Data
Models
Inventories

PARIS

Process Attribution of Regional Emissions

GA 101081430, RIA

Draft Annexes to National Inventory Reports

Deliverable 2.1	
Delivery due date Annex I	PM 22 | 31/10/2024
Actual date of submission	19/11/2024
Lead beneficiary: [acronym]	Work package: 2 Nature: Report Dissemination level: PU
Responsible scientist	A. Manning, UK Met Office
Contributors	A. Ganesan, H. de Longueville, A. Danjou, B. Murphy (University of Bristol) S. Henne, D. Brito Melo (Empa) A. Ramsden, A. Redington, P. Andrews (UK Met Office)
Internal reviewers	A. Ganesan, University of Bristol, co-coordinator, A. Manning, UK Met Office, WP2 lead
Version: 0.1	

Horizon Europe Cluster 5: Climate, energy and mobility
"This project has received funding from the European Union's Horizon Europe Research and Innovation programme under HORIZON-CL5-2022-D1-02 Grant Agreement No 101081430 - PARIS".

Table of content

1. Changes with respect to the DoA (Description of the Action)

No changes with respect to the DoA.

2. Dissemination and uptake

These draft Annexes to the National Inventory Reports are provided to the national inventory compilers of the eight focus countries of the project (UK, Netherlands, Ireland, Italy, Switzerland, Germany, Norway, Hungary). The Annexes provide a comparison between the emissions reported annually in NIRs versus those that are derived from atmospheric measurements ("top-down").

The Annexes provide an assessment of 1) gases or processes for which there are significant discrepancies between NIR and top-down, 2) gases that show consistency between NIR and top-down, and 3) regions that are not currently constrained by the observational network and are "blind" to the top-down estimates.

3. Short Summary of results

Inversion results were derived for eight focus countries (UK, Netherlands, Ireland, Italy, Switzerland, Germany, Norway, Hungary) for the period 2018-2023 using three inverse systems. National emissions and spatial distributions are presented and tabulated for methane, nitrous oxide and reported F-gases and compared to reported values. The specific gases estimated for each country varied depending on the available observational constraint in the measurement networks. In addition, Northern and Southern Hemisphere background concentration trends are provided for a global context.

4. Evidence of accomplishment

The eight draft Annexes are available as individual reports. All associated inverse modelling results (grid-distributed and country-aggregated fluxes) are provided as netcdf files.

4.1 Introduction | Background of the deliverable | milestone

There are only a few countries worldwide, and only two in Europe (the UK and Switzerland), who currently routinely report their emissions using bottom-up (inventory) and top-down (atmospheric data-based) methods together. The central aim of this project is to significantly increase the uptake of this joint approach to emissions evaluation. For each of the eight focus countries, national emissions were derived using atmospheric data from the European measurement networks. These results and comparisons to the National Inventory Reports (NIR) are documented in draft Annexes to the NIR for each focus country. Each draft Annex contains an Introduction section that describes the background to the document.

In this document, global concentration trends and national emissions estimates derived from atmospheric observations ("inverse estimates") are presented for each reported gas. Comparing the emissions submitted in national inventories with those calculated using atmospheric observations allows for emissions to be assessed using two fundamentally different approaches. Substantial differences can highlight areas that could warrant further investigation.

4.2 Scope of the deliverable | milestone

National emissions estimates for methane, nitrous oxide, HFC-134a, HFC-143a, HFC-125, HFC-32, HFC-227ea. HFC-245fa, HFC-23, HFC-365mfc, HFC-152a, HFC-43-10-mee over 2018-2023 using three inverse methods for the eight focus countries. Not all gases were estimated for each country, due to limitations in the observational network.

4.3 Content of the deliverable | milestone

An overview of the methodology, the work carried out, and results are described within the Annex reports. For ease, the introductory text from the Annexes is reproduced here. Data files containing the emissions estimates will be uploaded to the ICOS portal.

Global concentration trends for each gas are first shown using annual average concentrations from Mace Head, Ireland (Northern Hemisphere) and Kennaook/Cape Grim, Tasmania, Australia (Southern Hemisphere). Data from these stations were selected to exclude regionally-polluted air masses and therefore represents northern and southern hemispheric concentration trends. Mace Head observations were supported by the National Aeronautics and Space Administration (NASA) and the UK Department of Energy, Security and Net Zero (DESNZ), and Kennaook/Cape Grim observations by NASA and the Australian Bureau of Meteorology.

Observations of European concentrations of greenhouse gases used to derive national inverse emission estimates were collected from many different networks and providers. Methane and nitrous oxide concentrations originated from the European ICOS (Integrated Carbon Observation System) network, the UK DECC (Deriving Emissions related to Climate Change) network and other national or individual initiatives. F-gas observations were made by affiliates of the AGAGE (Advanced Global Atmospheric Gases Experiment) network. Observations from additional stations across Europe were supported by the Horizon-EU PARIS (Process Attribution of Regional Emissions) project. The observation stations used to derive emissions for each gas are shown in the corresponding sections of this document.

Inversion-based emissions estimates were derived using one atmospheric transport model but with multiple inverse models allowing a better quantification of the uncertainties associated with inverse modelling. The atmospheric transport model provides the link between surface fluxes and concentrations measured at the observing stations. Although the uncertainty associated with the atmospheric transport model is considered in the statistical inversion approach, it may be underestimated when only using a single transport model. The atmospheric transport model used is the Numerical Atmospheric dispersion Modelling Environment (NAME) Jones et al., 2007 a backwards-running Lagrangian Particle Dispersion Model (LPDM) that simulates the recent transport of air to each observing station. The NAME model has been widely used in the estimation of greenhouse gases emissions (Ganesan et al., 2015, Rigby et al., 2019, Manning et al., 2021).

The three inverse methods used are InTEM (Inversion Technique for Emission Modelling, Manning et al., 2021), ELRIS (Empa Lagrangian Regional Inversion System, Henne et al., 2016, Katharopoulos et al., 2023), and RHIME (Regional Hierarchical Inverse Modelling Environment, Ganesan et al., 2014). All three inverse methods estimate emissions within Europe along with boundary conditions that account for the concentration of the air entering Europe. All three systems started from the same set of a priori emissions that were either derived from the global EDGAR emission inventory (version 8, European Commission:

Joint Research Centre, 2023} or a uniform land-based emission, depending on the gas. A natural emission component, from the WETCHARTS product, was included in the methane prior. The same observational dataset was used by each inverse model, but data selection (i.e., filtering datasets for specific conditions) and treatment of uncertainties were chosen separately and hence differ. The three methods also differ in their statistical approaches for estimating emissions.

Emission estimates are presented for the period 2008-2023. Emissions for the full 2008-2023 period were derived with the InTEM model only, while emissions from 2018-2023 are presented as a combined result using the three inverse models.

For the 2008-2023 InTEM results, a 2-year inversion resolution, incrementing annually, was used for all gases except CH_4 and N_2O, where the resolution was monthly. For the recent 2018-2023 period, for all three models, the inversion resolution was one month for CH_4 and N_2O in order to capture the seasonality of the emissions, a one-year average over these results is also presented. For the fluorinated gases, a 1-year inversion resolution was adopted, with a 3-year moving average applied to the results. The uncertainty shown is the minimum/maximum of the uncertainties from the three results.

4.4 Conclusion and possible impact

These draft Annexes are used to guide discussions with the national inventory compilers of the focus countries and to build collaboration between inventory and atmospheric modelling teams. The national inventory compilers may choose to use the information provided in the draft Annexes to guide where further work is needed to reconcile large uncertainties or discrepancies. The countries can choose to include these draft Annexes in their NIRs.

4.5 References

European Commission: Joint Research Centre et al. (2023). GHG emissions of all world countries – 2023. Publications Office of the European Union. doi: 10.2760/953322.

Ganesan, A. L. et al. (2014). "Characterization of uncertainties in atmospheric trace gas inversions using hierarchical Bayesian methods". In: Atmospheric Chemistry and Physics 14.8, pp. 3855–3864. doi:10.5194/acp-14-3855-2014.

Ganesan, A. L. et al. (2015). "Quantifying methane and nitrous oxide emissions from the UK and Ireland using a national-scale monitoring network". In: Atmos. Chem. Phys. 15.11, pp. 6393–6406. doi: 10.5194/acp- 15- 6393- 2015.

Henne, S. et al. (2016). "Validation of the Swiss methane emission inventory by atmospheric observations and inverse modelling". In: Atmospheric Chemistry and Physics 16.6, pp. 3683–3710. doi: 10.5194/acp-16-3683-2016.

Jones, A.R. et al. (2007). "The U.K. Met Office's next-generation atmospheric dispersion model, NAMEIII, in Borrego C. and Norman A.-L. (Eds)". In: Air Pollution Modeling and its Application XVII (Proceedings of the 27th NATO/CCMS International Technical Meeting on Air Pollution Modelling and its Application), Springer, pp. 580–589.

Katharopoulos, I. et al. (2023). "Impact of transport model resolution and a priori assumptions on inverse modeling of Swiss F-gas emissions". In: Atmos. Chem. Phys. 23.22, pp. 14159–14186. doi: 10.5194/acp-23-14159-2023.

Manning, A. J. et al. (2021). "Evidence of a recent decline in UK emissions of hydrofluorocarbons determined by the InTEM inverse model and atmospheric measurements". In: Atmospheric Chemistry and Physics 21.16, pp. 12739–12755. doi: 10 . 5194/acp - 21 - 12739 - 2021.

Rigby, M. et al. (2019). "Increase in CFC-11 emissions from eastern China based on atmospheric observations". In: Nature 569, pp. 546–550. doi: 10.1038/s41586-019-1193-4. url: https://doi.org/10.1038/s41586-019-1193-4.

5. History of the document

Version	Author(s)	Date	Changes
0.1	A. Manning, A. Ganesan, S. Henne, D. Brito Melo, A. Ramsden, H. De Longueville, A. Danjou, B. Murphy, P. Andrews	18/11/2024	

Draft Inventory Annex
Germany 2024

18th November, 2024

1 Introduction

In this document, global concentration trends and national emissions estimates derived from atmospheric observations ("inverse estimates") are presented for each reported gas. Comparing the emissions submitted in national inventories with those calculated using atmospheric observations allows for emissions to be assessed using two fundamentally different approaches. Substantial differences can highlight areas that could warrant further investigation.

Global concentration trends for each gas are first shown using annual average concentrations from Mace Head, Ireland (Northern Hemisphere) and Kennaook/Cape Grim, Tasmania, Australia (Southern Hemisphere). Data from these stations were selected to exclude regionally-polluted air masses and therefore represents northern and southern hemispheric concentration trends. Mace Head observations were supported by the National Aeronautics and Space Administration (NASA) and the UK Department of Energy, Security and Net Zero (DESNZ), and Kennaook/Cape Grim observations by NASA and the Australian Bureau of Meteorology.

Observations of European concentrations of greenhouse gases used to derive national inverse emission estimates were collected from many different networks and providers. Methane and nitrous oxide concentrations originated from the European ICOS (Integrated Carbon Observation System) network, the UK DECC (Deriving Emissions related to Climate Change) network and other national or individual initiatives. F-gas observations were made by affiliates of the AGAGE (Advanced Global Atmospheric Gases Experiment) network. Observations from from additional stations across Europe were supported by the Horizon-EU PARIS (Process Attribution of Regional Emissions) project. The observation stations used to derive emissions for each gas are shown in the corresponding sections of this document.

Inversion-based emissions estimates were derived using one atmospheric transport model but with multiple inverse models allowing a better quantification of the uncertainties associated with inverse modelling. The atmospheric transport model provides the link between surface fluxes and concentrations measured at the observing stations. Although the uncertainty associated with the atmospheric transport model is considered in the statistical inversion approach, it may be underestimated when only using a single transport model. The atmospheric transport model used is the Numerical Atmospheric dispersion Modelling Environment (NAME) (Jones et al., 2007), a backwards-running Lagrangian Particle Dispersion Model (LPDM) that simulates the recent transport of air to each observing station. The NAME model has been widely used in the estimation of greenhouse gases emissions (Ganesan et al., 2015; Rigby et al., 2019; Manning et al., 2021).

The three inverse methods used are InTEM (Inversion Technique for Emission Modelling, Manning et al., 2021), ELRIS (Empa Lagrangian Regional Inversion System, Henne et al., 2016; Katharopoulos et al., 2023), and RHIME (Regional Hierarchical Inverse Modelling Environment, Ganesan et al., 2014). All three inverse methods estimate emissions within Europe along with boundary conditions that account for the concentration of the air entering Europe. All three systems started from the same set of a priori emissions that were either derived from the global EDGAR emission inventory (version 8, European Commission: Joint Research et al., 2023) or a uniform land-based emission, depending on the gas. A natural emission component, from the WETCHARTS product, was included in the methane prior. The same observational dataset was used by each inverse model, but data selection (i.e., filtering datasets for specific conditions) and treatment of uncertainties were chosen separately and hence differ. The three methods also differ in their statistical approaches for estimating emissions.

Emission estimates are presented for the period 2008-2023. Emissions for the full 2008-2023 period were derived with the InTEM model only, while emissions from 2018-2023 are presented as a combined result using the three inverse models.

For the 2008-2023 InTEM results, a 2-year inversion resolution, incrementing annually, was used for all gases except CH_4nd N_2, where the resolution was monthly. For the recent 2018-2023 period, for all three models, the inversion resolution was one month for CH_4 and N_2O in order to capture the seasonality of the emissions, a one-year average over these results is also presented. For the fluorinated gases, a 1-year

inversion resolution was adopted, with a 3-year moving average applied to the results. The uncertainty shown is the minimum/maximum of the uncertainties from the three results.

2 Global Concentration Trends

2.1 Methane (CH_4)

Figure 2.1.1: Background Northern Hemisphere monthly concentrations of CH_4 estimated from MHD, Ireland observations are shown in red, and background Southern Hemisphere monthly concentrations from CGO, Tasmania are shown in blue. Grey shading represents provisional data.

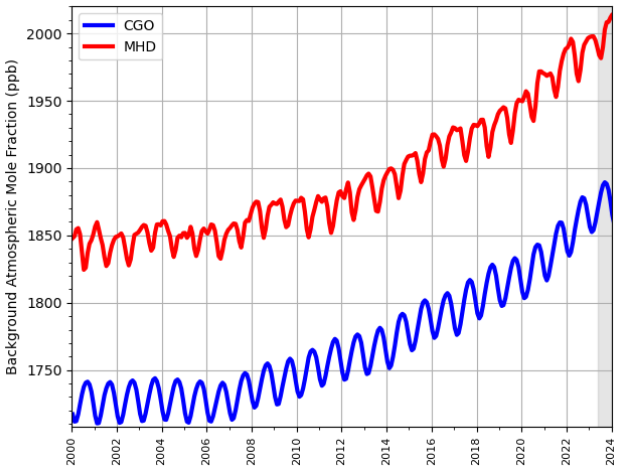

2.2 Nitrous Oxide (N_2O)

Figure 2.2.1: Background Northern Hemisphere monthly concentrations of N_2O estimated from MHD, Ireland observations are shown in red, and background Southern Hemisphere monthly concentrations from CGO, Tasmania are shown in blue. Grey shading represents provisional data.

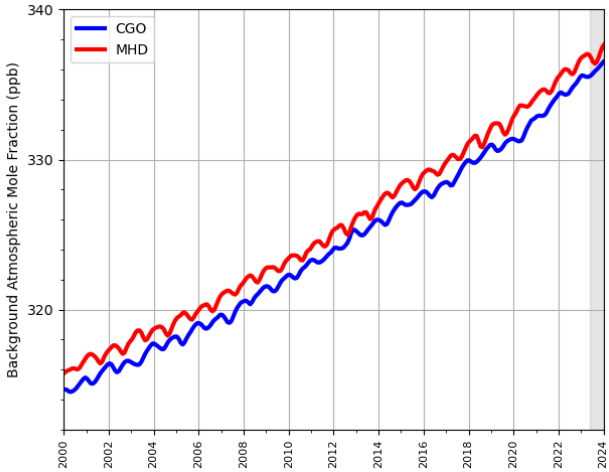

2.3 Hydrofluorocarbons (HFCs)

Figure 2.3.1: Background Northern Hemisphere monthly concentrations of six HFCs estimated from MHD, Ireland observations are shown in red, and background Southern Hemisphere monthly concentrations from CGO, Tasmania are shown in blue. Grey shading represents provisional data.

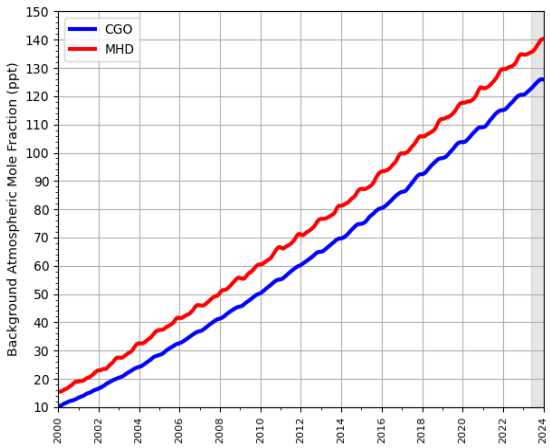

(a) HFC-134a

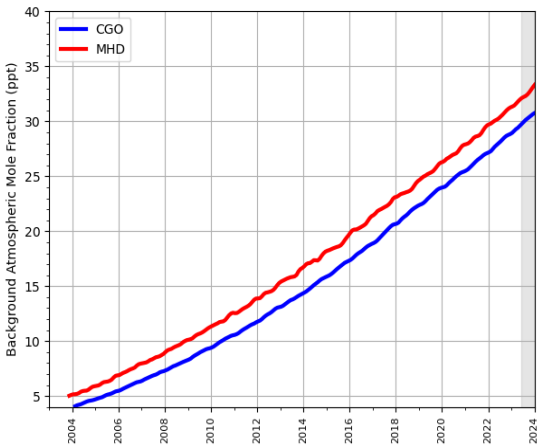

(b) HFC-143a

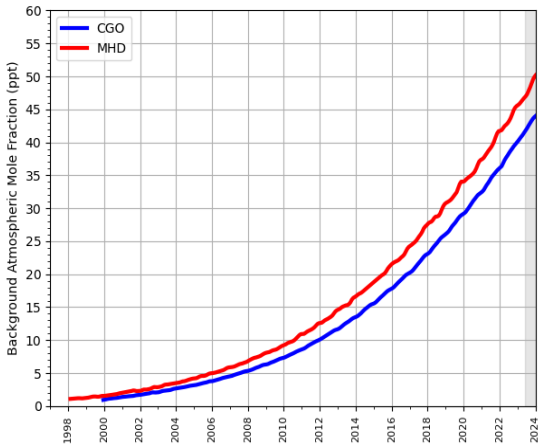

(c) HFC-125

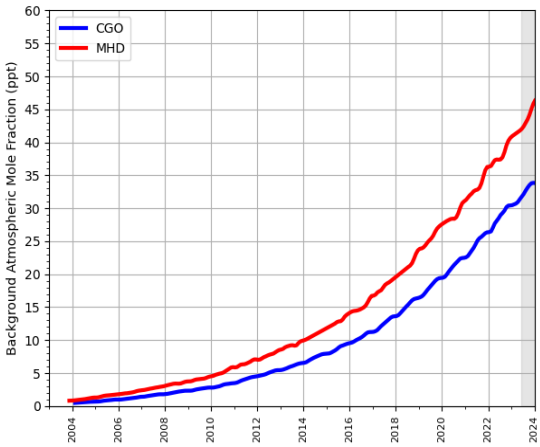

(d) HFC-32

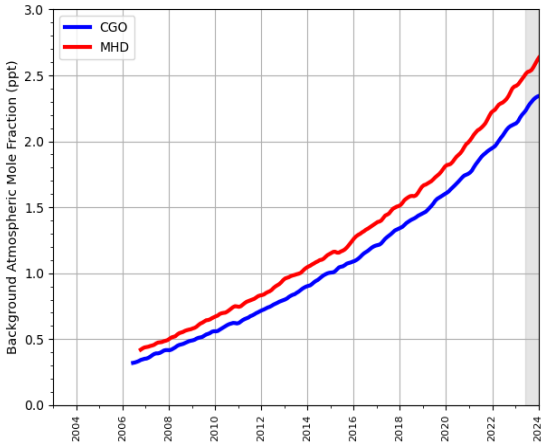

(e) HFC-227ea

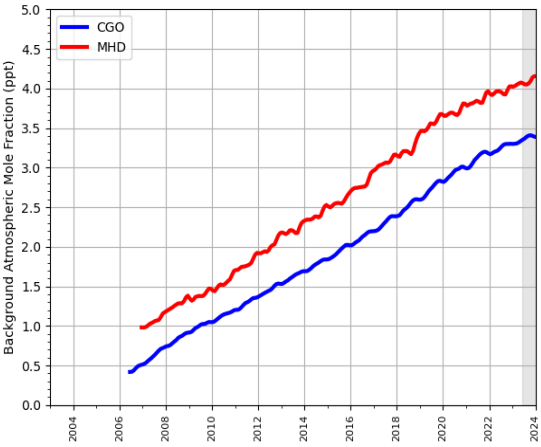

(f) HFC-245fa

Figure 2.3.2: Background Northern Hemisphere monthly concentrations of four HFCs estimated from MHD, Ireland observations are shown in red, and background Southern Hemisphere monthly concentrations from CGO, Tasmania are shown in blue. Grey shading represents provisional data.

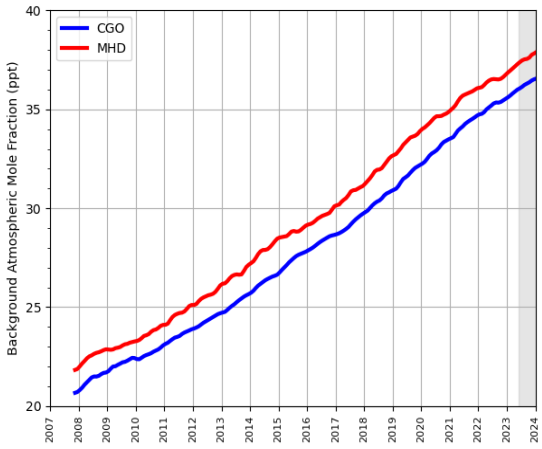

(a) HFC-23

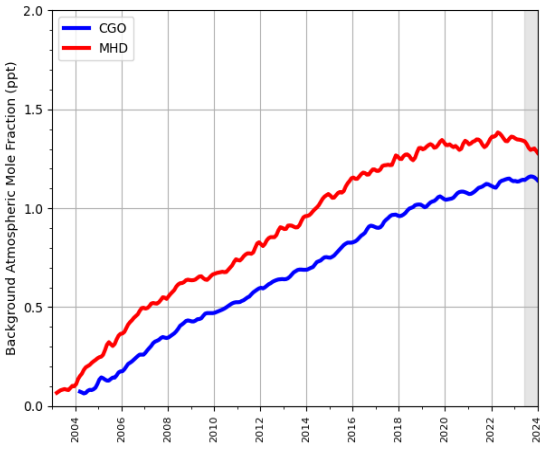

(b) HFC-365mfc

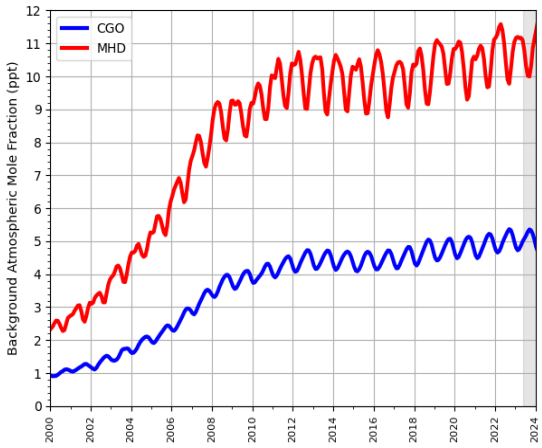

(c) HFC-152a

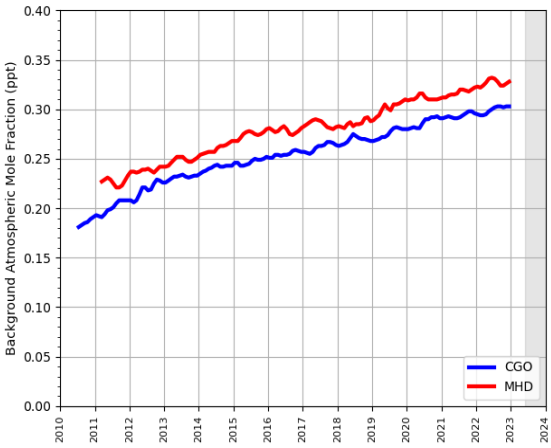

(d) HFC-43-10-mee

2.4 Perfluorocarbons (PFCs)

Figure 2.4.1: Background Northern Hemisphere monthly concentrations of four PFCs estimated from MHD, Ireland observations are shown in red, and background Southern Hemisphere monthly concentrations from CGO, Tasmania are shown in blue. Grey shading represents provisional data.

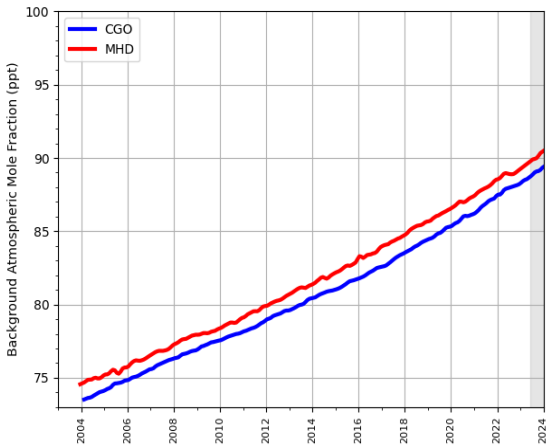

(a) PFC-14

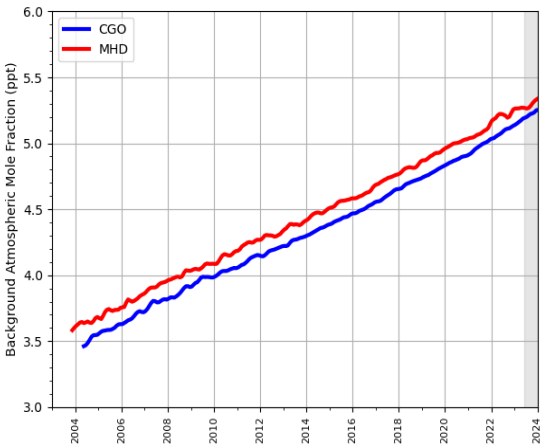

(b) PFC-116

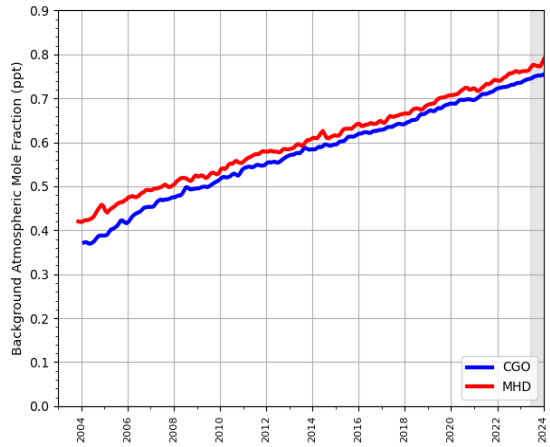

(c) PFC-218

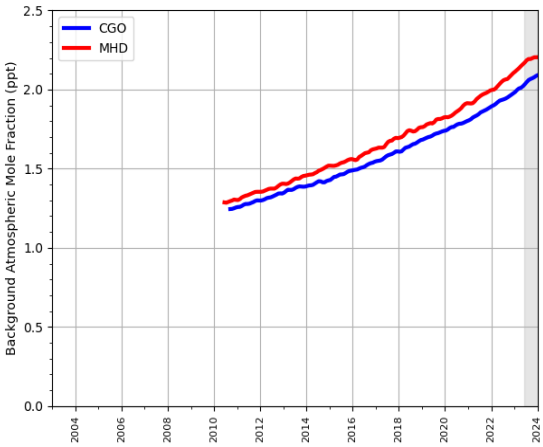

(d) PFC-318

3 Key findings

- Methane (CH_4): Overall, inverse models estimate higher emissions than the inventory (Figure 4.0.2). Between 2018 and 2022, the mean over the three inverse models is 15-30 % higher than the inventory. Moreover, the decreasing trend reported in the inventory is not confirmed by the models. CH_4 emissions are maximum in the northwest of the country, which is largely dominated by intense agriculture (Figure 4.0.5). High emissions are also obtained in the neighbouring countries, which makes it challenging to fully differentiate the German emissions from those from the Benelux region. Higher emissions are obtained during the winter months (Figures 4.0.4 and 4.0.6). The seasonality is mainly observed in rural areas, which indicates that it is related to agricultural emissions.
- Nitrous oxide (N_2O): The inverse results show a stronger year-to-year variability than the inventory (Figure 5.0.2). Between 2018 and 2022, the mean over the three inverse models is 5-30 % higher than the inventory. N_2O emissions are maximum in the northwest of the country and in the Rhine region between Mannheim and Darmstadt (Figure 5.0.5). Higher emissions are obtained during the summer months (Figures 5.0.4 and 5.0.6). The strongest seasonality is seen in the northwest of the country, again indicating a seasonality in agricultural emissions.
- Hydrofluorocarbons (HFCs): The European measurement network for HFCs and PFCs is significantly smaller than for methane and nitrous oxide (Figure 6.0.1). This increases the uncertainty of the model predictions. Overall, higher emissions are obtained from the inverse models. However, the inventory values are within the estimated model uncertainty. Most important aspects for individual gases are the increasing trend of HFC-32 and the decreasing trend of HFC-134a that is visible in both reporting and inverse modelling.
- Perfluorocarbons (PFCs): PFC emissions in Germany are small in comparison to the remaining greenhouse gases investigated. The sporadic nature of the emissions and the sparse measurement network result in high model uncertainties. Relatively high emissions of PFC-318 around Essen could be investigated (Figure 7.4.2).
- Sulphur hexafluoride (SF_6): A reasonable agreement is obtained between the inverse results and the inventory (Figure 8.0.2). High emissions are obtained in the southwest of the country, where a factory of SF_6 is known to exist. Note that all inverse models assumed uniform emissions of SF_6 over Germany as the prior spatial distribution and pick up the emission hot spot solely based on the atmospheric observations.

Table 1: Emissions estimation for the main greenhouse gases of focus in $\mathrm{TgCO_2{-}eq \cdot yr^{-1}}$ according to the National Inventory Report (NIR) 2024 and the inversions done in the PARIS project. For the PARIS estimation, the mean of the 3 inversion models is displayed, along with a range of uncertainty estimated via the half distance between the maximum and minimum uncertainties of the different models.

		2018	2019	2020	2021	2022	2023
CH_4	NIR 2024	58	55	54	53	52	
	PARIS mean	66 ± 4	63 ± 5	64 ± 6	67 ± 8	68 ± 6	70 ± 7
N_2O	NIR 2024	27	26	25	25	24	
	PARIS mean	34 ± 4	31 ± 2	29 ± 2	33 ± 2	25 ± 2	31 ± 2
Total HFCs[(1)]	NIR 2024	9.3	8.6	8.1	7.9	7.6	
	PARIS mean	9.9 ± 2.5	10.6 ± 2.3	10.5 ± 2.1	9.7 ± 1.9	8.8 ± 2.4	8.3 ± 2.3
Total PFCs[(2)]	NIR 2024	0.3	0.2	0.2	0.2	0.2	
	PARIS mean	0.4 ± 0.3	0.4 ± 0.4	0.5 ± 0.4	0.5 ± 0.4	0.6 ± 0.5	0.6 ± 0.5
SF_6	NIR 2024	4.0	4.0	3.1	2.7	2.0	
	PARIS mean	2.7 ± 0.7	2.6 ± 0.7	2.5 ± 0.6	2.3 ± 0.6	2.1 ± 0.5	1.9 ± 0.6

(1) Sum of HFC emissions presented in Table 2, except HFC-4310mee.
(2) Sum of PFC emissions presented in Table 3.

4 Methane (CH_4)

Figure 4.0.1: Total source sensitivity of CH_4 observing sites as calculated by the NAME transport model for the year (left) 2018 and (right) 2023 and used in the inversions. Observing stations active in each year are marked with red dots. Areas with visible land surface represent regions for which emissions can be observed well from the network. Shaded or dark areas represent regions for which limited emission information can be obtained from the network.

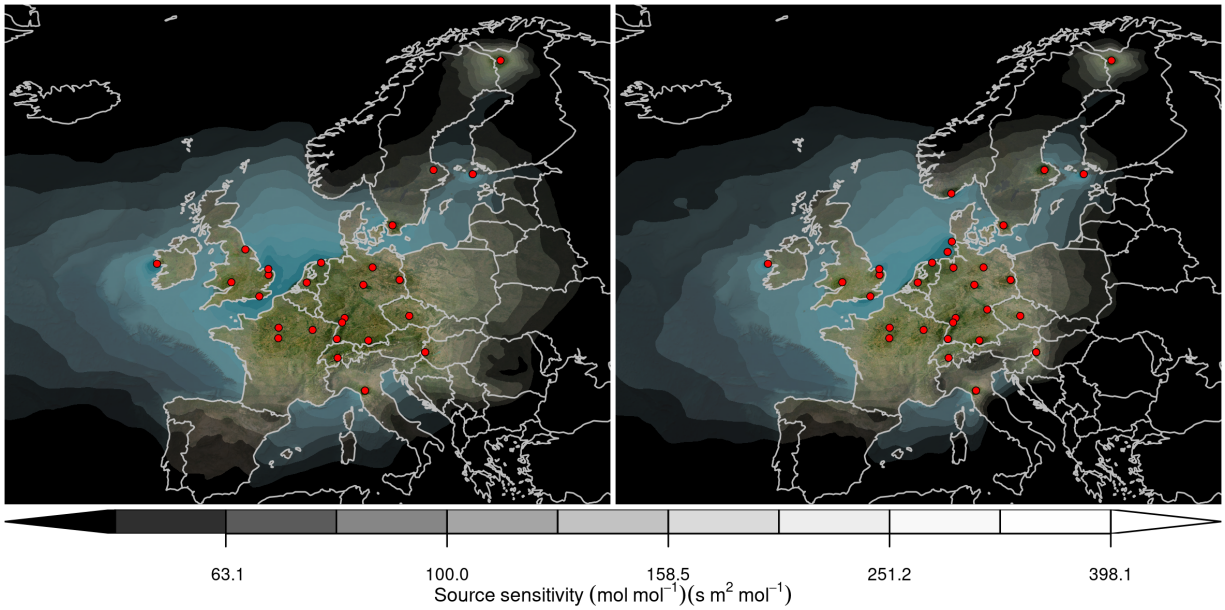

Figure 4.0.2: Verification of the German emissions inventory estimates for CH_4. Modelled annual emissions are given as the mean from all models (black line and grey shading) and the individual result from InTEM (blue line and shading). National inventory annual totals are given as grey bars.

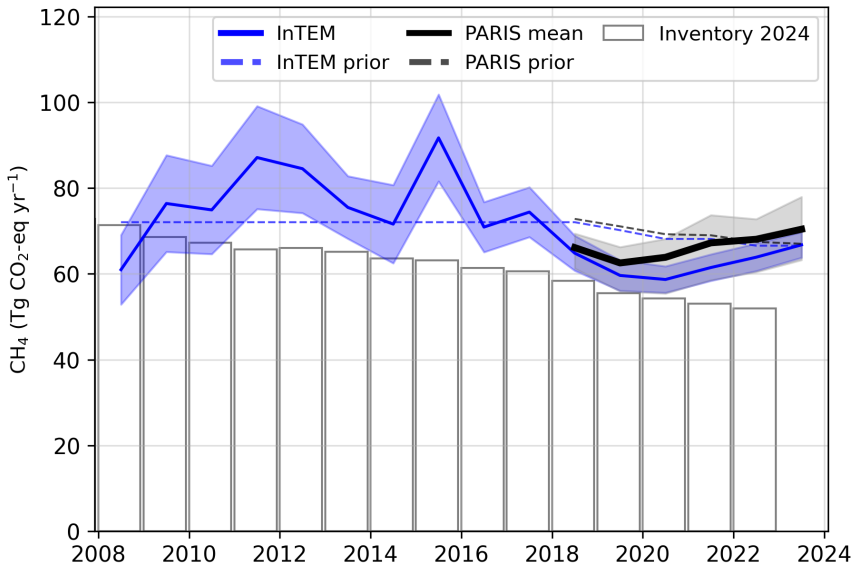

Figure 4.0.3: Verification of the German emissions inventory estimates for CH_4 (zoom in to 2018-2023). Modelled annual emissions are given as the mean from all models (black line and grey shading) and the individual result from InTEM (blue line and shading). National inventory annual totals are given as grey bars.

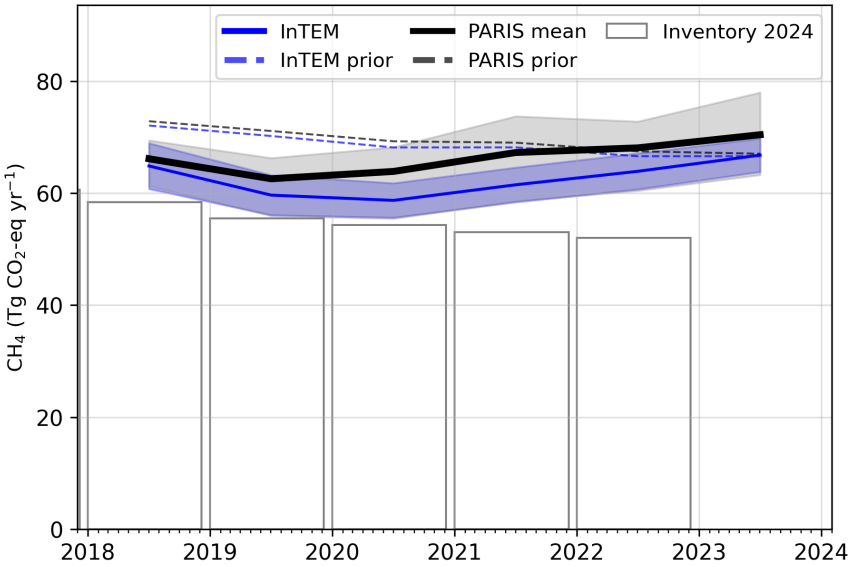

Figure 4.0.4: Verification of the German emissions inventory estimates for CH_4 (zoom in to 2018-2023). Modelled monthly emissions are given as the mean from all models (black line and grey shading) and the individual result from InTEM (blue line and shading). National inventory annual totals are given as grey bars.

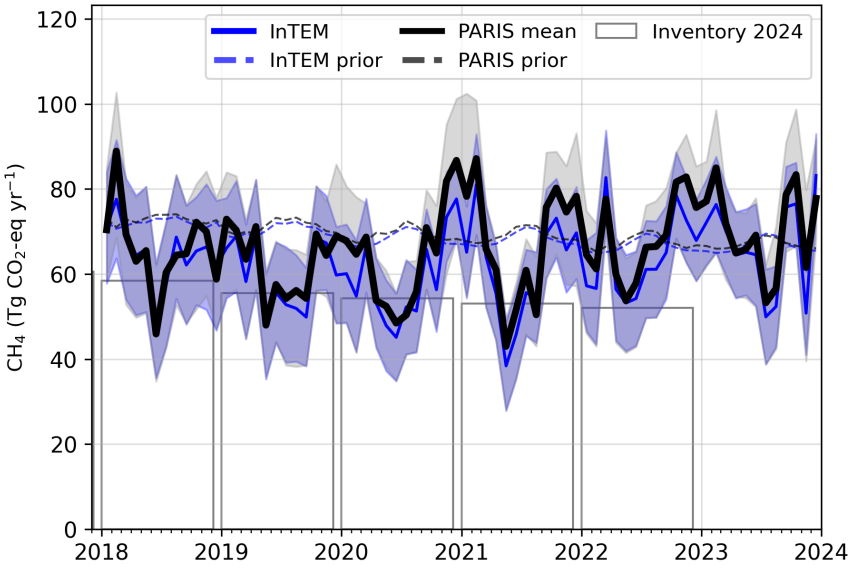

Figure 4.0.5: Spatial distribution of the German average modelled emissions of CH_4 during the period of 2018-2023 (mean from all models). Observing stations are marked with red circles and highly-populated cities are marked with red triangles.

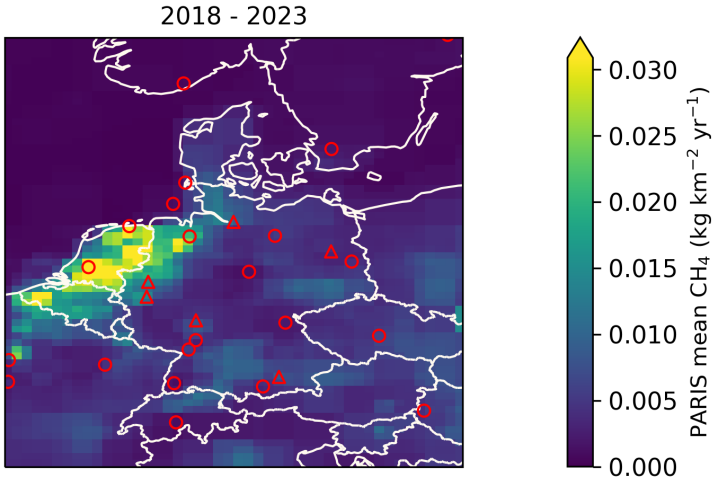

Figure 4.0.6: Spatial distribution of the seasonal deviation from the mean. The deviation is defined as the modelled German seasonally averaged CH_4 emissions over 2018-2023 minus the average over the whole period. The mean across all models is shown. Observing stations are marked with red circles and highly-populated cities are marked with red triangles.

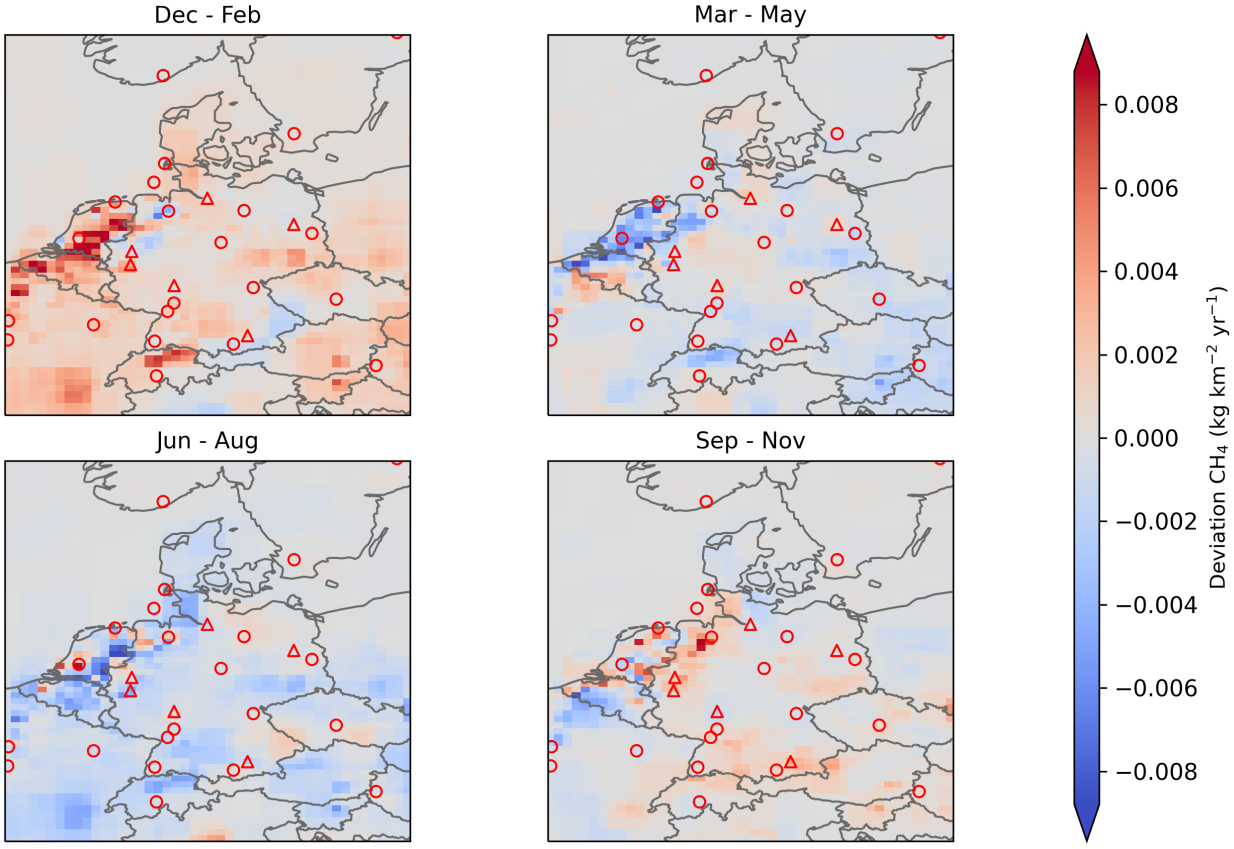

5 Nitrous Oxide (N_2O)

Figure 5.0.1: Total source sensitivity of N_2O observing sites as calculated by the NAME transport model for the year (left) 2018 and (right) 2023 and used in the inversions. Observing stations active in each year are marked with red dots. Areas with visible land surface represent regions for which emissions can be observed well from the network. Shaded or dark areas represent regions for which limited emission information can be obtained from the network.

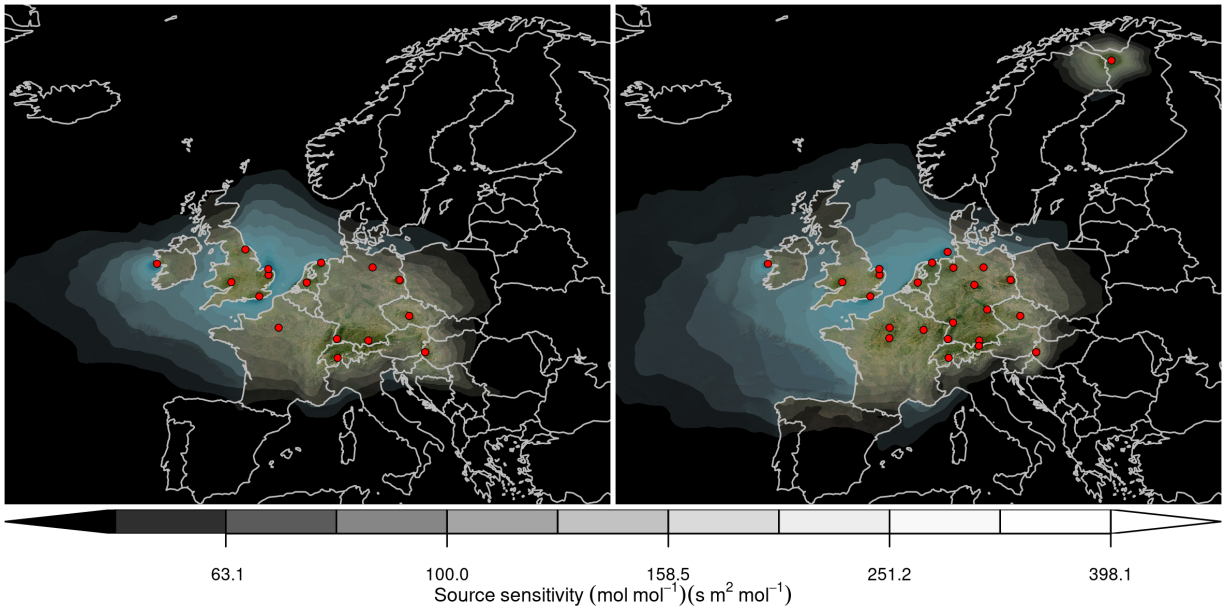

Figure 5.0.2: Verification of the German emissions inventory estimates for N_2O. Modelled annual emissions are given as the mean from all models (black line and grey shading) and the individual result from InTEM (blue line and shading). National inventory annual totals are given as grey bars.

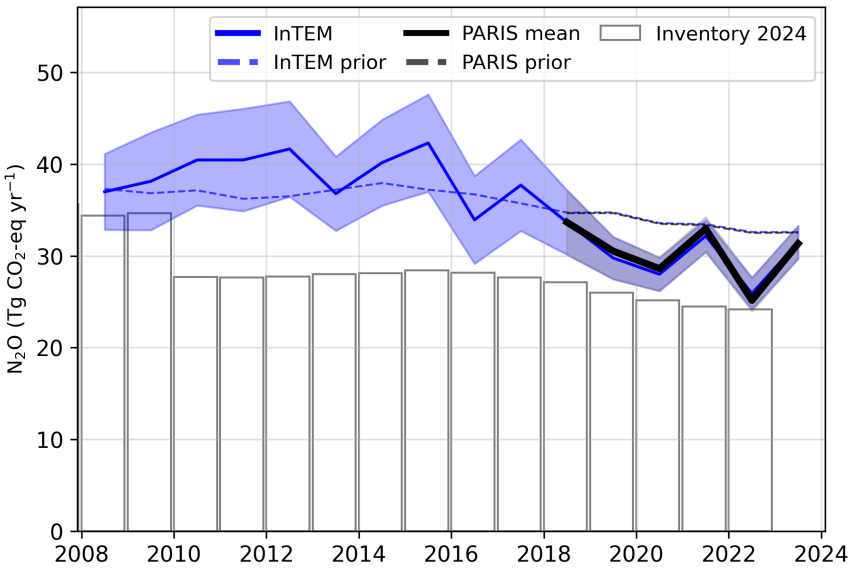

Figure 5.0.3: Verification of the German emissions inventory estimates for N_2O (zoom in to 2018-2023). Modelled annual emissions are given as the mean from all models (black line and grey shading) and the individual result from InTEM (blue line and shading). National inventory annual totals are given as grey bars.

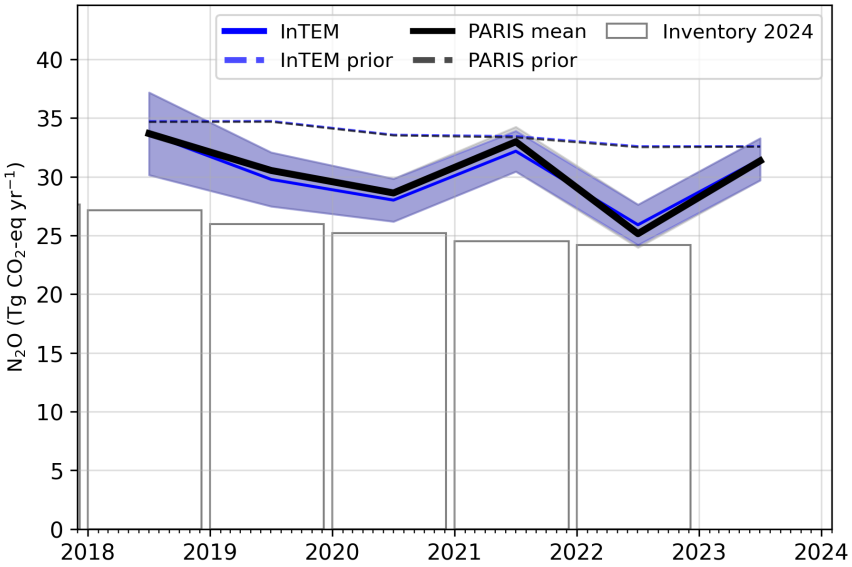

Figure 5.0.4: Verification of the German emissions inventory estimates for N_2O (zoom in to 2018-2023). Modelled monthly emissions are given as the mean from all models (black line and grey shading) and the individual result from InTEM (blue line and shading). National inventory annual totals are given as grey bars.

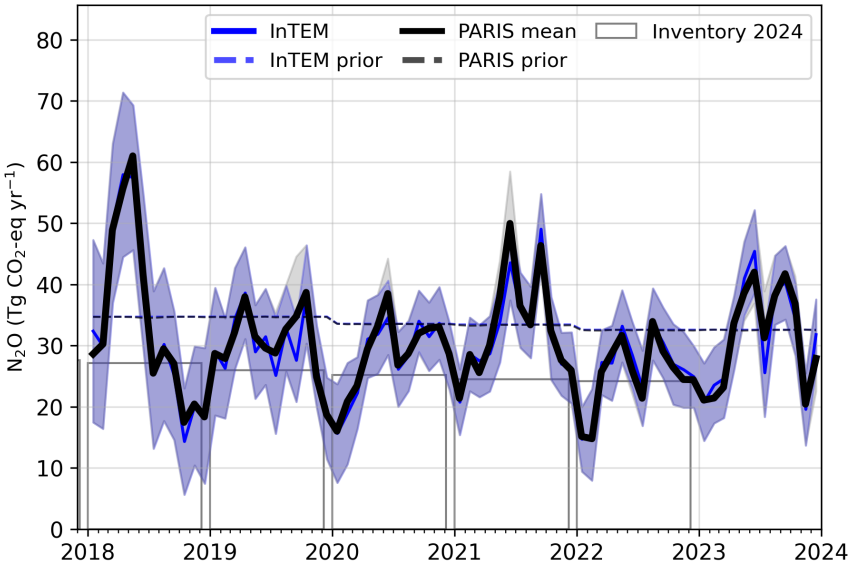

Figure 5.0.5: Spatial distribution of the German average modelled emissions of N_2O during the period of 2018-2023 (mean from all models). Observing stations are marked with red circles and highly-populated cities are marked with red triangles.

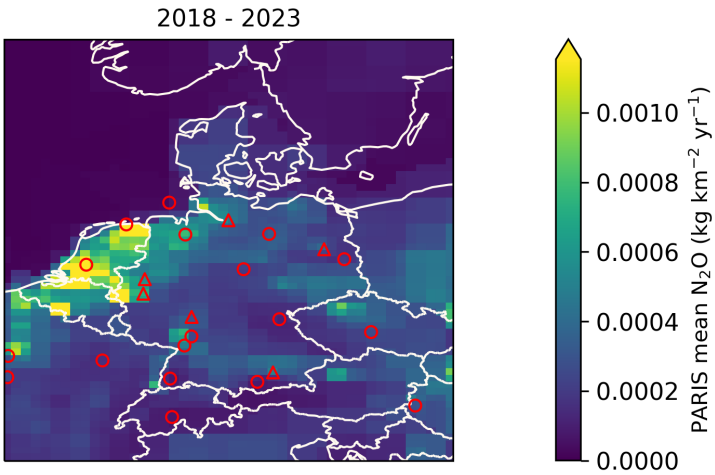

Figure 5.0.6: Spatial distribution of the seasonal deviation from the mean. The deviation is defined as the modelled German seasonally averaged N_2O emissions over 2018-2023 minus the average over the whole period. The mean across all models is shown. Observing stations are marked with red circles and highly-populated cities are marked with red triangles.

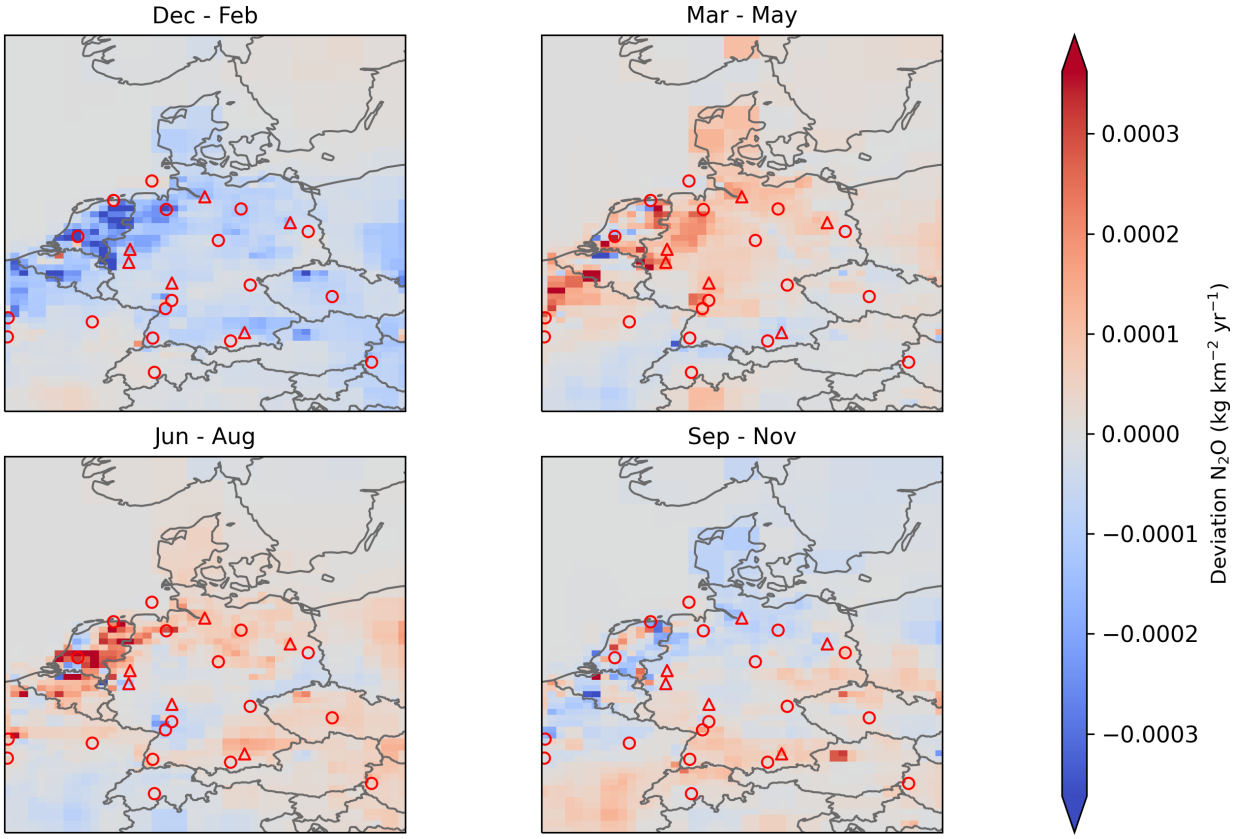

6 Hydrofluorocarbons (HFCs)

Figure 6.0.1: Total source sensitivity of HFCs/PFCs observing sites as calculated by the NAME transport model for the year (left) 2018 and (right) 2023 and used in the inversions. Observing stations active in each year are marked with red dots. Areas with visible land surface represent regions for which emissions can be observed well from the network. Shaded or dark areas represent regions for which limited emission information can be obtained from the network.

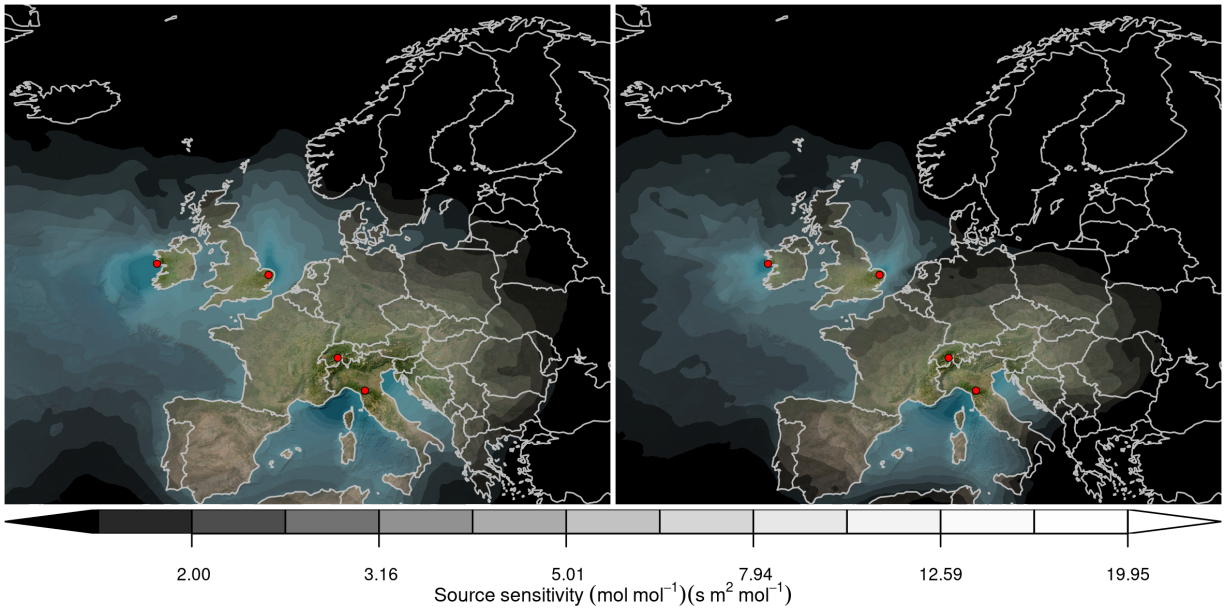

6.1 HFC-32

Figure 6.1.1: Verification of the German emissions inventory estimates for HFC-32. Modelled annual emissions are given as the mean from all models (black line and grey shading) and the individual result from InTEM (blue line and shading). National inventory annual totals are given as grey bars.

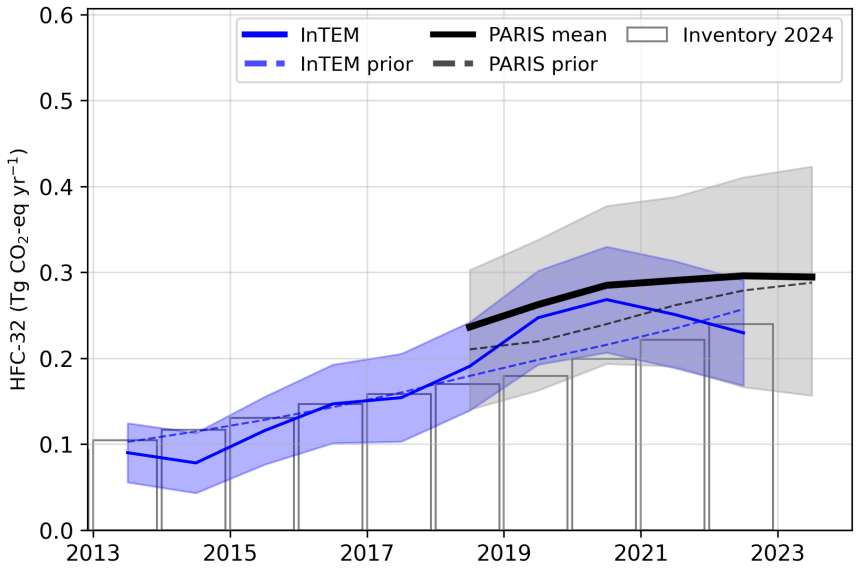

Figure 6.1.2: Spatial distribution of the German average modelled emissions of HFC-32 during the period of 2018-2023 (mean from all models). Observing stations are marked with red circles and highly-populated cities are marked with red triangles.

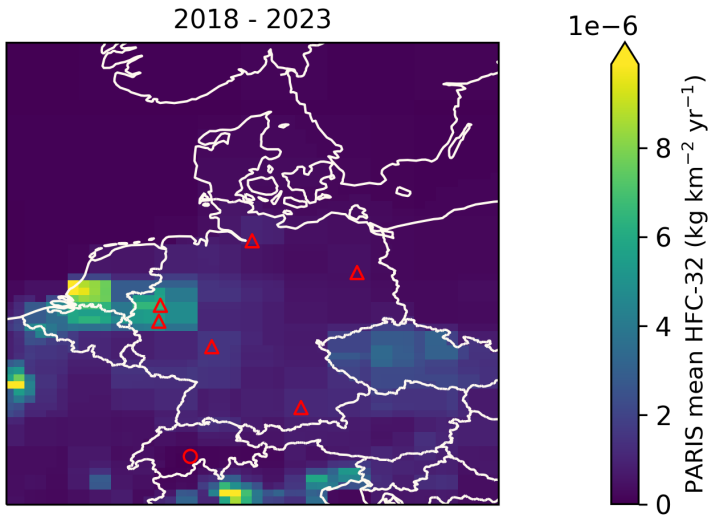

6.2 HFC-125

Figure 6.2.1: Verification of the German emissions inventory estimates for HFC-125. Modelled annual emissions are given as the mean from all models (black line and grey shading) and the individual result from InTEM (blue line and shading). National inventory annual totals are given as grey bars.

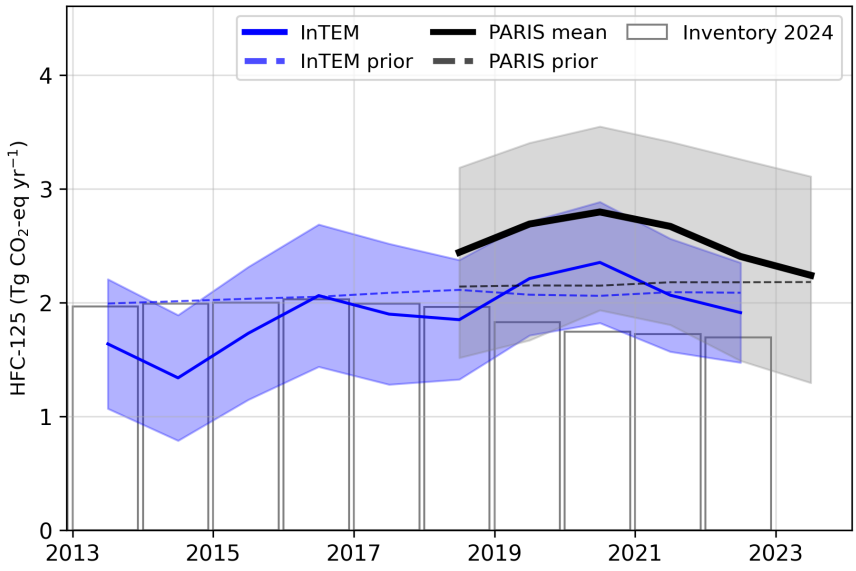

Figure 6.2.2: Spatial distribution of the German average modelled emissions of HFC-125 during the period of 2018-2023 (mean from all models). Observing stations are marked with red circles and highly-populated cities are marked with red triangles.

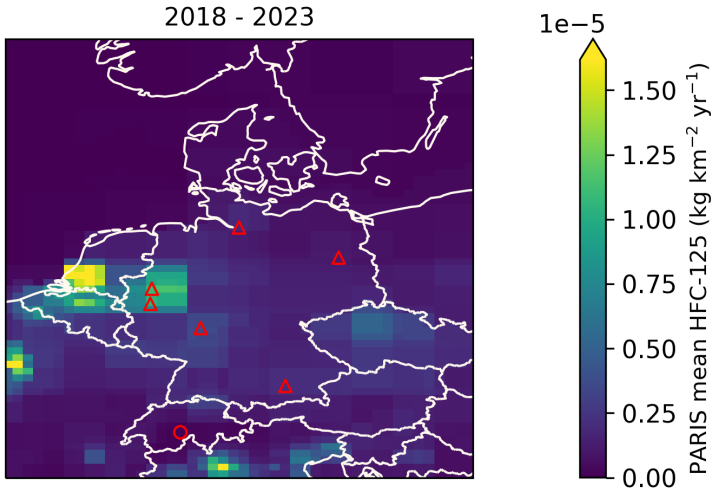

6.3 HFC-134a

Figure 6.3.1: Verification of the German emissions inventory estimates for HFC-134a. Modelled annual emissions are given as the mean from all models (black line and grey shading) and the individual result from InTEM (blue line and shading). National inventory annual totals are given as grey bars.

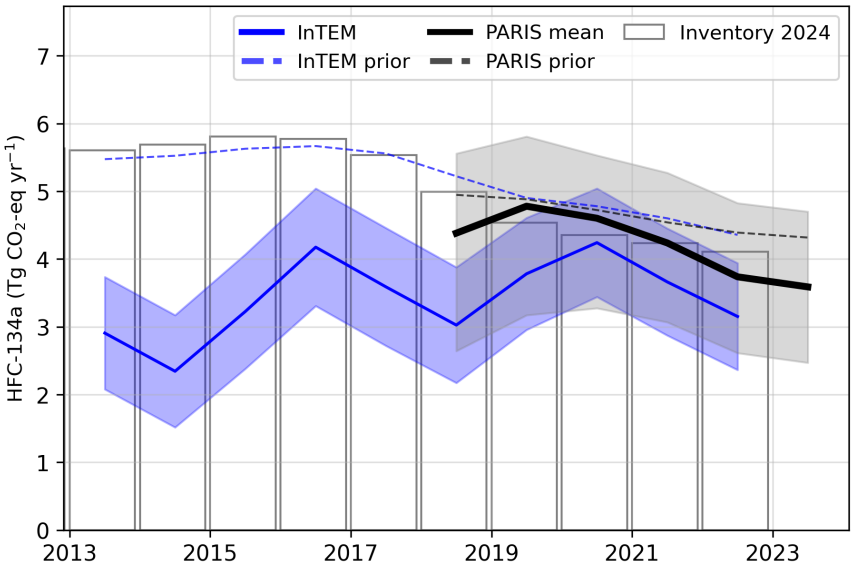

Figure 6.3.2: Spatial distribution of the German average modelled emissions of HFC-134a during the period of 2018-2023 (mean from all models). Observing stations are marked with red circles and highly-populated cities are marked with red triangles.

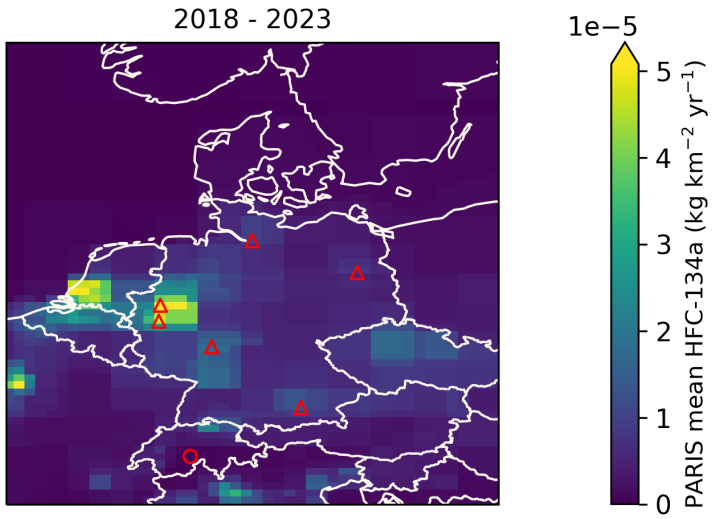

6.4 HFC-143a

Figure 6.4.1: Verification of the German emissions inventory estimates for HFC-143a. Modelled annual emissions are given as the mean from all models (black line and grey shading) and the individual result from InTEM (blue line and shading). National inventory annual totals are given as grey bars.

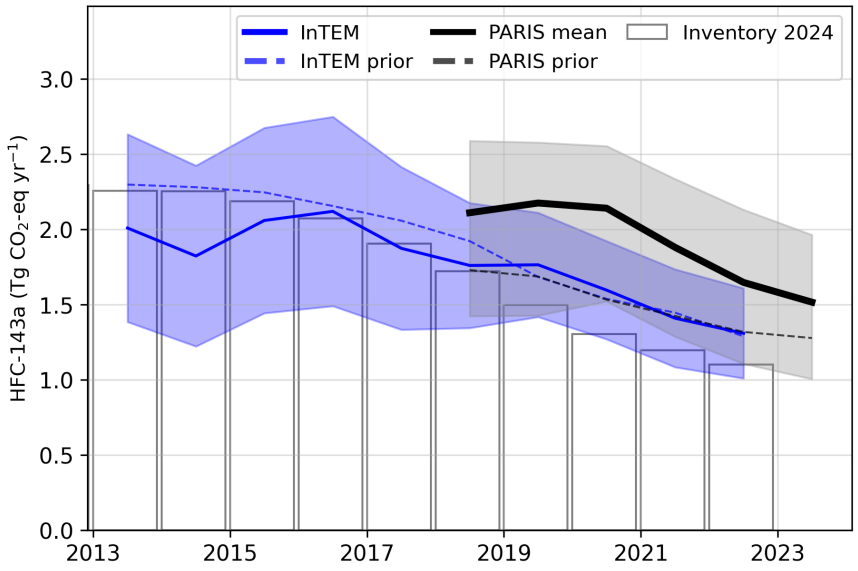

Figure 6.4.2: Spatial distribution of the German average modelled emissions of HFC-143a during the period of 2018-2023 (mean from all models). Observing stations are marked with red circles and highly-populated cities are marked with red triangles.

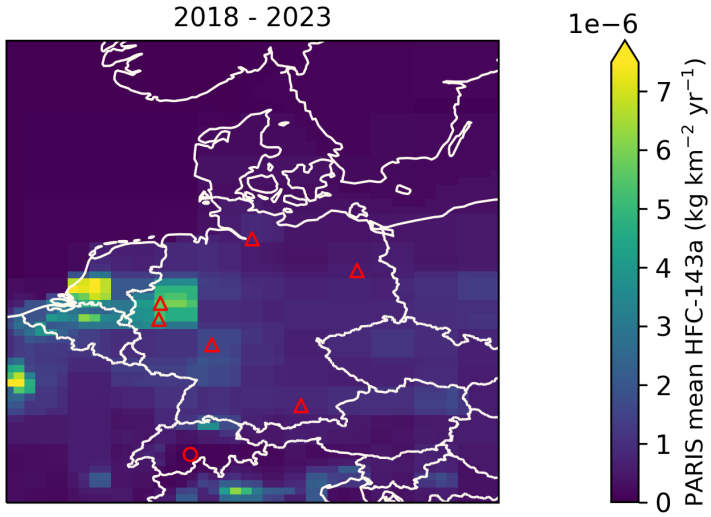

6.5 Total HFCs

Figure 6.5.1: Verification of the German emissions inventory estimates for total HFCs. Modelled annual emissions are given as the mean from all models (black line and grey shading) and the individual result from InTEM (blue line and shading). National inventory annual totals are given as grey bars.

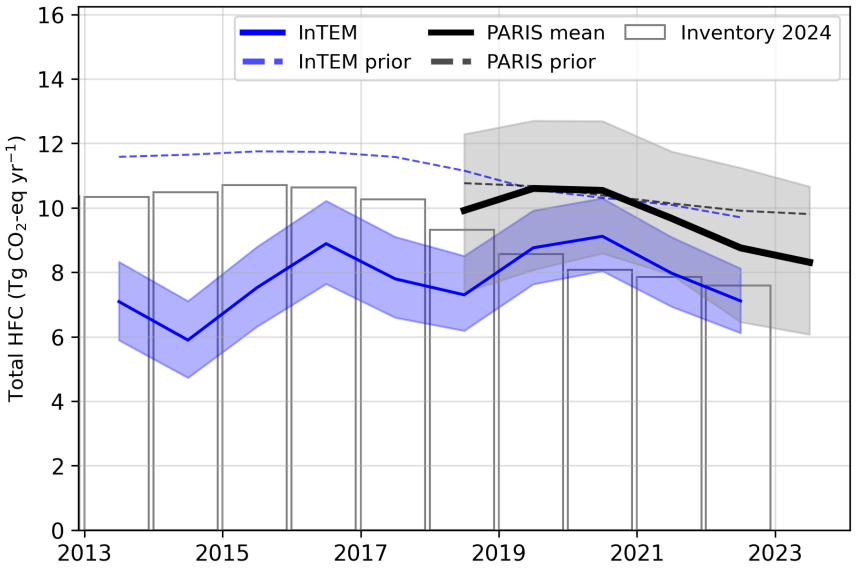

Table 2: Emissions estimation for HFCs in $\mathrm{TgCO_2{-}eq \cdot yr^{-1}}$ according to the National Inventory Report (NIR) 2024 and the inversions done in the PARIS project. For the PARIS estimation, the mean of the 3 inversion models is displayed, along with a range of uncertainty estimated via the half distance between the maximum and minimum uncertainties of the different models.

		2018	2019	2020	2021	2022	2023
HFC-23	NIR 2024	0.08	0.07	0.06	0.08	0.05	
	PARIS mean	0.41 ± 0.57	0.37 ± 0.51	0.40 ± 0.57	0.32 ± 0.55	0.43 ± 0.65	0.44 ± 0.65
HFC-32	NIR 2024	0.17	0.18	0.20	0.22	0.24	
	PARIS mean	0.24 ± 0.08	0.26 ± 0.09	0.28 ± 0.09	0.29 ± 0.10	0.30 ± 0.12	0.29 ± 0.13
HFC-125	NIR 2024	1.96	1.83	1.74	1.72	1.69	
	PARIS mean	2.44 ± 0.84	2.69 ± 0.87	2.80 ± 0.81	2.67 ± 0.80	2.40 ± 0.89	2.24 ± 0.91
HFC-134a	NIR 2024	5.00	4.54	4.35	4.24	4.11	
	PARIS mean	4.38 ± 1.46	4.78 ± 1.32	4.60 ± 1.13	4.24 ± 1.10	3.74 ± 1.11	3.59 ± 1.11
HFC-143a	NIR 2024	1.72	1.50	1.30	1.20	1.10	
	PARIS mean	2.11 ± 0.58	2.17 ± 0.58	2.14 ± 0.52	1.88 ± 0.52	1.65 ± 0.51	1.52 ± 0.48
HFC-152a	NIR 2024	0.04	0.03	0.02	0.01	0.01	
	PARIS mean	0.03 ± 0.02	0.03 ± 0.02	0.02 ± 0.02	0.02 ± 0.02	0.01 ± 0.01	0.01 ± 0.01
HFC-227ea	NIR 2024	0.14	0.14	0.12	0.11	0.11	
	PARIS mean	0.15 ± 0.14	0.14 ± 0.13	0.15 ± 0.13	0.16 ± 0.13	0.16 ± 0.13	0.16 ± 0.13
HFC-245fa	NIR 2024	0.12	0.12	0.18	0.19	0.19	
	PARIS mean	0.05 ± 0.06	0.05 ± 0.05	0.05 ± 0.05	0.04 ± 0.04	0.03 ± 0.03	0.02 ± 0.02
HFC-365mfc	NIR 2024	0.09	0.17	0.09	0.08	0.08	
	PARIS mean	0.10 ± 0.06	0.10 ± 0.05	0.09 ± 0.05	0.07 ± 0.04	0.04 ± 0.03	0.03 ± 0.03
HFC-4310mee	NIR 2024	0.00	0.00	0.00	0.00	0.00	
	PARIS mean	0.01 ± 0.02	0.01 ± 0.01	0.01 ± 0.01	0.01 ± 0.01	0.01 ± 0.01	[1]

[1] HFC-4310mee emissions were not estimated for 2023 due to lack of atmospheric observations.

7 Perfluorocarbons (PFCs)

7.1 PFC-14

Figure 7.1.1: Verification of the German emissions inventory estimates for PFC-14. Modelled annual emissions are given as the mean from all models (black line and grey shading) and the individual result from InTEM (blue line and shading). National inventory annual totals are given as grey bars.

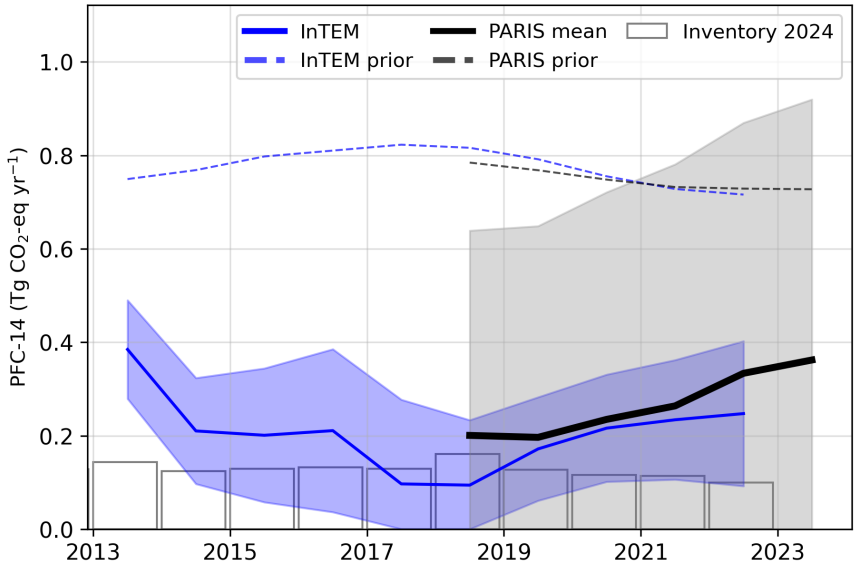

Figure 7.1.2: Spatial distribution of the German average modelled emissions of PFC-14 during the period of 2018-2023 (mean from all models). Observing stations are marked with red circles and highly-populated cities are marked with red triangles.

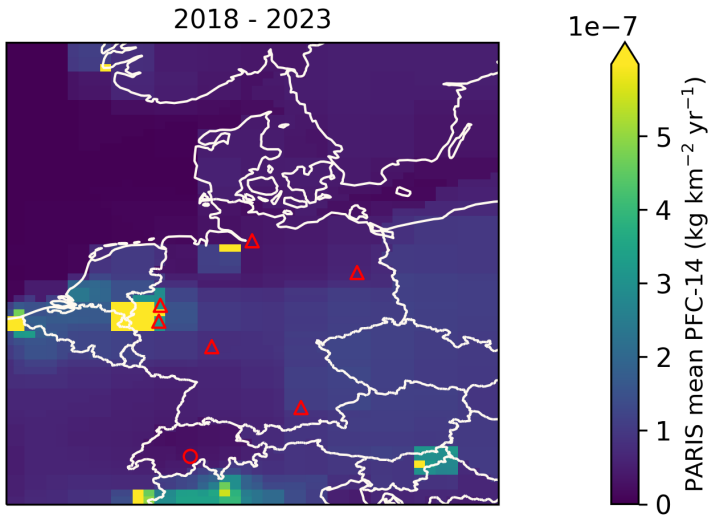

7.2 PFC-116

Figure 7.2.1: Verification of the German emissions inventory estimates for PFC-116. Modelled annual emissions are given as the mean from all models (black line and grey shading) and the individual result from InTEM (blue line and shading). National inventory annual totals are given as grey bars.

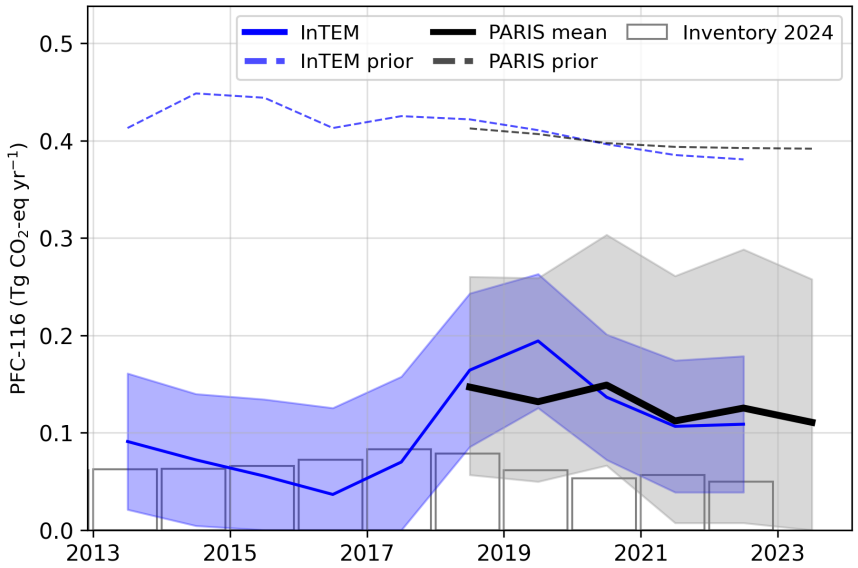

Figure 7.2.2: Spatial distribution of the German average modelled emissions of PFC-116 during the period of 2018-2023 (mean from all models). Observing stations are marked with red circles and highly-populated cities are marked with red triangles.

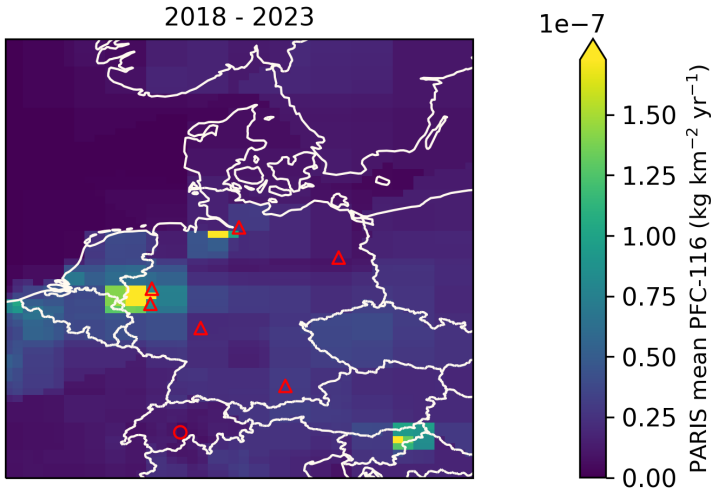

7.3 PFC-218

Figure 7.3.1: Verification of the German emissions inventory estimates for PFC-218. Modelled annual emissions are given as the mean from all models (black line and grey shading) and the individual result from InTEM (blue line and shading). National inventory annual totals are given as grey bars.

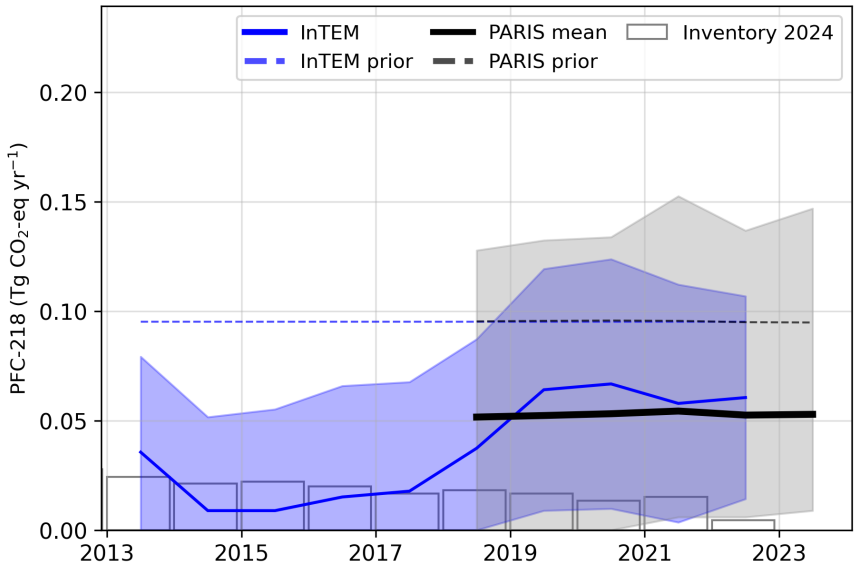

Figure 7.3.2: Spatial distribution of the German average modelled emissions of PFC-218 during the period of 2018-2023 (mean from all models). Observing stations are marked with red circles and highly-populated cities are marked with red triangles.

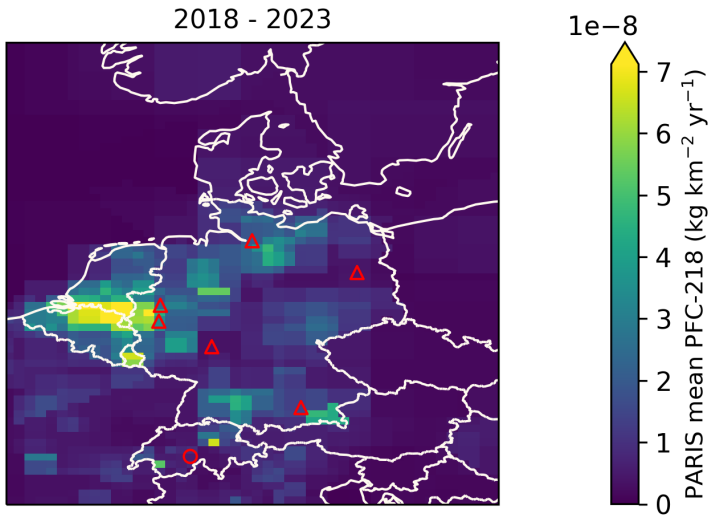

7.4 PFC-318

Figure 7.4.1: Verification of the German emissions inventory estimates for PFC-318. Modelled annual emissions are given as the mean from all models (black line and grey shading) and the individual result from InTEM (blue line and shading). National inventory annual totals are given as grey bars.

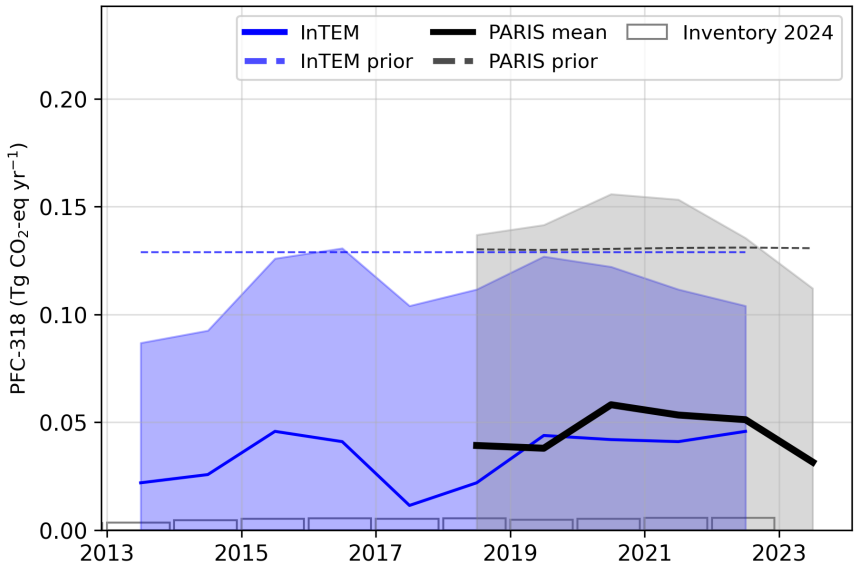

Figure 7.4.2: Spatial distribution of the German average modelled emissions of PFC-318 during the period of 2018-2023 (mean from all models). Observing stations are marked with red circles and highly-populated cities are marked with red triangles.

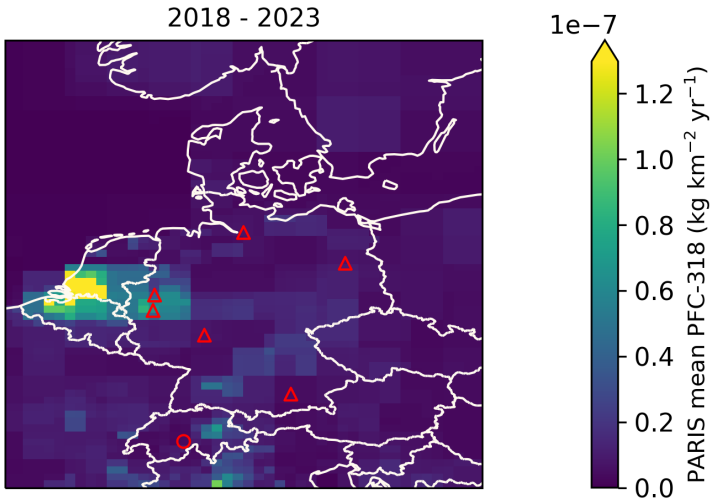

7.5 Total PFCs

Figure 7.5.1: Verification of the German emissions inventory estimates for total PFCs. Modelled annual emissions are given as the mean from all models (black line and grey shading) and the individual result from InTEM (blue line and shading). National inventory annual totals are given as grey bars.

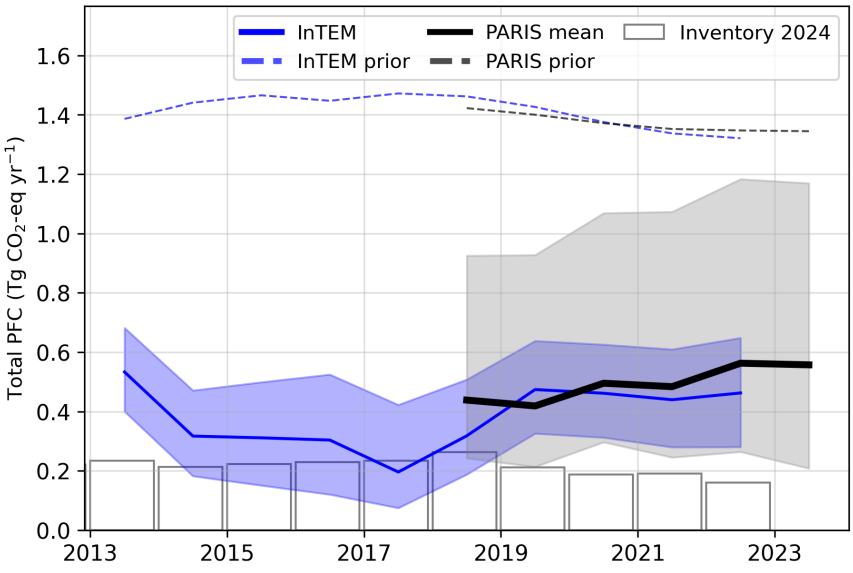

Table 3: Emissions estimation for PFCs in $\mathrm{TgCO_2{-}eq \cdot yr^{-1}}$ according to the National Inventory Report (NIR) 2024 and the inversions done in the PARIS project. For the PARIS estimation, the mean of the 3 inversion models is displayed, along with a range of uncertainty estimated via the half distance between the maximum and minimum uncertainties of the different models.

		2018	2019	2020	2021	2022	2023
PFC-14	NIR 2024	0.161	0.128	0.116	0.114	0.100	
	PARIS mean	0.20 ± 0.32	0.20 ± 0.32	0.23 ± 0.36	0.26 ± 0.39	0.33 ± 0.43	0.36 ± 0.46
PFC-116	NIR 2024	0.079	0.062	0.053	0.056	0.050	
	PARIS mean	0.15 ± 0.10	0.13 ± 0.10	0.15 ± 0.12	0.11 ± 0.13	0.13 ± 0.14	0.11 ± 0.13
PFC-218	NIR 2024	0.018	0.017	0.014	0.015	0.005	
	PARIS mean	0.05 ± 0.06	0.05 ± 0.07	0.05 ± 0.07	0.05 ± 0.07	0.05 ± 0.07	0.05 ± 0.07
PFC-318	NIR 2024	0.005	0.005	0.005	0.006	0.006	
	PARIS mean	0.04 ± 0.07	0.04 ± 0.07	0.06 ± 0.08	0.05 ± 0.08	0.05 ± 0.07	0.03 ± 0.06

8 Sulphur hexafluoride (SF_6)

Figure 8.0.1: Total source sensitivity of SF_6 observing sites as calculated by the NAME transport model for the year (left) 2018 and (right) 2023 and used in the inversions. Observing stations active in each year are marked with red dots. Areas with visible land surface represent regions for which emissions can be observed well from the network. Shaded or dark areas represent regions for which limited emission information can be obtained from the network.

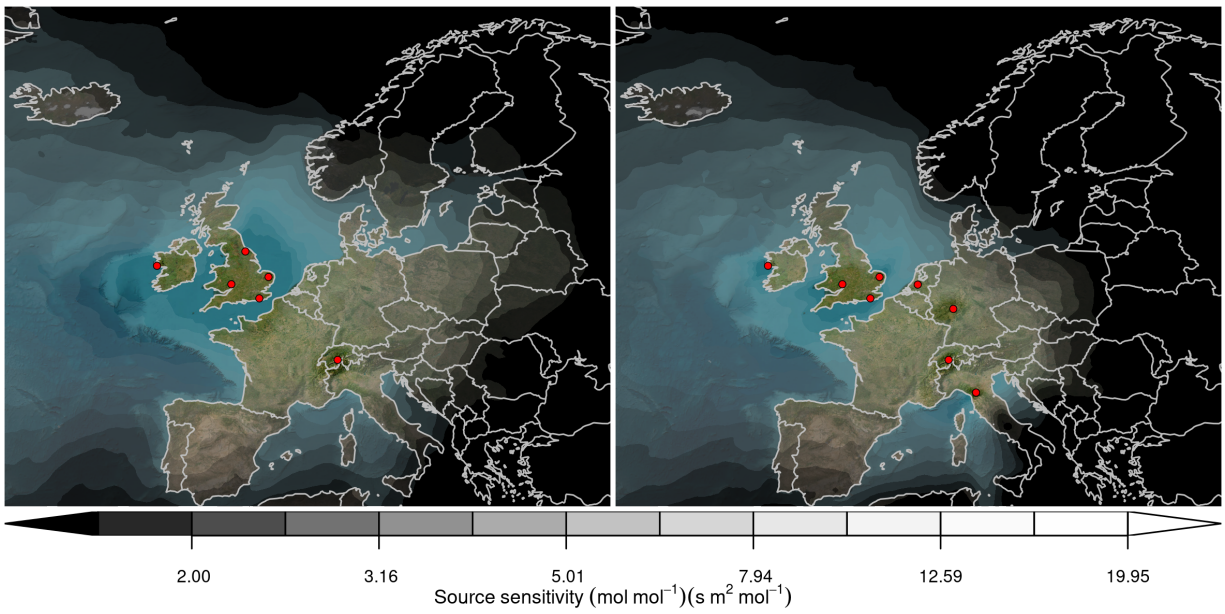

Figure 8.0.2: Verification of the German emissions inventory estimates for SF_6. Modelled annual emissions are given as the mean from all models (black line and grey shading) and the individual result from InTEM (blue line and shading). National inventory annual totals are given as grey bars.

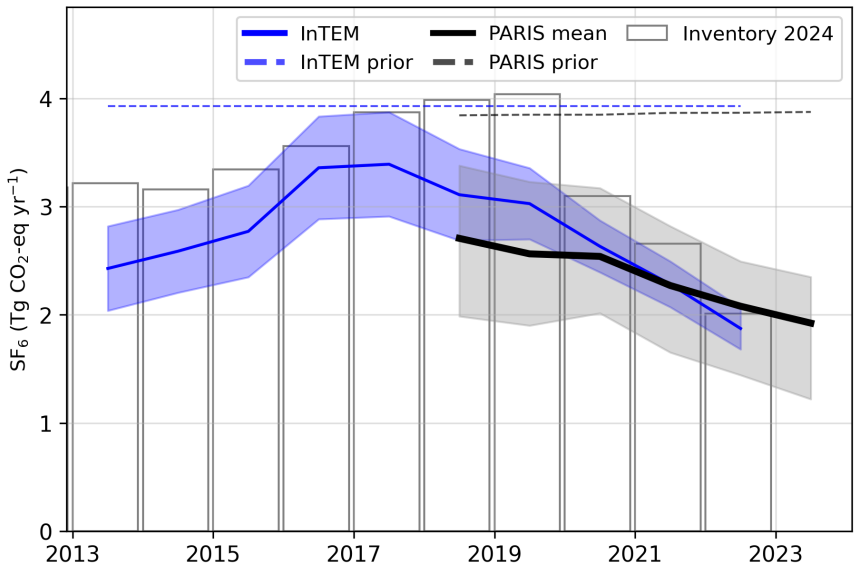

Figure 8.0.3: Spatial distribution of the German average modelled emissions of SF_6 during the period of 2018-2023 (mean from all models). Observing stations are marked with red circles and highly-populated cities are marked with red triangles.

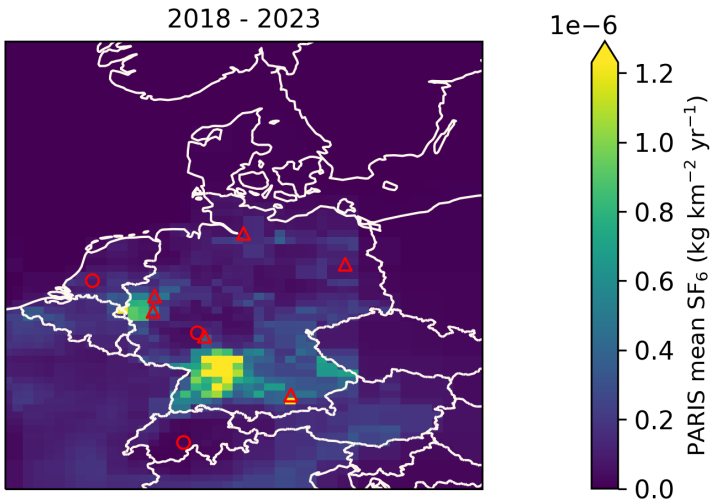

References

European Commission: Joint Research, Centre et al. (2023). *GHG emissions of all world countries – 2023*. Publications Office of the European Union. DOI: 10.2760/953322.

Ganesan, A. L. et al. (2014). "Characterization of uncertainties in atmospheric trace gas inversions using hierarchical Bayesian methods". In: *Atmospheric Chemistry and Physics* 14.8, pp. 3855–3864. DOI: 10.5194/acp-14-3855-2014. URL: http://www.atmos-chem-phys.net/14/3855/2014/http://www.atmos-chem-phys.net/14/3855/2014/acp-14-3855-2014.pdf.

Ganesan, A. L. et al. (2015). "Quantifying methane and nitrous oxide emissions from the UK and Ireland using a national-scale monitoring network". In: *Atmos. Chem. Phys.* 15.11, pp. 6393–6406. DOI: 10.5194/acp-15-6393-2015. URL: https://www.atmos-chem-phys.net/15/6393/2015/https://www.atmos-chem-phys.net/15/6393/2015/acp-15-6393-2015.pdf.

Henne, S. et al. (2016). "Validation of the Swiss methane emission inventory by atmospheric observations and inverse modelling". In: *Atmospheric Chemistry and Physics* 16.6, pp. 3683–3710. DOI: 10.5194/acp-16-3683-2016. URL: http://www.atmos-chem-phys.net/16/3683/2016/.

Jones, A.R. et al. (2007). "The U.K. Met Office's next-generation atmospheric dispersion model, NAME III, in Borrego C. and Norman A.-L. (Eds)". In: *Air Pollution Modeling and its Application XVII (Proceedings of the 27th NATO/CCMS International Technical Meeting on Air Pollution Modelling and its Application), Springer*, pp. 580–589.

Katharopoulos, I. et al. (2023). "Impact of transport model resolution and a priori assumptions on inverse modeling of Swiss F-gas emissions". In: *Atmos. Chem. Phys.* 23.22, pp. 14159–14186. DOI: 10.5194/acp-23-14159-2023. URL: https://acp.copernicus.org/articles/23/14159/2023/.

Manning, A. J. et al. (2021). "Evidence of a recent decline in UK emissions of hydrofluorocarbons determined by the InTEM inverse model and atmospheric measurements". In: *Atmospheric Chemistry and Physics* 21.16, pp. 12739–12755. DOI: 10.5194/acp-21-12739-2021. URL: https://acp.copernicus.org/articles/21/12739/2021/.

Rigby, M. et al. (2019). "Increase in CFC-11 emissions from eastern China based on atmospheric observations". In: *Nature* 569, pp. 546–550. DOI: 10.1038/s41586-019-1193-4. URL: https://doi.org/10.1038/s41586-019-1193-4.

Draft Inventory Annex
Hungary 2024

18th November, 2024

1 Introduction

In this document, global concentration trends and national emissions estimates derived from atmospheric observations ("inverse estimates") are presented for each reported gas. Comparing the emissions submitted in national inventories with those calculated using atmospheric observations allows for emissions to be assessed using two fundamentally different approaches. Substantial differences can highlight areas that could warrant further investigation.

Global concentration trends for each gas are first shown using annual average concentrations from Mace Head, Ireland (Northern Hemisphere) and Kennaook/Cape Grim, Tasmania, Australia (Southern Hemisphere). Data from these stations were selected to exclude regionally-polluted air masses and therefore represents northern and southern hemispheric concentration trends. Mace Head observations were supported by the National Aeronautics and Space Administration (NASA) and the UK Department of Energy, Security and Net Zero (DESNZ), and Kennaook/Cape Grim observations by NASA and the Australian Bureau of Meteorology.

Observations of European concentrations of greenhouse gases used to derive national inverse emission estimates were collected from many different networks and providers. Methane and nitrous oxide concentrations originated from the European ICOS (Integrated Carbon Observation System) network, the UK DECC (Deriving Emissions related to Climate Change) network and other national or individual initiatives. F-gas observations were made by affiliates of the AGAGE (Advanced Global Atmospheric Gases Experiment) network. Observations from from additional stations across Europe were supported by the Horizon-EU PARIS (Process Attribution of Regional Emissions) project. The observation stations used to derive emissions for each gas are shown in the corresponding sections of this document.

Inversion-based emissions estimates were derived using one atmospheric transport model but with multiple inverse models allowing a better quantification of the uncertainties associated with inverse modelling. The atmospheric transport model provides the link between surface fluxes and concentrations measured at the observing stations. Although the uncertainty associated with the atmospheric transport model is considered in the statistical inversion approach, it may be underestimated when only using a single transport model. The atmospheric transport model used is the Numerical Atmospheric dispersion Modelling Environment (NAME) (Jones et al., 2007), a backwards-running Lagrangian Particle Dispersion Model (LPDM) that simulates the recent transport of air to each observing station. The NAME model has been widely used in the estimation of greenhouse gases emissions (Ganesan et al., 2015; Rigby et al., 2019; Manning et al., 2021).

The three inverse methods used are InTEM (Inversion Technique for Emission Modelling, Manning et al., 2021), ELRIS (Empa Lagrangian Regional Inversion System, Henne et al., 2016; Katharopoulos et al., 2023), and RHIME (Regional Hierarchical Inverse Modelling Environment, Ganesan et al., 2014). All three inverse methods estimate emissions within Europe along with boundary conditions that account for the concentration of the air entering Europe. All three systems started from the same set of a priori emissions that were either derived from the global EDGAR emission inventory (version 8, European Commission: Joint Research et al., 2023) or a uniform land-based emission, depending on the gas. A natural emission component, from the WETCHARTS product, was included in the methane prior. The same observational dataset was used by each inverse model, but data selection (i.e., filtering datasets for specific conditions) and treatment of uncertainties were chosen separately and hence differ. The three methods also differ in their statistical approaches for estimating emissions.

Emission estimates are presented for the period 2008-2023. Emissions for the full 2008-2023 period were derived with the InTEM model only, while emissions from 2018-2023 are presented as a combined result using the three inverse models.

For the 2008-2023 InTEM results, a 2-year inversion resolution, incrementing annually, was used for all gases except CH_4nd N_2, where the resolution was monthly. For the recent 2018-2023 period, for all three models, the inversion resolution was one month for CH_4 and N_2O in order to capture the seasonality of the emissions, a one-year average over these results is also presented. For the fluorinated gases, a 1-year

inversion resolution was adopted, with a 3-year moving average applied to the results. The uncertainty shown is the minimum/maximum of the uncertainties from the three results.

2 Global Concentration Trends

2.1 Methane (CH_4)

Figure 2.1.1: Background Northern Hemisphere monthly concentrations of CH_4 estimated from MHD, Ireland observations are shown in red, and background Southern Hemisphere monthly concentrations from CGO, Tasmania are shown in blue. Grey shading represents provisional data.

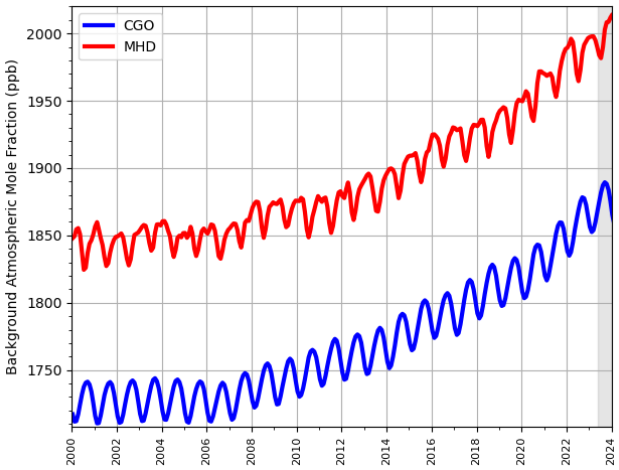

2.2 Nitrous Oxide (N_2O)

Figure 2.2.1: Background Northern Hemisphere monthly concentrations of N_2O estimated from MHD, Ireland observations are shown in red, and background Southern Hemisphere monthly concentrations from CGO, Tasmania are shown in blue. Grey shading represents provisional data.

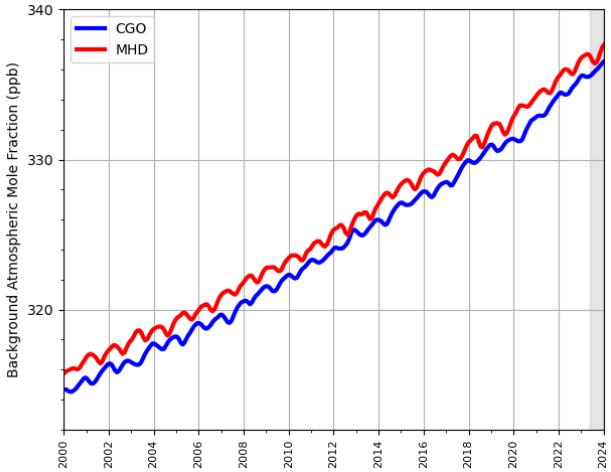

2.3 Hydrofluorocarbons (HFCs)

Figure 2.3.1: Background Northern Hemisphere monthly concentrations of six HFCs estimated from MHD, Ireland observations are shown in red, and background Southern Hemisphere monthly concentrations from CGO, Tasmania are shown in blue. Grey shading represents provisional data.

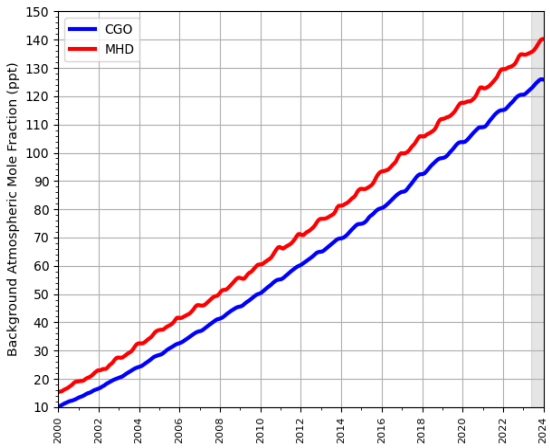

(a) HFC-134a

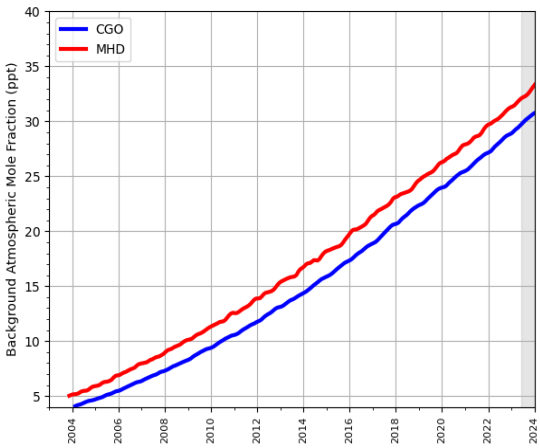

(b) HFC-143a

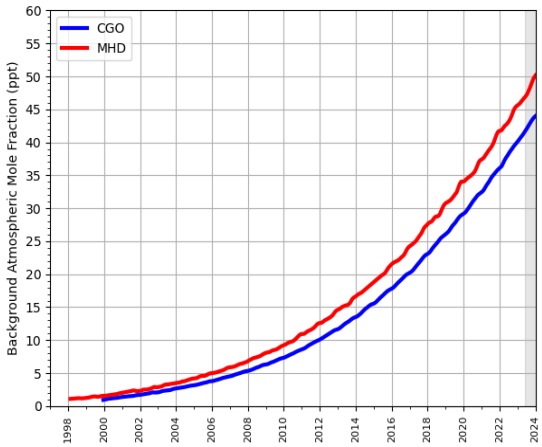

(c) HFC-125

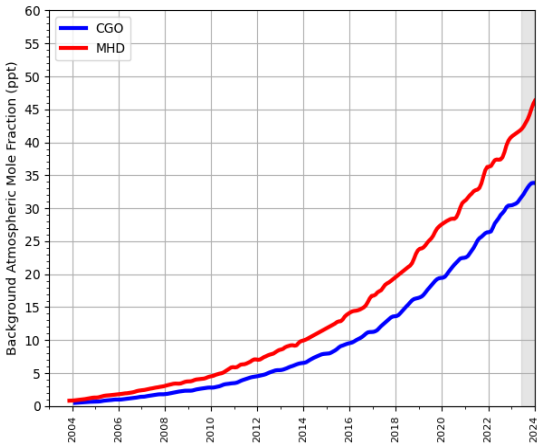

(d) HFC-32

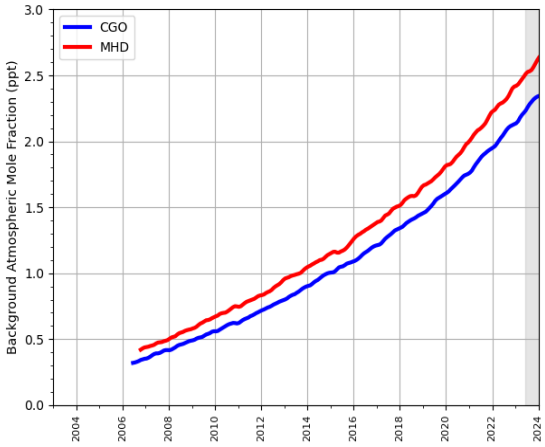

(e) HFC-227ea

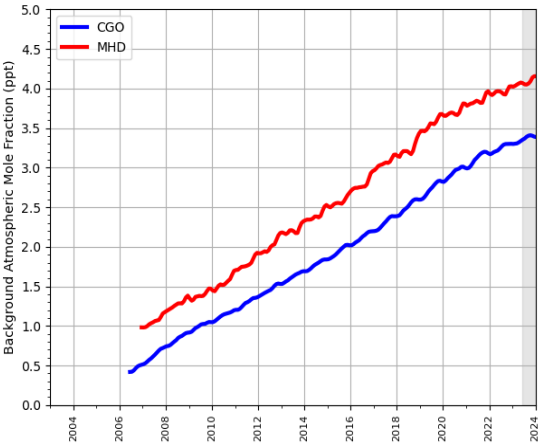

(f) HFC-245fa

Figure 2.3.2: Background Northern Hemisphere monthly concentrations of four HFCs estimated from MHD, Ireland observations are shown in red, and background Southern Hemisphere monthly concentrations from CGO, Tasmania are shown in blue. Grey shading represents provisional data.

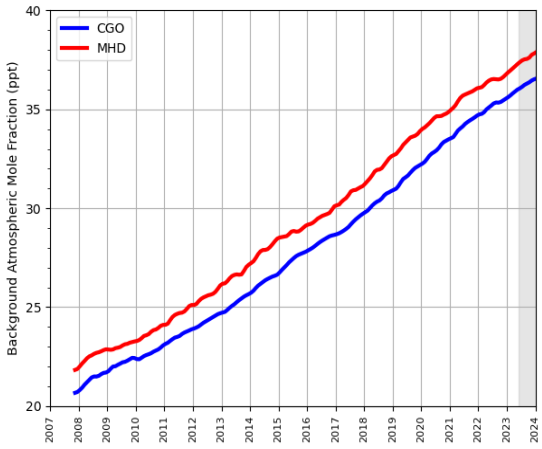

(a) HFC-23

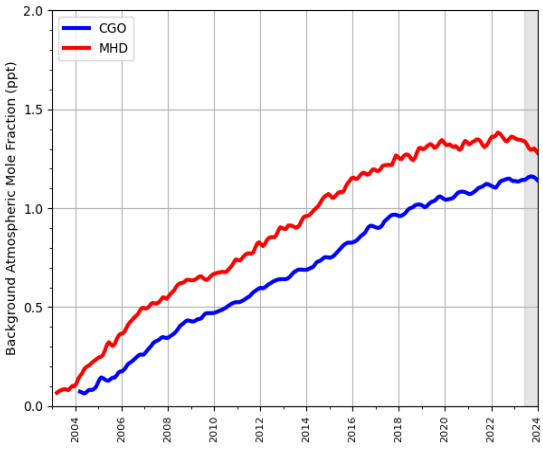

(b) HFC-365mfc

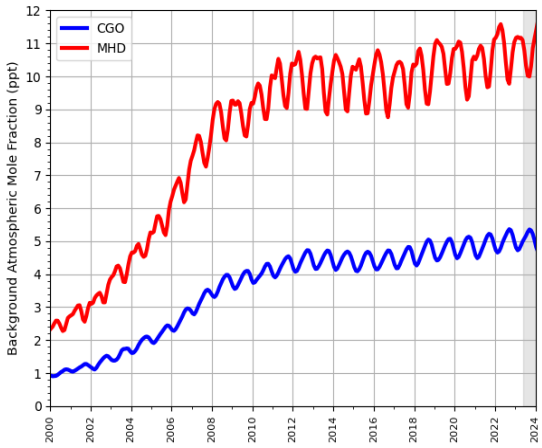

(c) HFC-152a

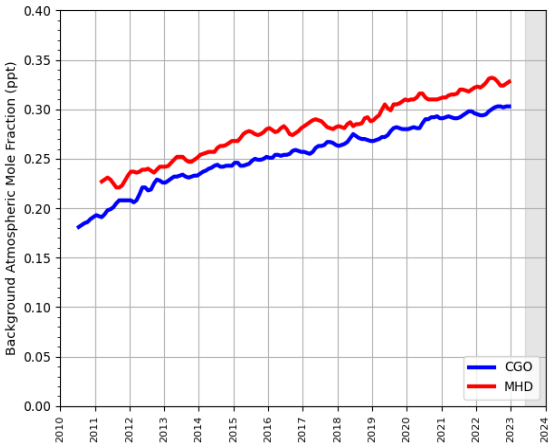

(d) HFC-43-10-mee

2.4 Perfluorocarbons (PFCs)

Figure 2.4.1: Background Northern Hemisphere monthly concentrations of four PFCs estimated from MHD, Ireland observations are shown in red, and background Southern Hemisphere monthly concentrations from CGO, Tasmania are shown in blue. Grey shading represents provisional data.

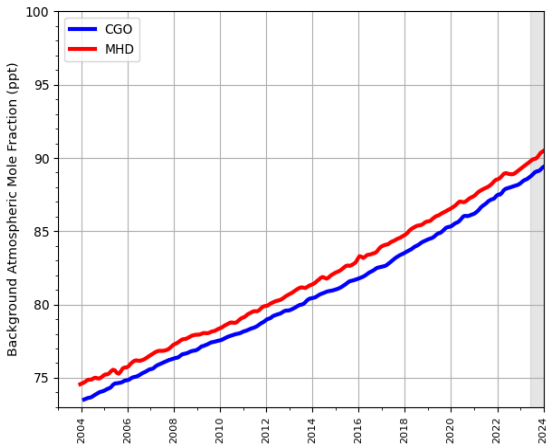

(a) PFC-14

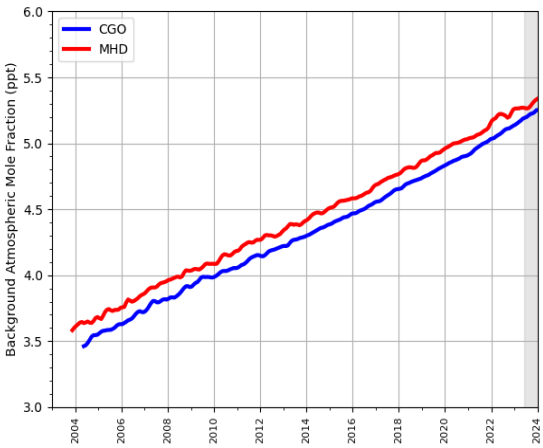

(b) PFC-116

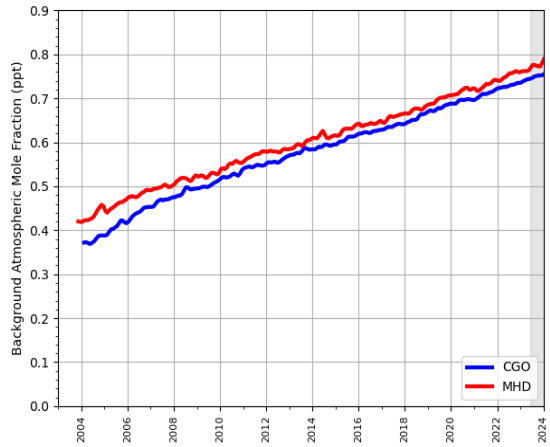

(c) PFC-218

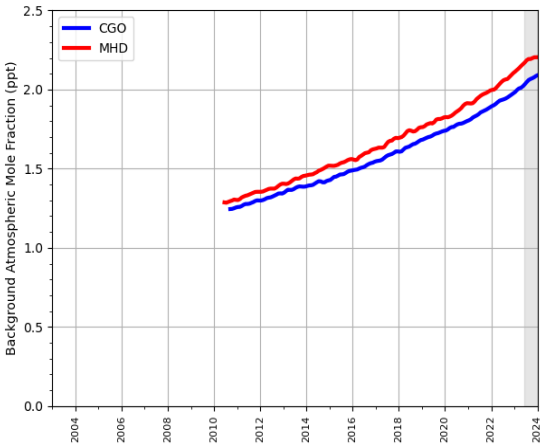

(d) PFC-318

3 Key findings

- General note: The presented inverse modelling estimates of Hungarian emissions currently are limited by the sparsity of atmospheric observations in south-eastern Europe. For the inversion period 2018-2023, the only available observations within the Hungarian domain were those of CH_4 and N_2O from the Hungarian tall tower site Hegyhátsál close to the western border with Austria. Limited source sensitivity towards eastern Hungary results from the current observing network. As part of the PARIS project, flask sampling of halogenated species was initiated at Hegyhátsál in 2024. Previously, limited source sensitivity from observations at Jungfraujoch, Switzerland, and Monte Cimone, Italy, is not sufficient to derive Hungarian halogenated species emissions with any degree of certainty.
- Methane (CH_4): Inverse results are about 50 % larger than inventory estimates between 2018 and 2022 (Figure 4.0.2). No significant temporal trend is discernable in both data sets. Highest emissions are obtained for the western part of Hungary, potentially driven by the stronger observational constraint in this area (Figure 4.0.4). The inverse results indicate a pronounced seasonality in the methane emissions, broadly spread over the domain. The results show that these are maximum in winter (Figures 4.0.3 and 4.0.5).
- Nitrous oxide (N_2O): Inverse results are significantly larger, about double, than inventory estimates between 2018 and 2022 (Figure 5.0.2). As for CH_4, highest emissions are obtained for the western part of the country (Figure 5.0.4). The inverse results indicate a considerable seasonality in the nitrous oxide emissions with a maximum in summer and autumn most likely related to emissions from agricultural soils. This feature is widespread in the Hungarian domain, with an exception in neighbouring Slovakia (Figures 5.0.3 and 5.0.5).
- Hydrofluorocarbons (HFCs): Due to the limited observational constraint very large uncertainties remain in the Hungarian HFC emissions estimates obtained from inverse modelling. For most HFCs, these estimates stay relatively close to the a priori values (Figure 6.5.1), the latter being generally larger than the inventory and not showing a decrease in recent years. The downward tendency in the inversely estimated emissions, followed by an increase in recent years, is statistically not significant. Incorporating the novel flask observations from Hegyhátsál should improve estimates in future inverse modelling.
- Perfluorocarbons (PFCs): Due to the limited observational constraint very large uncertainties remain in the Hungarian PFC emissions estimates obtained from inverse modelling. These estimates are mostly smaller than their a priori values, but associated with uncertainties larger than 100 % (Figure 7.5.1). Incorporating the novel flask observations from Hegyhátsál should improve estimates in future inverse modelling.
- Sulphur hexafluoride (SF_6): Similar to HFCs and PFCs, no conclusions can be drawn from the current uncertain inverse emission estimates of SF_6. The inverse estimates stay in close agreement with the a priori assumption, which for this gas is in line with the national inventory (Figure 8.0.2).

Table 1: Emissions estimation of CH_4 and N_2O in $\mathrm{TgCO_2{-}eq \cdot yr^{-1}}$ according to the National Inventory Report (NIR) 2024 and the inversions undertaken in the PARIS project. For the PARIS estimation, the mean of the 3 inversion models is displayed, along with a range of uncertainty estimated via the half distance between the maximum and minimum uncertainties of the different models.

		2018	2019	2020	2021	2022	2023
CH_4	NIR 2024	9.4	9.3	9.2	9.0	8.8	
	PARIS mean	14.9 ± 4.7	15.5 ± 6.1	15.8 ± 5.2	17.1 ± 7.5	13.3 ± 4.8	16.0 ± 5.6
N_2O	NIR 2024	4.3	4.3	4.5	4.5	3.7	
	PARIS mean	7.1 ± 1.9	8.9 ± 3.0	9.0 ± 3.4	9.8 ± 3.7	7.1 ± 1.6	8.5 ± 2.8

4 Methane (CH_4)

Figure 4.0.1: Total source sensitivity of CH_4 observing sites as calculated by the NAME transport model for the year (left) 2018 and (right) 2023 and used in the inversions. Observing stations active in each year are marked with red dots. Areas with visible land surface represent regions for which emissions can be observed well from the network. Shaded or dark areas represent regions for which limited emission information can be obtained from the network.

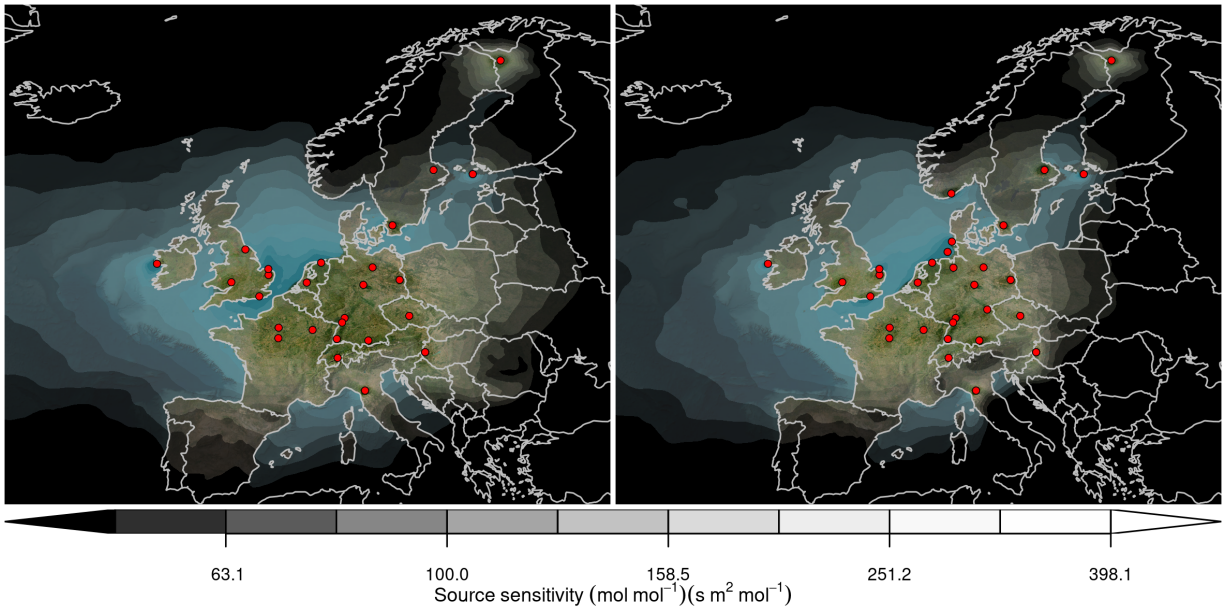

Figure 4.0.2: Verification of the Hungarian emissions inventory estimates for CH_4 (zoom in to 2018-2023). Modelled annual emissions are given as the mean from all models (black line and grey shading) and the individual result from InTEM (blue line and shading). National inventory annual totals are given as grey bars.

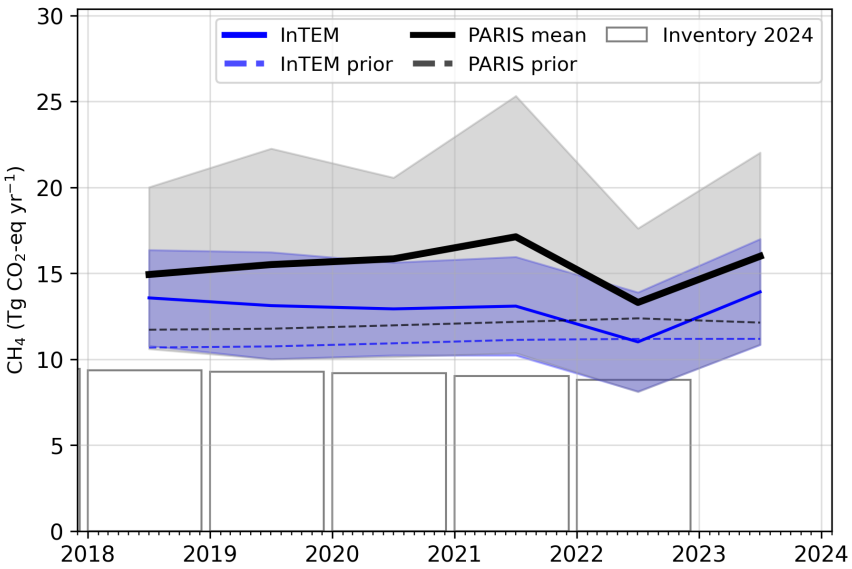

Figure 4.0.3: Verification of the Hungarian emissions inventory estimates for CH_4 (zoom in to 2018-2023). Modelled monthly emissions are given as the mean from all models (black line and grey shading) and the individual result from InTEM (blue line and shading). National inventory annual totals are given as grey bars.

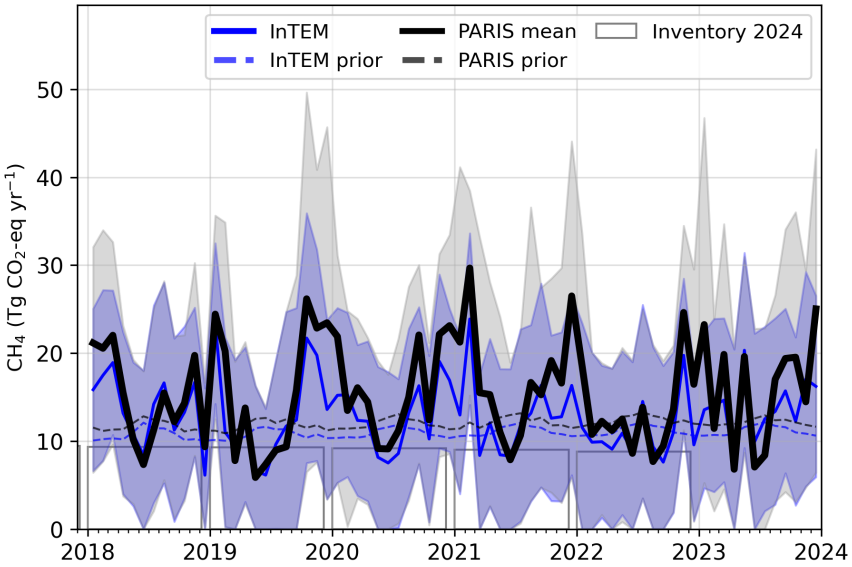

Figure 4.0.4: Spatial distribution of the Hungarian average modelled emissions of CH_4 during the period of 2018-2023 (mean from all models). Observing stations are marked with red circles and highly-populated cities are marked with red triangles.

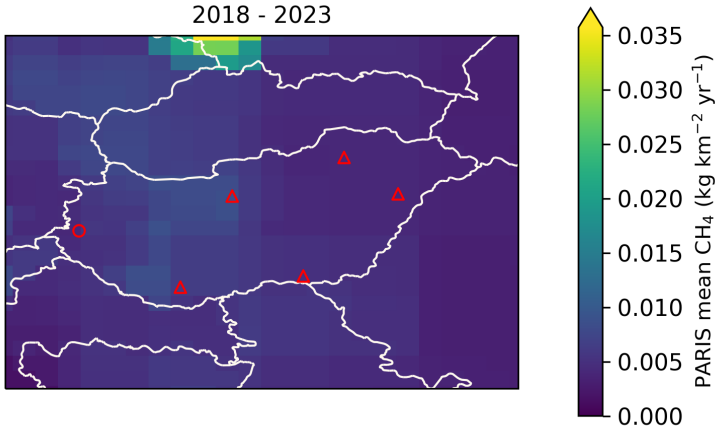

Figure 4.0.5: Spatial distribution of the seasonal deviation from the mean. The deviation is defined as the modelled Hungarian seasonally averaged CH_4 emissions over 2018-2023 minus the average over the whole period. The mean across all models is shown. Observing stations are marked with red circles and highly-populated cities are marked with red triangles.

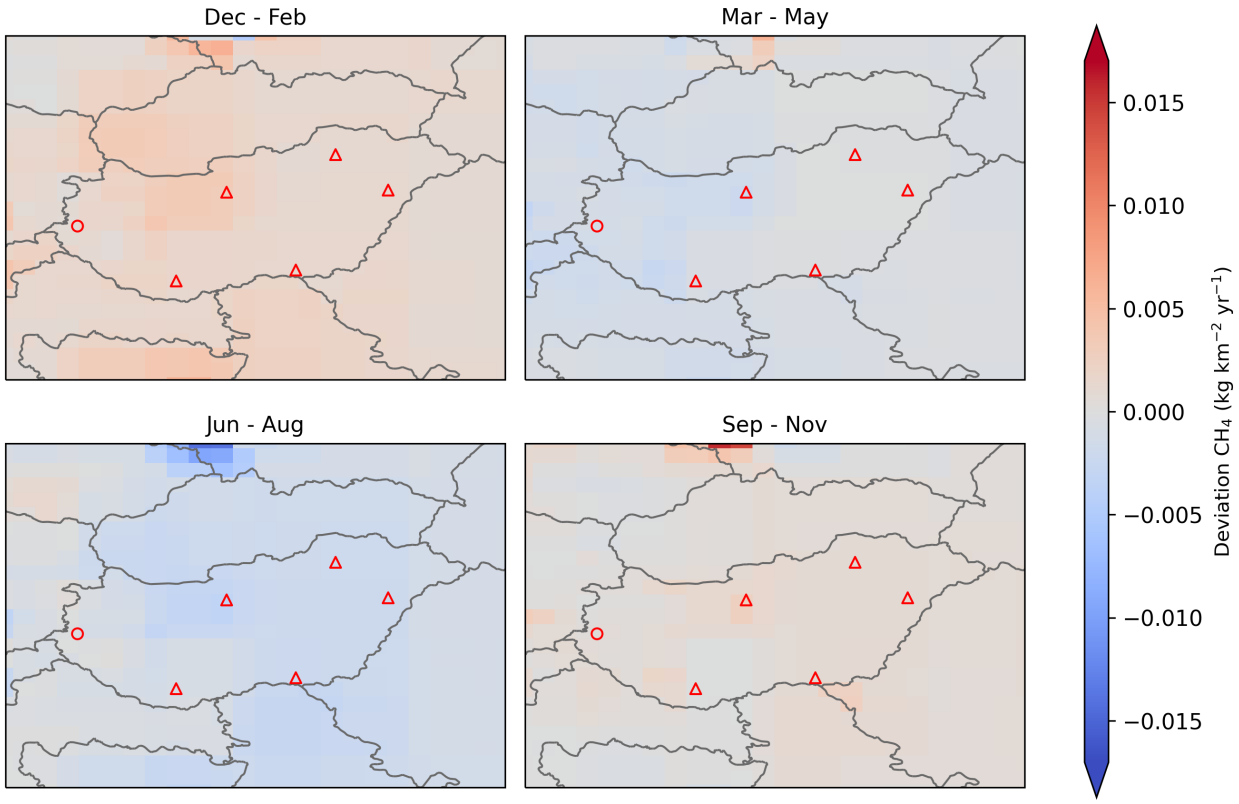

5 Nitrous Oxide (N_2O)

Figure 5.0.1: Total source sensitivity of N_2O observing sites as calculated by the NAME transport model for the year (left) 2018 and (right) 2023 and used in the inversions. Observing stations active in each year are marked with red dots. Areas with visible land surface represent regions for which emissions can be observed well from the network. Shaded or dark areas represent regions for which limited emission information can be obtained from the network.

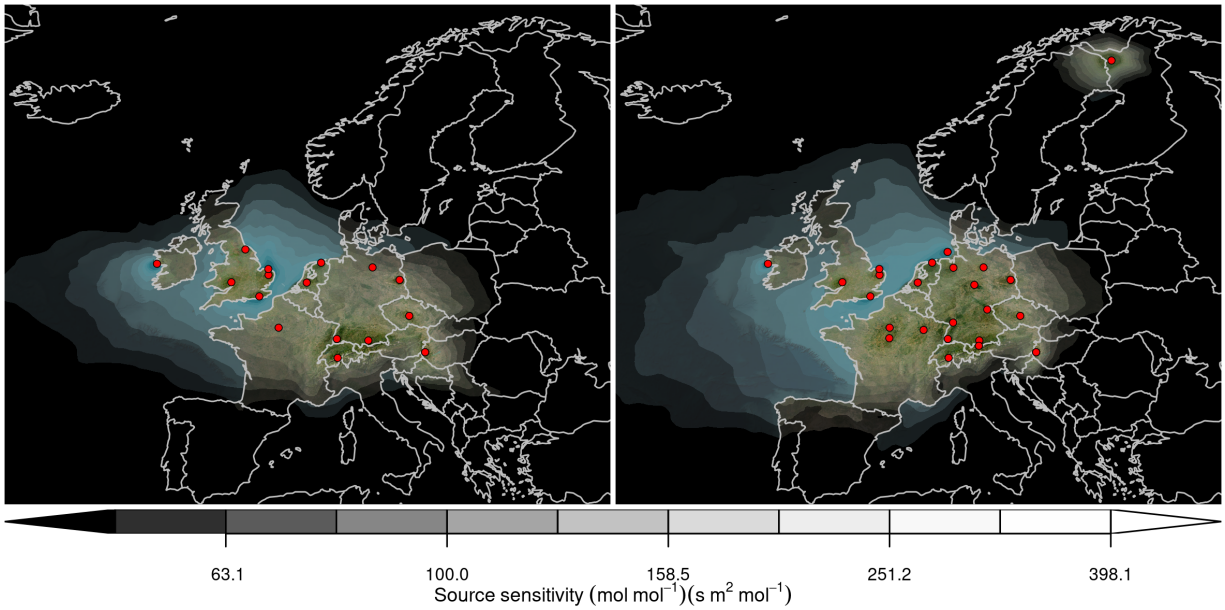

Figure 5.0.2: Verification of the Hungarian emissions inventory estimates for N_2O (zoom in to 2018-2023). Modelled annual emissions are given as the mean from all models (black line and grey shading) and the individual result from InTEM (blue line and shading). National inventory annual totals are given as grey bars.

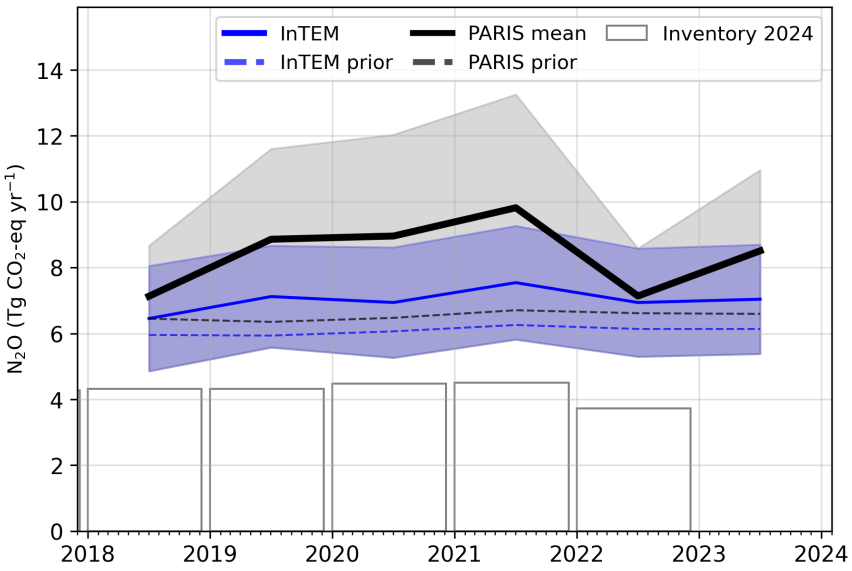

Figure 5.0.3: Verification of the Hungarian emissions inventory estimates for N_2O (zoom in to 2018-2023). Modelled monthly emissions are given as the mean from all models (black line and grey shading) and the individual result from InTEM (blue line and shading). National inventory annual totals are given as grey bars.

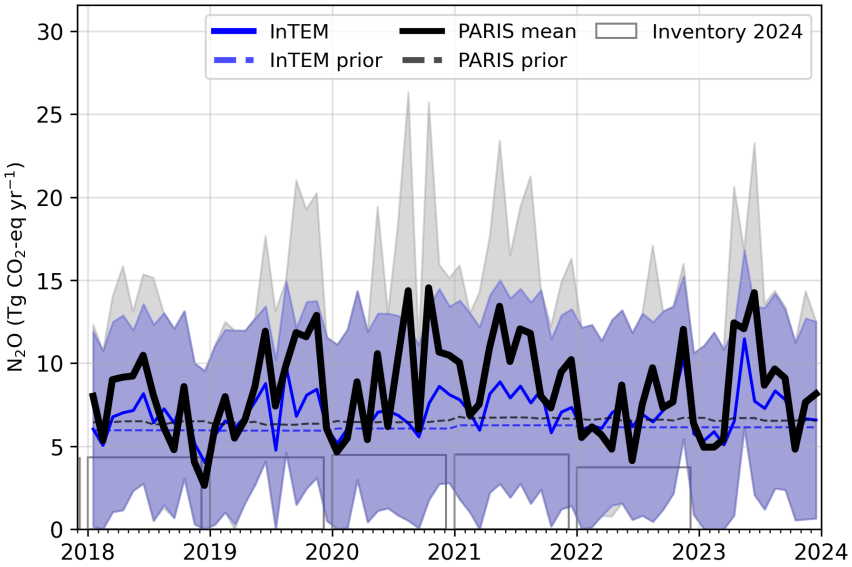

Figure 5.0.4: Spatial distribution of the Hungarian average modelled emissions of N_2O during the period of 2018-2023 (mean from all models). Observing stations are marked with red circles and highly-populated cities are marked with red triangles.

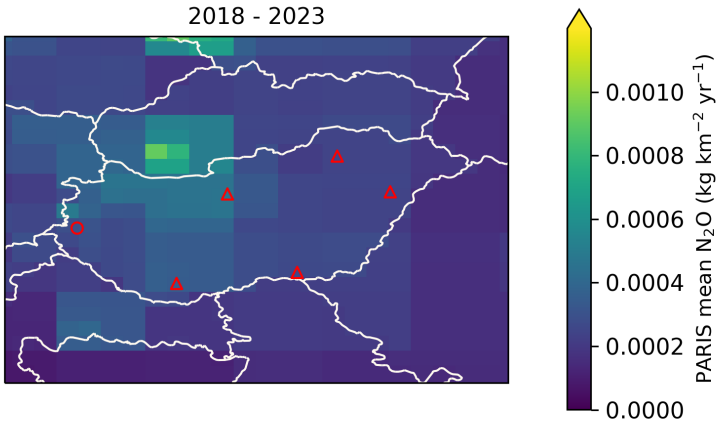

Figure 5.0.5: Spatial distribution of the seasonal deviation from the mean. The deviation is defined as the modelled Hungarian seasonally averaged N_2O emissions over 2018-2023 minus the average over the whole period. The mean across all models is shown. Observing stations are marked with red circles and highly-populated cities are marked with red triangles.

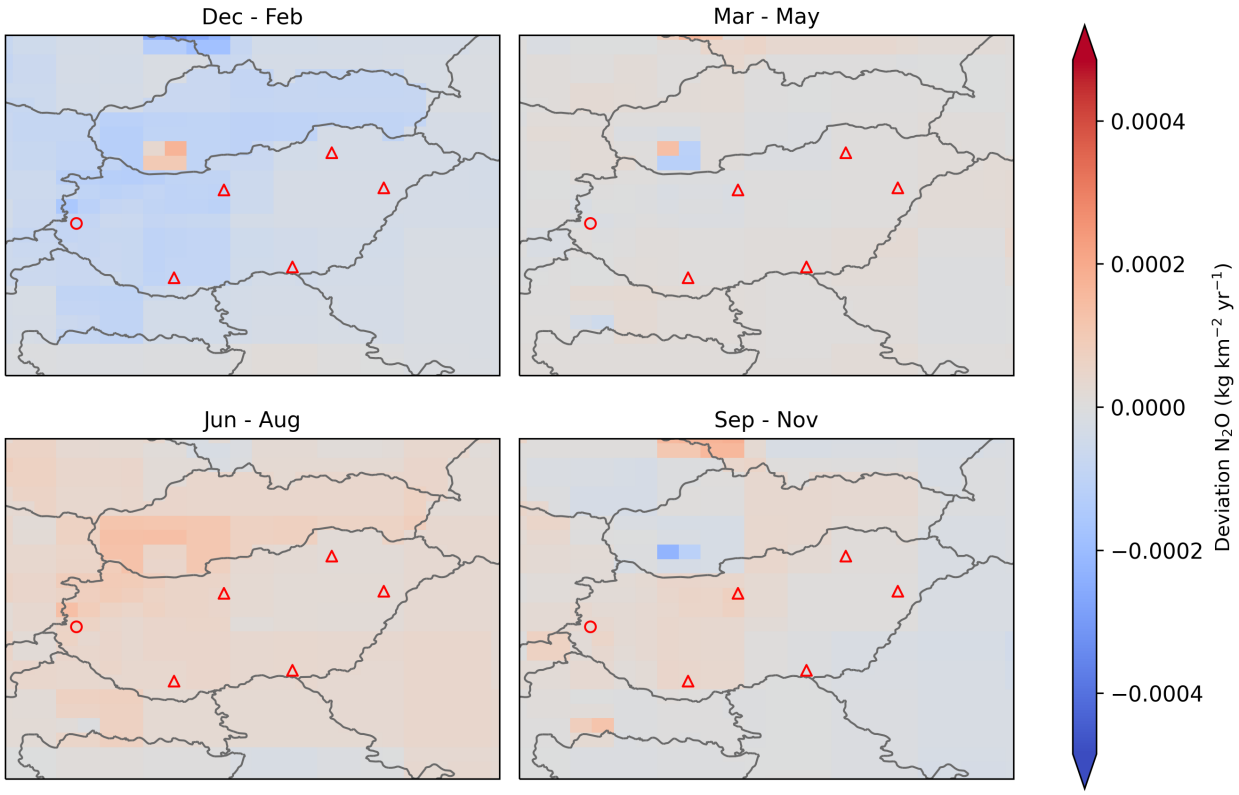

6 Hydrofluorocarbons (HFCs)

Figure 6.0.1: Total source sensitivity of HFCs/PFCs observing sites as calculated by the NAME transport model for the year (left) 2018 and (right) 2023 and used in the inversions. Observing stations active in each year are marked with red dots. Areas with visible land surface represent regions for which emissions can be observed well from the network. Shaded or dark areas represent regions for which limited emission information can be obtained from the network.

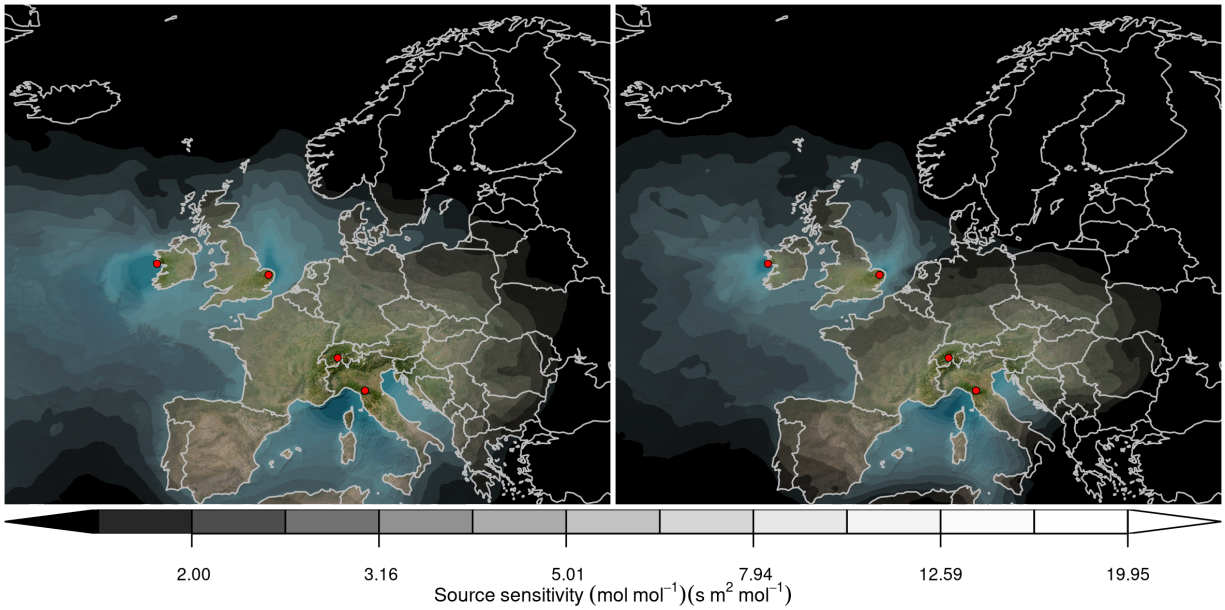

6.1 HFC-32

Figure 6.1.1: Verification of the Hungarian emissions inventory estimates for HFC-32. Modelled annual emissions are given as the mean from all models (black line and grey shading) and the individual result from InTEM (blue line and shading). National inventory annual totals are given as grey bars.

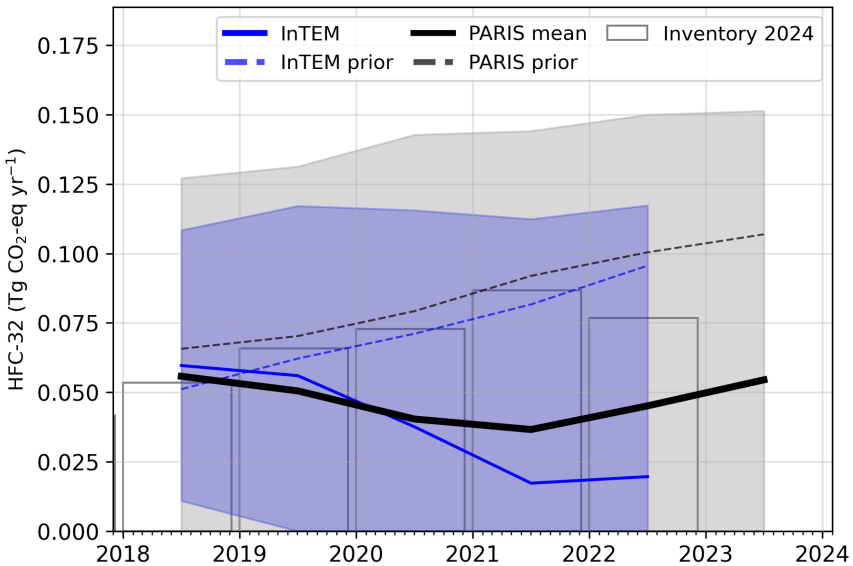

Figure 6.1.2: Spatial distribution of the Hungarian average modelled emissions of HFC-32 during the period of 2018-2023 (mean from all models). Observing stations are marked with red circles and highly-populated cities are marked with red triangles.

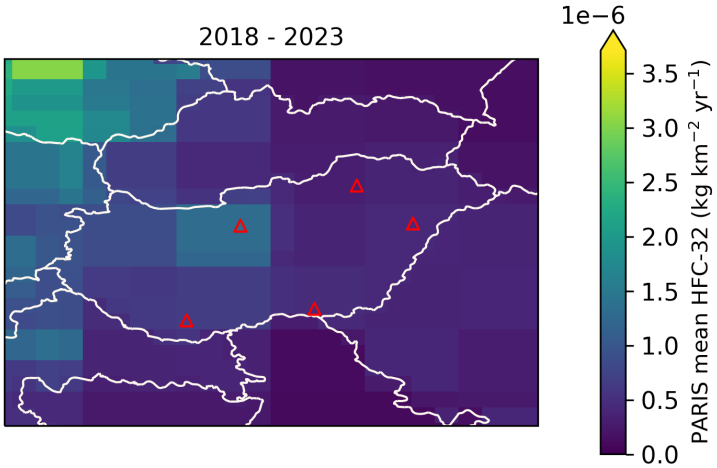

6.2 HFC-125

Figure 6.2.1: Verification of the Hungarian emissions inventory estimates for HFC-125. Modelled annual emissions are given as the mean from all models (black line and grey shading) and the individual result from InTEM (blue line and shading). National inventory annual totals are given as grey bars.

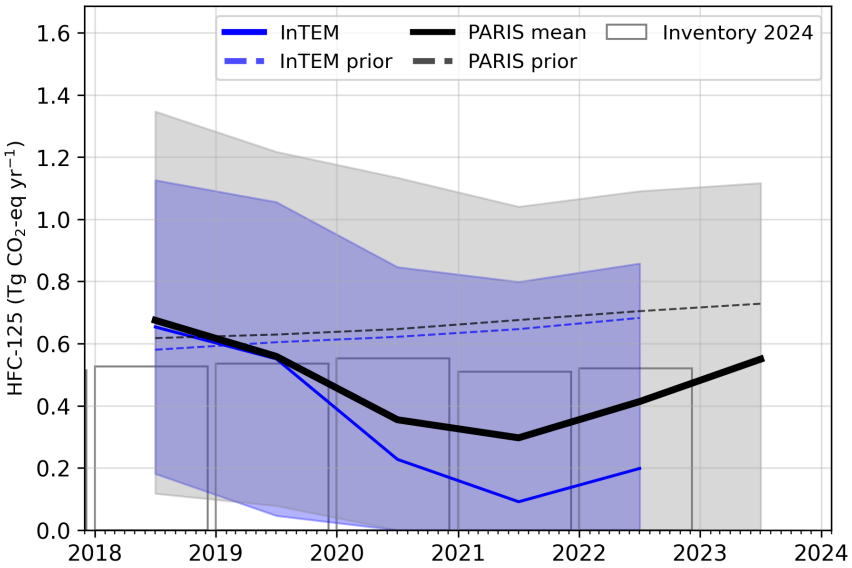

Figure 6.2.2: Spatial distribution of the Hungarian average modelled emissions of HFC-125 during the period of 2018-2023 (mean from all models). Observing stations are marked with red circles and highly-populated cities are marked with red triangles.

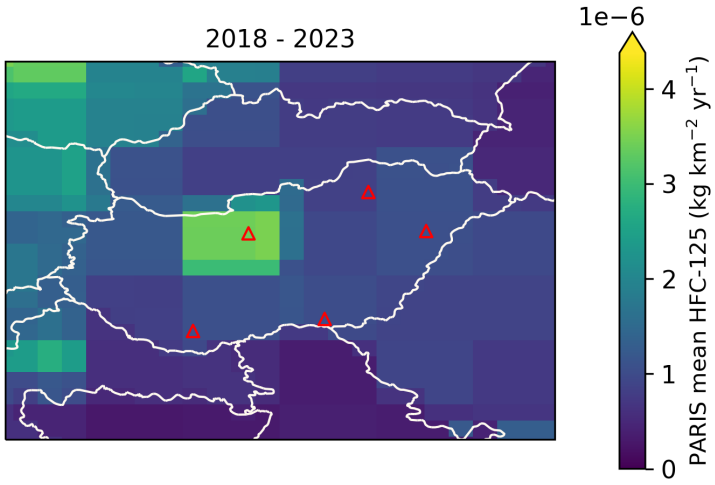

6.3 HFC-134a

Figure 6.3.1: Verification of the Hungarian emissions inventory estimates for HFC-134a. Modelled annual emissions are given as the mean from all models (black line and grey shading) and the individual result from InTEM (blue line and shading). National inventory annual totals are given as grey bars.

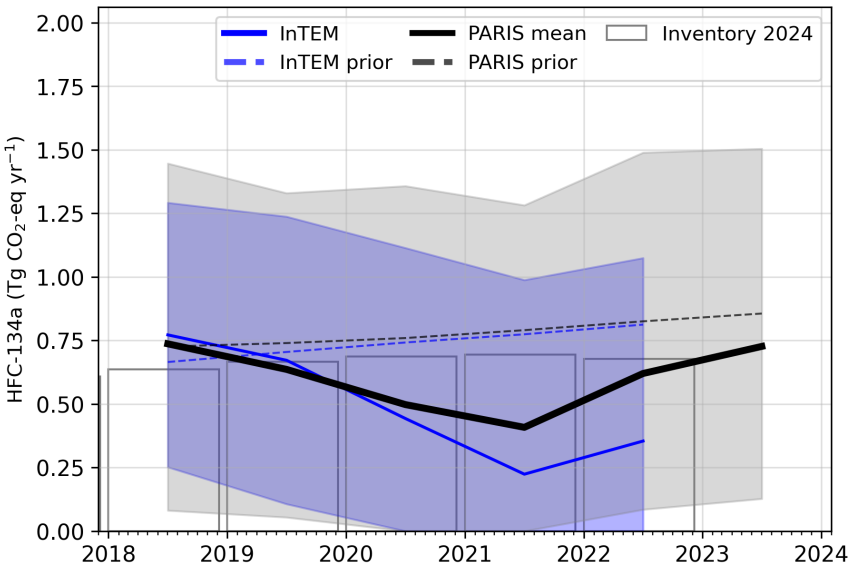

Figure 6.3.2: Spatial distribution of the Hungarian average modelled emissions of HFC-134a during the period of 2018-2023 (mean from all models). Observing stations are marked with red circles and highly-populated cities are marked with red triangles.

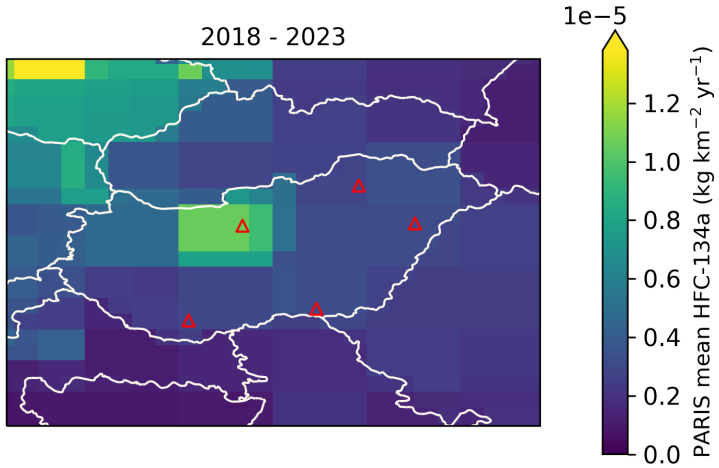

6.4 HFC-143a

Figure 6.4.1: Verification of the Hungarian emissions inventory estimates for HFC-143a. Modelled annual emissions are given as the mean from all models (black line and grey shading) and the individual result from InTEM (blue line and shading). National inventory annual totals are given as grey bars.

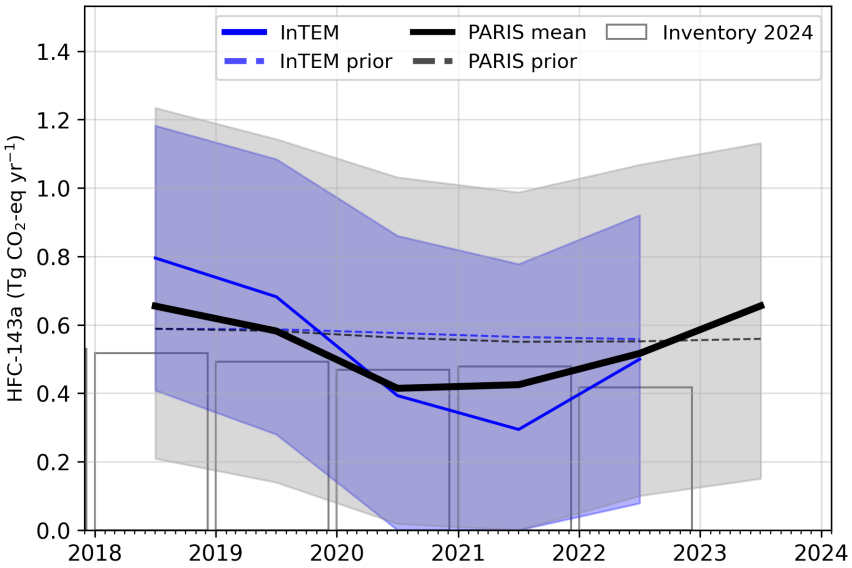

Figure 6.4.2: Spatial distribution of the Hungarian average modelled emissions of HFC-143a during the period of 2018-2023 (mean from all models). Observing stations are marked with red circles and highly-populated cities are marked with red triangles.

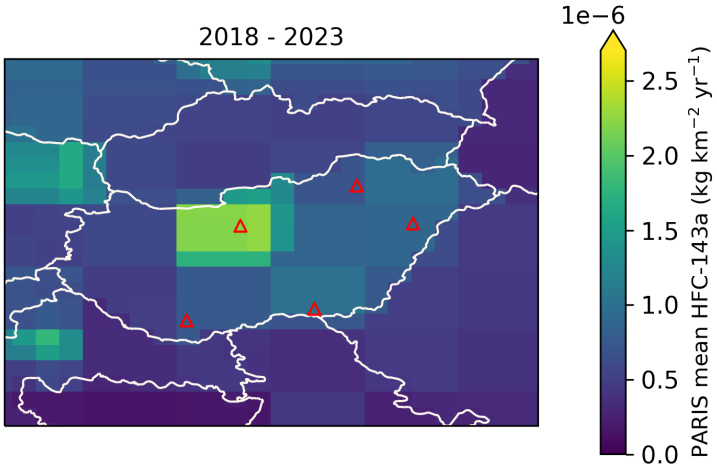

6.5 Total HFCs

Figure 6.5.1: Verification of the Hungarian emissions inventory estimates for total HFCs. Modelled annual emissions are given as the mean from all models (black line and grey shading) and the individual result from InTEM (blue line and shading). National inventory annual totals are given as grey bars.

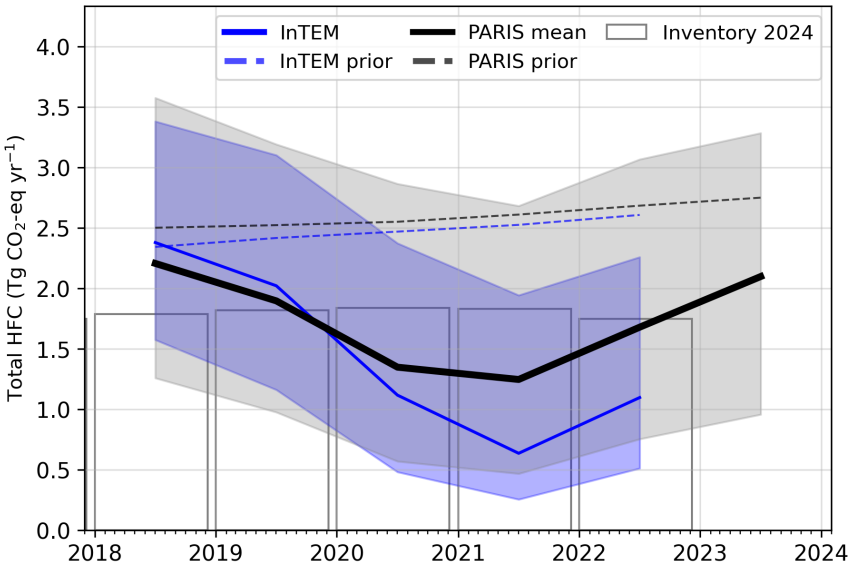

Table 2: Emissions estimation for HFCs in $\mathrm{TgCO_2{-}eq \cdot yr^{-1}}$ according to the National Inventory Report (NIR) 2024 and the inversions done in the PARIS project. For the PARIS estimation, the mean of the 3 inversion models is displayed, along with a range of uncertainty estimated via the half distance between the maximum and minimum uncertainties of the different models.

		2018	2019	2020	2021	2022	2023
HFC-23	NIR 2024	0.003	0.005	0.005	0.005	0.006	
	PARIS mean	0.024 ± 0.350	0.022 ± 0.363	0.019 ± 0.400	0.063 ± 0.448	0.067 ± 0.446	0.092 ± 0.455
HFC-32	NIR 2024	0.053	0.066	0.073	0.087	0.077	
	PARIS mean	0.06 ± 0.06	0.05 ± 0.07	0.04 ± 0.07	0.04 ± 0.07	0.05 ± 0.07	0.05 ± 0.08
HFC-125	NIR 2024	0.526	0.535	0.552	0.510	0.520	
	PARIS mean	0.68 ± 0.61	0.56 ± 0.57	0.36 ± 0.57	0.30 ± 0.52	0.41 ± 0.55	0.55 ± 0.56
HFC-134a	NIR 2024	0.636	0.667	0.686	0.695	0.677	
	PARIS mean	0.74 ± 0.68	0.64 ± 0.64	0.50 ± 0.68	0.41 ± 0.64	0.62 ± 0.70	0.73 ± 0.69
HFC-143a	NIR 2024	0.517	0.493	0.469	0.479	0.417	
	PARIS mean	0.65 ± 0.51	0.58 ± 0.50	0.41 ± 0.51	0.43 ± 0.49	0.52 ± 0.48	0.66 ± 0.49
HFC-152a	NIR 2024	0.000	0.000	0.000	0.000	0.000	
	PARIS mean	0.005 ± 0.013	0.006 ± 0.014	0.004 ± 0.013	0.005 ± 0.015	0.004 ± 0.015	0.005 ± 0.016
HFC-227ea	NIR 2024	0.022	0.023	0.023	0.023	0.021	
	PARIS mean	0.016 ± 0.058	0.012 ± 0.057	0.006 ± 0.065	0.003 ± 0.069	0.004 ± 0.063	0.005 ± 0.056
HFC-245fa	NIR 2024	0.000	0.000	0.000	0.000	0.000	
	PARIS mean	0.024 ± 0.033	0.016 ± 0.031	0.003 ± 0.029	0.003 ± 0.030	0.004 ± 0.025	0.005 ± 0.021
HFC-365mfc	NIR 2024	0.028	0.030	0.031	0.031	0.028	
	PARIS mean	0.015 ± 0.030	0.013 ± 0.027	0.008 ± 0.027	0.005 ± 0.027	0.004 ± 0.023	0.004 ± 0.021
HFC-4310mee	NIR 2024	0.000	0.000	0.000	0.000	0.000	
	PARIS mean	0.001 ± 0.015	0.001 ± 0.016	0.001 ± 0.019	0.001 ± 0.017	0.000 ± 0.016	[1]

[1] HFC-4310mee emissions were not estimated for 2023 due to lack of atmospheric observations.

7 Perfluorocarbons (PFCs)

7.1 PFC-14

Figure 7.1.1: Verification of the Hungarian emissions inventory estimates for PFC-14. Modelled annual emissions are given as the mean from all models (black line and grey shading) and the individual result from InTEM (blue line and shading). National inventory annual totals are given as grey bars.

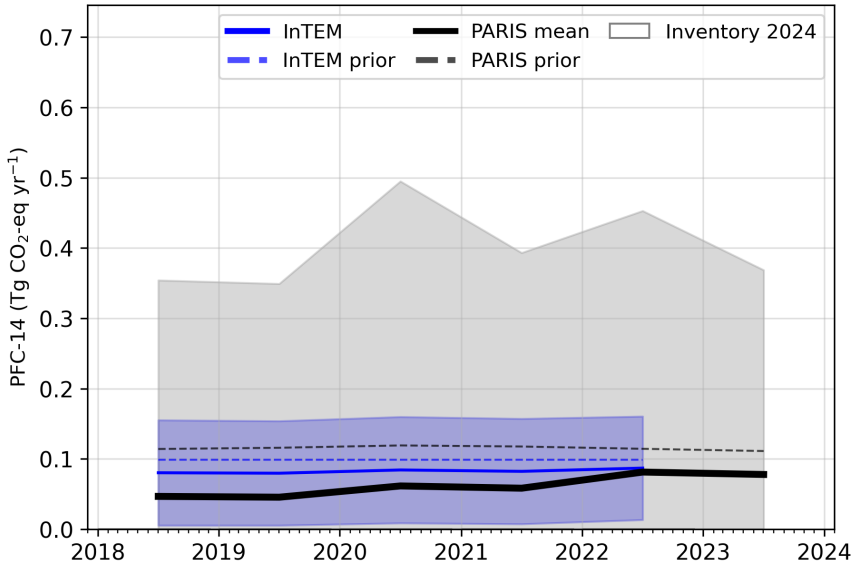

Figure 7.1.2: Spatial distribution of the Hungarian average modelled emissions of PFC-14 during the period of 2018-2023 (mean from all models). Observing stations are marked with red circles and highly-populated cities are marked with red triangles.

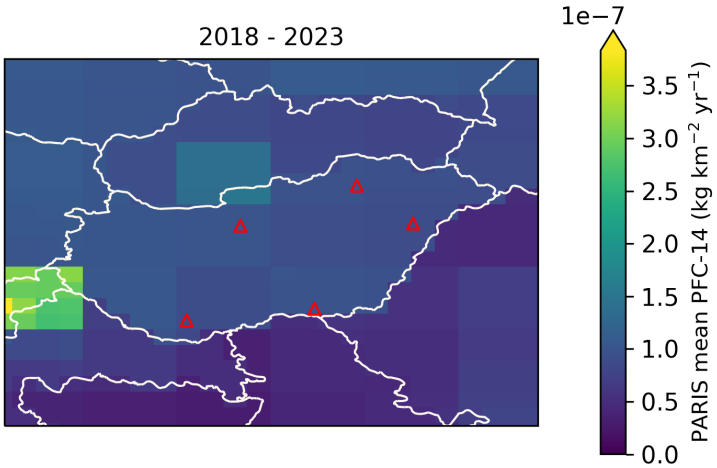

7.2 PFC-116

Figure 7.2.1: Verification of the Hungarian emissions inventory estimates for PFC-116. Modelled annual emissions are given as the mean from all models (black line and grey shading) and the individual result from InTEM (blue line and shading). National inventory annual totals are given as grey bars.

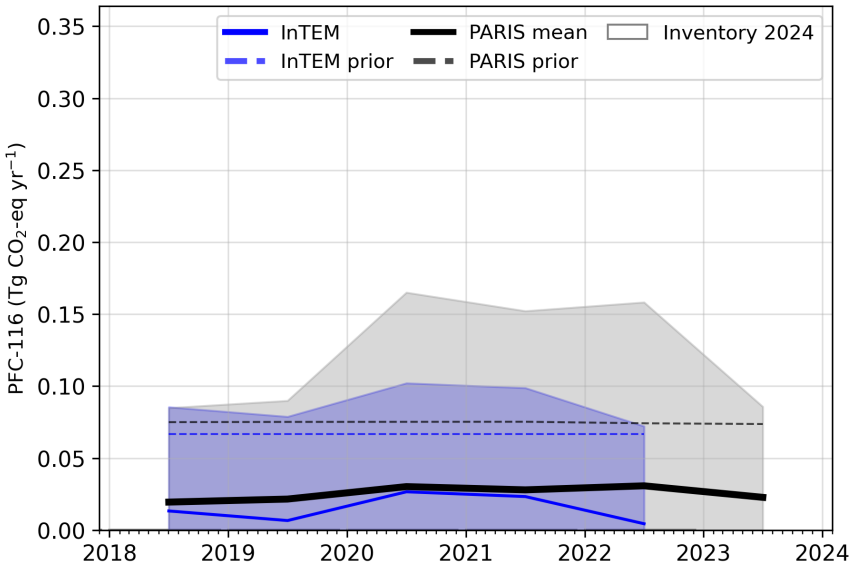

Figure 7.2.2: Spatial distribution of the Hungarian average modelled emissions of PFC-116 during the period of 2018-2023 (mean from all models). Observing stations are marked with red circles and highly-populated cities are marked with red triangles.

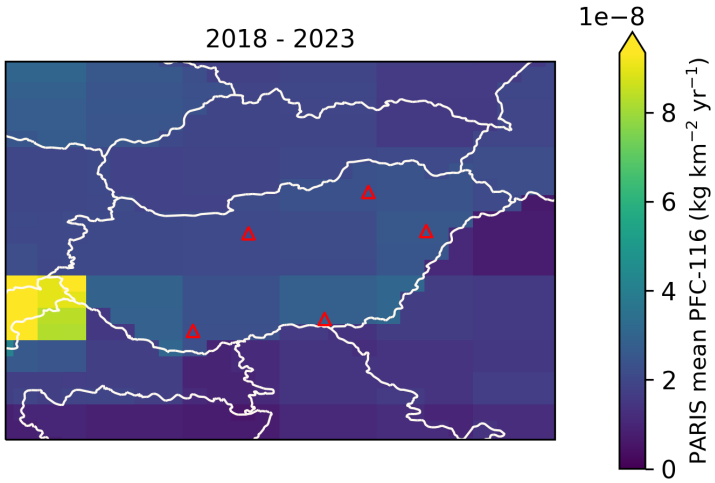

7.3 PFC-218

Figure 7.3.1: Verification of the Hungarian emissions inventory estimates for PFC-218. Modelled annual emissions are given as the mean from all models (black line and grey shading) and the individual result from InTEM (blue line and shading). National inventory annual totals are given as grey bars.

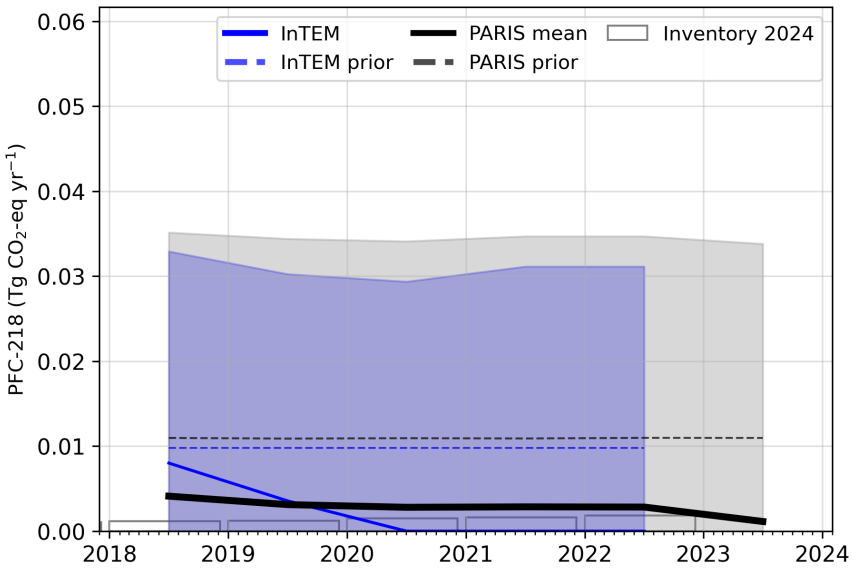

Figure 7.3.2: Spatial distribution of the Hungarian average modelled emissions of PFC-218 during the period of 2018-2023 (mean from all models). Observing stations are marked with red circles and highly-populated cities are marked with red triangles.

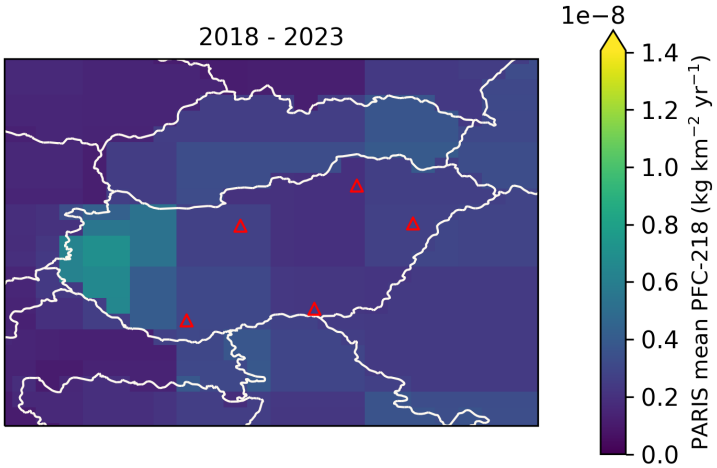

7.4 PFC-318

Figure 7.4.1: Verification of the Hungarian emissions inventory estimates for PFC-318. Modelled annual emissions are given as the mean from all models (black line and grey shading) and the individual result from InTEM (blue line and shading). National inventory annual totals are given as grey bars.

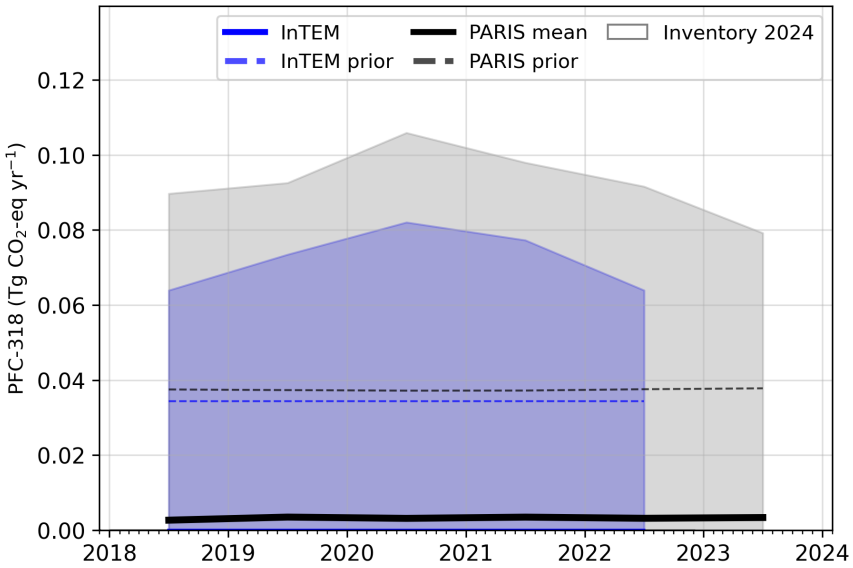

Figure 7.4.2: Spatial distribution of the Hungarian average modelled emissions of PFC-318 during the period of 2018-2023 (mean from all models). Observing stations are marked with red circles and highly-populated cities are marked with red triangles.

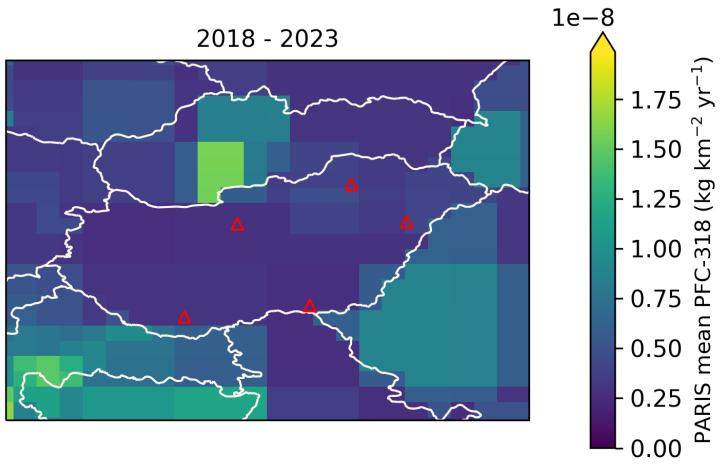

7.5 Total PFCs

Figure 7.5.1: Verification of the Hungarian emissions inventory estimates for total PFCs. Modelled annual emissions are given as the mean from all models (black line and grey shading) and the individual result from InTEM (blue line and shading). National inventory annual totals are given as grey bars.

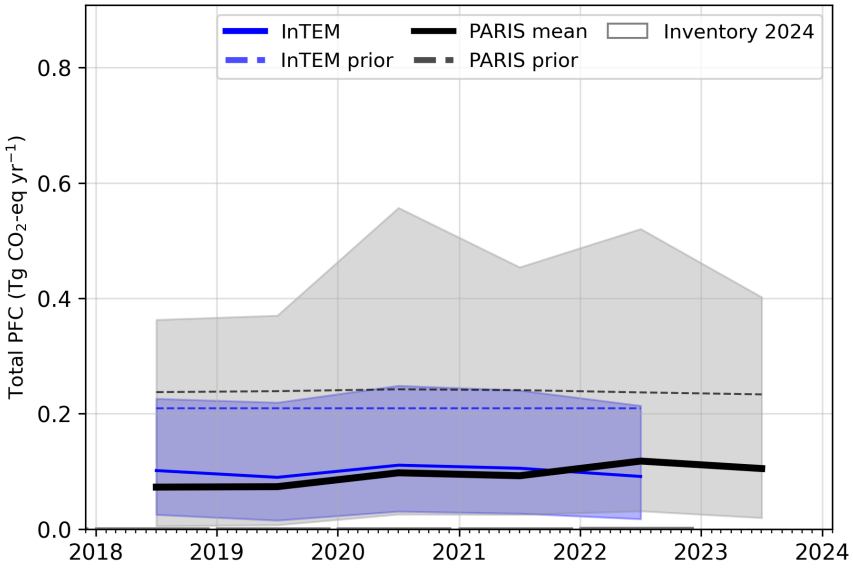

Table 3: Emissions estimation for PFCs in $\mathrm{TgCO_2{-}eq \cdot yr^{-1}}$ according to the National Inventory Report (NIR) 2024 and the inversions done in the PARIS project. For the PARIS estimation, the mean of the 3 inversion models is displayed, along with a range of uncertainty estimated via the half distance between the maximum and minimum uncertainties of the different models.

		2018	2019	2020	2021	2022	2023
PFC-14	NIR 2024	0.000	0.000	0.000	0.000	0.000	
	PARIS mean	0.047 ± 0.177	0.045 ± 0.175	0.061 ± 0.247	0.058 ± 0.197	0.081 ± 0.226	0.078 ± 0.184
PFC-116	NIR 2024	0.000	0.000	0.000	0.000	0.000	
	PARIS mean	0.019 ± 0.042	0.022 ± 0.045	0.030 ± 0.083	0.028 ± 0.076	0.031 ± 0.079	0.023 ± 0.043
PFC-218	NIR 2024	0.001	0.001	0.001	0.002	0.002	
	PARIS mean	0.004 ± 0.018	0.003 ± 0.017	0.003 ± 0.017	0.003 ± 0.017	0.003 ± 0.017	0.001 ± 0.017
PFC-318	NIR 2024	0.000	0.000	0.000	0.000	0.000	
	PARIS mean	0.003 ± 0.045	0.003 ± 0.046	0.003 ± 0.053	0.003 ± 0.049	0.003 ± 0.046	0.003 ± 0.040

8 Sulphur hexafluoride (SF_6)

Figure 8.0.1: Total source sensitivity of SF_6 observing sites as calculated by the NAME transport model for the year (left) 2018 and (right) 2023 and used in the inversions. Observing stations active in each year are marked with red dots. Areas with visible land surface represent regions for which emissions can be observed well from the network. Shaded or dark areas represent regions for which limited emission information can be obtained from the network.

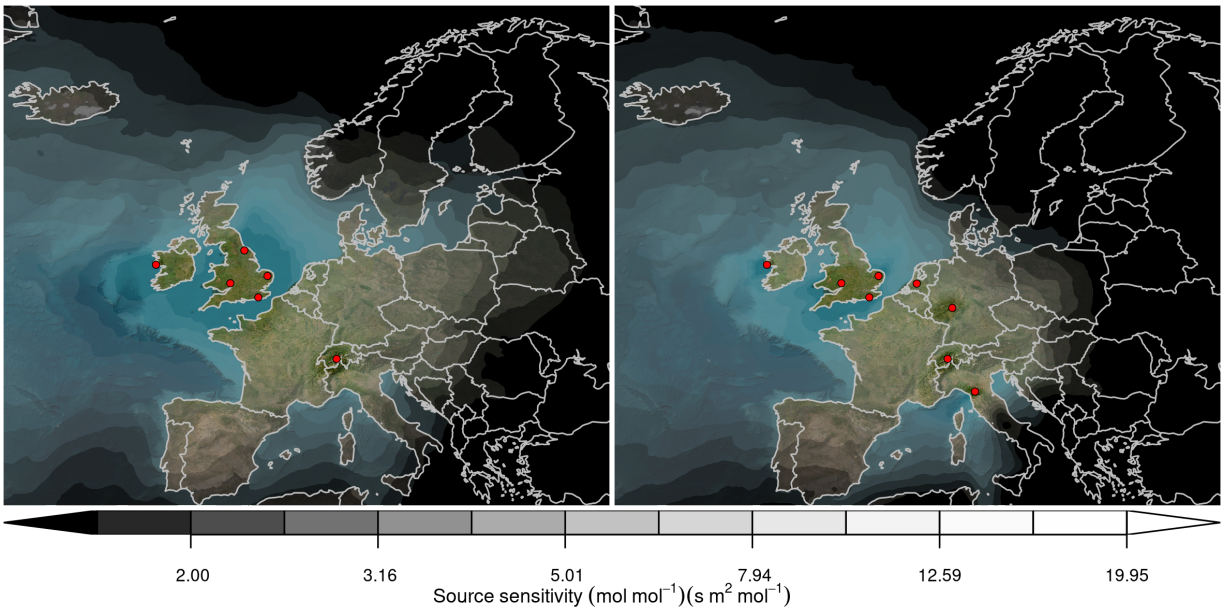

Figure 8.0.2: Verification of the Hungarian emissions inventory estimates for SF_6. Modelled annual emissions are given as the mean from all models (black line and grey shading) and the individual result from InTEM (blue line and shading). National inventory annual totals are given as grey bars.

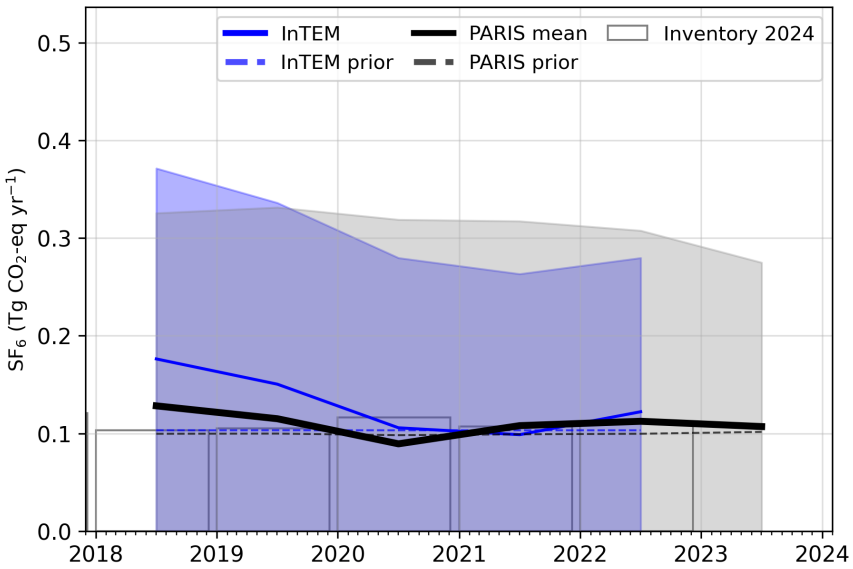

Figure 8.0.3: Spatial distribution of the Hungarian average modelled emissions of SF_6 during the period of 2018-2023 (mean from all models). Observing stations are marked with red circles and highly-populated cities are marked with red triangles.

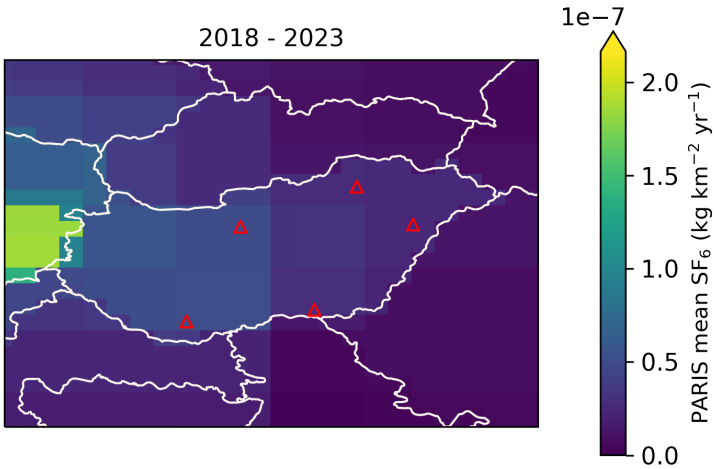

References

European Commission: Joint Research, Centre et al. (2023). *GHG emissions of all world countries – 2023*. Publications Office of the European Union. DOI: 10.2760/953322.

Ganesan, A. L. et al. (2014). "Characterization of uncertainties in atmospheric trace gas inversions using hierarchical Bayesian methods". In: *Atmospheric Chemistry and Physics* 14.8, pp. 3855–3864. DOI: 10.5194/acp-14-3855-2014. URL: http://www.atmos-chem-phys.net/14/3855/2014/http://www.atmos-chem-phys.net/14/3855/2014/acp-14-3855-2014.pdf.

Ganesan, A. L. et al. (2015). "Quantifying methane and nitrous oxide emissions from the UK and Ireland using a national-scale monitoring network". In: *Atmos. Chem. Phys.* 15.11, pp. 6393–6406. DOI: 10.5194/acp-15-6393-2015. URL: https://www.atmos-chem-phys.net/15/6393/2015/https://www.atmos-chem-phys.net/15/6393/2015/acp-15-6393-2015.pdf.

Henne, S. et al. (2016). "Validation of the Swiss methane emission inventory by atmospheric observations and inverse modelling". In: *Atmospheric Chemistry and Physics* 16.6, pp. 3683–3710. DOI: 10.5194/acp-16-3683-2016. URL: http://www.atmos-chem-phys.net/16/3683/2016/.

Jones, A.R. et al. (2007). "The U.K. Met Office's next-generation atmospheric dispersion model, NAME III, in Borrego C. and Norman A.-L. (Eds)". In: *Air Pollution Modeling and its Application XVII (Proceedings of the 27th NATO/CCMS International Technical Meeting on Air Pollution Modelling and its Application), Springer*, pp. 580–589.

Katharopoulos, I. et al. (2023). "Impact of transport model resolution and a priori assumptions on inverse modeling of Swiss F-gas emissions". In: *Atmos. Chem. Phys.* 23.22, pp. 14159–14186. DOI: 10.5194/acp-23-14159-2023. URL: https://acp.copernicus.org/articles/23/14159/2023/.

Manning, A. J. et al. (2021). "Evidence of a recent decline in UK emissions of hydrofluorocarbons determined by the InTEM inverse model and atmospheric measurements". In: *Atmospheric Chemistry and Physics* 21.16, pp. 12739–12755. DOI: 10.5194/acp-21-12739-2021. URL: https://acp.copernicus.org/articles/21/12739/2021/.

Rigby, M. et al. (2019). "Increase in CFC-11 emissions from eastern China based on atmospheric observations". In: *Nature* 569, pp. 546–550. DOI: 10.1038/s41586-019-1193-4. URL: https://doi.org/10.1038/s41586-019-1193-4.

Draft Inventory Annex
Italy 2024

18th November, 2024

1 Introduction

In this document, global concentration trends and national emissions estimates derived from atmospheric observations ("inverse estimates") are presented for each reported gas. Comparing the emissions submitted in national inventories with those calculated using atmospheric observations allows for emissions to be assessed using two fundamentally different approaches. Substantial differences can highlight areas that could warrant further investigation.

Global concentration trends for each gas are first shown using annual average concentrations from Mace Head, Ireland (Northern Hemisphere) and Kennaook/Cape Grim, Tasmania, Australia (Southern Hemisphere). Data from these stations were selected to exclude regionally-polluted air masses and therefore represents northern and southern hemispheric concentration trends. Mace Head observations were supported by the National Aeronautics and Space Administration (NASA) and the UK Department of Energy, Security and Net Zero (DESNZ), and Kennaook/Cape Grim observations by NASA and the Australian Bureau of Meteorology.

Observations of European concentrations of greenhouse gases used to derive national inverse emission estimates were collected from many different networks and providers. Methane and nitrous oxide concentrations originated from the European ICOS (Integrated Carbon Observation System) network, the UK DECC (Deriving Emissions related to Climate Change) network and other national or individual initiatives. F-gas observations were made by affiliates of the AGAGE (Advanced Global Atmospheric Gases Experiment) network. Observations from from additional stations across Europe were supported by the Horizon-EU PARIS (Process Attribution of Regional Emissions) project. The observation stations used to derive emissions for each gas are shown in the corresponding sections of this document.

Inversion-based emissions estimates were derived using one atmospheric transport model but with multiple inverse models allowing a better quantification of the uncertainties associated with inverse modelling. The atmospheric transport model provides the link between surface fluxes and concentrations measured at the observing stations. Although the uncertainty associated with the atmospheric transport model is considered in the statistical inversion approach, it may be underestimated when only using a single transport model. The atmospheric transport model used is the Numerical Atmospheric dispersion Modelling Environment (NAME) (Jones et al., 2007), a backwards-running Lagrangian Particle Dispersion Model (LPDM) that simulates the recent transport of air to each observing station. The NAME model has been widely used in the estimation of greenhouse gases emissions (Ganesan et al., 2015; Rigby et al., 2019; Manning et al., 2021).

The three inverse methods used are InTEM (Inversion Technique for Emission Modelling, Manning et al., 2021), ELRIS (Empa Lagrangian Regional Inversion System, Henne et al., 2016; Katharopoulos et al., 2023), and RHIME (Regional Hierarchical Inverse Modelling Environment, Ganesan et al., 2014). All three inverse methods estimate emissions within Europe along with boundary conditions that account for the concentration of the air entering Europe. All three systems started from the same set of a priori emissions that were either derived from the global EDGAR emission inventory (version 8, European Commission: Joint Research et al., 2023) or a uniform land-based emission, depending on the gas. A natural emission component, from the WETCHARTS product, was included in the methane prior. The same observational dataset was used by each inverse model, but data selection (i.e., filtering datasets for specific conditions) and treatment of uncertainties were chosen separately and hence differ. The three methods also differ in their statistical approaches for estimating emissions.

Emission estimates are presented for the period 2008-2023. Emissions for the full 2008-2023 period were derived with the InTEM model only, while emissions from 2018-2023 are presented as a combined result using the three inverse models.

For the 2008-2023 InTEM results, a 2-year inversion resolution, incrementing annually, was used for all gases except CH_4nd N_2, where the resolution was monthly. For the recent 2018-2023 period, for all three models, the inversion resolution was one month for CH_4 and N_2O in order to capture the seasonality of the emissions, a one-year average over these results is also presented. For the fluorinated gases, a 1-year

inversion resolution was adopted, with a 3-year moving average applied to the results. The uncertainty shown is the minimum/maximum of the uncertainties from the three results.

2 Global Concentration Trends

2.1 Methane (CH_4)

Figure 2.1.1: Background Northern Hemisphere monthly concentrations of CH_4 estimated from MHD, Ireland observations are shown in red, and background Southern Hemisphere monthly concentrations from CGO, Tasmania are shown in blue. Grey shading represents provisional data.

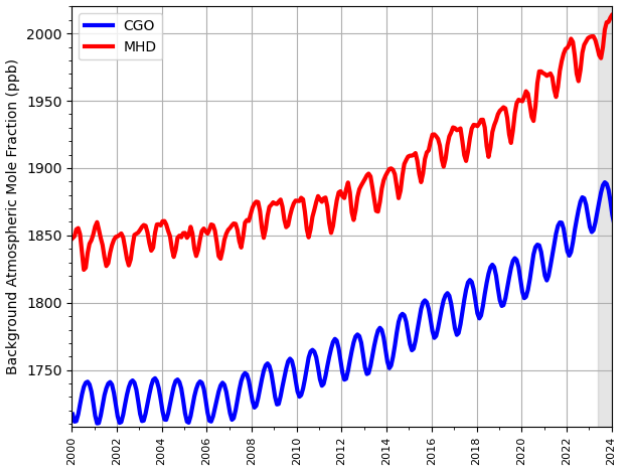

2.2 Nitrous Oxide (N_2O)

Figure 2.2.1: Background Northern Hemisphere monthly concentrations of N_2O estimated from MHD, Ireland observations are shown in red, and background Southern Hemisphere monthly concentrations from CGO, Tasmania are shown in blue. Grey shading represents provisional data.

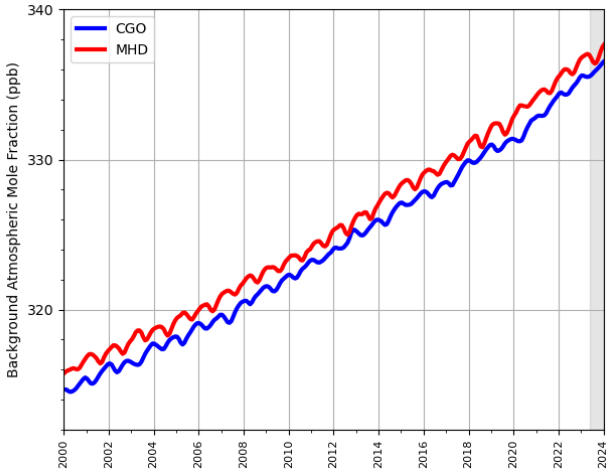

2.3 Hydrofluorocarbons (HFCs)

Figure 2.3.1: Background Northern Hemisphere monthly concentrations of six HFCs estimated from MHD, Ireland observations are shown in red, and background Southern Hemisphere monthly concentrations from CGO, Tasmania are shown in blue. Grey shading represents provisional data.

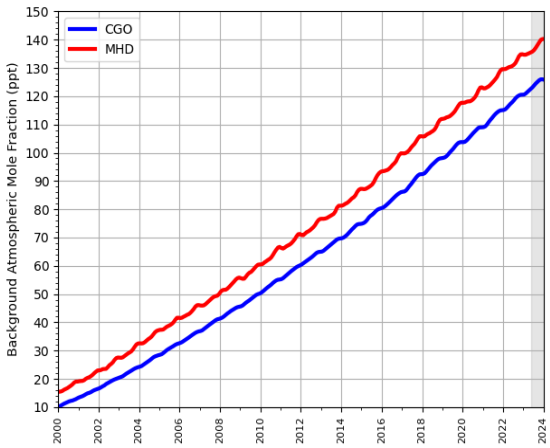

(a) HFC-134a

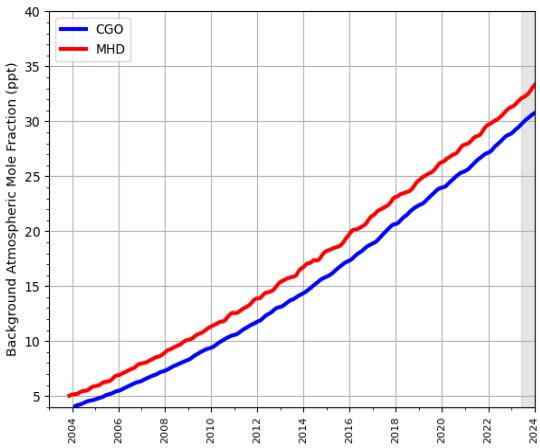

(b) HFC-143a

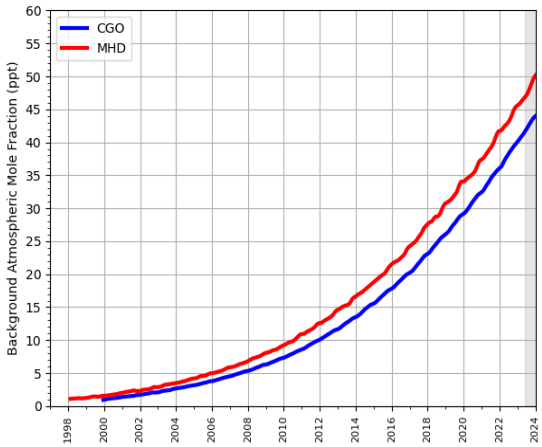

(c) HFC-125

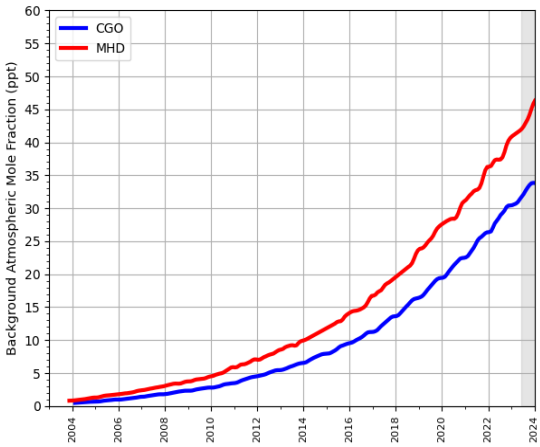

(d) HFC-32

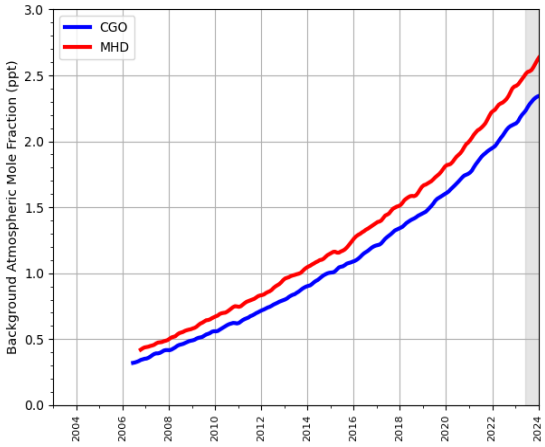

(e) HFC-227ea

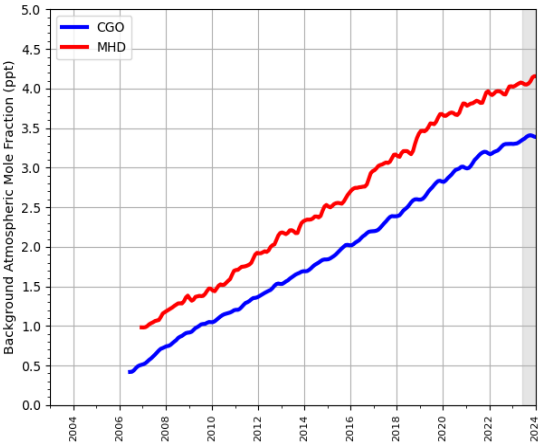

(f) HFC-245fa

Figure 2.3.2: Background Northern Hemisphere monthly concentrations of four HFCs estimated from MHD, Ireland observations are shown in red, and background Southern Hemisphere monthly concentrations from CGO, Tasmania are shown in blue. Grey shading represents provisional data.

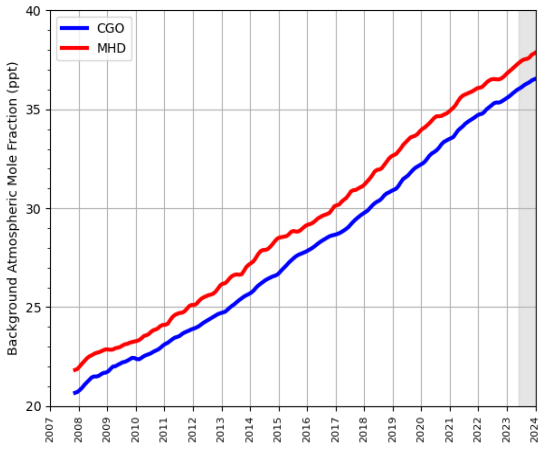

(a) HFC-23

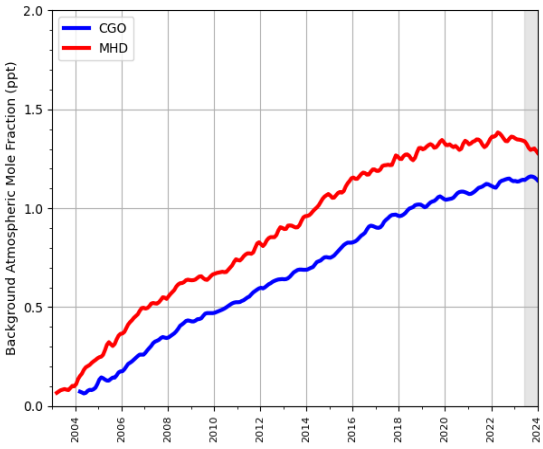

(b) HFC-365mfc

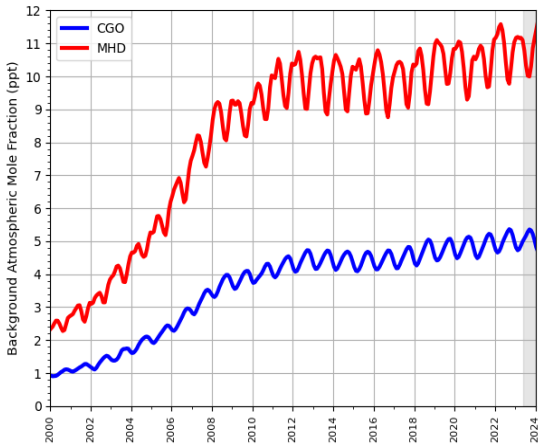

(c) HFC-152a

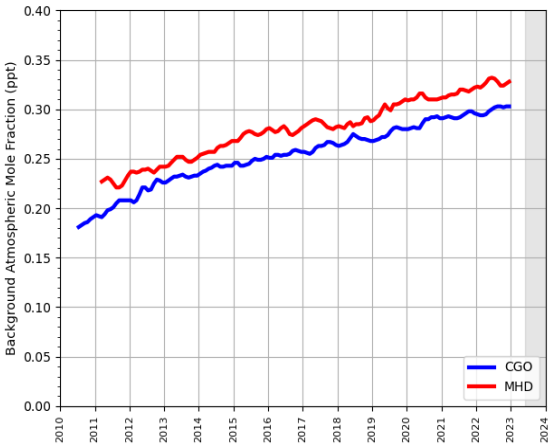

(d) HFC-43-10-mee

2.4 Perfluorocarbons (PFCs)

Figure 2.4.1: Background Northern Hemisphere monthly concentrations of four PFCs estimated from MHD, Ireland observations are shown in red, and background Southern Hemisphere monthly concentrations from CGO, Tasmania are shown in blue. Grey shading represents provisional data.

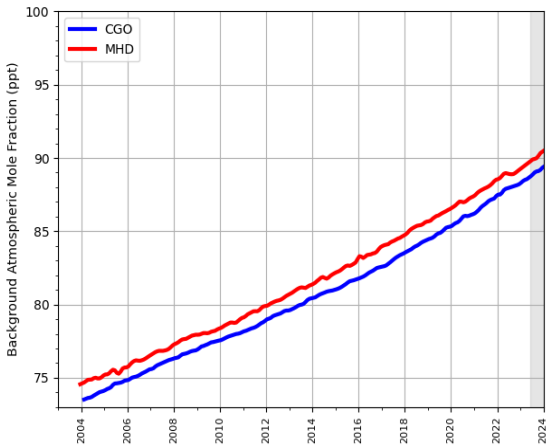

(a) PFC-14

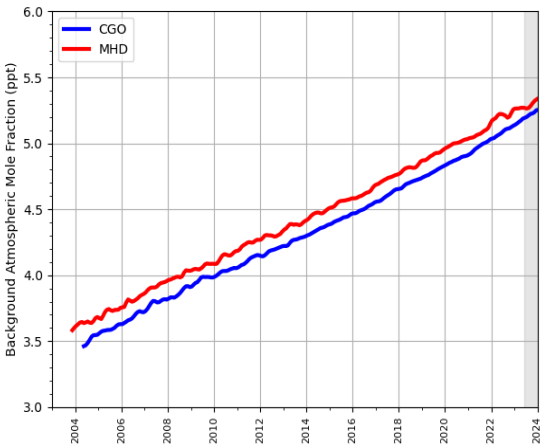

(b) PFC-116

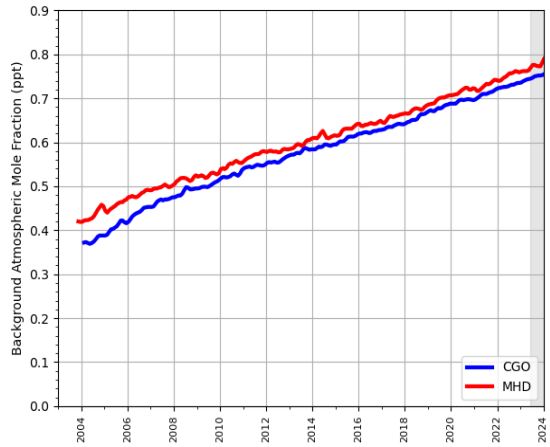

(c) PFC-218

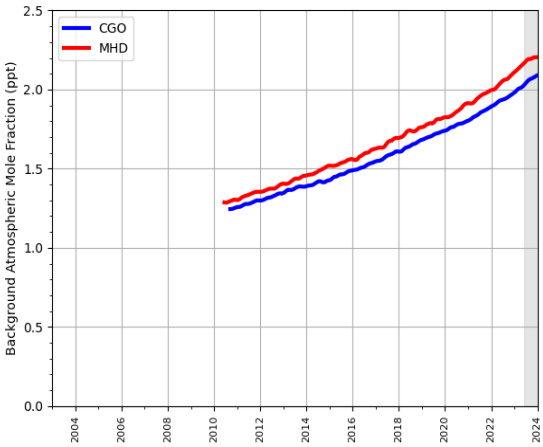

(d) PFC-318

3 Key findings

- The observation network used in this report has very little sensitivity to southern Italy. The new station in Sicily that started in 2024, will be extremely useful in filling this gap. All of the subsequent results are based on the assumption that either southern Italian emissions are relatively small or that the prior has sufficient skill. This assumption will be tested next year with the improved observational network.
- All of the inversion estimates are potentially impacted by a weak constraint on the concentration of air arriving from the south. If this is estimated too high then the emissions in southern Italy will be lower to compensate. The new station in Sicily will address this issue. In addition, next year, the estimates will include Lampadusa methane observations.
- PFC spatial maps for PFC-14 and PFC-318 are of note as they identify specific areas of emission in NW Italy.

Table 1: Emissions estimation for the main greenhouse gases of focus in $\mathrm{TgCO_2{-}eq \cdot yr^{-1}}$ according to the National Inventory Report (NIR) 2024 and the inversions done in the PARIS project. For the PARIS estimation, the mean of the 3 inversion models is displayed, along with a range of uncertainty estimated via the half distance between the maximum and minimum uncertainties of the different models.

		2018	2019	2020	2021	2022	2023
CH_4	NIR 2024	48	47	48	48	46	
	PARIS mean	24 ± 6	21 ± 7	25 ± 9	24 ± 8	25 ± 7	26 ± 9
N_2O	NIR 2024	18	17	18	18	16	
	PARIS mean	10 ± 3	15 ± 3	16 ± 3	16 ± 3	15 ± 4	14 ± 3
Total HFCs[(1)]	NIR 2024	11.4	11.1	10.0	9.4	9.1	
	PARIS mean	7.5 ± 1.8	7.2 ± 1.7	6.4 ± 1.6	6.3 ± 1.5	5.9 ± 1.5	6.2 ± 1.6
Total PFCs[(2)]	NIR 2024	1.5	0.9	0.5	0.4	0.4	
	PARIS mean	0.5 ± 0.4	0.5 ± 0.4	0.5 ± 0.5	0.5 ± 0.5	0.4 ± 0.4	0.4 ± 0.3
SF_6	NIR 2024	0.5	0.4	0.3	0.3	0.4	
	PARIS mean	0.9 ± 0.6	1.1 ± 0.7	1.2 ± 0.8	1.2 ± 0.8	1.1 ± 0.6	1.0 ± 0.9

[(1)] Sum of HFC emissions presented in Table 2, except HFC-4310mee.
[(2)] Sum of PFC emissions presented in Table 3.

4 Methane (CH_4)

Figure 4.0.1: Total source sensitivity of CH_4 observing sites as calculated by the NAME transport model for the year (left) 2018 and (right) 2023 and used in the inversions. Observing stations active in each year are marked with red dots. Areas with visible land surface represent regions for which emissions can be observed well from the network. Shaded or dark areas represent regions for which limited emission information can be obtained from the network.

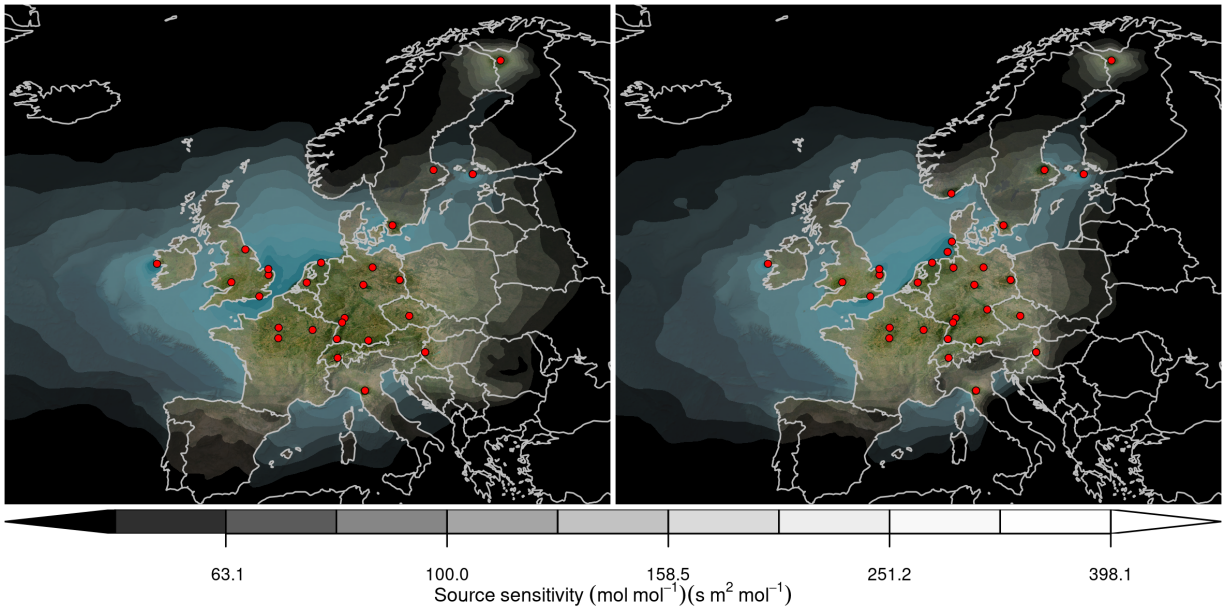

Figure 4.0.2: Verification of the Italian emissions inventory estimates for CH_4. Modelled annual emissions are given as the mean from all models (black line and grey shading) and the individual result from InTEM (blue line and shading). National inventory annual totals are given as grey bars.

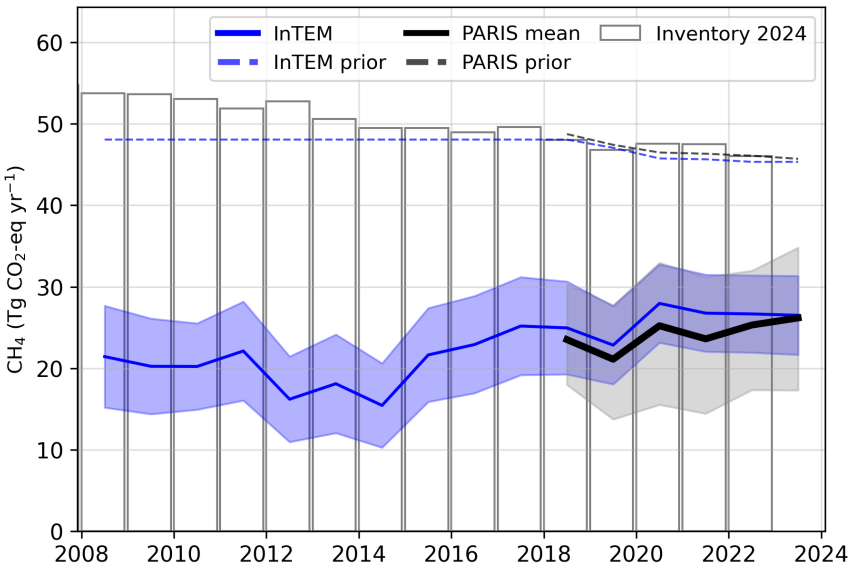

Figure 4.0.3: Verification of the Italian emissions inventory estimates for CH_4 (zoom in to 2018-2023). Modelled annual emissions are given as the mean from all models (black line and grey shading) and the individual result from InTEM (blue line and shading). National inventory annual totals are given as grey bars.

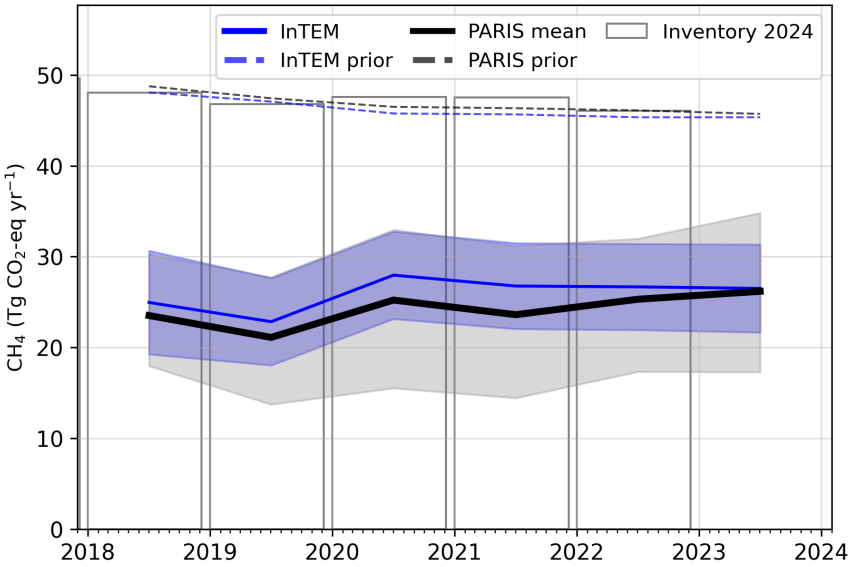

Figure 4.0.4: Verification of the Italian emissions inventory estimates for CH_4 (zoom in to 2018-2023). Modelled monthly emissions are given as the mean from all models (black line and grey shading) and the individual result from InTEM (blue line and shading). National inventory annual totals are given as grey bars.

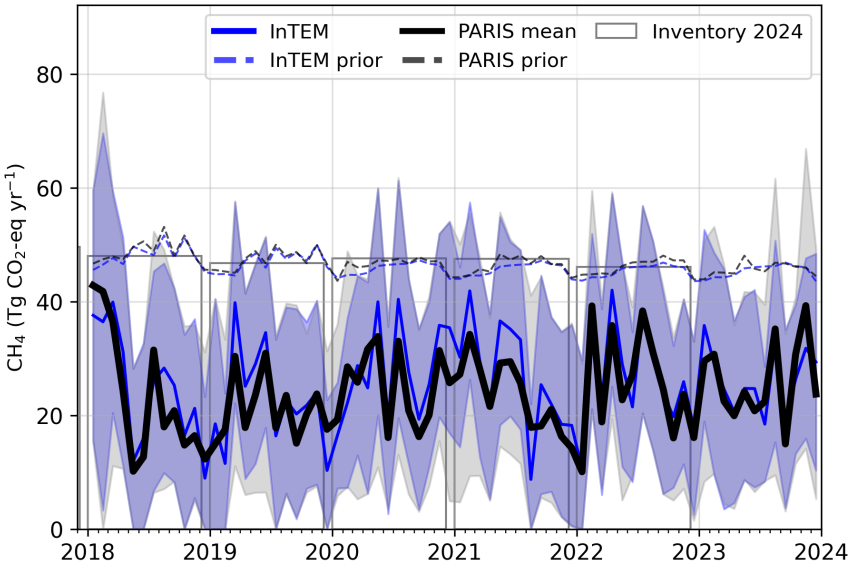

Figure 4.0.5: Spatial distribution of the Italian average modelled emissions of CH_4 during the period of 2018-2023 (mean from all models). Observing stations are marked with red circles and highly-populated cities are marked with red triangles.

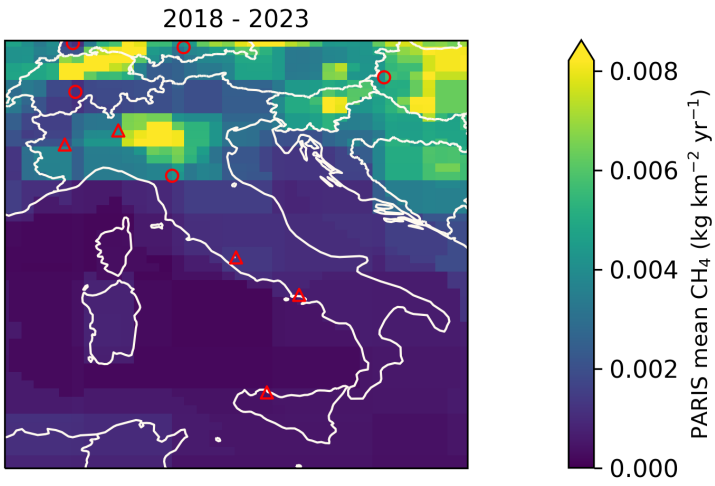

Figure 4.0.6: Spatial distribution of the seasonal deviation from the mean. The deviation is defined as the modelled Italian seasonally averaged CH_4 emissions over 2018-2023 minus the average over the whole period. The mean across all models is shown. Observing stations are marked with red circles and highly-populated cities are marked with red triangles.

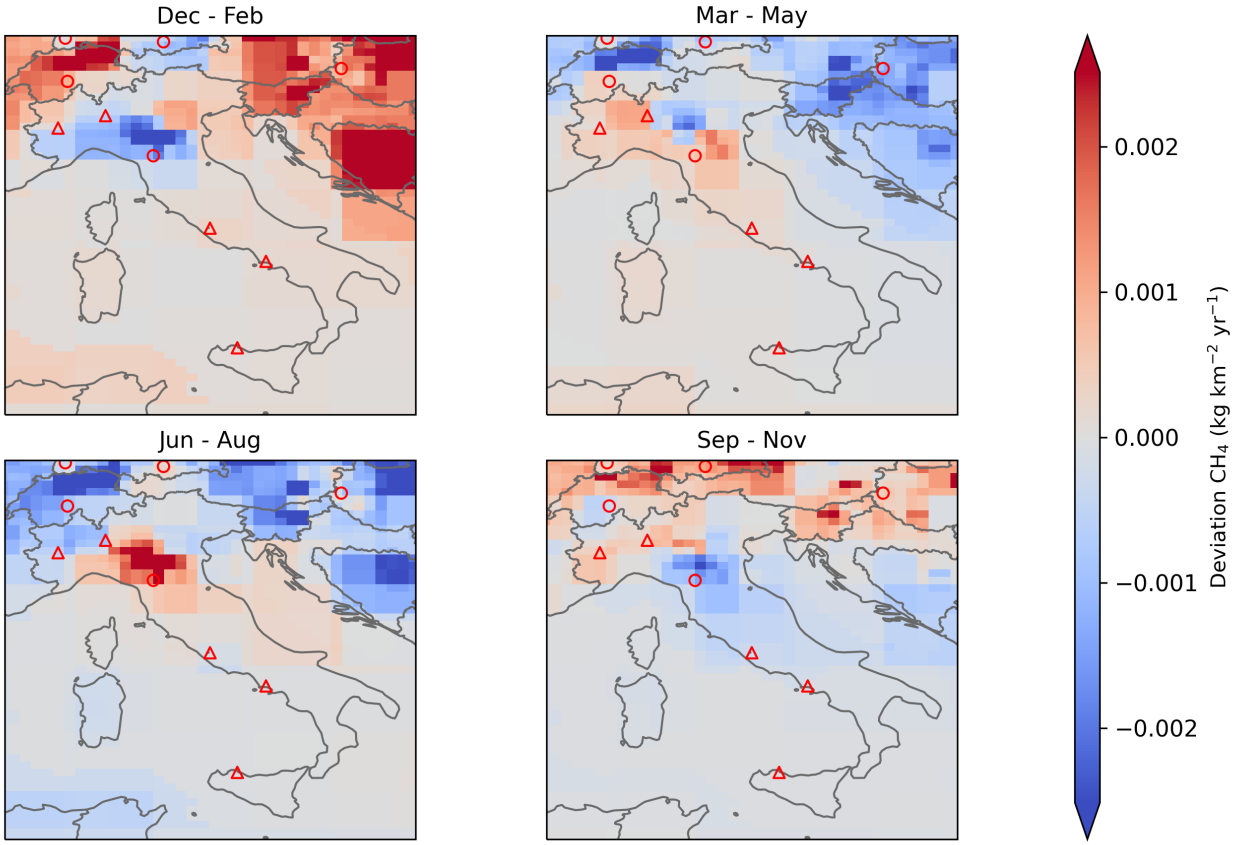

5 Nitrous Oxide (N_2O)

Figure 5.0.1: Total source sensitivity of N_2O observing sites as calculated by the NAME transport model for the year (left) 2018 and (right) 2023 and used in the inversions. Observing stations active in each year are marked with red dots. Areas with visible land surface represent regions for which emissions can be observed well from the network. Shaded or dark areas represent regions for which limited emission information can be obtained from the network.

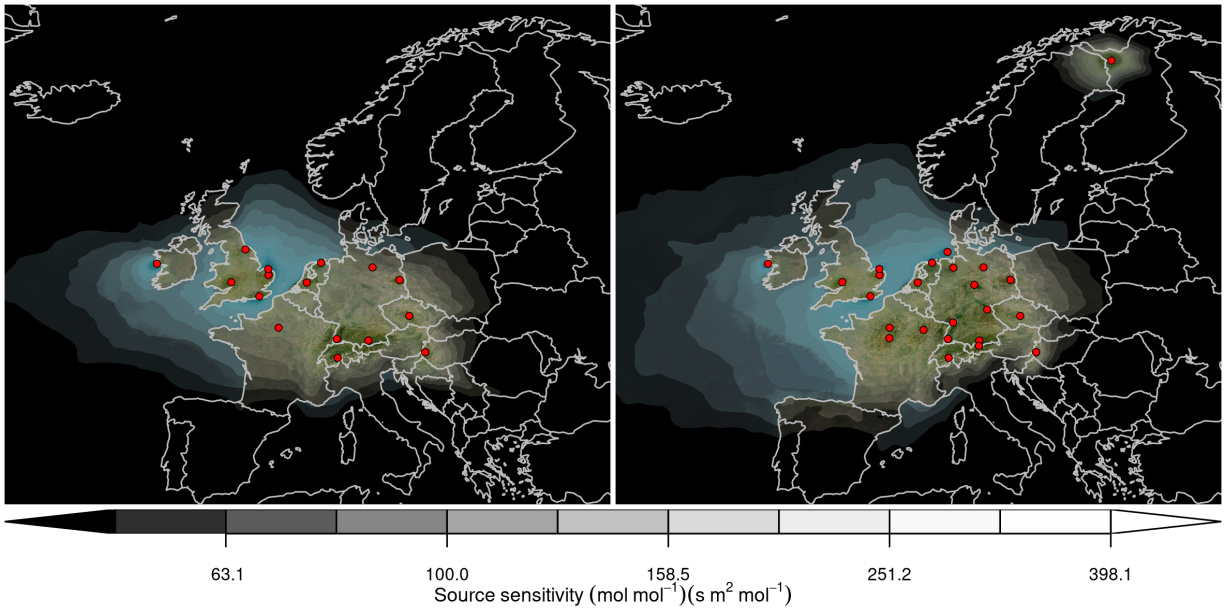

Figure 5.0.2: Verification of the Italian emissions inventory estimates for N_2O. Modelled annual emissions are given as the mean from all models (black line and grey shading) and the individual result from InTEM (blue line and shading). National inventory annual totals are given as grey bars.

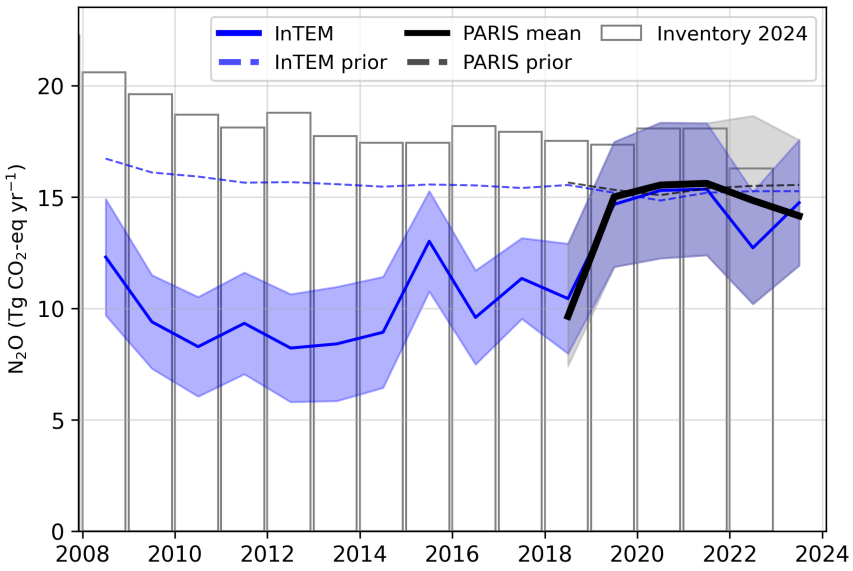

Figure 5.0.3: Verification of the Italian emissions inventory estimates for N_2O (zoom in to 2018-2023). Modelled annual emissions are given as the mean from all models (black line and grey shading) and the individual result from InTEM (blue line and shading). National inventory annual totals are given as grey bars.

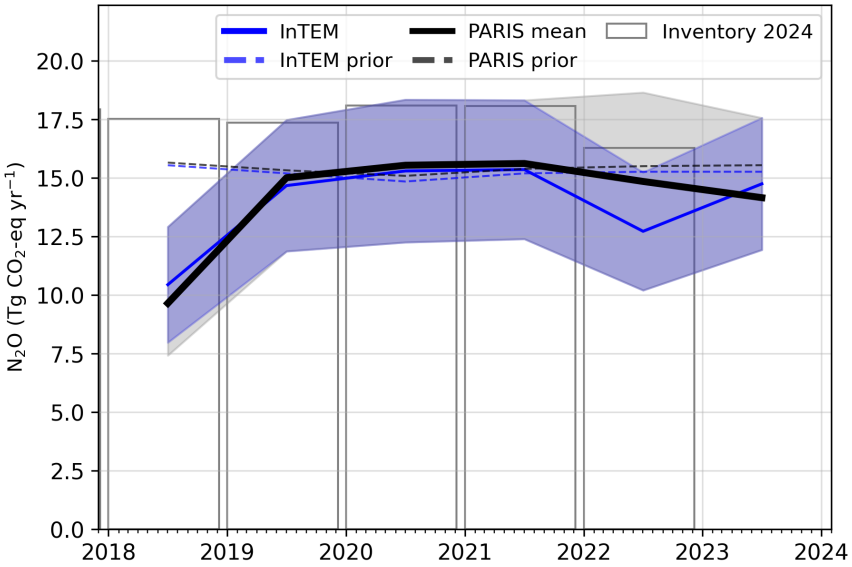

Figure 5.0.4: Verification of the Italian emissions inventory estimates for N_2O (zoom in to 2018-2023). Modelled monthly emissions are given as the mean from all models (black line and grey shading) and the individual result from InTEM (blue line and shading). National inventory annual totals are given as grey bars.

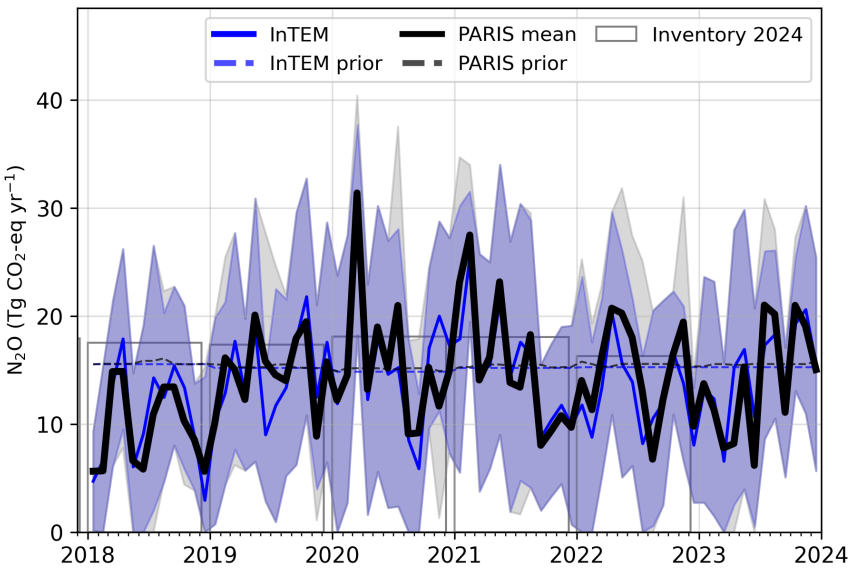

Figure 5.0.5: Spatial distribution of the Italian average modelled emissions of N_2O during the period of 2018-2023 (mean from all models). Observing stations are marked with red circles and highly-populated cities are marked with red triangles.

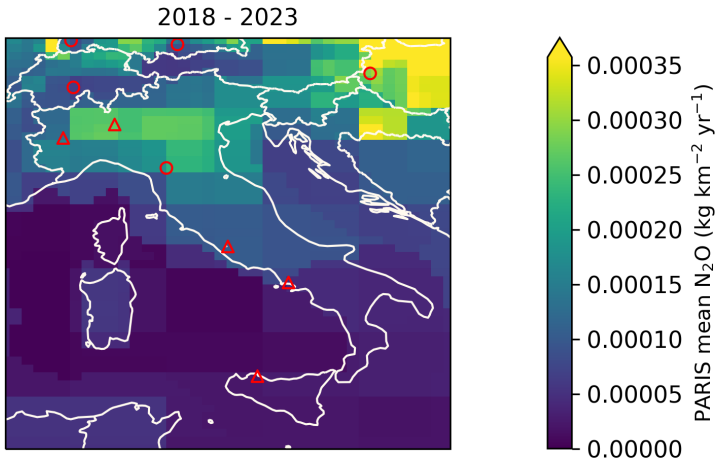

Figure 5.0.6: Spatial distribution of the seasonal deviation from the mean. The deviation is defined as the modelled Italian seasonally averaged N_2O emissions over 2018-2023 minus the average over the whole period. The mean across all models is shown. Observing stations are marked with red circles and highly-populated cities are marked with red triangles.

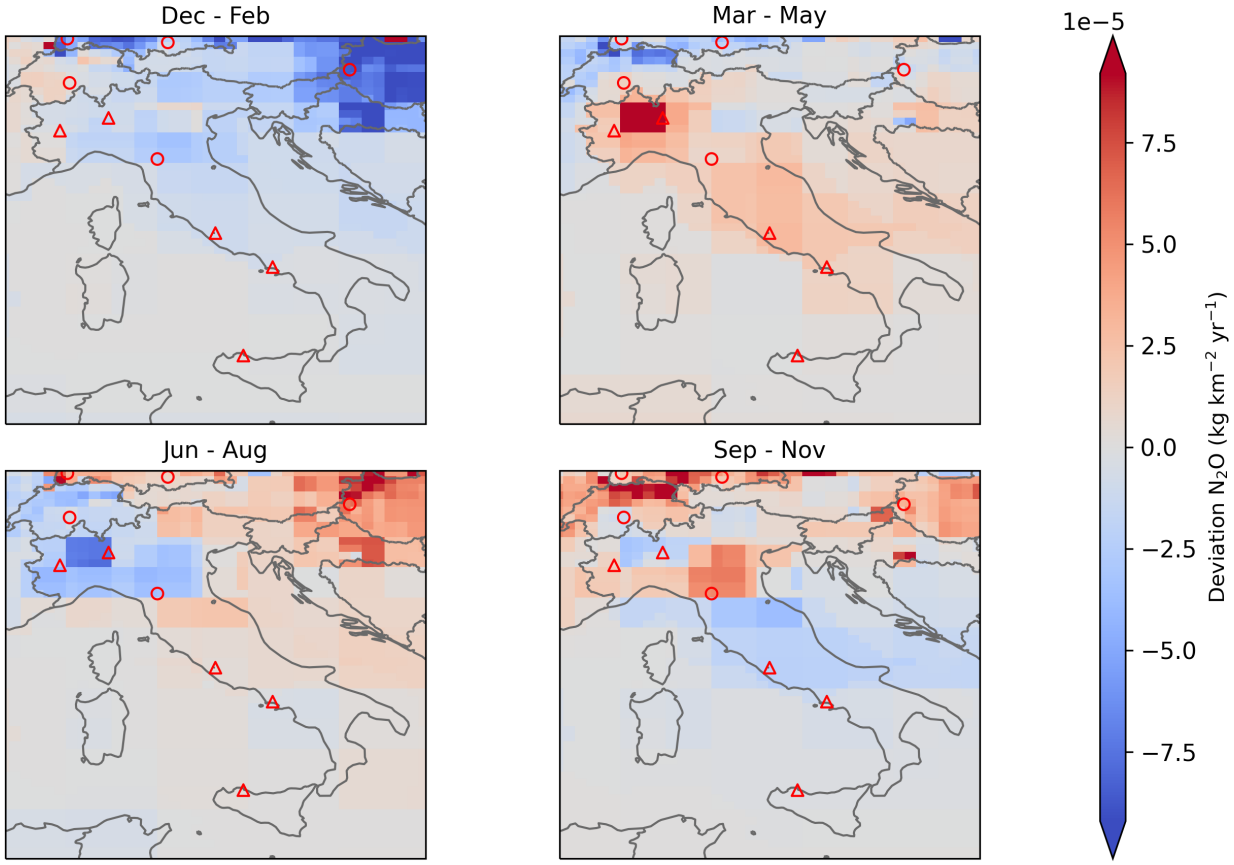

6 Hydrofluorocarbons (HFCs)

Figure 6.0.1: Total source sensitivity of HFCs/PFCs observing sites as calculated by the NAME transport model for the year (left) 2018 and (right) 2023 and used in the inversions. Observing stations active in each year are marked with red dots. Areas with visible land surface represent regions for which emissions can be observed well from the network. Shaded or dark areas represent regions for which limited emission information can be obtained from the network.

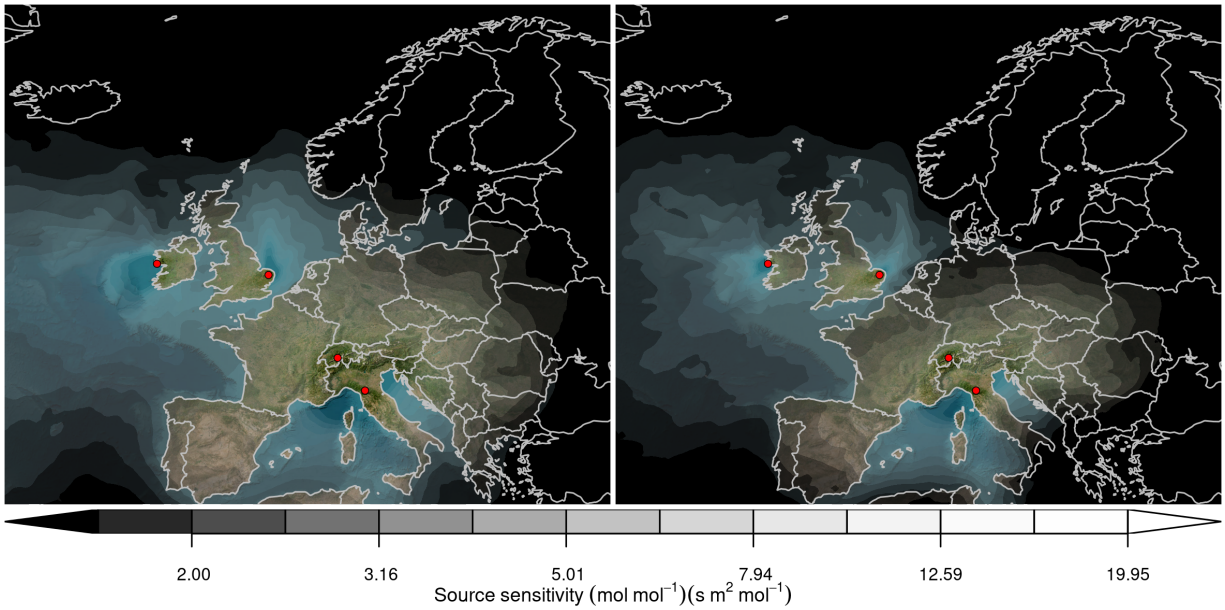

6.1 HFC-32

Figure 6.1.1: Verification of the Italian emissions inventory estimates for HFC-32. Modelled annual emissions are given as the mean from all models (black line and grey shading) and the individual result from InTEM (blue line and shading). National inventory annual totals are given as grey bars.

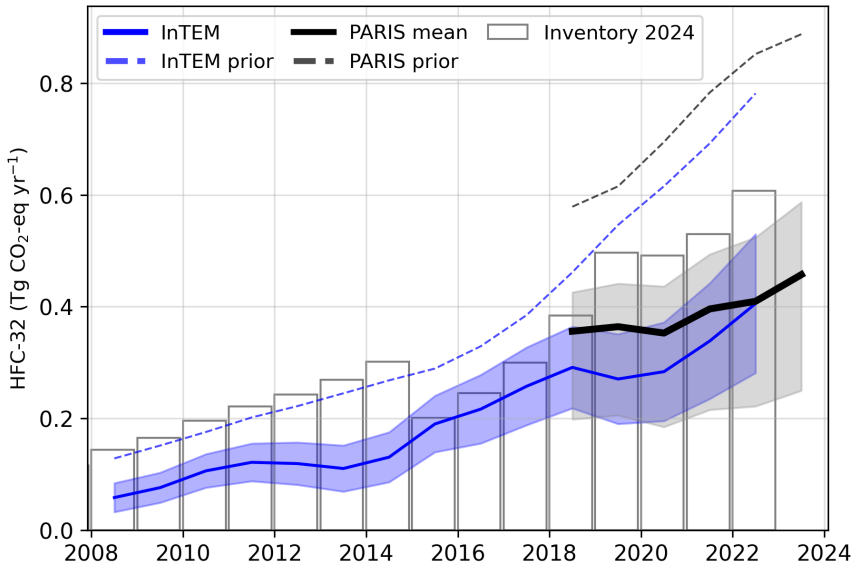

Figure 6.1.2: Spatial distribution of the Italian average modelled emissions of HFC-32 during the period of 2018-2023 (mean from all models). Observing stations are marked with red circles and highly-populated cities are marked with red triangles.

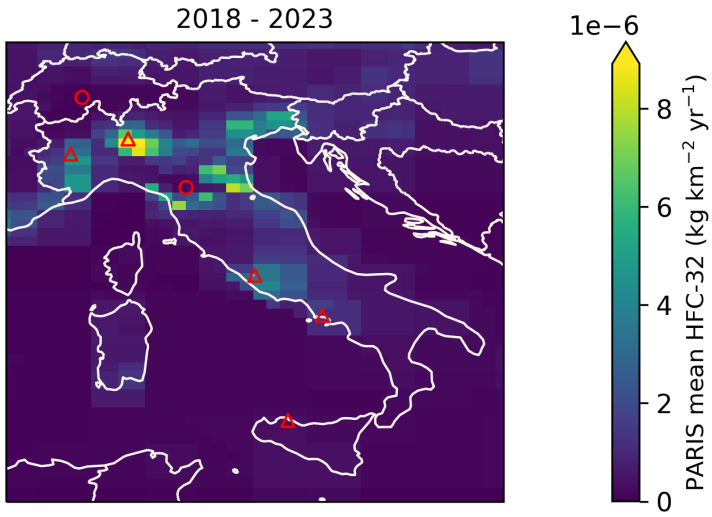

6.2 HFC-125

Figure 6.2.1: Verification of the Italian emissions inventory estimates for HFC-125. Modelled annual emissions are given as the mean from all models (black line and grey shading) and the individual result from InTEM (blue line and shading). National inventory annual totals are given as grey bars.

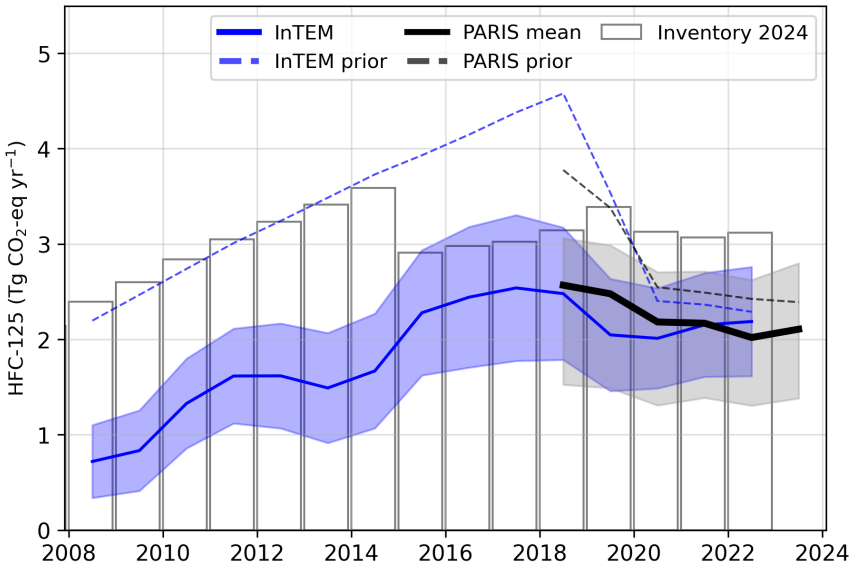

Figure 6.2.2: Spatial distribution of the Italian average modelled emissions of HFC-125 during the period of 2018-2023 (mean from all models). Observing stations are marked with red circles and highly-populated cities are marked with red triangles.

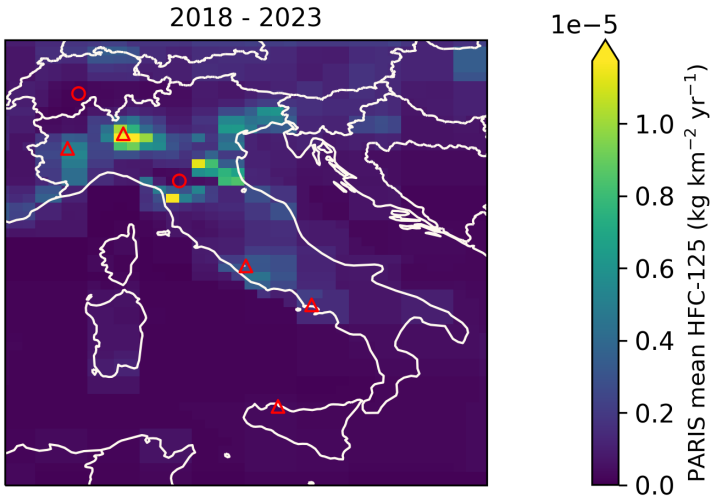

6.3 HFC-134a

Figure 6.3.1: Verification of the Italian emissions inventory estimates for HFC-134a. Modelled annual emissions are given as the mean from all models (black line and grey shading) and the individual result from InTEM (blue line and shading). National inventory annual totals are given as grey bars.

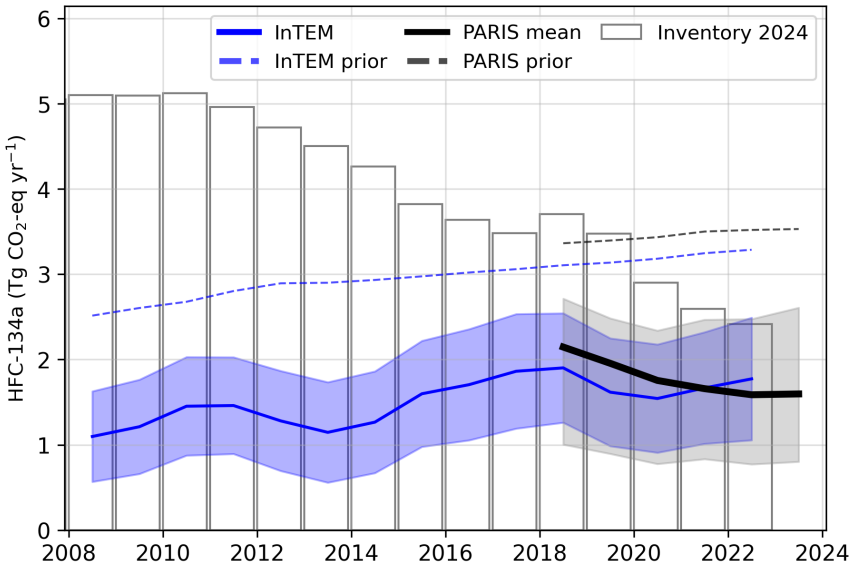

Figure 6.3.2: Spatial distribution of the Italian average modelled emissions of HFC-134a during the period of 2018-2023 (mean from all models). Observing stations are marked with red circles and highly-populated cities are marked with red triangles.

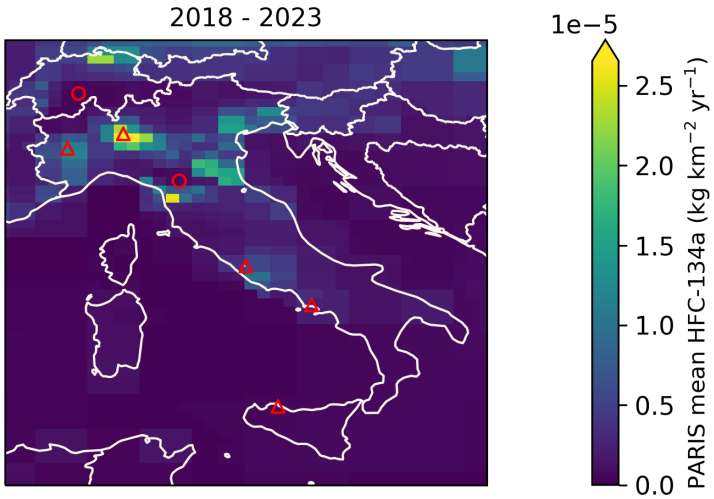

6.4 HFC-143a

Figure 6.4.1: Verification of the Italian emissions inventory estimates for HFC-143a. Modelled annual emissions are given as the mean from all models (black line and grey shading) and the individual result from InTEM (blue line and shading). National inventory annual totals are given as grey bars.

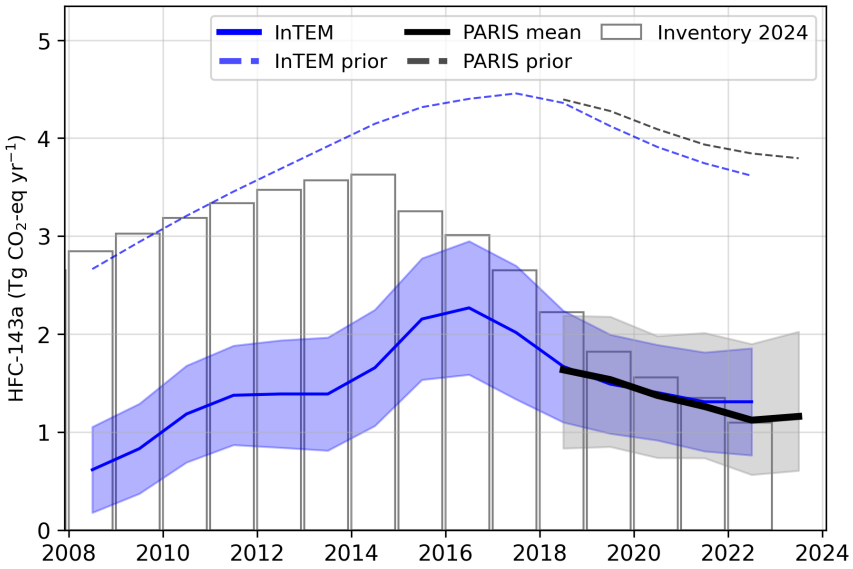

Figure 6.4.2: Spatial distribution of the Italian average modelled emissions of HFC-143a during the period of 2018-2023 (mean from all models). Observing stations are marked with red circles and highly-populated cities are marked with red triangles.

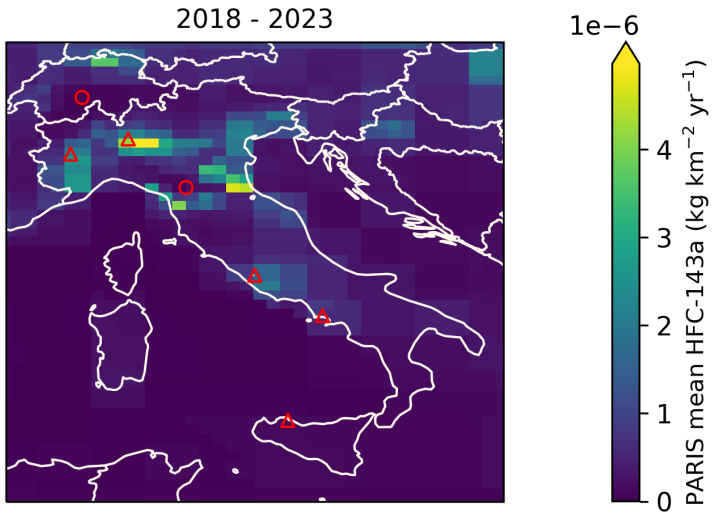

6.5 Total HFCs

Figure 6.5.1: Verification of the Italian emissions inventory estimates for total HFCs. Modelled annual emissions are given as the mean from all models (black line and grey shading) and the individual result from InTEM (blue line and shading). National inventory annual totals are given as grey bars.

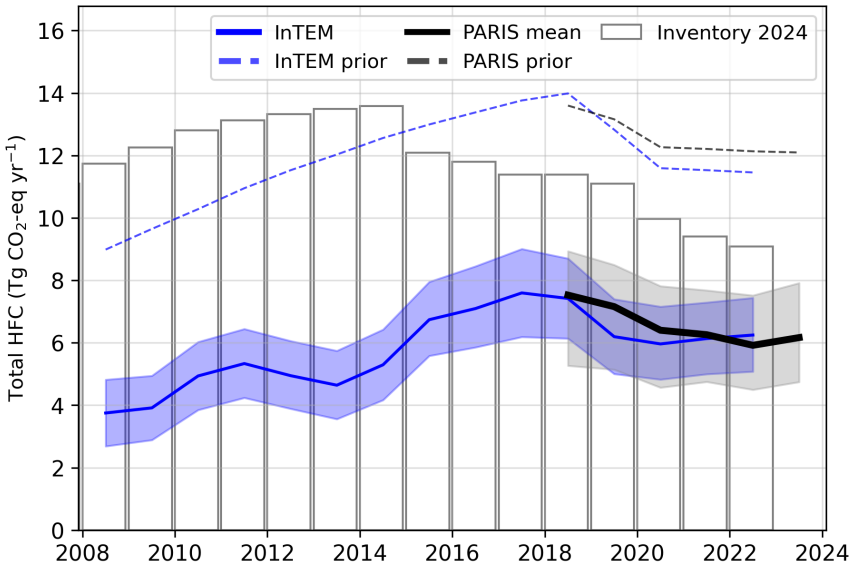

Table 2: Emissions estimation for HFCs in $\mathrm{TgCO_2{-}eq \cdot yr^{-1}}$ according to the National Inventory Report (NIR) 2024 and the inversions done in the PARIS project. For the PARIS estimation, the mean of the 3 inversion models is displayed, along with a range of uncertainty estimated via the half distance between the maximum and minimum uncertainties of the different models.

		2018	2019	2020	2021	2022	2023
HFC-23	NIR 2024	0.29	0.29	0.28	0.27	0.27	
	PARIS mean	0.65 ± 0.70	0.68 ± 0.77	0.61 ± 0.77	0.66 ± 0.76	0.67 ± 0.78	0.73 ± 0.87
HFC-32	NIR 2024	0.38	0.50	0.49	0.53	0.61	
	PARIS mean	0.36 ± 0.11	0.36 ± 0.12	0.35 ± 0.13	0.40 ± 0.14	0.41 ± 0.15	0.46 ± 0.17
HFC-125	NIR 2024	3.14	3.39	3.13	3.07	3.12	
	PARIS mean	2.57 ± 0.77	2.48 ± 0.75	2.18 ± 0.70	2.17 ± 0.66	2.02 ± 0.66	2.11 ± 0.71
HFC-134a	NIR 2024	3.70	3.47	2.90	2.59	2.41	
	PARIS mean	2.15 ± 0.85	1.96 ± 0.79	1.75 ± 0.78	1.66 ± 0.82	1.59 ± 0.85	1.60 ± 0.90
HFC-143a	NIR 2024	2.22	1.82	1.56	1.35	1.10	
	PARIS mean	1.64 ± 0.68	1.54 ± 0.66	1.37 ± 0.62	1.26 ± 0.64	1.12 ± 0.67	1.16 ± 0.71
HFC-152a	NIR 2024	0.00	0.00	0.00	0.00	0.00	
	PARIS mean	0.01 ± 0.01	0.01 ± 0.01	0.01 ± 0.01	0.01 ± 0.01	0.01 ± 0.01	0.01 ± 0.02
HFC-227ea	NIR 2024	1.38	1.39	1.39	1.39	1.38	
	PARIS mean	0.06 ± 0.07	0.06 ± 0.07	0.05 ± 0.08	0.05 ± 0.09	0.05 ± 0.09	0.05 ± 0.09
HFC-245fa	NIR 2024	0.25	0.24	0.22	0.21	0.20	
	PARIS mean	0.05 ± 0.05	0.04 ± 0.05	0.03 ± 0.05	0.03 ± 0.04	0.02 ± 0.03	0.02 ± 0.02
HFC-365mfc	NIR 2024	0.00	0.00	0.00	0.00	0.00	
	PARIS mean	0.05 ± 0.04	0.04 ± 0.04	0.04 ± 0.03	0.04 ± 0.04	0.04 ± 0.04	0.04 ± 0.04
HFC-4310mee	NIR 2024	0.00	0.00	0.00	0.00	0.00	
	PARIS mean	0.02 ± 0.02	0.01 ± 0.02	0.01 ± 0.02	0.01 ± 0.02	0.01 ± 0.01	[1]

[1] HFC-4310mee emissions were not estimated for 2023 due to lack of atmospheric observations.

7 Perfluorocarbons (PFCs)

7.1 PFC-14

Figure 7.1.1: Verification of the Italian emissions inventory estimates for PFC-14. Modelled annual emissions are given as the mean from all models (black line and grey shading) and the individual result from InTEM (blue line and shading). National inventory annual totals are given as grey bars.

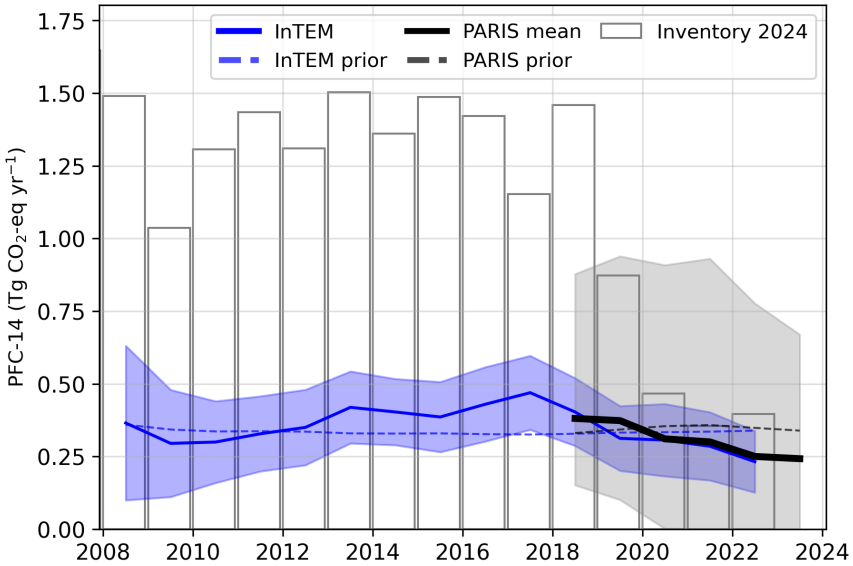

Figure 7.1.2: Spatial distribution of the Italian average modelled emissions of PFC-14 during the period of 2018-2023 (mean from all models). Observing stations are marked with red circles and highly-populated cities are marked with red triangles.

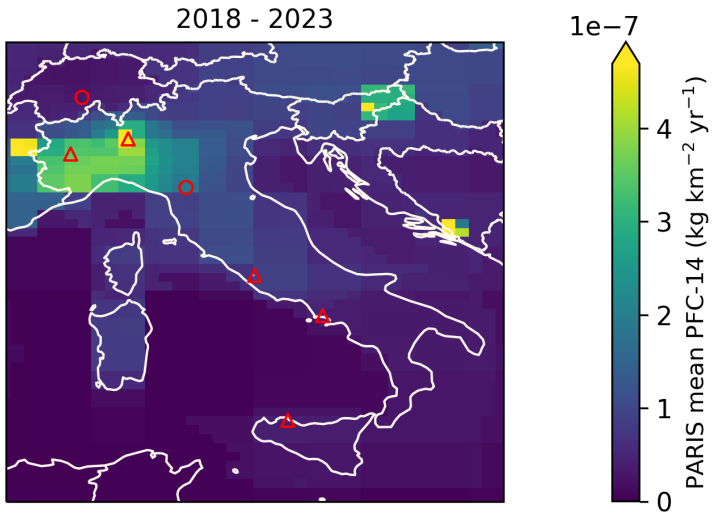

7.2 PFC-116

Figure 7.2.1: Verification of the Italian emissions inventory estimates for PFC-116. Modelled annual emissions are given as the mean from all models (black line and grey shading) and the individual result from InTEM (blue line and shading). National inventory annual totals are given as grey bars.

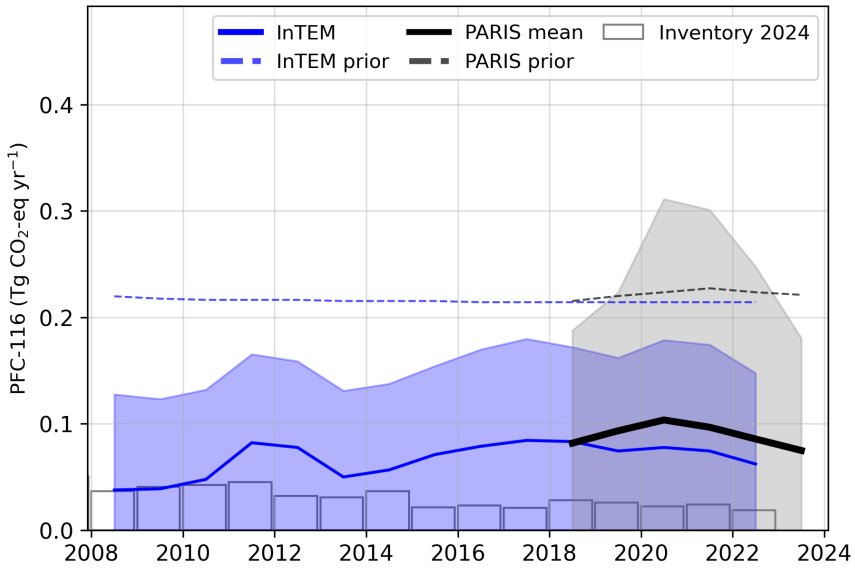

Figure 7.2.2: Spatial distribution of the Italian average modelled emissions of PFC-116 during the period of 2018-2023 (mean from all models). Observing stations are marked with red circles and highly-populated cities are marked with red triangles.

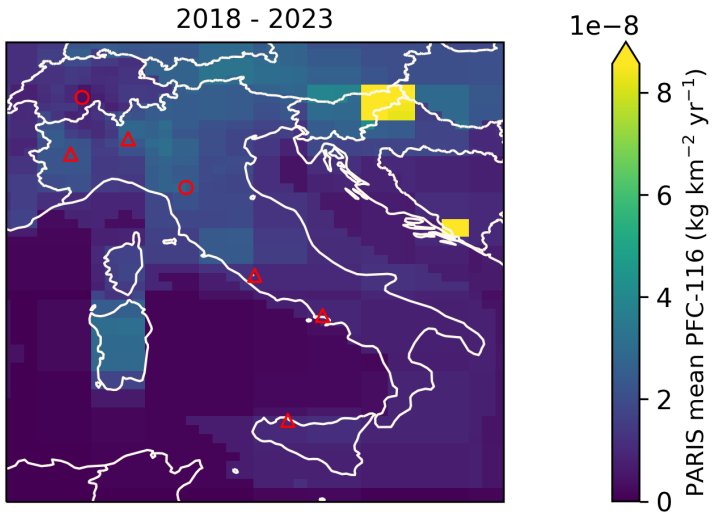

7.3 PFC-218

Figure 7.3.1: Verification of the Italian emissions inventory estimates for PFC-218. Modelled annual emissions are given as the mean from all models (black line and grey shading) and the individual result from InTEM (blue line and shading). National inventory annual totals are given as grey bars.

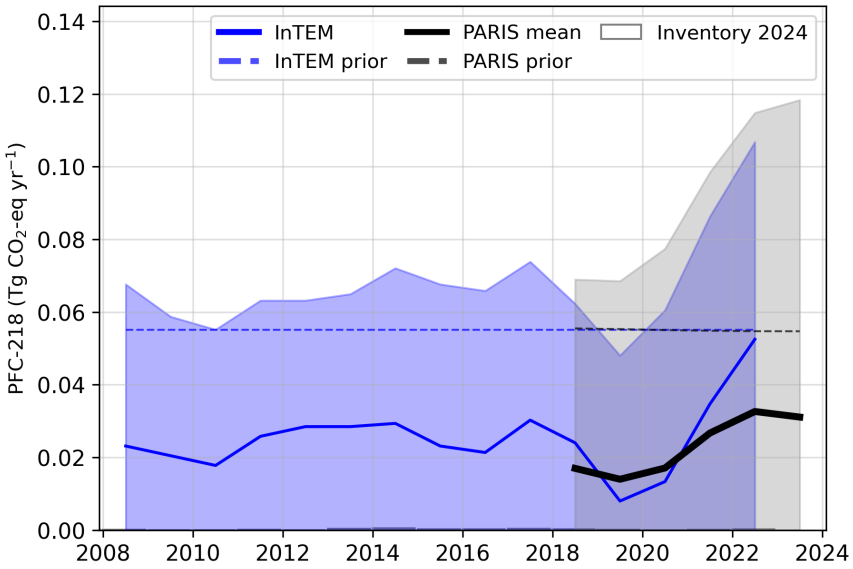

Figure 7.3.2: Spatial distribution of the Italian average modelled emissions of PFC-218 during the period of 2018-2023 (mean from all models). Observing stations are marked with red circles and highly-populated cities are marked with red triangles.

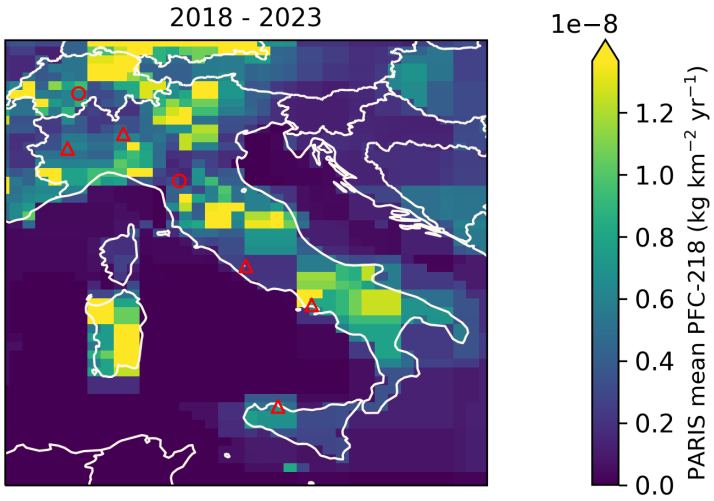

7.4 PFC-318

Figure 7.4.1: Verification of the Italian emissions inventory estimates for PFC-318. Modelled annual emissions are given as the mean from all models (black line and grey shading) and the individual result from InTEM (blue line and shading). National inventory annual totals are given as grey bars.

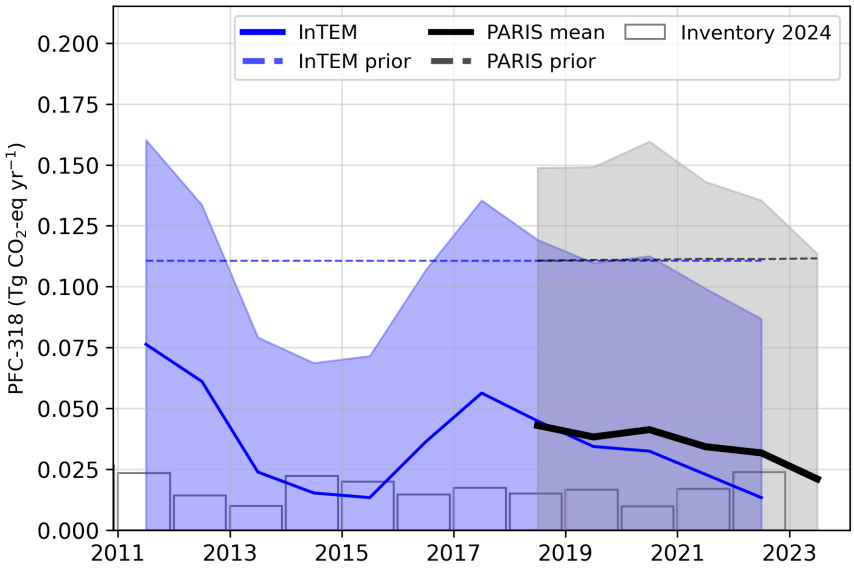

Figure 7.4.2: Spatial distribution of the Italian average modelled emissions of PFC-318 during the period of 2018-2023 (mean from all models). Observing stations are marked with red circles and highly-populated cities are marked with red triangles.

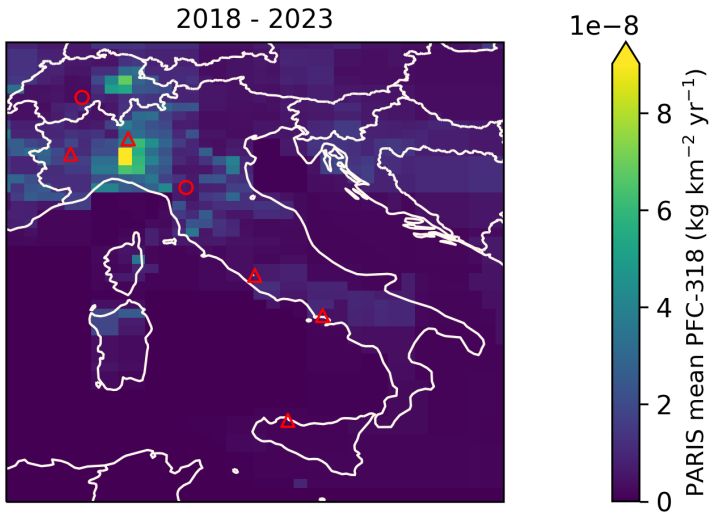

7.5 Total PFCs

Figure 7.5.1: Verification of the Italian emissions inventory estimates for total PFCs. Modelled annual emissions are given as the mean from all models (black line and grey shading) and the individual result from InTEM (blue line and shading). National inventory annual totals are given as grey bars.

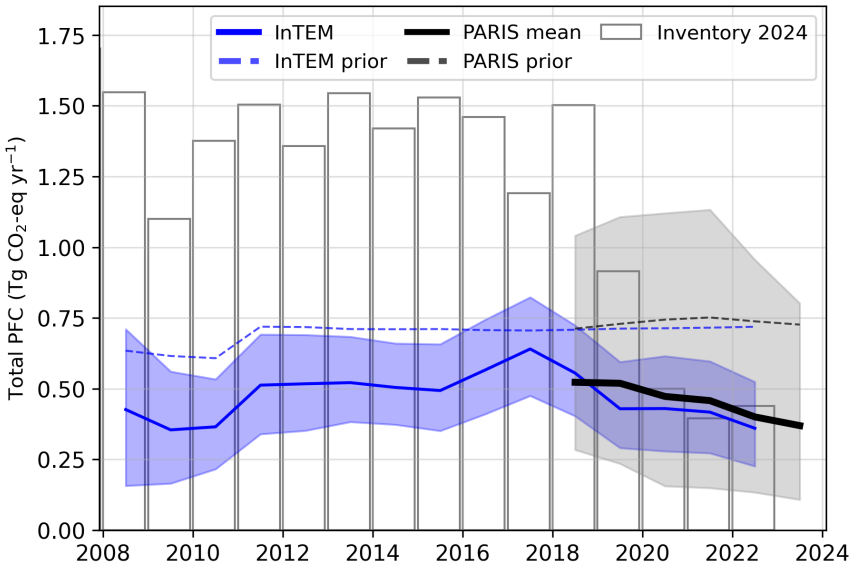

Table 3: Emissions estimation for PFCs in $\mathrm{TgCO_2{-}eq \cdot yr^{-1}}$ according to the National Inventory Report (NIR) 2024 and the inversions done in the PARIS project. For the PARIS estimation, the mean of the 3 inversion models is displayed, along with a range of uncertainty estimated via the half distance between the maximum and minimum uncertainties of the different models.

		2018	2019	2020	2021	2022	2023
PFC-14	NIR 2024	1.46	0.87	0.47	0.35	0.40	
	PARIS mean	0.38 ± 0.36	0.37 ± 0.42	0.31 ± 0.45	0.30 ± 0.47	0.25 ± 0.39	0.24 ± 0.33
PFC-116	NIR 2024	0.03	0.03	0.02	0.02	0.02	
	PARIS mean	0.08 ± 0.09	0.09 ± 0.11	0.10 ± 0.16	0.10 ± 0.15	0.09 ± 0.12	0.07 ± 0.09
PFC-218	NIR 2024	0.00	0.00	0.00	0.00	0.00	
	PARIS mean	0.02 ± 0.03	0.01 ± 0.03	0.02 ± 0.04	0.03 ± 0.05	0.03 ± 0.06	0.03 ± 0.06
PFC-318	NIR 2024	0.02	0.02	0.01	0.02	0.02	
	PARIS mean	0.04 ± 0.07	0.04 ± 0.07	0.04 ± 0.08	0.03 ± 0.07	0.03 ± 0.07	0.02 ± 0.06

References

European Commission: Joint Research, Centre et al. (2023). *GHG emissions of all world countries – 2023*. Publications Office of the European Union. DOI: 10.2760/953322.

Ganesan, A. L. et al. (2014). "Characterization of uncertainties in atmospheric trace gas inversions using hierarchical Bayesian methods". In: *Atmospheric Chemistry and Physics* 14.8, pp. 3855–3864. DOI: 10.5194/acp-14-3855-2014. URL: http://www.atmos-chem-phys.net/14/3855/2014/http://www.atmos-chem-phys.net/14/3855/2014/acp-14-3855-2014.pdf.

Ganesan, A. L. et al. (2015). "Quantifying methane and nitrous oxide emissions from the UK and Ireland using a national-scale monitoring network". In: *Atmos. Chem. Phys.* 15.11, pp. 6393–6406. DOI: 10.5194/acp-15-6393-2015. URL: https://www.atmos-chem-phys.net/15/6393/2015/https://www.atmos-chem-phys.net/15/6393/2015/acp-15-6393-2015.pdf.

Henne, S. et al. (2016). "Validation of the Swiss methane emission inventory by atmospheric observations and inverse modelling". In: *Atmospheric Chemistry and Physics* 16.6, pp. 3683–3710. DOI: 10.5194/acp-16-3683-2016. URL: http://www.atmos-chem-phys.net/16/3683/2016/.

Jones, A.R. et al. (2007). "The U.K. Met Office's next-generation atmospheric dispersion model, NAME III, in Borrego C. and Norman A.-L. (Eds)". In: *Air Pollution Modeling and its Application XVII (Proceedings of the 27th NATO/CCMS International Technical Meeting on Air Pollution Modelling and its Application), Springer*, pp. 580–589.

Katharopoulos, I. et al. (2023). "Impact of transport model resolution and a priori assumptions on inverse modeling of Swiss F-gas emissions". In: *Atmos. Chem. Phys.* 23.22, pp. 14159–14186. DOI: 10.5194/acp-23-14159-2023. URL: https://acp.copernicus.org/articles/23/14159/2023/.

Manning, A. J. et al. (2021). "Evidence of a recent decline in UK emissions of hydrofluorocarbons determined by the InTEM inverse model and atmospheric measurements". In: *Atmospheric Chemistry and Physics* 21.16, pp. 12739–12755. DOI: 10.5194/acp-21-12739-2021. URL: https://acp.copernicus.org/articles/21/12739/2021/.

Rigby, M. et al. (2019). "Increase in CFC-11 emissions from eastern China based on atmospheric observations". In: *Nature* 569, pp. 546–550. DOI: 10.1038/s41586-019-1193-4. URL: https://doi.org/10.1038/s41586-019-1193-4.

Draft Inventory Annex
Netherlands 2024

18th November, 2024

1 Introduction

In this document, global concentration trends and national emissions estimates derived from atmospheric observations ("inverse estimates") are presented for each reported gas. Comparing the emissions submitted in national inventories with those calculated using atmospheric observations allows for emissions to be assessed using two fundamentally different approaches. Substantial differences can highlight areas that could warrant further investigation.

Global concentration trends for each gas are first shown using annual average concentrations from Mace Head, Ireland (Northern Hemisphere) and Kennaook/Cape Grim, Tasmania, Australia (Southern Hemisphere). Data from these stations were selected to exclude regionally-polluted air masses and therefore represents northern and southern hemispheric concentration trends. Mace Head observations were supported by the National Aeronautics and Space Administration (NASA) and the UK Department of Energy, Security and Net Zero (DESNZ), and Kennaook/Cape Grim observations by NASA and the Australian Bureau of Meteorology.

Observations of European concentrations of greenhouse gases used to derive national inverse emission estimates were collected from many different networks and providers. Methane and nitrous oxide concentrations originated from the European ICOS (Integrated Carbon Observation System) network, the UK DECC (Deriving Emissions related to Climate Change) network and other national or individual initiatives. F-gas observations were made by affiliates of the AGAGE (Advanced Global Atmospheric Gases Experiment) network. Observations from from additional stations across Europe were supported by the Horizon-EU PARIS (Process Attribution of Regional Emissions) project. The observation stations used to derive emissions for each gas are shown in the corresponding sections of this document.

Inversion-based emissions estimates were derived using one atmospheric transport model but with multiple inverse models allowing a better quantification of the uncertainties associated with inverse modelling. The atmospheric transport model provides the link between surface fluxes and concentrations measured at the observing stations. Although the uncertainty associated with the atmospheric transport model is considered in the statistical inversion approach, it may be underestimated when only using a single transport model. The atmospheric transport model used is the Numerical Atmospheric dispersion Modelling Environment (NAME) (Jones et al., 2007), a backwards-running Lagrangian Particle Dispersion Model (LPDM) that simulates the recent transport of air to each observing station. The NAME model has been widely used in the estimation of greenhouse gases emissions (Ganesan et al., 2015; Rigby et al., 2019; Manning et al., 2021).

The three inverse methods used are InTEM (Inversion Technique for Emission Modelling, Manning et al., 2021), ELRIS (Empa Lagrangian Regional Inversion System, Henne et al., 2016; Katharopoulos et al., 2023), and RHIME (Regional Hierarchical Inverse Modelling Environment, Ganesan et al., 2014). All three inverse methods estimate emissions within Europe along with boundary conditions that account for the concentration of the air entering Europe. All three systems started from the same set of a priori emissions that were either derived from the global EDGAR emission inventory (version 8, European Commission: Joint Research et al., 2023) or a uniform land-based emission, depending on the gas. A natural emission component, from the WETCHARTS product, was included in the methane prior. The same observational dataset was used by each inverse model, but data selection (i.e., filtering datasets for specific conditions) and treatment of uncertainties were chosen separately and hence differ. The three methods also differ in their statistical approaches for estimating emissions.

Emission estimates are presented for the period 2008-2023. Emissions for the full 2008-2023 period were derived with the InTEM model only, while emissions from 2018-2023 are presented as a combined result using the three inverse models.

For the 2008-2023 InTEM results, a 2-year inversion resolution, incrementing annually, was used for all gases except CH_4nd N_2, where the resolution was monthly. For the recent 2018-2023 period, for all three models, the inversion resolution was one month for CH_4 and N_2O in order to capture the seasonality of the emissions, a one-year average over these results is also presented. For the fluorinated gases, a 1-year

inversion resolution was adopted, with a 3-year moving average applied to the results. The uncertainty shown is the minimum/maximum of the uncertainties from the three results.

2 Global Concentration Trends

2.1 Methane (CH_4)

Figure 2.1.1: Background Northern Hemisphere monthly concentrations of CH_4 estimated from MHD, Ireland observations are shown in red, and background Southern Hemisphere monthly concentrations from CGO, Tasmania are shown in blue. Grey shading represents provisional data.

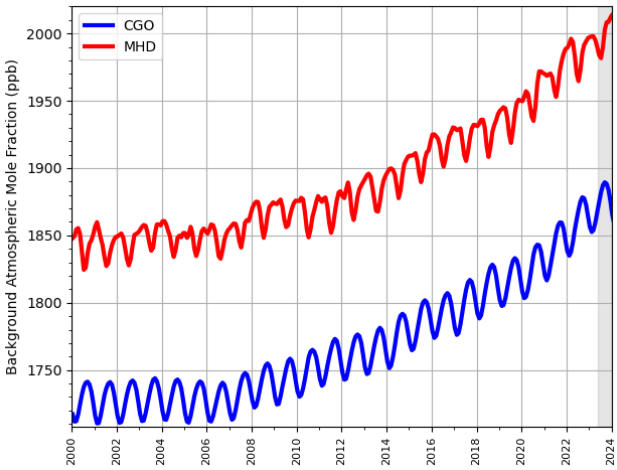

2.2 Nitrous Oxide (N_2O)

Figure 2.2.1: Background Northern Hemisphere monthly concentrations of N_2O estimated from MHD, Ireland observations are shown in red, and background Southern Hemisphere monthly concentrations from CGO, Tasmania are shown in blue. Grey shading represents provisional data.

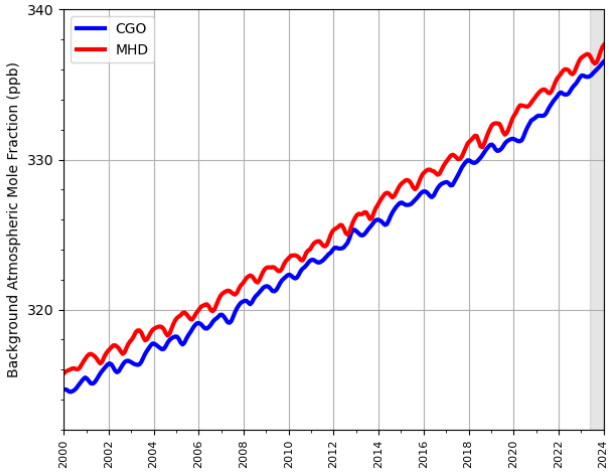

2.3 Hydrofluorocarbons (HFCs)

Figure 2.3.1: Background Northern Hemisphere monthly concentrations of six HFCs estimated from MHD, Ireland observations are shown in red, and background Southern Hemisphere monthly concentrations from CGO, Tasmania are shown in blue. Grey shading represents provisional data.

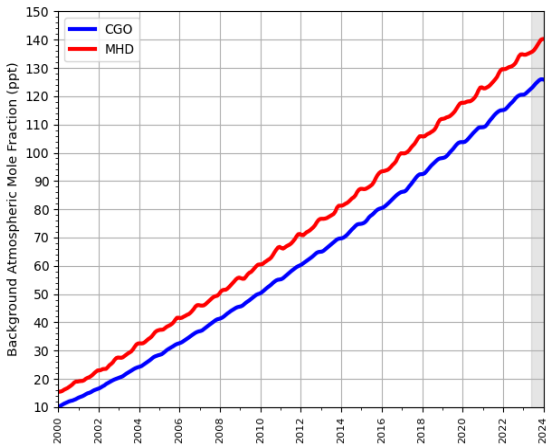

(a) HFC-134a

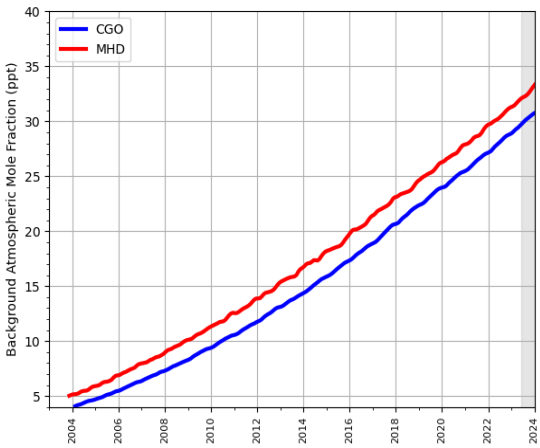

(b) HFC-143a

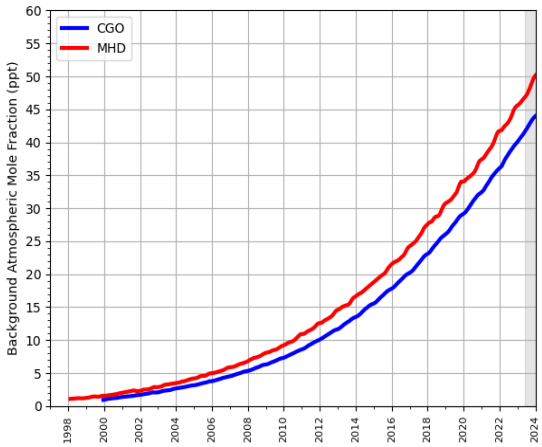

(c) HFC-125

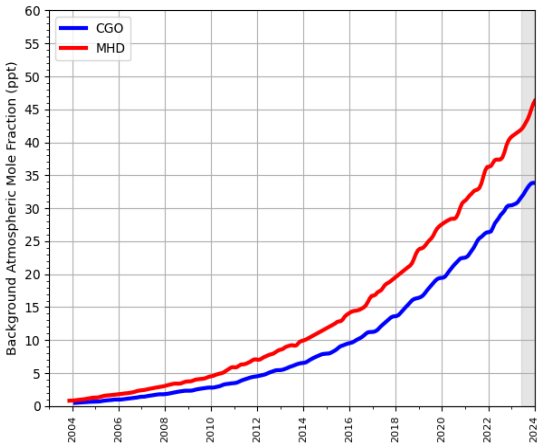

(d) HFC-32

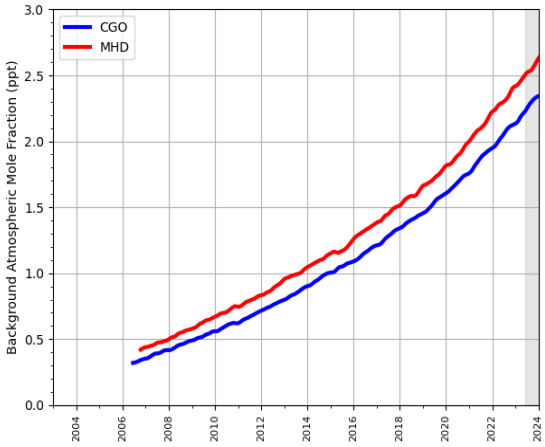

(e) HFC-227ea

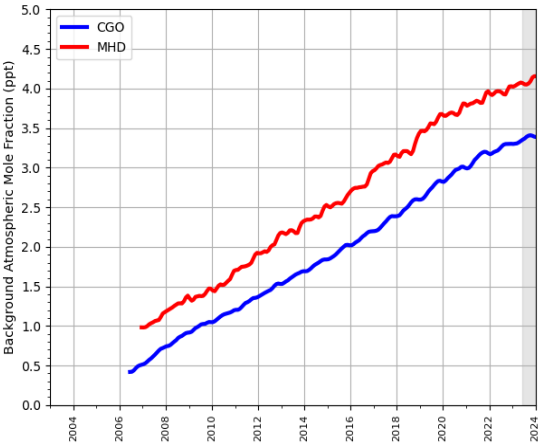

(f) HFC-245fa

Figure 2.3.2: Background Northern Hemisphere monthly concentrations of four HFCs estimated from MHD, Ireland observations are shown in red, and background Southern Hemisphere monthly concentrations from CGO, Tasmania are shown in blue. Grey shading represents provisional data.

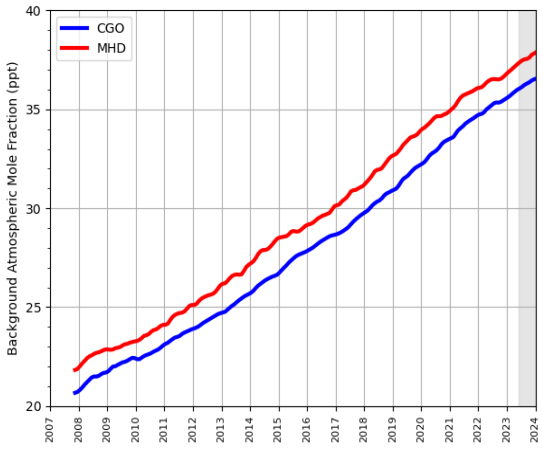

(a) HFC-23

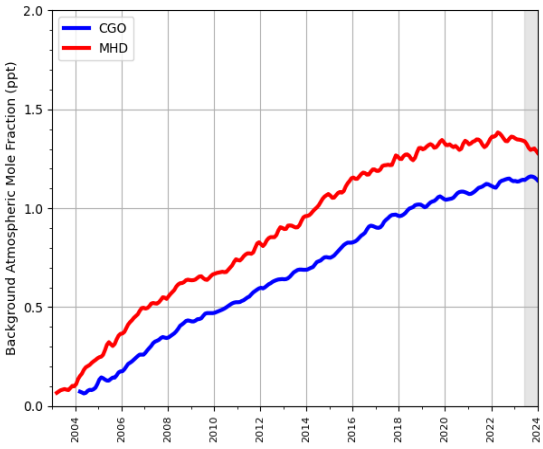

(b) HFC-365mfc

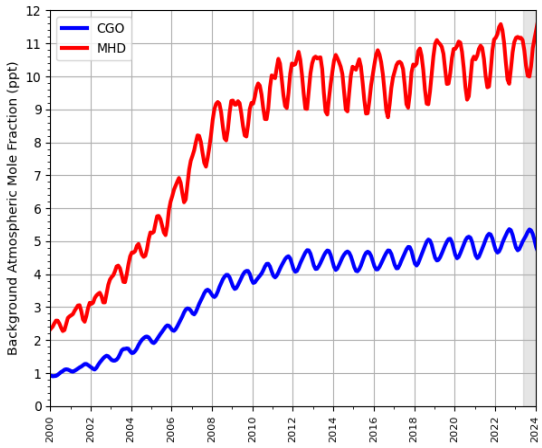

(c) HFC-152a

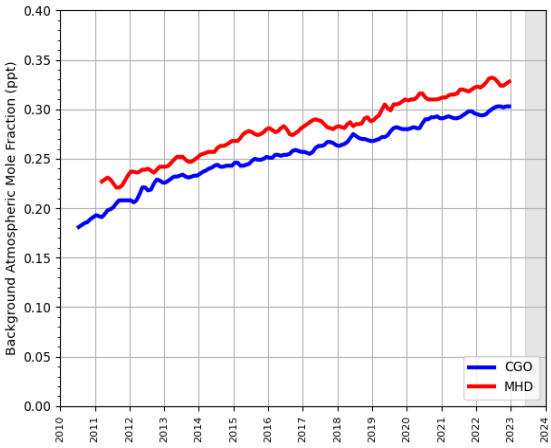

(d) HFC-43-10-mee

2.4 Perfluorocarbons (PFCs)

Figure 2.4.1: Background Northern Hemisphere monthly concentrations of four PFCs estimated from MHD, Ireland observations are shown in red, and background Southern Hemisphere monthly concentrations from CGO, Tasmania are shown in blue. Grey shading represents provisional data.

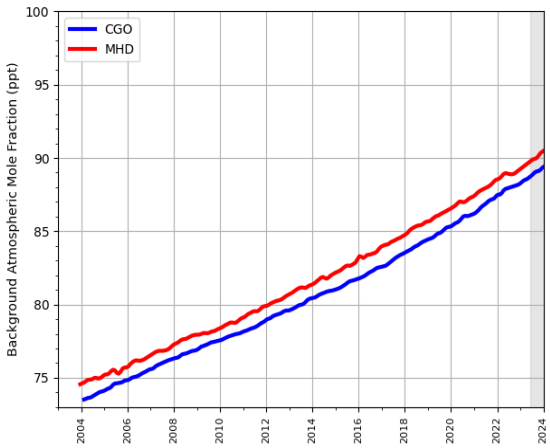

(a) PFC-14

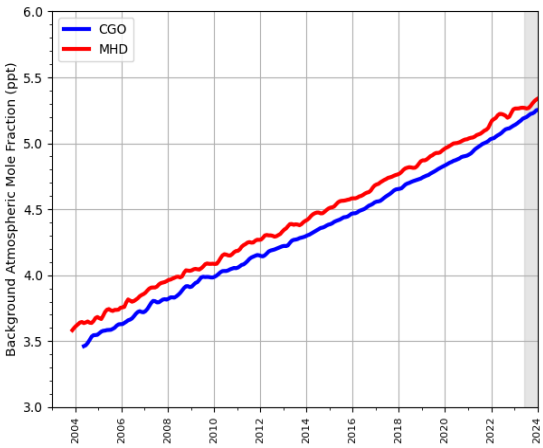

(b) PFC-116

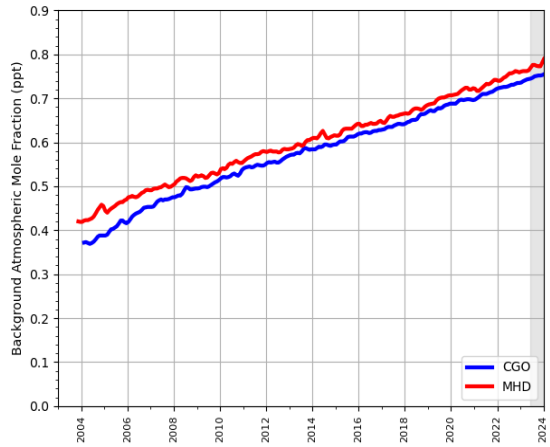

(c) PFC-218

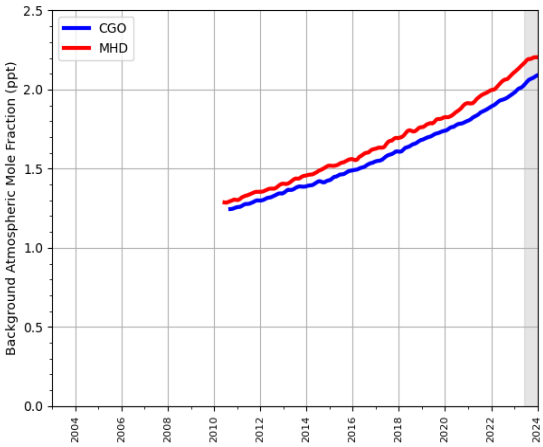

(d) PFC-318

3 Key findings

- Methane (CH_4): Inversion results are around 50 % higher than the inventory estimates. The inclusion of the observations from LUT has a strong impact on the model results and requires further investigation. In most years the inverse models estimate a pronounced seasonal cycle in emissions with the maximum in winter.
- Nitrous oxide (N_2O): Inversion results are around 25 % higher than the inventory estimates. In all years the inverse models estimate a pronounced seasonal cycle in emissions with the maximum in late spring or early summer. Unusual concentrated emissions are estimated in SE Netherlands and in southern Belgium and require further investigation and understanding.
- Hydrofluorocarbons (HFCs): The inverse models generally estimate significantly higher emissions than those reported in the inventory. The decline in recent years in the inventory is not seen in the inverse results, except for HFC-143a, although the inverse model uncertainties are high. The inverse model emissions are concentrated to the SW of the Netherlands. Note, the InTEM-only estimates use Cabauw observations from 2021 and are estimated over two-year periods.
- Perfluorocarbons (PFCs): The inverse results reveal some notable areas of emission, in the SE for PFC-14 and PFC-116 and in the SW for PFC-318. The inverse model resolution means that it is difficult for them to correctly allocate these emissions to a specific country. The inverse model estimates are higher than those reported in the inventory although the uncertainties are very high. Note, the InTEM-only estimates use Cabauw observations from 2021 and are estimated over two-year periods.
- Sulphur hexafluoride (SF_6): The inverse model estimates reveal a significant source in the SW of the Netherlands or western Germany close to the border, given the resolution of the models it is not possible, currently, to be more precise. The trend estimated by the inversions is too uncertain to be reliable at the moment, data from future years will make this clearer.

Table 1: Emissions estimation for the main greenhouse gases of focus in $\mathrm{TgCO_2{-}eq \cdot yr^{-1}}$ according to the National Inventory Report (NIR) 2024 and the inversions done in the PARIS project. For the PARIS estimation, the mean of the 3 inversion models is displayed, along with a range of uncertainty estimated via the half distance between the maximum and minimum uncertainties of the different models.

		2018	2019	2020	2021	2022	2023
CH_4	NIR 2024	20	20	19	19	19	
	PARIS mean	30 ± 4	31 ± 3	30 ± 4	31 ± 5	32 ± 4	32 ± 3
N_2O	NIR 2024	8	8	7	7	7	
	PARIS mean	10 ± 2	11 ± 2	11 ± 2	11 ± 2	10 ± 2	10 ± 1
Total HFCs[(1)]	NIR 2024	1.1	1.1	0.9	1.0	0.9	
	PARIS mean	3.0 ± 0.8	2.7 ± 0.8	2.3 ± 0.8	2.4 ± 0.9	2.8 ± 0.9	3.0 ± 0.9
Total PFCs[(2)]	NIR 2024	0.0	0.0	0.0	0.0	0.0	
	PARIS mean	0.1 ± 0.1	0.1 ± 0.1	0.1 ± 0.1	0.1 ± 0.1	0.1 ± 0.1	0.1 ± 0.1
SF_6	NIR 2024	0.1	0.1	0.1	0.1	0.1	
	PARIS mean	0.1 ± 0.1	0.1 ± 0.1	0.1 ± 0.1	0.1 ± 0.1	0.1 ± 0.1	0.2 ± 0.2

(1) Sum of HFC emissions presented in Table 2, except HFC-4310mee.
(2) Sum of PFC emissions presented in Table 3.

4 Methane (CH_4)

Figure 4.0.1: Total source sensitivity of CH_4 observing sites as calculated by the NAME transport model for the year (left) 2018 and (right) 2023 and used in the inversions. Observing stations active in each year are marked with red dots. Areas with visible land surface represent regions for which emissions can be observed well from the network. Shaded or dark areas represent regions for which limited emission information can be obtained from the network.

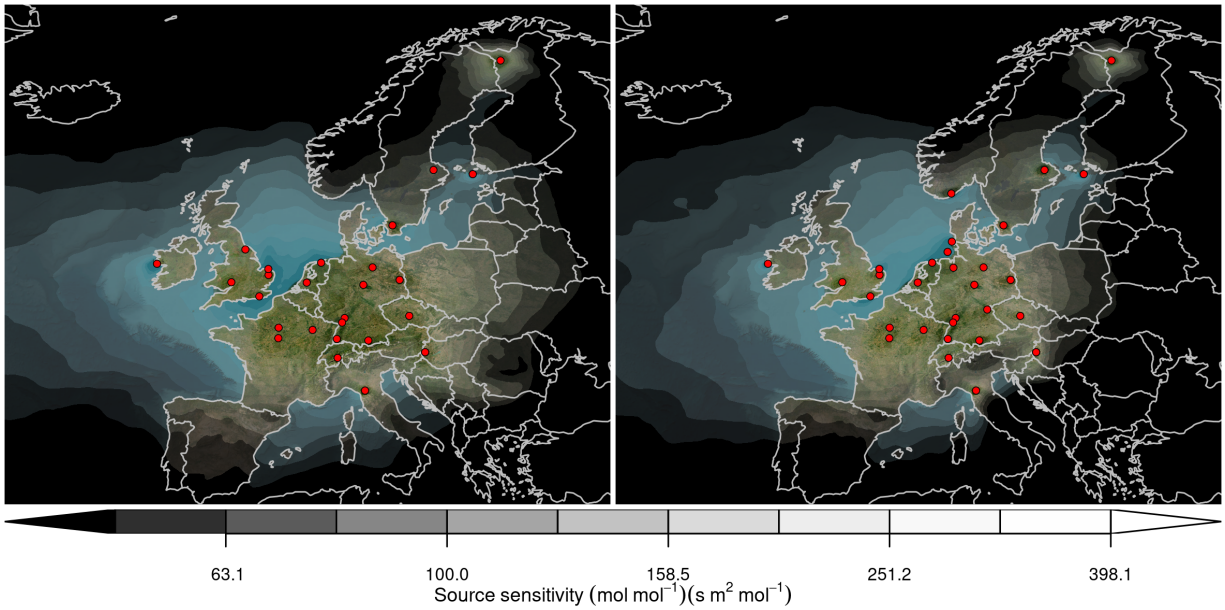

Figure 4.0.2: Verification of the Dutch emissions inventory estimates for CH_4. Modelled annual emissions are given as the mean from all models (black line and grey shading) and the individual result from InTEM (blue line and shading). National inventory annual totals are given as grey bars.

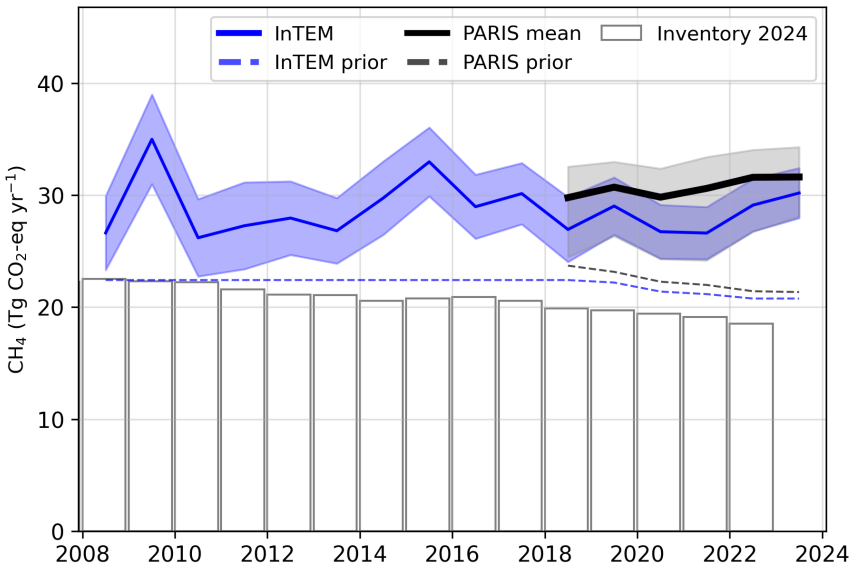

Figure 4.0.3: Verification of the Dutch emissions inventory estimates for CH_4 (zoom in to 2018-2023). Modelled annual emissions are given as the mean from all models (black line and grey shading) and the individual result from InTEM (blue line and shading). National inventory annual totals are given as grey bars.

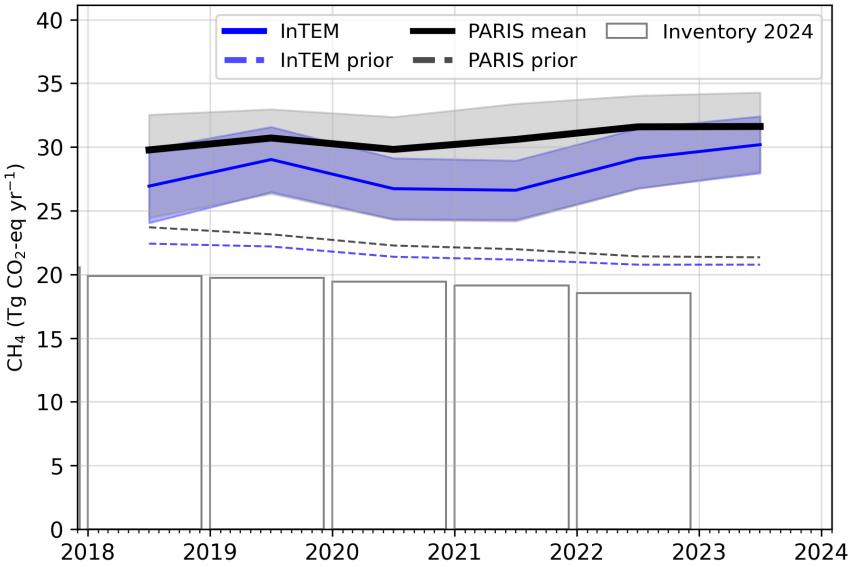

Figure 4.0.4: Verification of the Dutch emissions inventory estimates for CH_4 (zoom in to 2018-2023). Modelled monthly emissions are given as the mean from all models (black line and grey shading) and the individual result from InTEM (blue line and shading). National inventory annual totals are given as grey bars.

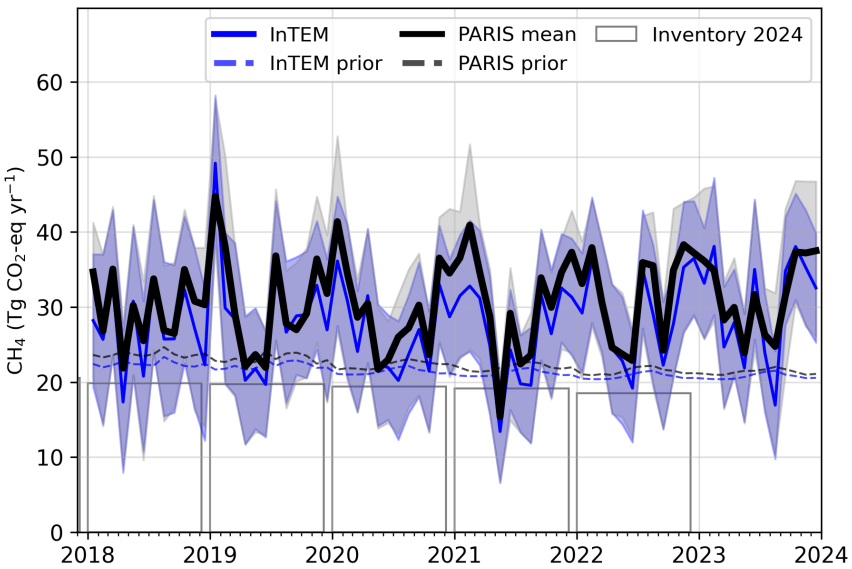

Figure 4.0.5: Spatial distribution of the Dutch average modelled emissions of CH_4 during the period of 2018-2023 (mean from all models). Observing stations are marked with red circles and highly-populated cities are marked with red triangles.

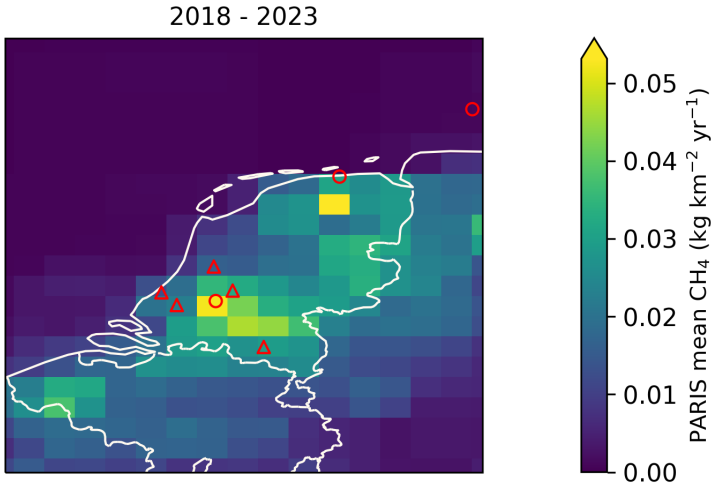

Figure 4.0.6: Spatial distribution of the seasonal deviation from the mean. The deviation is defined as the modelled Dutch seasonally averaged CH_4 emissions over 2018-2023 minus the average over the whole period. The mean across all models is shown. Observing stations are marked with red circles and highly-populated cities are marked with red triangles.

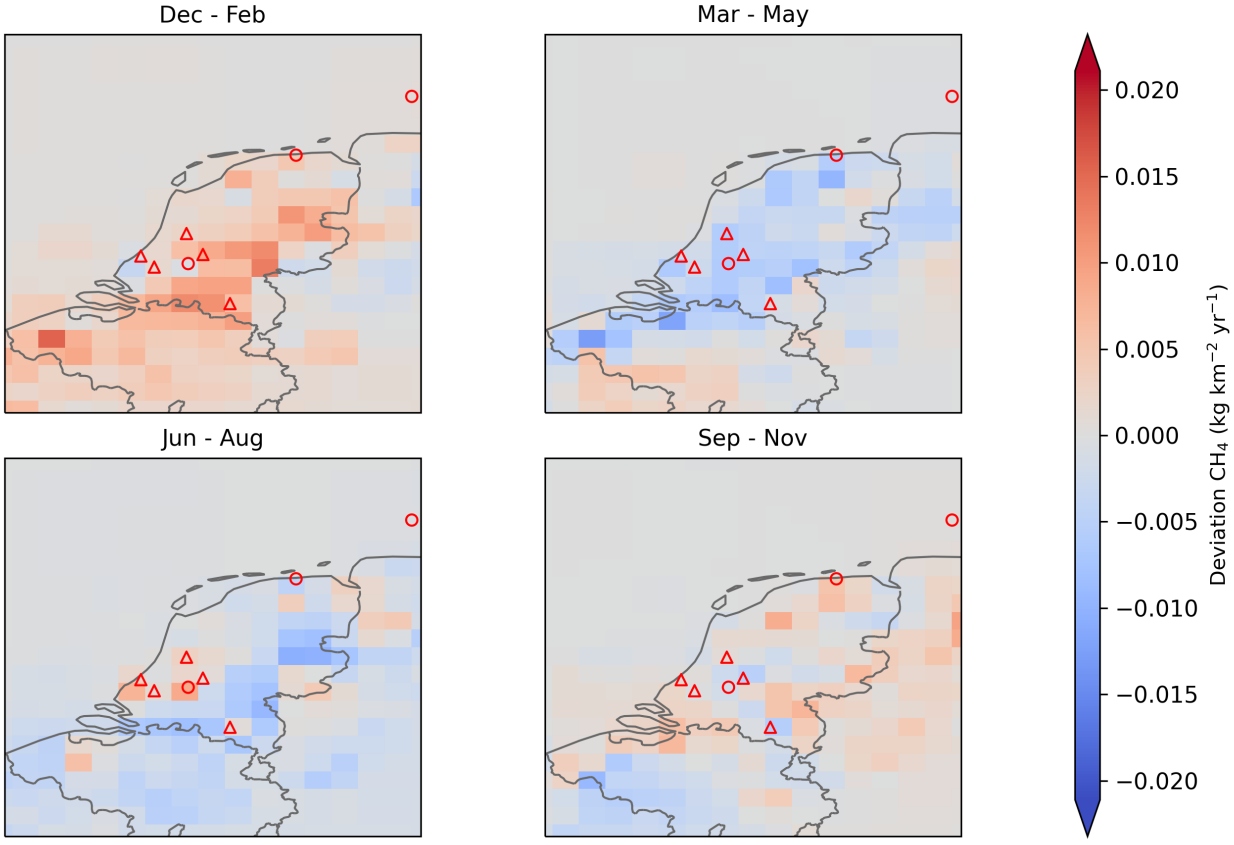

5 Nitrous Oxide (N_2O)

Figure 5.0.1: Total source sensitivity of N_2O observing sites as calculated by the NAME transport model for the year (left) 2018 and (right) 2023 and used in the inversions. Observing stations active in each year are marked with red dots. Areas with visible land surface represent regions for which emissions can be observed well from the network. Shaded or dark areas represent regions for which limited emission information can be obtained from the network.

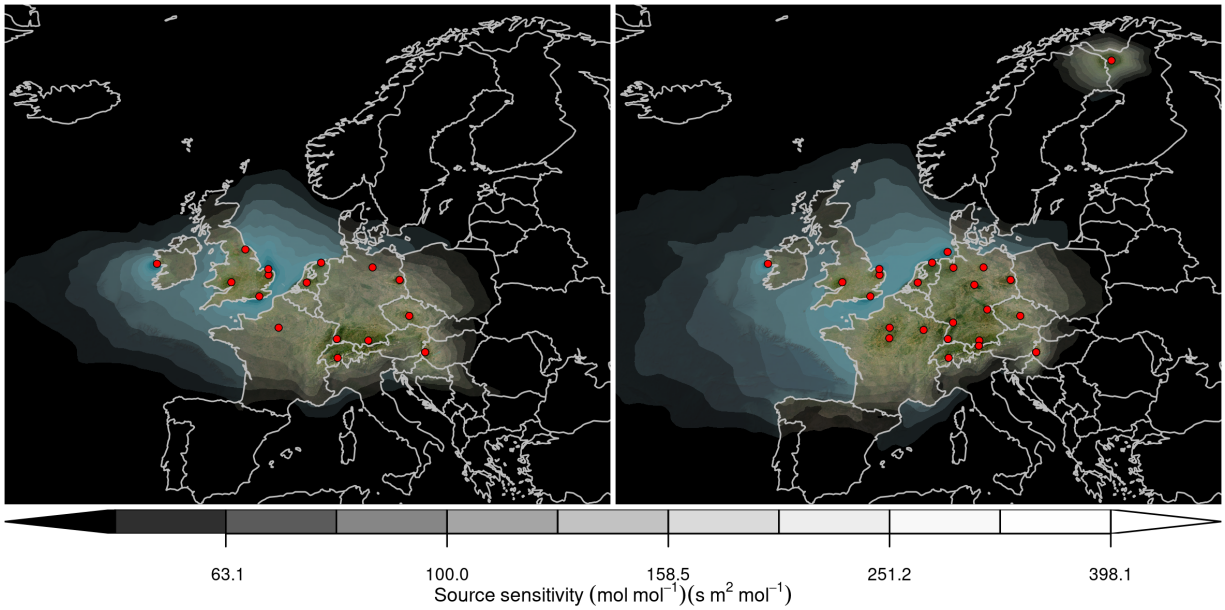

Figure 5.0.2: Verification of the Dutch emissions inventory estimates for N_2O. Modelled annual emissions are given as the mean from all models (black line and grey shading) and the individual result from InTEM (blue line and shading). National inventory annual totals are given as grey bars.

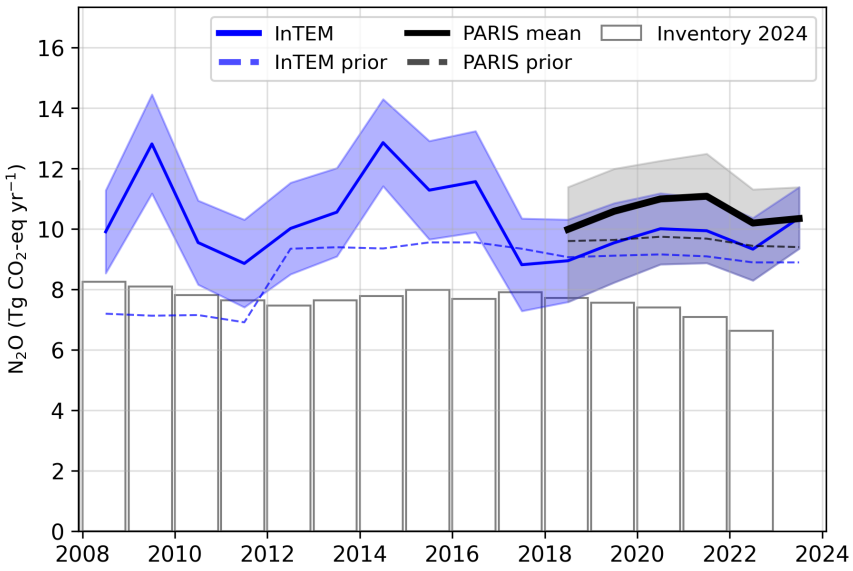

Figure 5.0.3: Verification of the Dutch emissions inventory estimates for N_2O (zoom in to 2018-2023). Modelled annual emissions are given as the mean from all models (black line and grey shading) and the individual result from InTEM (blue line and shading). National inventory annual totals are given as grey bars.

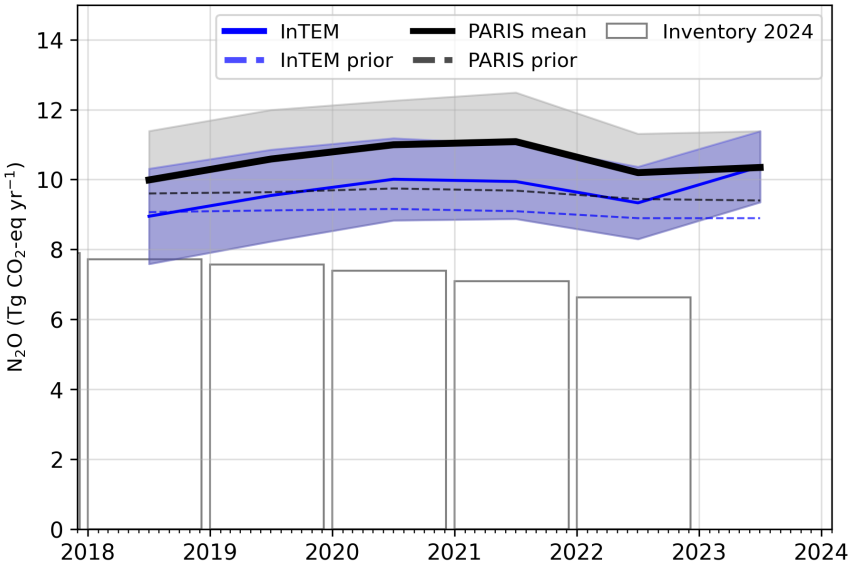

Figure 5.0.4: Verification of the Dutch emissions inventory estimates for N_2O (zoom in to 2018-2023). Modelled monthly emissions are given as the mean from all models (black line and grey shading) and the individual result from InTEM (blue line and shading). National inventory annual totals are given as grey bars.

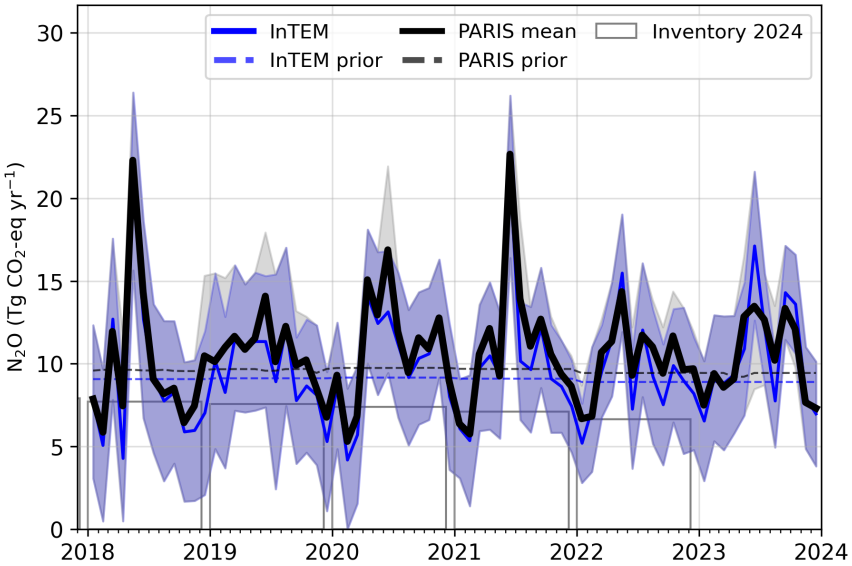

Figure 5.0.5: Spatial distribution of the Dutch average modelled emissions of N_2O during the period of 2018-2023 (mean from all models). Observing stations are marked with red circles and highly-populated cities are marked with red triangles.

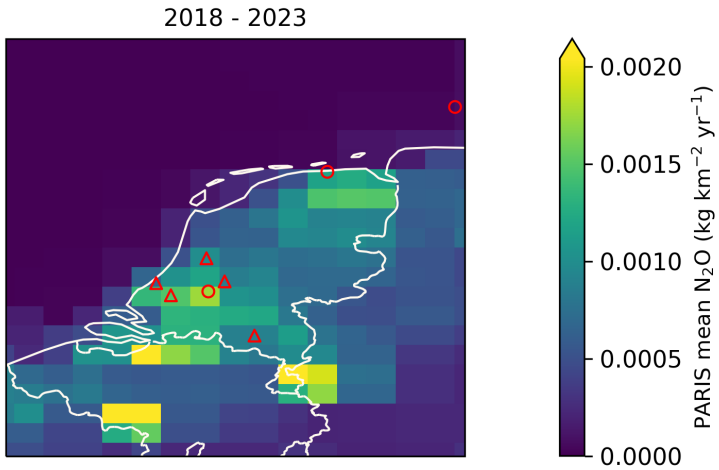

Figure 5.0.6: Spatial distribution of the seasonal deviation from the mean. The deviation is defined as the modelled Dutch seasonally averaged N_2O emissions over 2018-2023 minus the average over the whole period. The mean across all models is shown. Observing stations are marked with red circles and highly-populated cities are marked with red triangles.

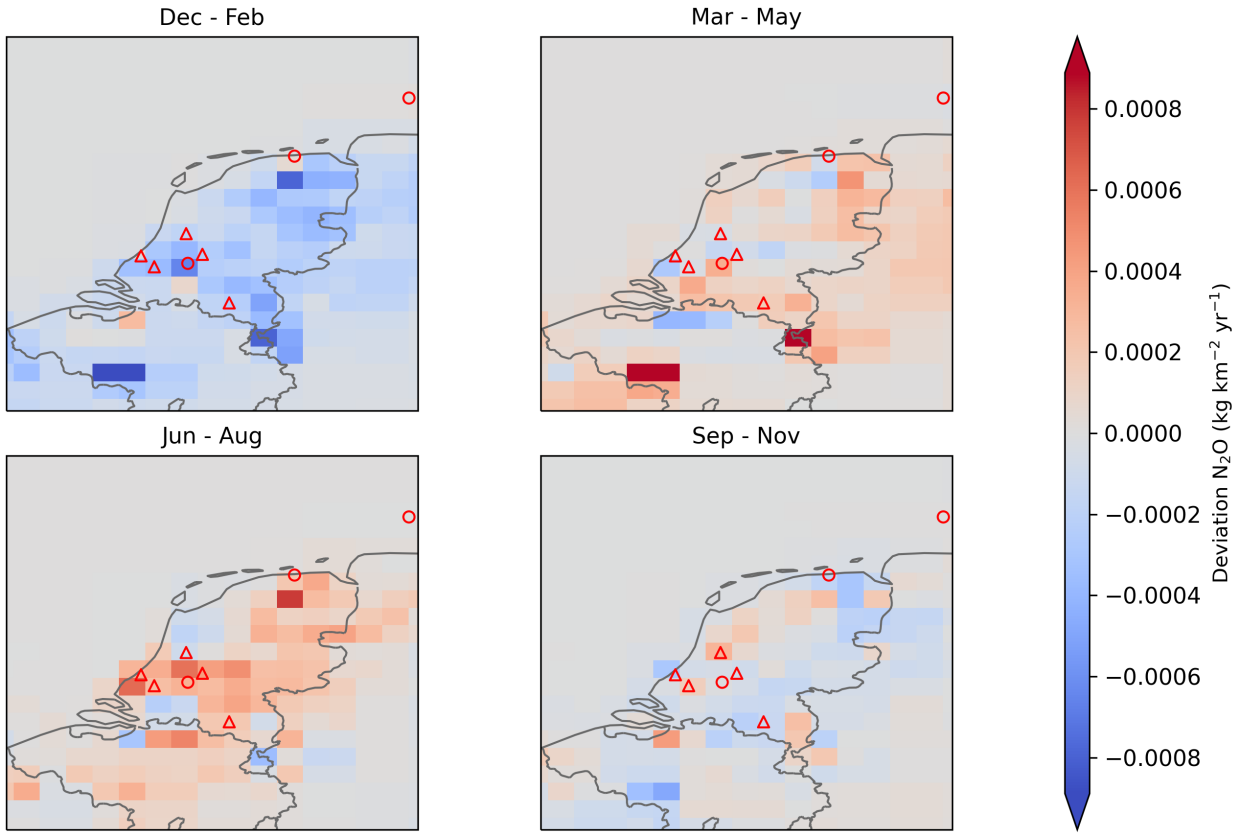

6 Hydrofluorocarbons (HFCs)

Figure 6.0.1: Total source sensitivity of HFCs/PFCs observing sites as calculated by the NAME transport model for the year (left) 2018 and (right) 2023 and used in the inversions. Observing stations active in each year are marked with red dots. Areas with visible land surface represent regions for which emissions can be observed well from the network. Shaded or dark areas represent regions for which limited emission information can be obtained from the network.

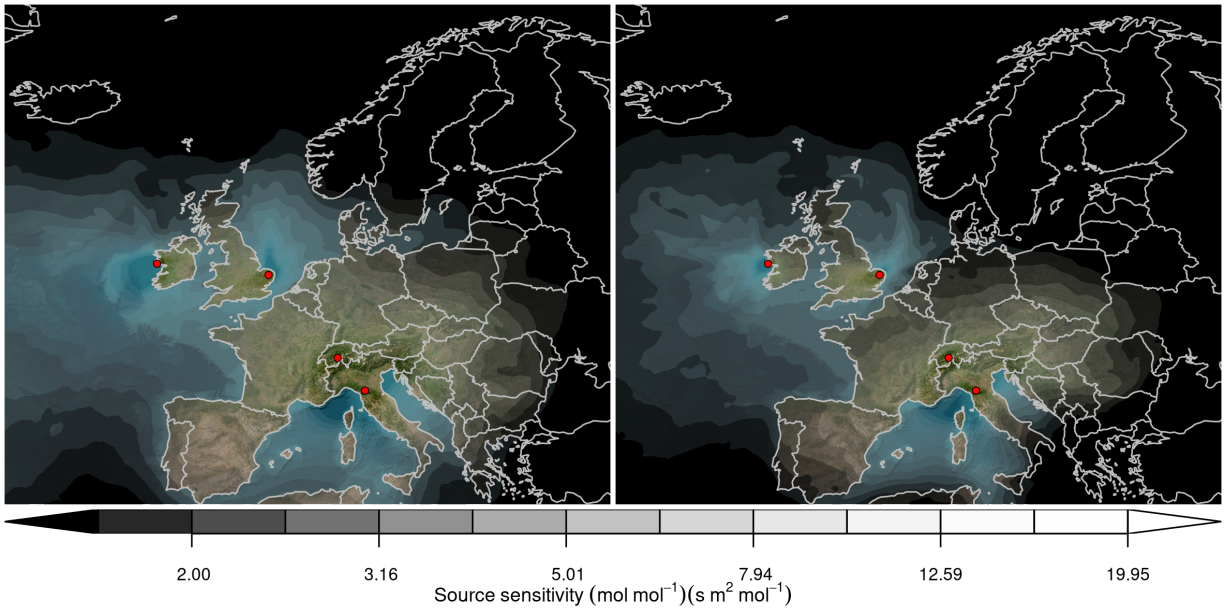

6.1 HFC-32

Figure 6.1.1: Verification of the Dutch emissions inventory estimates for HFC-32. Modelled annual emissions are given as the mean from all models (black line and grey shading) and the individual result from InTEM (blue line and shading). National inventory annual totals are given as grey bars.

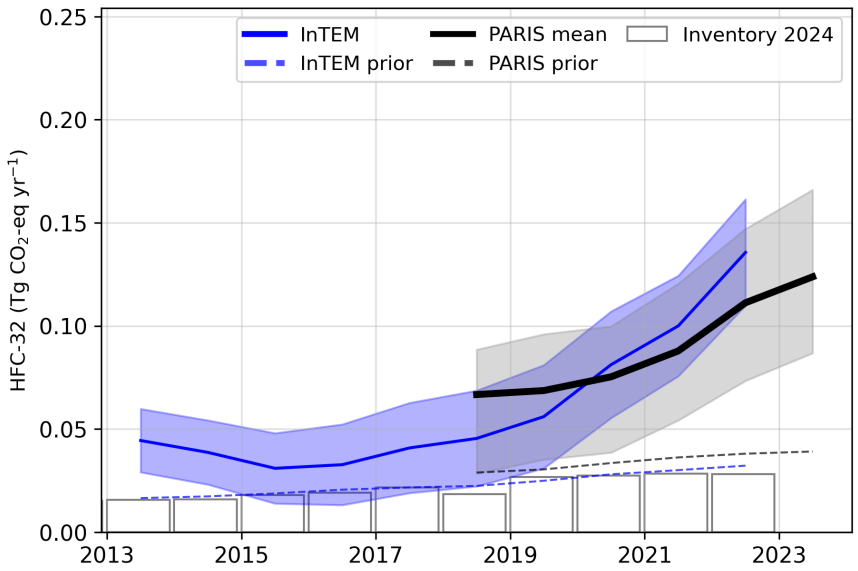

Figure 6.1.2: Spatial distribution of the Dutch average modelled emissions of HFC-32 during the period of 2018-2023 (mean from all models). Observing stations are marked with red circles and highly-populated cities are marked with red triangles.

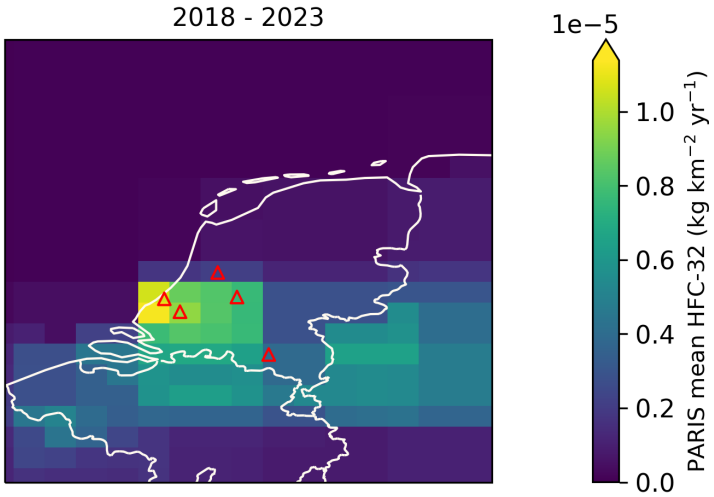

6.2 HFC-125

Figure 6.2.1: Verification of the Dutch emissions inventory estimates for HFC-125. Modelled annual emissions are given as the mean from all models (black line and grey shading) and the individual result from InTEM (blue line and shading). National inventory annual totals are given as grey bars.

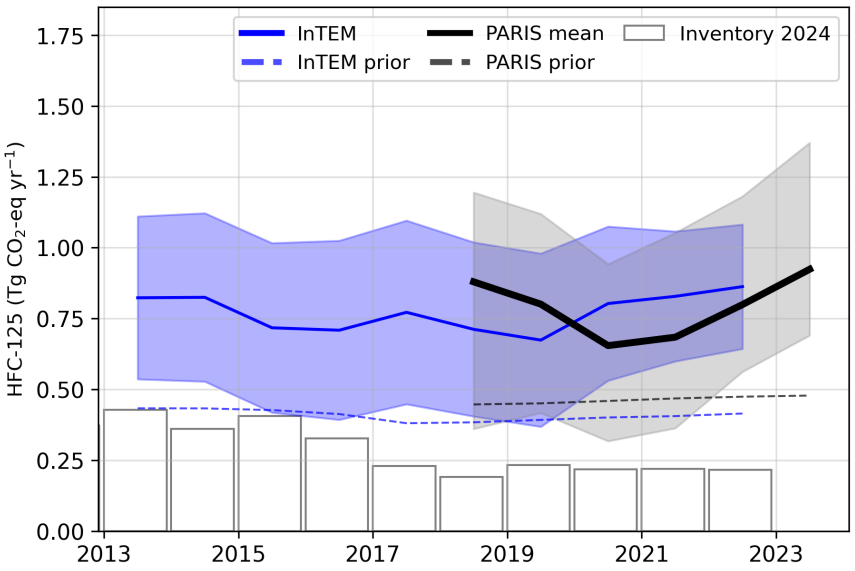

Figure 6.2.2: Spatial distribution of the Dutch average modelled emissions of HFC-125 during the period of 2018-2023 (mean from all models). Observing stations are marked with red circles and highly-populated cities are marked with red triangles.

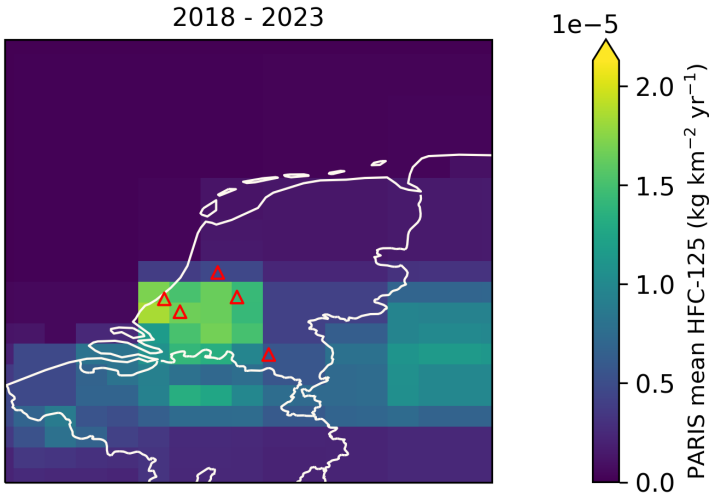

6.3 HFC-134a

Figure 6.3.1: Verification of the Dutch emissions inventory estimates for HFC-134a. Modelled annual emissions are given as the mean from all models (black line and grey shading) and the individual result from InTEM (blue line and shading). National inventory annual totals are given as grey bars.

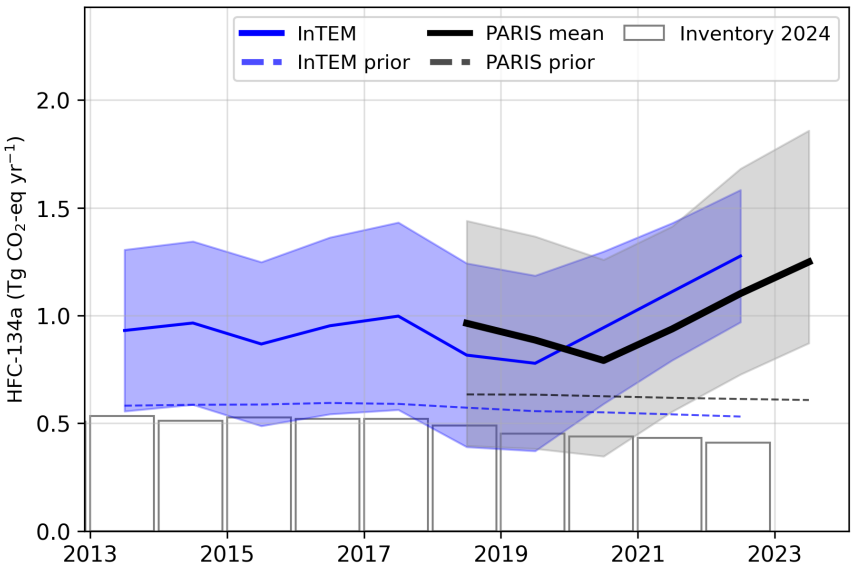

Figure 6.3.2: Spatial distribution of the Dutch average modelled emissions of HFC-134a during the period of 2018-2023 (mean from all models). Observing stations are marked with red circles and highly-populated cities are marked with red triangles.

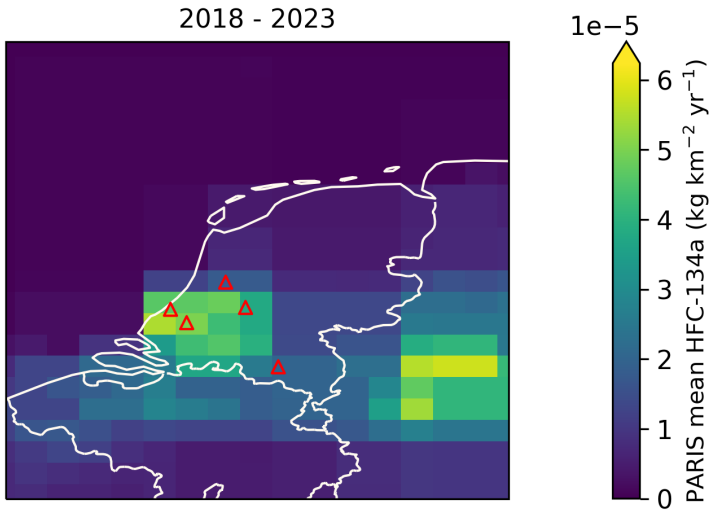

6.4 HFC-143a

Figure 6.4.1: Verification of the Dutch emissions inventory estimates for HFC-143a. Modelled annual emissions are given as the mean from all models (black line and grey shading) and the individual result from InTEM (blue line and shading). National inventory annual totals are given as grey bars.

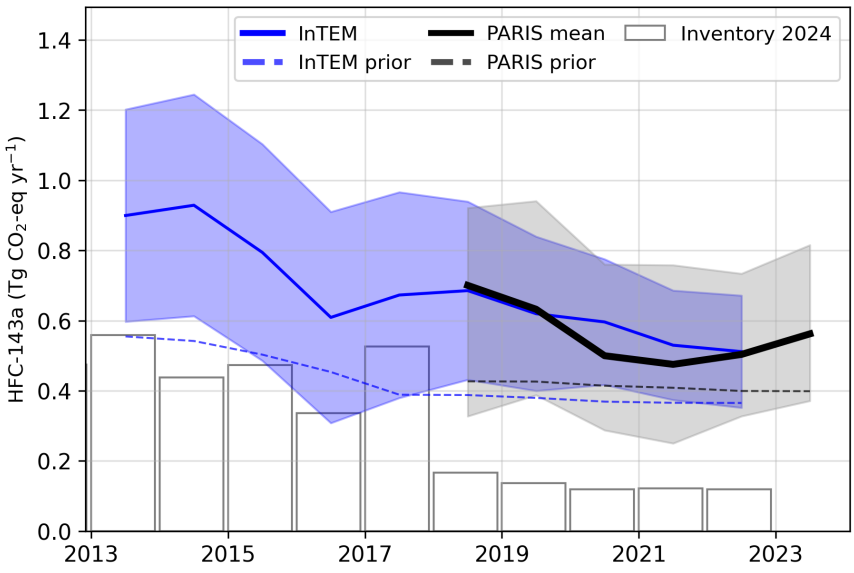

Figure 6.4.2: Spatial distribution of the Dutch average modelled emissions of HFC-143a during the period of 2018-2023 (mean from all models). Observing stations are marked with red circles and highly-populated cities are marked with red triangles.

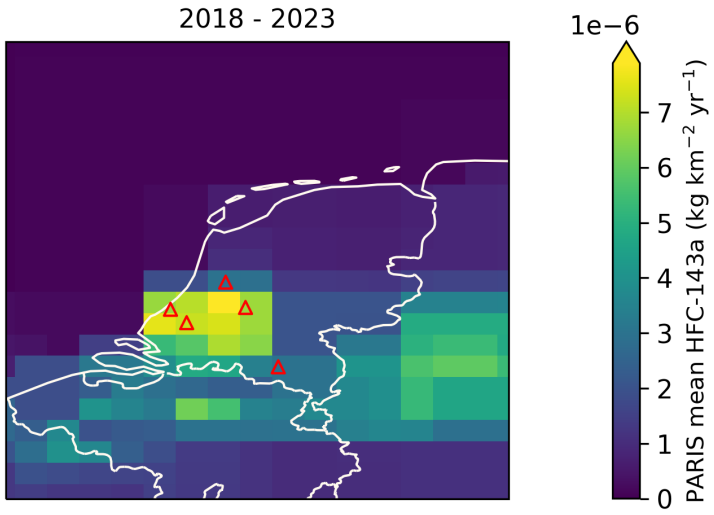

6.5 Total HFCs

Figure 6.5.1: Verification of the Dutch emissions inventory estimates for total HFCs. Modelled annual emissions are given as the mean from all models (black line and grey shading) and the individual result from InTEM (blue line and shading). National inventory annual totals are given as grey bars.

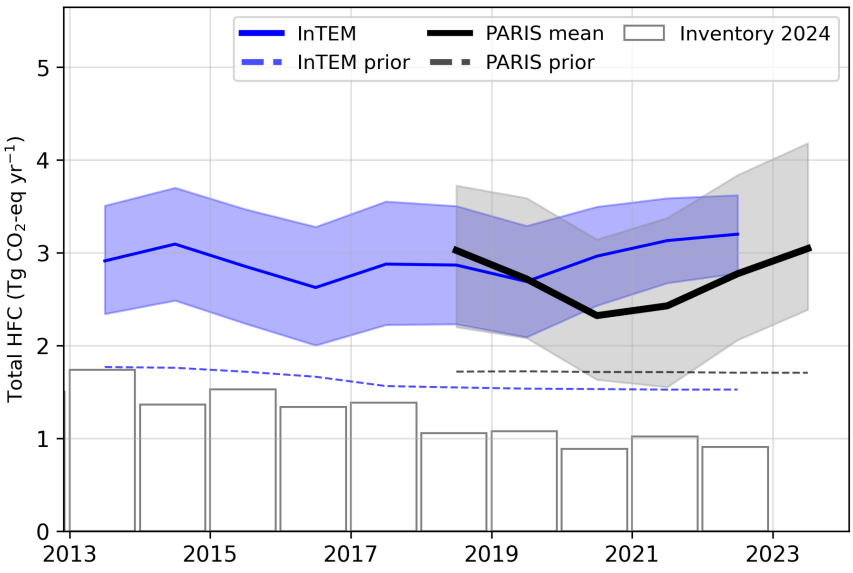

Table 2: Emissions estimation for HFCs in $\mathrm{TgCO_2{-}eq \cdot yr^{-1}}$ according to the National Inventory Report (NIR) 2024 and the inversions done in the PARIS project. For the PARIS estimation, the mean of the 3 inversion models is displayed, along with a range of uncertainty estimated via the half distance between the maximum and minimum uncertainties of the different models.

		2018	2019	2020	2021	2022	2023
HFC-23	NIR 2024	0.19	0.23	0.08	0.22	0.13	
	PARIS mean	0.27 ± 0.37	0.19 ± 0.30	0.19 ± 0.30	0.12 ± 0.27	0.16 ± 0.32	0.10 ± 0.27
HFC-32	NIR 2024	0.02	0.03	0.03	0.03	0.03	
	PARIS mean	0.07 ± 0.03	0.07 ± 0.03	0.08 ± 0.03	0.09 ± 0.03	0.11 ± 0.04	0.12 ± 0.04
HFC-125	NIR 2024	0.19	0.23	0.22	0.22	0.22	
	PARIS mean	0.88 ± 0.42	0.80 ± 0.35	0.65 ± 0.31	0.68 ± 0.34	0.80 ± 0.31	0.92 ± 0.34
HFC-134a	NIR 2024	0.49	0.45	0.44	0.43	0.41	
	PARIS mean	0.96 ± 0.52	0.89 ± 0.49	0.79 ± 0.46	0.94 ± 0.43	1.10 ± 0.48	1.25 ± 0.49
HFC-143a	NIR 2024	0.17	0.14	0.12	0.12	0.12	
	PARIS mean	0.70 ± 0.30	0.63 ± 0.28	0.50 ± 0.24	0.48 ± 0.25	0.50 ± 0.20	0.56 ± 0.22
HFC-152a	NIR 2024	0.00	0.00	0.00	0.00	0.00	
	PARIS mean	0.00 ± 0.00	0.00 ± 0.00	0.00 ± 0.00	0.00 ± 0.00	0.00 ± 0.00	0.00 ± 0.00
HFC-227ea	NIR 2024	0.00	0.00	0.00	0.00	0.00	
	PARIS mean	0.08 ± 0.07	0.08 ± 0.07	0.07 ± 0.06	0.07 ± 0.06	0.05 ± 0.05	0.05 ± 0.04
HFC-245fa	NIR 2024	0.00	0.00	0.00	0.00	0.00	
	PARIS mean	0.03 ± 0.02	0.03 ± 0.02	0.02 ± 0.02	0.02 ± 0.01	0.02 ± 0.01	0.02 ± 0.01
HFC-365mfc	NIR 2024	0.00	0.00	0.00	0.00	0.00	
	PARIS mean	0.03 ± 0.02	0.03 ± 0.02	0.02 ± 0.02	0.03 ± 0.02	0.02 ± 0.02	0.02 ± 0.01
HFC-4310mee	NIR 2024	0.00	0.00	0.00	0.00	0.00	
	PARIS mean	0.00 ± 0.01	0.00 ± 0.01	0.00 ± 0.00	0.00 ± 0.00	0.00 ± 0.00	[1]

[1] HFC-4310mee emissions were not estimated for 2023 due to lack of atmospheric observations.

7 Perfluorocarbons (PFCs)

7.1 PFC-14

Figure 7.1.1: Verification of the Dutch emissions inventory estimates for PFC-14. Modelled annual emissions are given as the mean from all models (black line and grey shading) and the individual result from InTEM (blue line and shading). National inventory annual totals are given as grey bars.

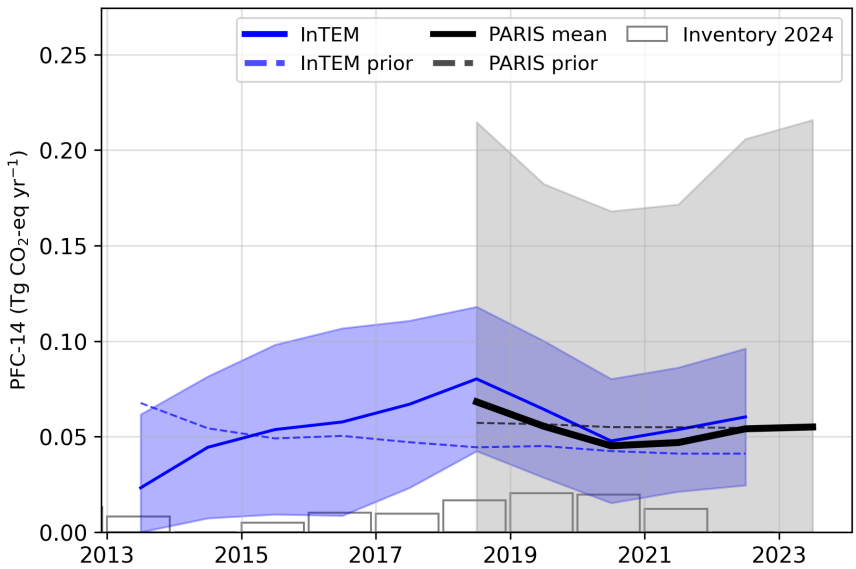

Figure 7.1.2: Spatial distribution of the Dutch average modelled emissions of PFC-14 during the period of 2018-2023 (mean from all models). Observing stations are marked with red circles and highly-populated cities are marked with red triangles.

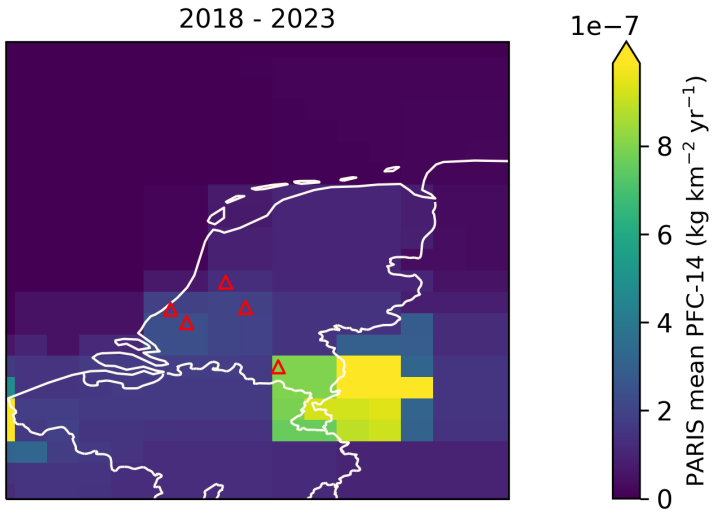

7.2 PFC-116

Figure 7.2.1: Verification of the Dutch emissions inventory estimates for PFC-116. Modelled annual emissions are given as the mean from all models (black line and grey shading) and the individual result from InTEM (blue line and shading). National inventory annual totals are given as grey bars.

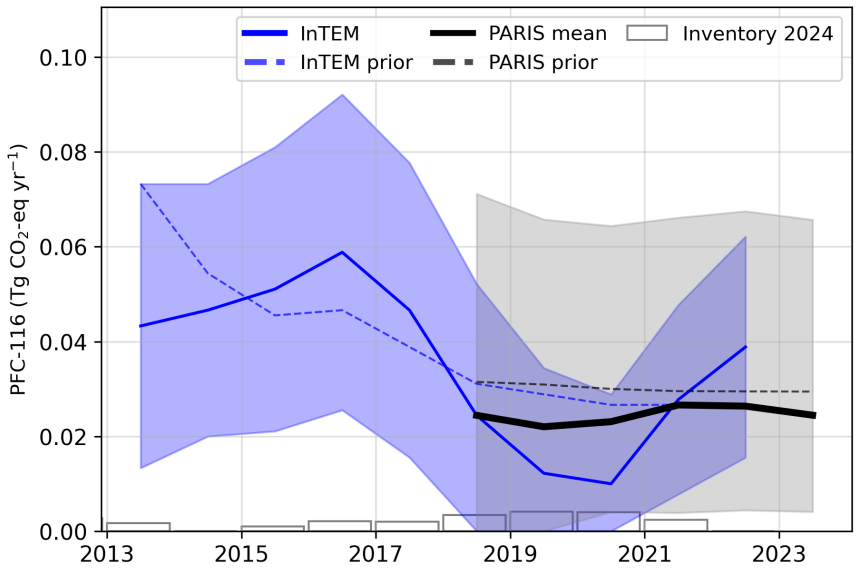

Figure 7.2.2: Spatial distribution of the Dutch average modelled emissions of PFC-116 during the period of 2018-2023 (mean from all models). Observing stations are marked with red circles and highly-populated cities are marked with red triangles.

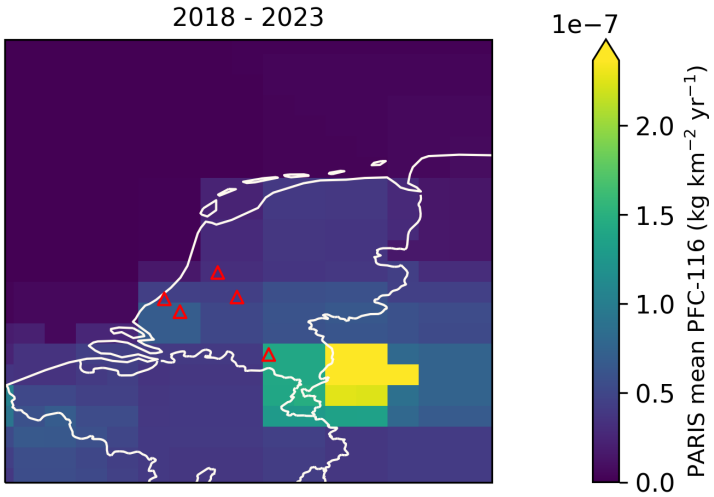

7.3 PFC-218

Figure 7.3.1: Verification of the Dutch emissions inventory estimates for PFC-218. Modelled annual emissions are given as the mean from all models (black line and grey shading) and the individual result from InTEM (blue line and shading). National inventory annual totals are given as grey bars.

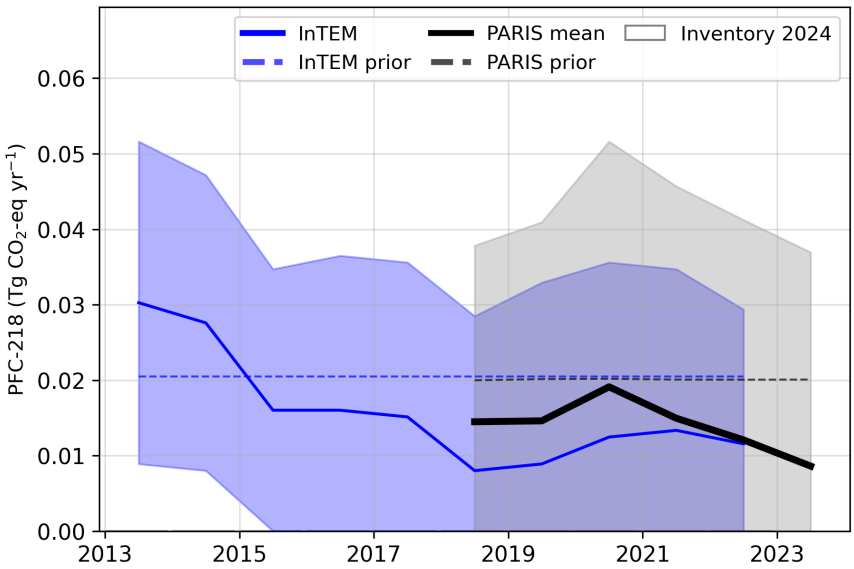

Figure 7.3.2: Spatial distribution of the Dutch average modelled emissions of PFC-218 during the period of 2018-2023 (mean from all models). Observing stations are marked with red circles and highly-populated cities are marked with red triangles.

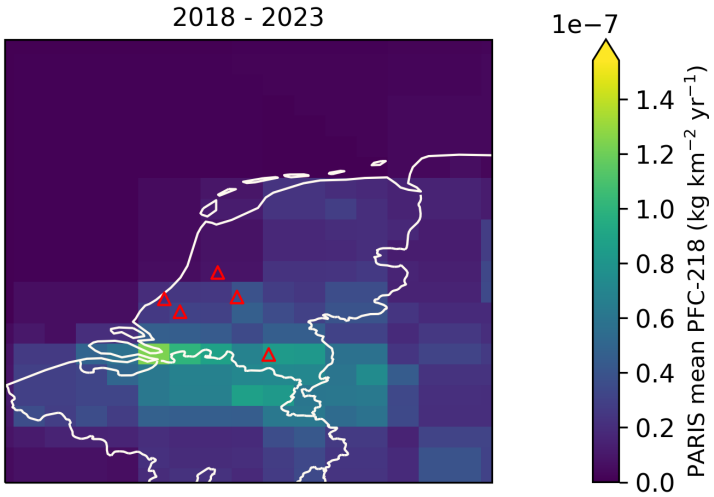

7.4 PFC-318

Figure 7.4.1: Verification of the Dutch emissions inventory estimates for PFC-318. Modelled annual emissions are given as the mean from all models (black line and grey shading) and the individual result from InTEM (blue line and shading). National inventory annual totals are given as grey bars.

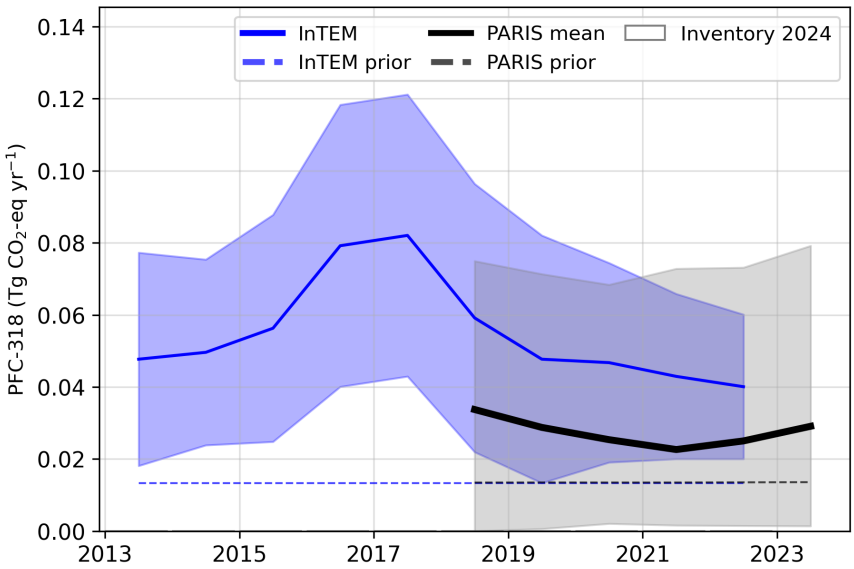

Figure 7.4.2: Spatial distribution of the Dutch average modelled emissions of PFC-318 during the period of 2018-2023 (mean from all models). Observing stations are marked with red circles and highly-populated cities are marked with red triangles.

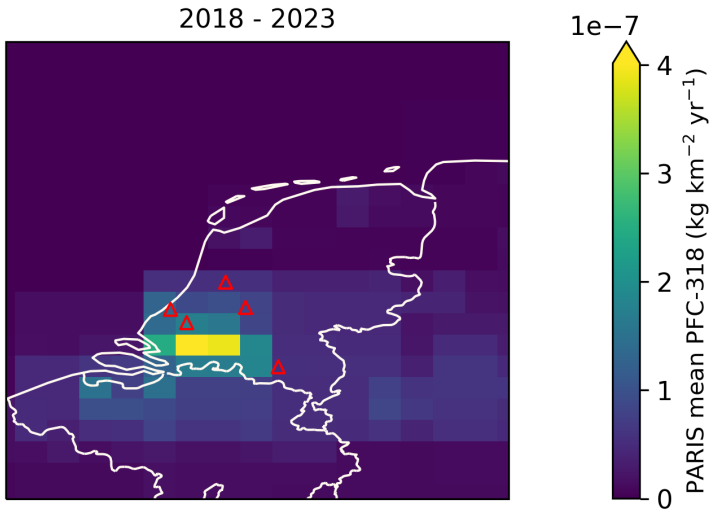

7.5 Total PFCs

Figure 7.5.1: Verification of the Dutch emissions inventory estimates for total PFCs. Modelled annual emissions are given as the mean from all models (black line and grey shading) and the individual result from InTEM (blue line and shading). National inventory annual totals are given as grey bars.

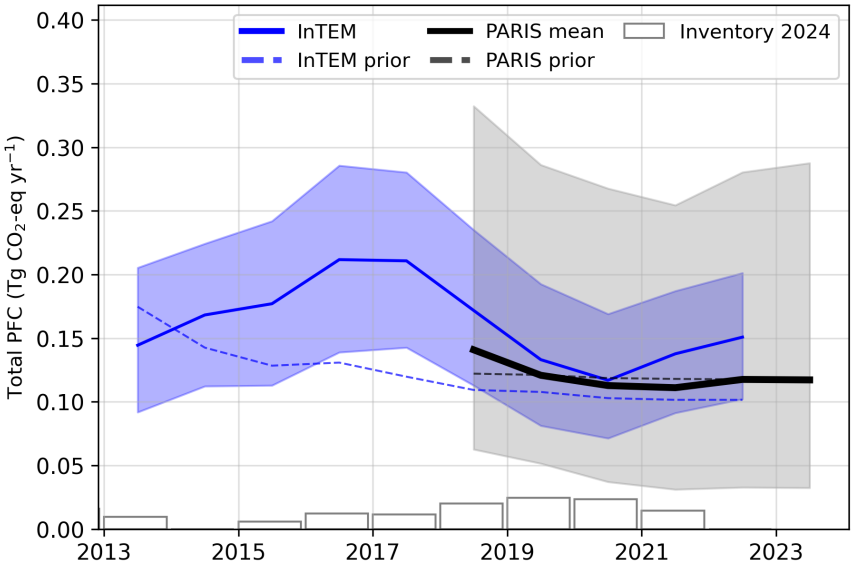

Table 3: Emissions estimation for PFCs in $\mathrm{TgCO_2{-}eq \cdot yr^{-1}}$ according to the National Inventory Report (NIR) 2024 and the inversions done in the PARIS project. For the PARIS estimation, the mean of the 3 inversion models is displayed, along with a range of uncertainty estimated via the half distance between the maximum and minimum uncertainties of the different models.

		2018	2019	2020	2021	2022	2023
PFC-14	NIR 2024	0.02	0.02	0.02	0.01	0.00	
	PARIS mean	0.07 ± 0.11	0.06 ± 0.09	0.05 ± 0.08	0.05 ± 0.09	0.05 ± 0.10	0.06 ± 0.11
PFC-116	NIR 2024	0.00	0.00	0.00	0.00	0.00	
	PARIS mean	0.02 ± 0.04	0.02 ± 0.03	0.02 ± 0.03	0.03 ± 0.03	0.03 ± 0.03	0.02 ± 0.03
PFC-218	NIR 2024	0.00	0.00	0.00	0.00	0.00	
	PARIS mean	0.01 ± 0.02	0.01 ± 0.02	0.02 ± 0.03	0.01 ± 0.02	0.01 ± 0.02	0.01 ± 0.02
PFC-318	NIR 2024	0.00	0.00	0.00	0.00	0.00	
	PARIS mean	0.03 ± 0.04	0.03 ± 0.04	0.03 ± 0.03	0.02 ± 0.04	0.03 ± 0.04	0.03 ± 0.04

8 Sulphur hexafluoride (SF_6)

Figure 8.0.1: Total source sensitivity of SF_6 observing sites as calculated by the NAME transport model for the year (left) 2018 and (right) 2023 and used in the inversions. Observing stations active in each year are marked with red dots. Areas with visible land surface represent regions for which emissions can be observed well from the network. Shaded or dark areas represent regions for which limited emission information can be obtained from the network.

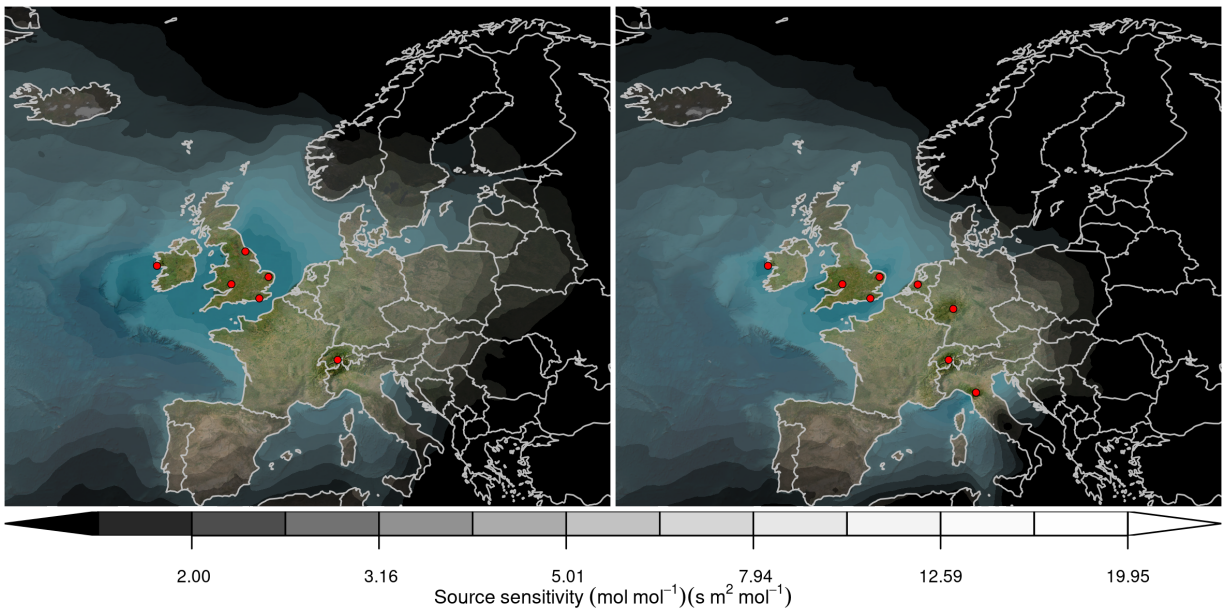

Figure 8.0.2: Verification of the Dutch emissions inventory estimates for SF_6. Modelled annual emissions are given as the mean from all models (black line and grey shading) and the individual result from InTEM (blue line and shading). National inventory annual totals are given as grey bars.

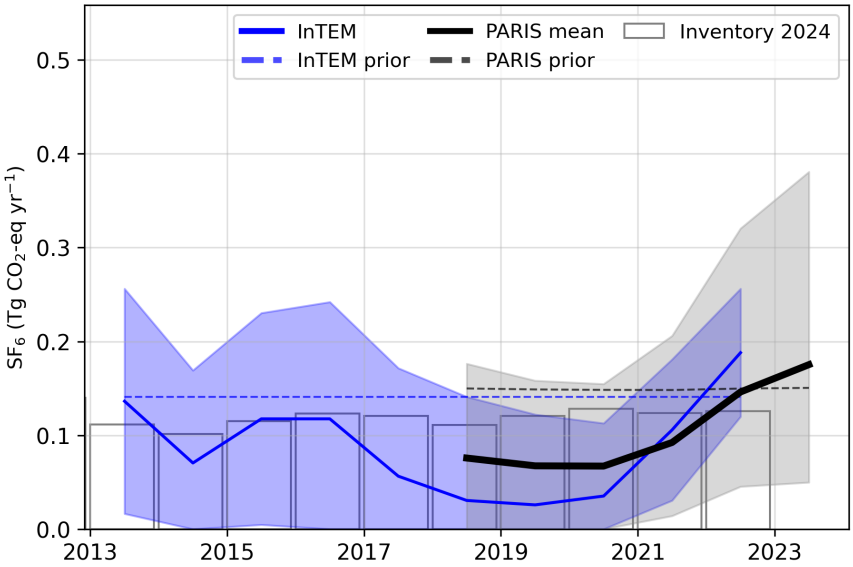

Figure 8.0.3: Spatial distribution of the Dutch average modelled emissions of SF_6 during the period of 2018-2023 (mean from all models). Observing stations are marked with red circles and highly-populated cities are marked with red triangles.

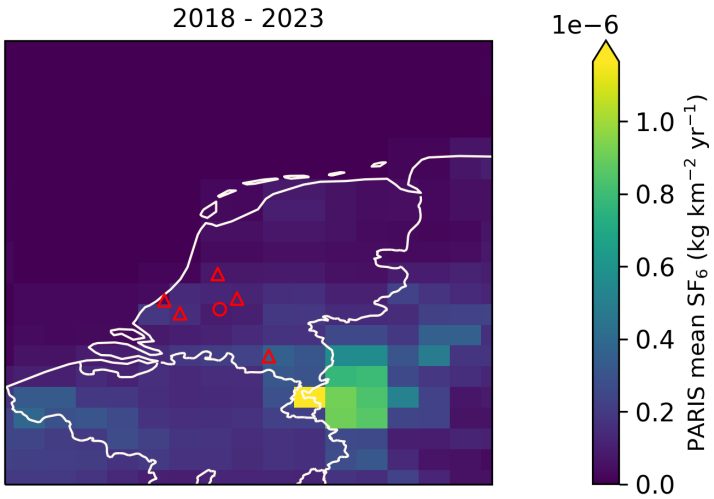

References

European Commission: Joint Research, Centre et al. (2023). *GHG emissions of all world countries – 2023*. Publications Office of the European Union. DOI: 10.2760/953322.

Ganesan, A. L. et al. (2014). "Characterization of uncertainties in atmospheric trace gas inversions using hierarchical Bayesian methods". In: *Atmospheric Chemistry and Physics* 14.8, pp. 3855–3864. DOI: 10.5194/acp-14-3855-2014. URL: http://www.atmos-chem-phys.net/14/3855/2014/http://www.atmos-chem-phys.net/14/3855/2014/acp-14-3855-2014.pdf.

Ganesan, A. L. et al. (2015). "Quantifying methane and nitrous oxide emissions from the UK and Ireland using a national-scale monitoring network". In: *Atmos. Chem. Phys.* 15.11, pp. 6393–6406. DOI: 10.5194/acp-15-6393-2015. URL: https://www.atmos-chem-phys.net/15/6393/2015/https://www.atmos-chem-phys.net/15/6393/2015/acp-15-6393-2015.pdf.

Henne, S. et al. (2016). "Validation of the Swiss methane emission inventory by atmospheric observations and inverse modelling". In: *Atmospheric Chemistry and Physics* 16.6, pp. 3683–3710. DOI: 10.5194/acp-16-3683-2016. URL: http://www.atmos-chem-phys.net/16/3683/2016/.

Jones, A.R. et al. (2007). "The U.K. Met Office's next-generation atmospheric dispersion model, NAME III, in Borrego C. and Norman A.-L. (Eds)". In: *Air Pollution Modeling and its Application XVII (Proceedings of the 27th NATO/CCMS International Technical Meeting on Air Pollution Modelling and its Application), Springer*, pp. 580–589.

Katharopoulos, I. et al. (2023). "Impact of transport model resolution and a priori assumptions on inverse modeling of Swiss F-gas emissions". In: *Atmos. Chem. Phys.* 23.22, pp. 14159–14186. DOI: 10.5194/acp-23-14159-2023. URL: https://acp.copernicus.org/articles/23/14159/2023/.

Manning, A. J. et al. (2021). "Evidence of a recent decline in UK emissions of hydrofluorocarbons determined by the InTEM inverse model and atmospheric measurements". In: *Atmospheric Chemistry and Physics* 21.16, pp. 12739–12755. DOI: 10.5194/acp-21-12739-2021. URL: https://acp.copernicus.org/articles/21/12739/2021/.

Rigby, M. et al. (2019). "Increase in CFC-11 emissions from eastern China based on atmospheric observations". In: *Nature* 569, pp. 546–550. DOI: 10.1038/s41586-019-1193-4. URL: https://doi.org/10.1038/s41586-019-1193-4.

Draft Inventory Annex
Norway 2024

18th November, 2024

1 Introduction

In this document, global concentration trends and national emissions estimates derived from atmospheric observations ("inverse estimates") are presented for each reported gas. Comparing the emissions submitted in national inventories with those calculated using atmospheric observations allows for emissions to be assessed using two fundamentally different approaches. Substantial differences can highlight areas that could warrant further investigation.

Global concentration trends for each gas are first shown using annual average concentrations from Mace Head, Ireland (Northern Hemisphere) and Kennaook/Cape Grim, Tasmania, Australia (Southern Hemisphere). Data from these stations were selected to exclude regionally-polluted air masses and therefore represents northern and southern hemispheric concentration trends. Mace Head observations were supported by the National Aeronautics and Space Administration (NASA) and the UK Department of Energy, Security and Net Zero (DESNZ), and Kennaook/Cape Grim observations by NASA and the Australian Bureau of Meteorology.

Observations of European concentrations of greenhouse gases used to derive national inverse emission estimates were collected from many different networks and providers. Methane and nitrous oxide concentrations originated from the European ICOS (Integrated Carbon Observation System) network, the UK DECC (Deriving Emissions related to Climate Change) network and other national or individual initiatives. F-gas observations were made by affiliates of the AGAGE (Advanced Global Atmospheric Gases Experiment) network. Observations from from additional stations across Europe were supported by the Horizon-EU PARIS (Process Attribution of Regional Emissions) project. The observation stations used to derive emissions for each gas are shown in the corresponding sections of this document.

Inversion-based emissions estimates were derived using one atmospheric transport model but with multiple inverse models allowing a better quantification of the uncertainties associated with inverse modelling. The atmospheric transport model provides the link between surface fluxes and concentrations measured at the observing stations. Although the uncertainty associated with the atmospheric transport model is considered in the statistical inversion approach, it may be underestimated when only using a single transport model. The atmospheric transport model used is the Numerical Atmospheric dispersion Modelling Environment (NAME) (Jones et al., 2007), a backwards-running Lagrangian Particle Dispersion Model (LPDM) that simulates the recent transport of air to each observing station. The NAME model has been widely used in the estimation of greenhouse gases emissions (Ganesan et al., 2015; Rigby et al., 2019; Manning et al., 2021).

The three inverse methods used are InTEM (Inversion Technique for Emission Modelling, Manning et al., 2021), ELRIS (Empa Lagrangian Regional Inversion System, Henne et al., 2016; Katharopoulos et al., 2023), and RHIME (Regional Hierarchical Inverse Modelling Environment, Ganesan et al., 2014). All three inverse methods estimate emissions within Europe along with boundary conditions that account for the concentration of the air entering Europe. All three systems started from the same set of a priori emissions that were either derived from the global EDGAR emission inventory (version 8, European Commission: Joint Research et al., 2023) or a uniform land-based emission, depending on the gas. A natural emission component, from the WETCHARTS product, was included in the methane prior. The same observational dataset was used by each inverse model, but data selection (i.e., filtering datasets for specific conditions) and treatment of uncertainties were chosen separately and hence differ. The three methods also differ in their statistical approaches for estimating emissions.

Emission estimates are presented for the period 2008-2023. Emissions for the full 2008-2023 period were derived with the InTEM model only, while emissions from 2018-2023 are presented as a combined result using the three inverse models.

For the 2008-2023 InTEM results, a 2-year inversion resolution, incrementing annually, was used for all gases except CH_4nd N_2, where the resolution was monthly. For the recent 2018-2023 period, for all three models, the inversion resolution was one month for CH_4 and N_2O in order to capture the seasonality of the emissions, a one-year average over these results is also presented. For the fluorinated gases, a 1-year

inversion resolution was adopted, with a 3-year moving average applied to the results. The uncertainty shown is the minimum/maximum of the uncertainties from the three results.

2 Global Concentration Trends

2.1 Methane (CH_4)

Figure 2.1.1: Background Northern Hemisphere monthly concentrations of CH_4 estimated from MHD, Ireland observations are shown in red, and background Southern Hemisphere monthly concentrations from CGO, Tasmania are shown in blue. Grey shading represents provisional data.

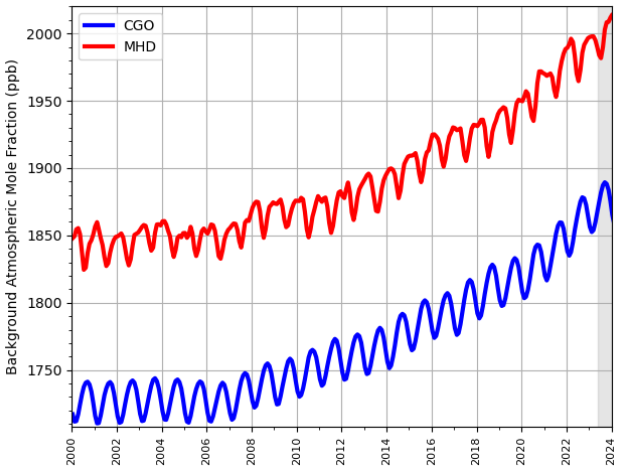

2.2 Nitrous Oxide (N_2O)

Figure 2.2.1: Background Northern Hemisphere monthly concentrations of N_2O estimated from MHD, Ireland observations are shown in red, and background Southern Hemisphere monthly concentrations from CGO, Tasmania are shown in blue. Grey shading represents provisional data.

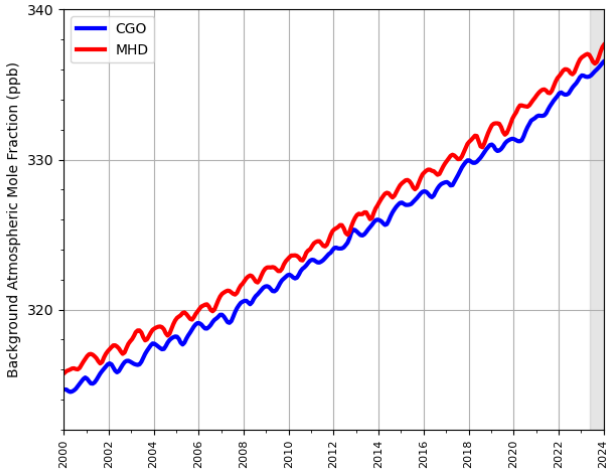

2.3 Hydrofluorocarbons (HFCs)

Figure 2.3.1: Background Northern Hemisphere monthly concentrations of six HFCs estimated from MHD, Ireland observations are shown in red, and background Southern Hemisphere monthly concentrations from CGO, Tasmania are shown in blue. Grey shading represents provisional data.

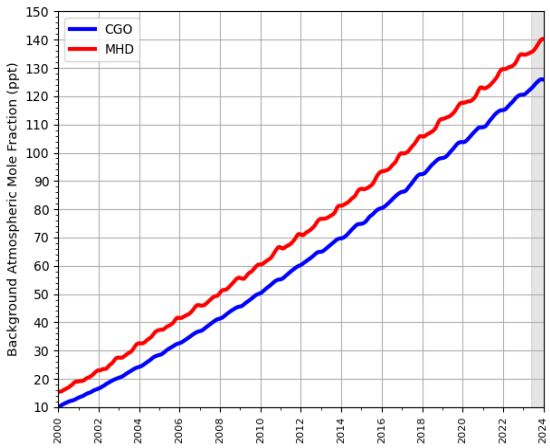

(a) HFC-134a

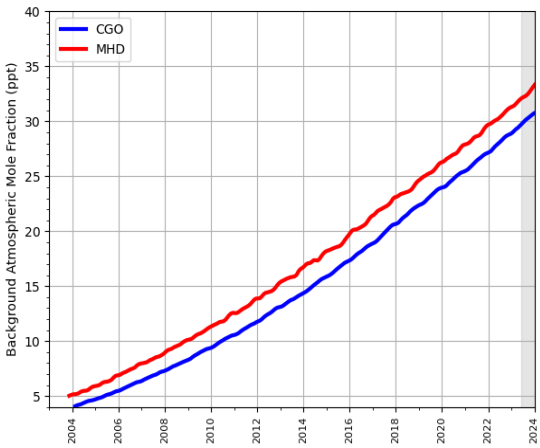

(b) HFC-143a

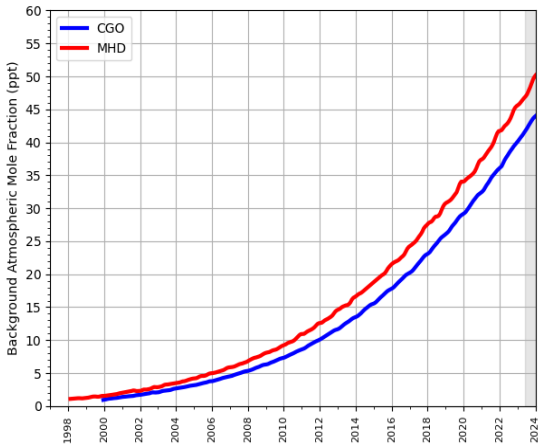

(c) HFC-125

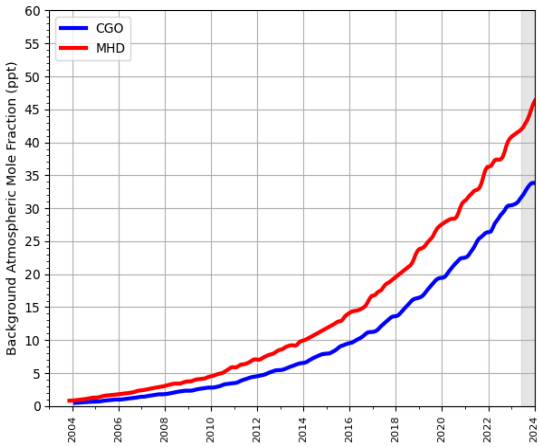

(d) HFC-32

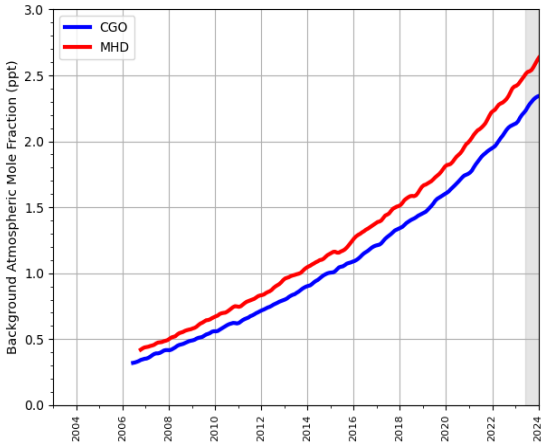

(e) HFC-227ea

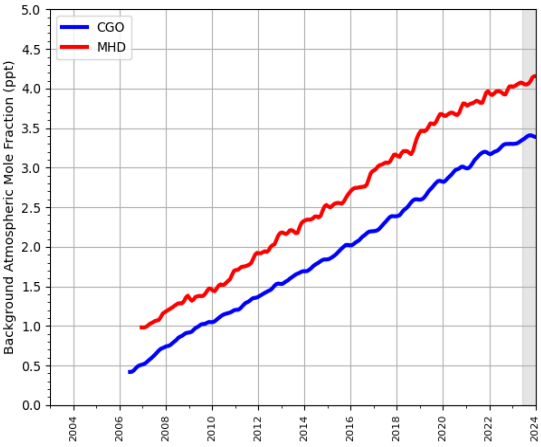

(f) HFC-245fa

Figure 2.3.2: Background Northern Hemisphere monthly concentrations of four HFCs estimated from MHD, Ireland observations are shown in red, and background Southern Hemisphere monthly concentrations from CGO, Tasmania are shown in blue. Grey shading represents provisional data.

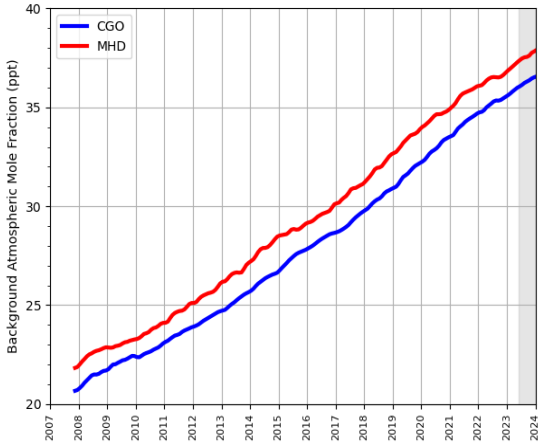

(a) HFC-23

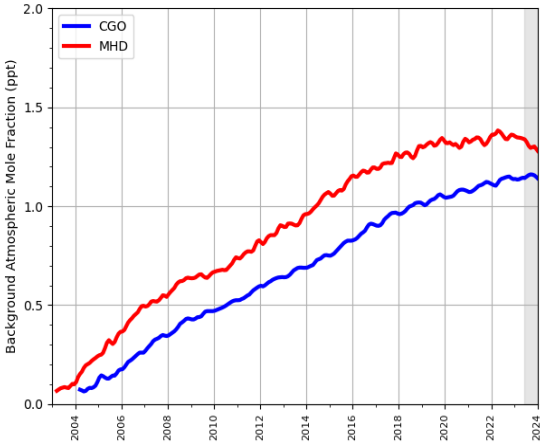

(b) HFC-365mfc

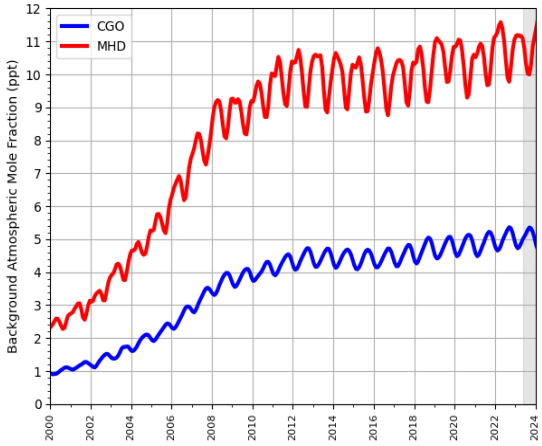

(c) HFC-152a

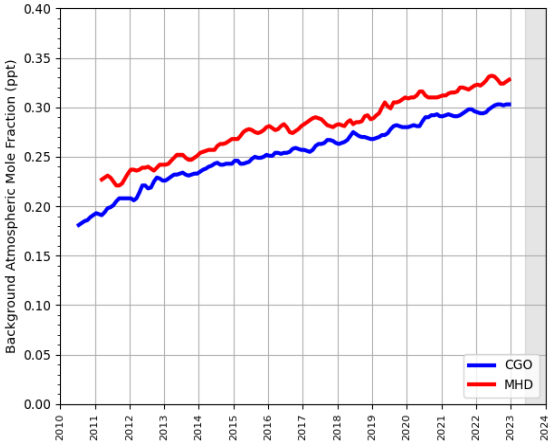

(d) HFC-43-10-mee

2.4 Perfluorocarbons (PFCs)

Figure 2.4.1: Background Northern Hemisphere monthly concentrations of four PFCs estimated from MHD, Ireland observations are shown in red, and background Southern Hemisphere monthly concentrations from CGO, Tasmania are shown in blue. Grey shading represents provisional data.

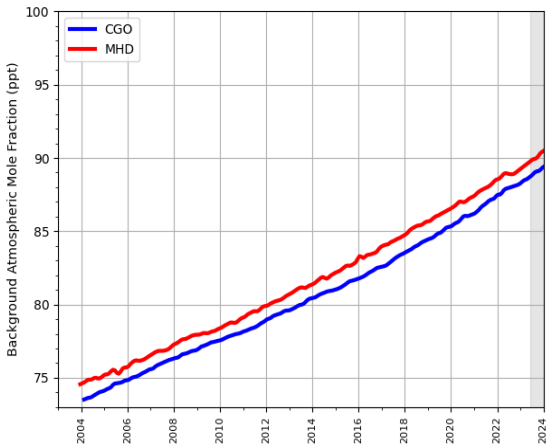

(a) PFC-14

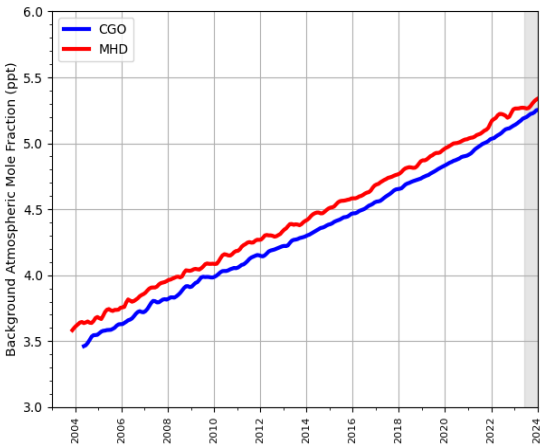

(b) PFC-116

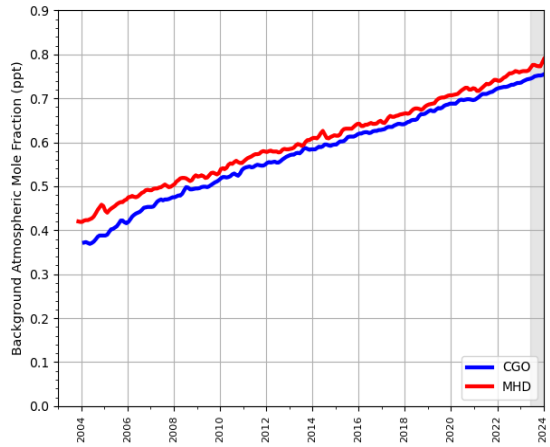

(c) PFC-218

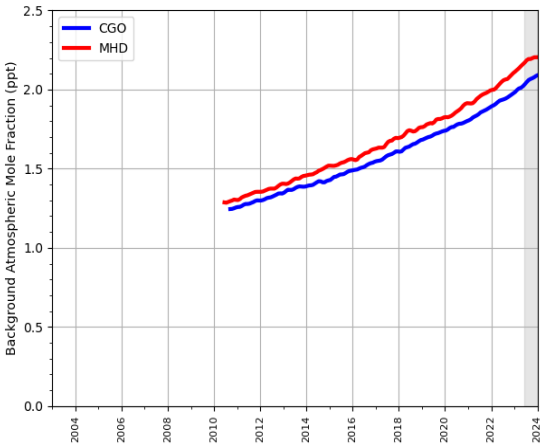

(d) PFC-318

3 Key findings

- Methane (CH_4): Inverse results are potentially marginally higher than the reported inventory estimates between 2018 and 2022. However the inverse results include all sources, both natural and anthropogenic, and the contribution from the natural sources is very uncertain. It is therefore difficult to glean much additional information. The EDGAR V8, plus natural components from WETCHARTS, prior emission distribution used in the inversions was significantly reduced by more than a factor of two.
- Hydrofluorocarbons (HFCs), perfluorocarbons (PFCs) and sulphur hexafluoride (SF_6): Due to the limited observational constraint very large uncertainties remain in the Norwegian emissions estimates obtained from inverse modelling for these gases. These estimates stay relatively close to the a priori values. Incorporating the new flask observations from Birkenes from 2024, and the use of observations from Zeppelin in Spitzbergen, will improve the estimates in future years.
- It is unlikely, given the current observational coverage, that inverse estimates from nitrous oxide (N_2O) will be viable.

Table 1: Emissions estimation of CH_4 in $\mathrm{TgCO_2{-}eq \cdot yr^{-1}}$ according to the National Inventory Report (NIR) 2024 and the inversions done in the PARIS project. For the PARIS estimation, the mean of the 3 inversion models is displayed, along with a range of uncertainty estimated via the half distance between the maximum and minimum uncertainties of the different models.

		2018	2019	2020	2021	2022	2023
CH_4	NIR 2024	6	6	5	5	nan	
	PARIS mean	10 ± 11	10 ± 12	8 ± 9	9 ± 9	9 ± 9	10 ± 9

4 Methane (CH_4)

Figure 4.0.1: Total source sensitivity of CH_4 observing sites as calculated by the NAME transport model for the year (left) 2018 and (right) 2023 and used in the inversions. Observing stations active in each year are marked with red dots. Areas with visible land surface represent regions for which emissions can be observed well from the network. Shaded or dark areas represent regions for which limited emission information can be obtained from the network.

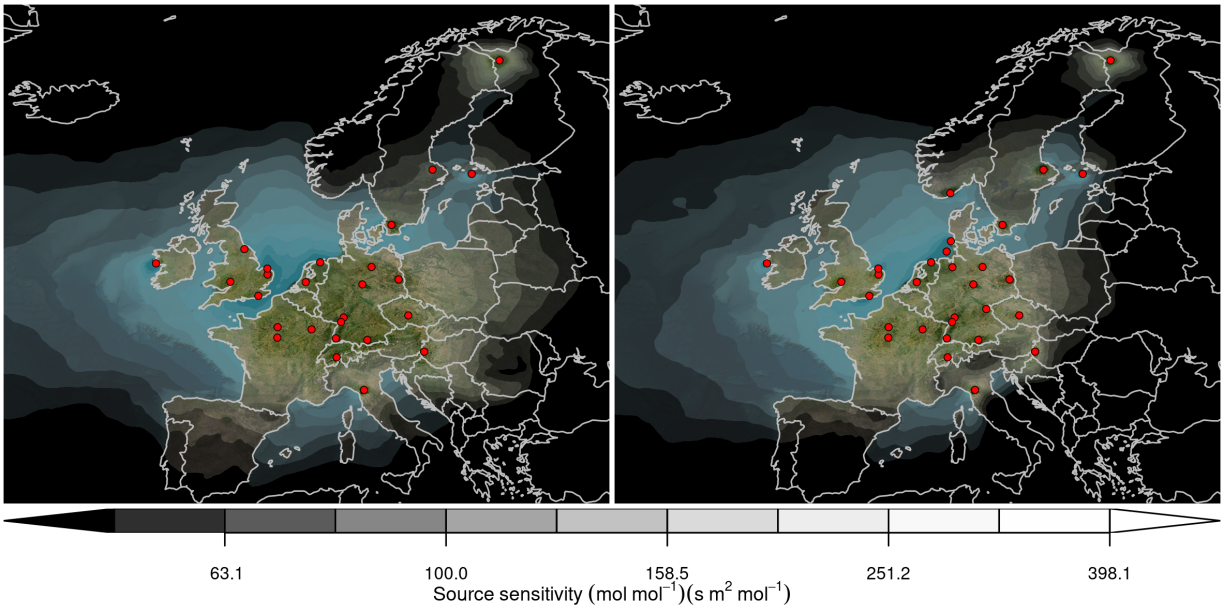

Figure 4.0.2: Verification of the Norwegian emissions inventory estimates for CH_4 (zoom in to 2018-2023). Modelled annual emissions are given as the mean from all models (black line and grey shading) and the individual result from InTEM (blue line and shading). National inventory annual totals are given as grey bars.

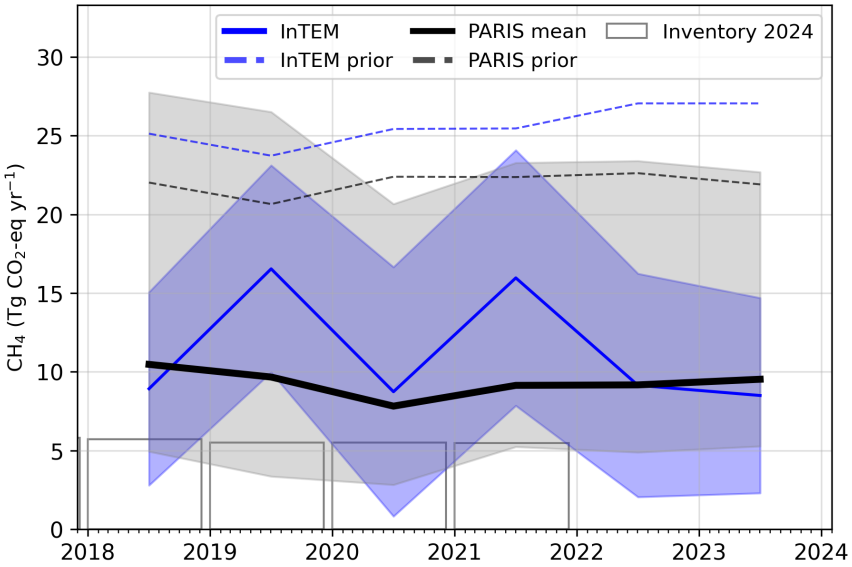

Figure 4.0.3: Verification of the Norwegian emissions inventory estimates for CH_4 (zoom in to 2018-2023). Modelled monthly emissions are given as the mean from all models (black line and grey shading) and the individual result from InTEM (blue line and shading). National inventory annual totals are given as grey bars.

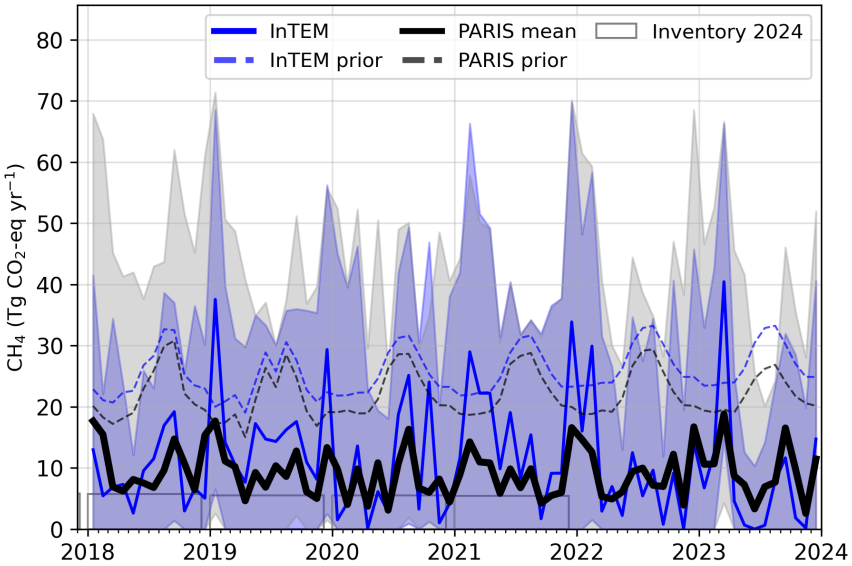

Figure 4.0.4: Spatial distribution of the Norwegian average modelled emissions of CH_4 during the period of 2018-2023 (mean from all models). Observing stations are marked with red circles and highly-populated cities are marked with red triangles.

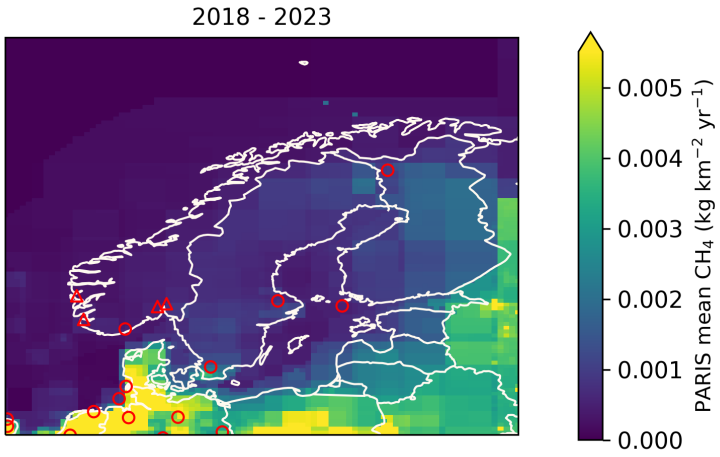

Figure 4.0.5: Spatial distribution of the seasonal deviation from the mean. The deviation is defined as the modelled Norwegian seasonally averaged CH_4 emissions over 2018-2023 minus the average over the whole period. The mean across all models is shown. Observing stations are marked with red circles and highly-populated cities are marked with red triangles.

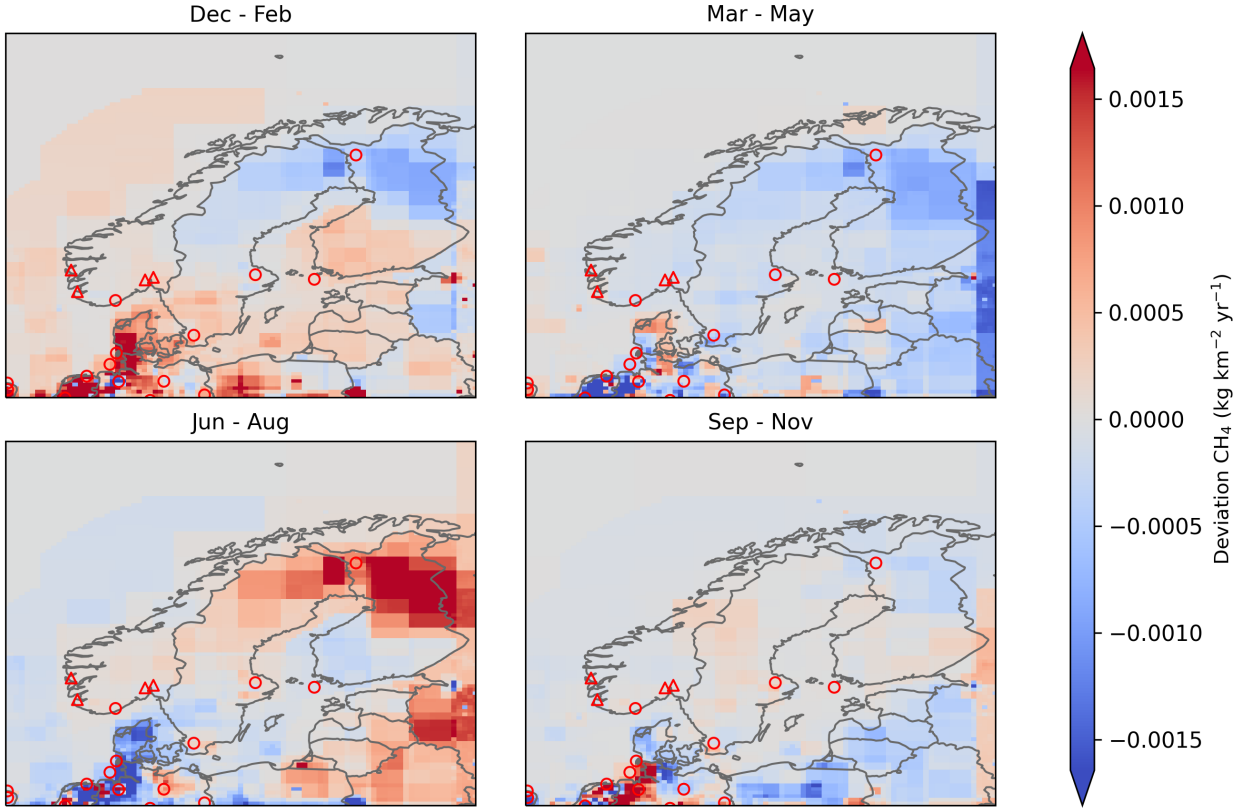

5 Nitrous Oxide (N_2O)

Figure 5.0.1: Total source sensitivity of N_2O observing sites as calculated by the NAME transport model for the year (left) 2018 and (right) 2023 and used in the inversions. Observing stations active in each year are marked with red dots. Areas with visible land surface represent regions for which emissions can be observed well from the network. Shaded or dark areas represent regions for which limited emission information can be obtained from the network.

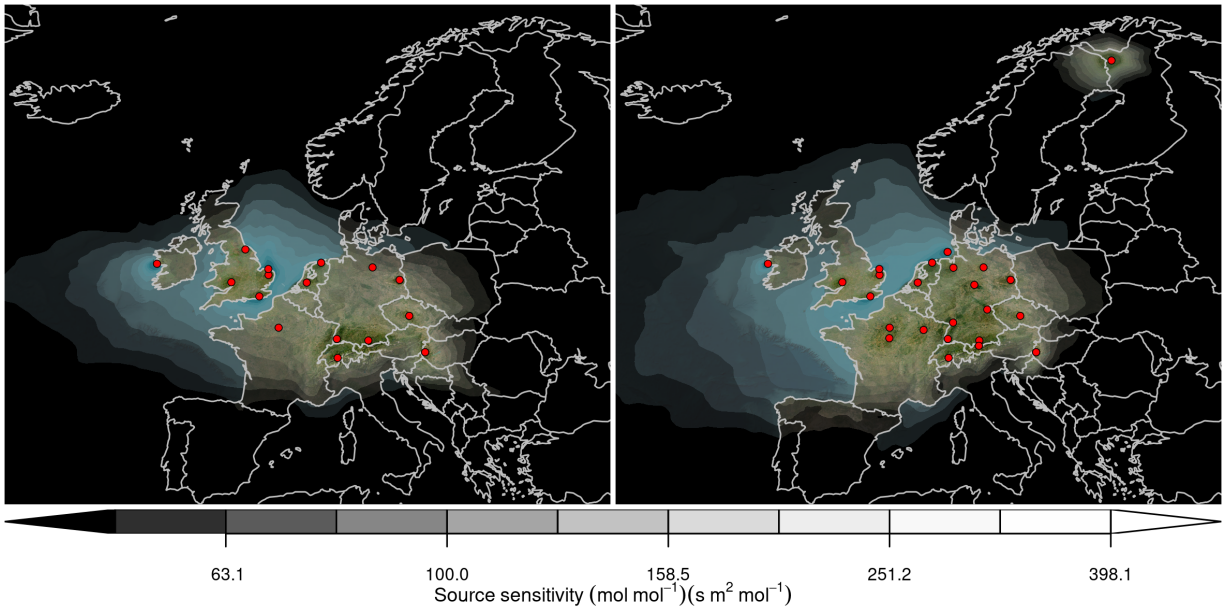

6 Hydrofluorocarbons (HFCs) and Perfluorocarbons (PFCs)

Figure 6.0.1: Total source sensitivity of HFCs/PFCs observing sites as calculated by the NAME transport model for the year (left) 2018 and (right) 2023 and used in the inversions. Observing stations active in each year are marked with red dots. Areas with visible land surface represent regions for which emissions can be observed well from the network. Shaded or dark areas represent regions for which limited emission information can be obtained from the network.

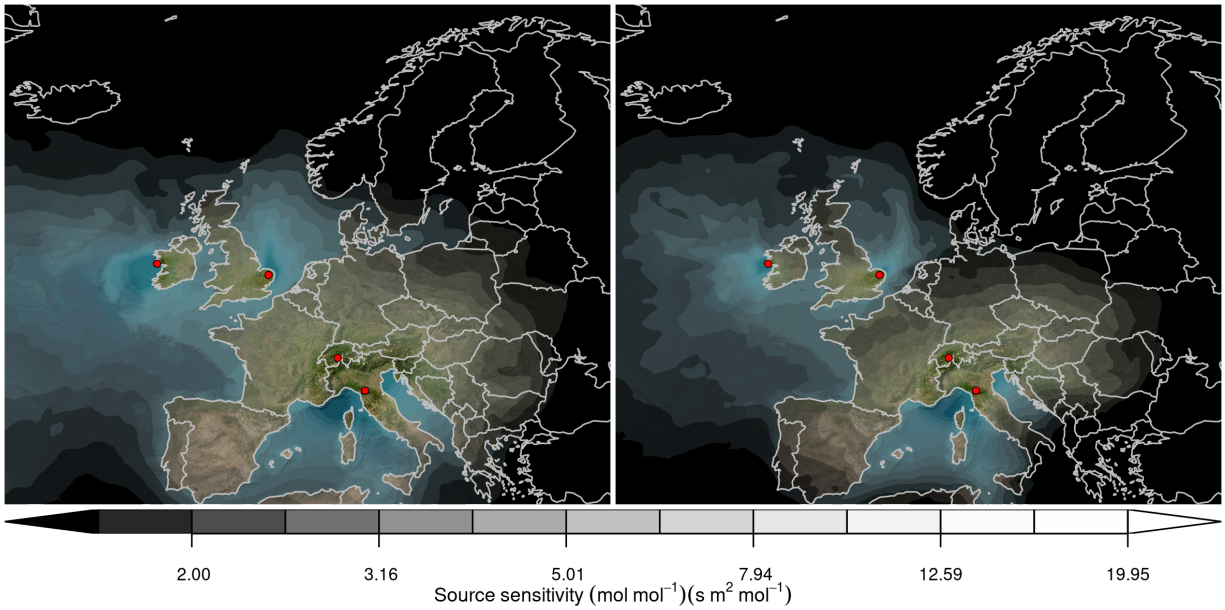

7 Sulphur hexafluoride (SF_6)

Figure 7.0.1: Total source sensitivity of SF_6 observing sites as calculated by the NAME transport model for the year (left) 2018 and (right) 2023 and used in the inversions. Observing stations active in each year are marked with red dots. Areas with visible land surface represent regions for which emissions can be observed well from the network. Shaded or dark areas represent regions for which limited emission information can be obtained from the network.

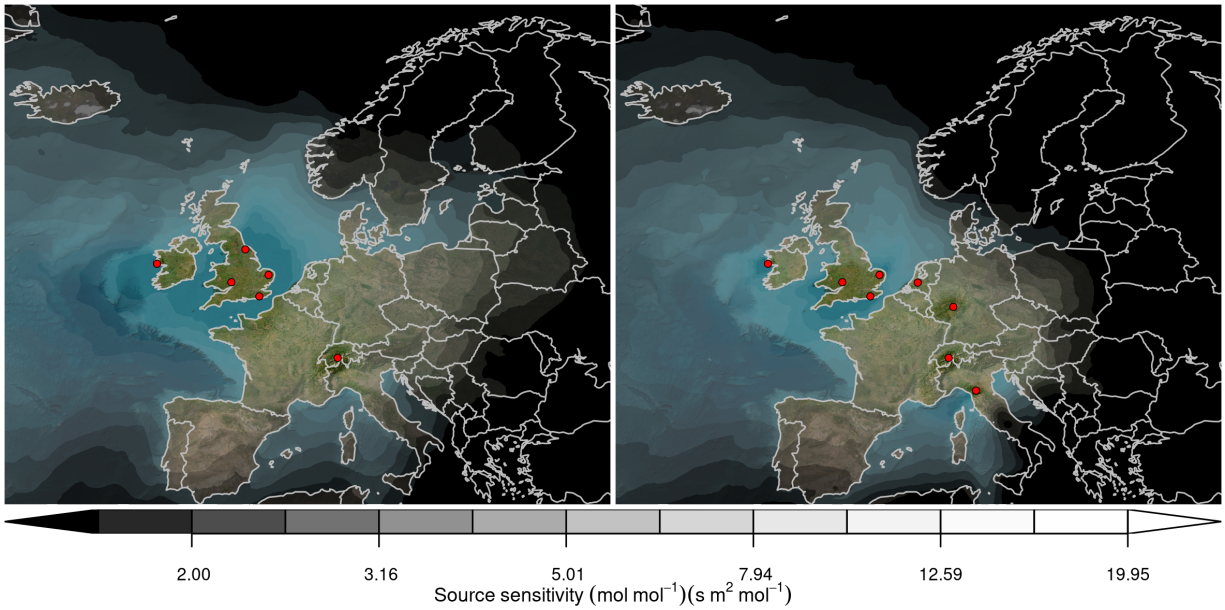

References

European Commission: Joint Research, Centre et al. (2023). *GHG emissions of all world countries – 2023*. Publications Office of the European Union. DOI: 10.2760/953322.

Ganesan, A. L. et al. (2014). "Characterization of uncertainties in atmospheric trace gas inversions using hierarchical Bayesian methods". In: *Atmospheric Chemistry and Physics* 14.8, pp. 3855–3864. DOI: 10.5194/acp-14-3855-2014. URL: http://www.atmos-chem-phys.net/14/3855/2014/http://www.atmos-chem-phys.net/14/3855/2014/acp-14-3855-2014.pdf.

Ganesan, A. L. et al. (2015). "Quantifying methane and nitrous oxide emissions from the UK and Ireland using a national-scale monitoring network". In: *Atmos. Chem. Phys.* 15.11, pp. 6393–6406. DOI: 10.5194/acp-15-6393-2015. URL: https://www.atmos-chem-phys.net/15/6393/2015/https://www.atmos-chem-phys.net/15/6393/2015/acp-15-6393-2015.pdf.

Henne, S. et al. (2016). "Validation of the Swiss methane emission inventory by atmospheric observations and inverse modelling". In: *Atmospheric Chemistry and Physics* 16.6, pp. 3683–3710. DOI: 10.5194/acp-16-3683-2016. URL: http://www.atmos-chem-phys.net/16/3683/2016/.

Jones, A.R. et al. (2007). "The U.K. Met Office's next-generation atmospheric dispersion model, NAME III, in Borrego C. and Norman A.-L. (Eds)". In: *Air Pollution Modeling and its Application XVII (Proceedings of the 27th NATO/CCMS International Technical Meeting on Air Pollution Modelling and its Application), Springer*, pp. 580–589.

Katharopoulos, I. et al. (2023). "Impact of transport model resolution and a priori assumptions on inverse modeling of Swiss F-gas emissions". In: *Atmos. Chem. Phys.* 23.22, pp. 14159–14186. DOI: 10.5194/acp-23-14159-2023. URL: https://acp.copernicus.org/articles/23/14159/2023/.

Manning, A. J. et al. (2021). "Evidence of a recent decline in UK emissions of hydrofluorocarbons determined by the InTEM inverse model and atmospheric measurements". In: *Atmospheric Chemistry and Physics* 21.16, pp. 12739–12755. DOI: 10.5194/acp-21-12739-2021. URL: https://acp.copernicus.org/articles/21/12739/2021/.

Rigby, M. et al. (2019). "Increase in CFC-11 emissions from eastern China based on atmospheric observations". In: *Nature* 569, pp. 546–550. DOI: 10.1038/s41586-019-1193-4. URL: https://doi.org/10.1038/s41586-019-1193-4.

Draft Inventory Annex
Switzerland 2024

18th November, 2024

1 Introduction

In this document, global concentration trends and national emissions estimates derived from atmospheric observations ("inverse estimates") are presented for each reported gas. Comparing the emissions submitted in national inventories with those calculated using atmospheric observations allows for emissions to be assessed using two fundamentally different approaches. Substantial differences can highlight areas that could warrant further investigation.

Global concentration trends for each gas are first shown using annual average concentrations from Mace Head, Ireland (Northern Hemisphere) and Kennaook/Cape Grim, Tasmania, Australia (Southern Hemisphere). Data from these stations were selected to exclude regionally-polluted air masses and therefore represents northern and southern hemispheric concentration trends. Mace Head observations were supported by the National Aeronautics and Space Administration (NASA) and the UK Department of Energy, Security and Net Zero (DESNZ), and Kennaook/Cape Grim observations by NASA and the Australian Bureau of Meteorology.

Observations of European concentrations of greenhouse gases used to derive national inverse emission estimates were collected from many different networks and providers. Methane and nitrous oxide concentrations originated from the European ICOS (Integrated Carbon Observation System) network, the UK DECC (Deriving Emissions related to Climate Change) network and other national or individual initiatives. F-gas observations were made by affiliates of the AGAGE (Advanced Global Atmospheric Gases Experiment) network. Observations from from additional stations across Europe were supported by the Horizon-EU PARIS (Process Attribution of Regional Emissions) project. The observation stations used to derive emissions for each gas are shown in the corresponding sections of this document.

Inversion-based emissions estimates were derived using one atmospheric transport model but with multiple inverse models allowing a better quantification of the uncertainties associated with inverse modelling. The atmospheric transport model provides the link between surface fluxes and concentrations measured at the observing stations. Although the uncertainty associated with the atmospheric transport model is considered in the statistical inversion approach, it may be underestimated when only using a single transport model. The atmospheric transport model used is the Numerical Atmospheric dispersion Modelling Environment (NAME) (Jones et al., 2007), a backwards-running Lagrangian Particle Dispersion Model (LPDM) that simulates the recent transport of air to each observing station. The NAME model has been widely used in the estimation of greenhouse gases emissions (Ganesan et al., 2015; Rigby et al., 2019; Manning et al., 2021).

The three inverse methods used are InTEM (Inversion Technique for Emission Modelling, Manning et al., 2021), ELRIS (Empa Lagrangian Regional Inversion System, Henne et al., 2016; Katharopoulos et al., 2023), and RHIME (Regional Hierarchical Inverse Modelling Environment, Ganesan et al., 2014). All three inverse methods estimate emissions within Europe along with boundary conditions that account for the concentration of the air entering Europe. All three systems started from the same set of a priori emissions that were either derived from the global EDGAR emission inventory (version 8, European Commission: Joint Research et al., 2023) or a uniform land-based emission, depending on the gas. A natural emission component, from the WETCHARTS product, was included in the methane prior. The same observational dataset was used by each inverse model, but data selection (i.e., filtering datasets for specific conditions) and treatment of uncertainties were chosen separately and hence differ. The three methods also differ in their statistical approaches for estimating emissions.

Emission estimates are presented for the period 2008-2023. Emissions for the full 2008-2023 period were derived with the InTEM model only, while emissions from 2018-2023 are presented as a combined result using the three inverse models.

For the 2008-2023 InTEM results, a 2-year inversion resolution, incrementing annually, was used for all gases except CH_4nd N_2, where the resolution was monthly. For the recent 2018-2023 period, for all three models, the inversion resolution was one month for CH_4 and N_2O in order to capture the seasonality of the emissions, a one-year average over these results is also presented. For the fluorinated gases, a 1-year

inversion resolution was adopted, with a 3-year moving average applied to the results. The uncertainty shown is the minimum/maximum of the uncertainties from the three results.

2 Global Concentration Trends

2.1 Methane (CH_4)

Figure 2.1.1: Background Northern Hemisphere monthly concentrations of CH_4 estimated from MHD, Ireland observations are shown in red, and background Southern Hemisphere monthly concentrations from CGO, Tasmania are shown in blue. Grey shading represents provisional data.

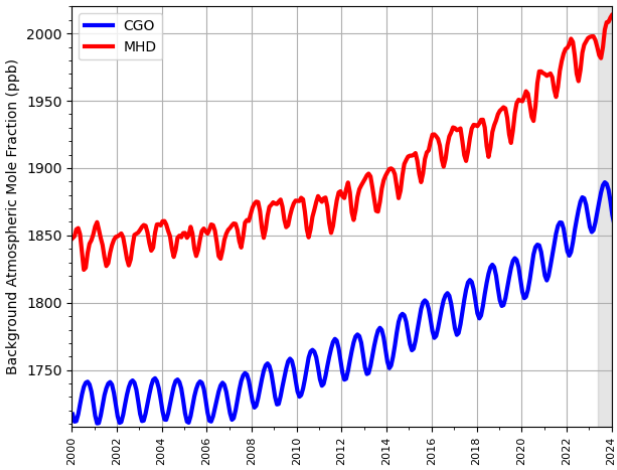

2.2 Nitrous Oxide (N_2O)

Figure 2.2.1: Background Northern Hemisphere monthly concentrations of N_2O estimated from MHD, Ireland observations are shown in red, and background Southern Hemisphere monthly concentrations from CGO, Tasmania are shown in blue. Grey shading represents provisional data.

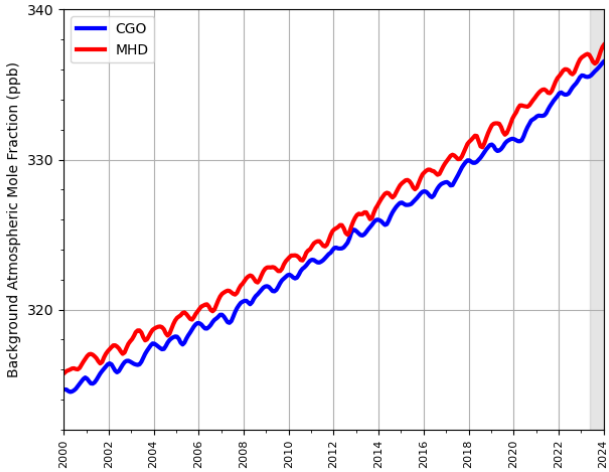

2.3 Hydrofluorocarbons (HFCs)

Figure 2.3.1: Background Northern Hemisphere monthly concentrations of six HFCs estimated from MHD, Ireland observations are shown in red, and background Southern Hemisphere monthly concentrations from CGO, Tasmania are shown in blue. Grey shading represents provisional data.

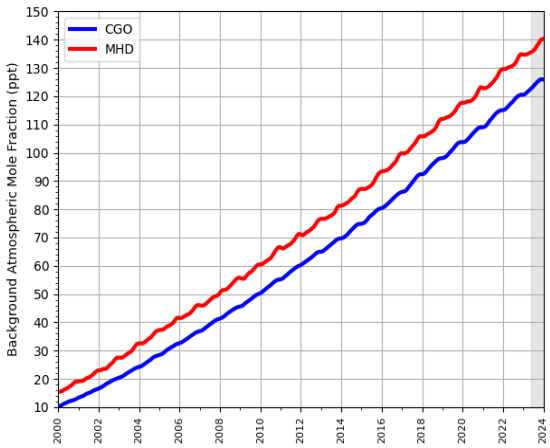

(a) HFC-134a

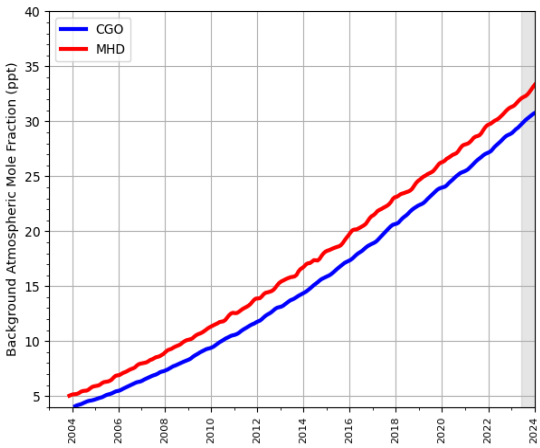

(b) HFC-143a

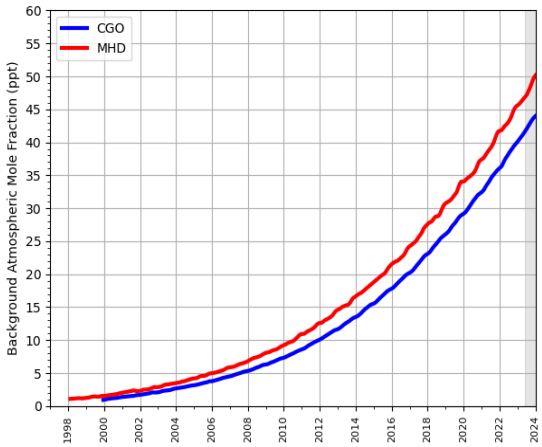

(c) HFC-125

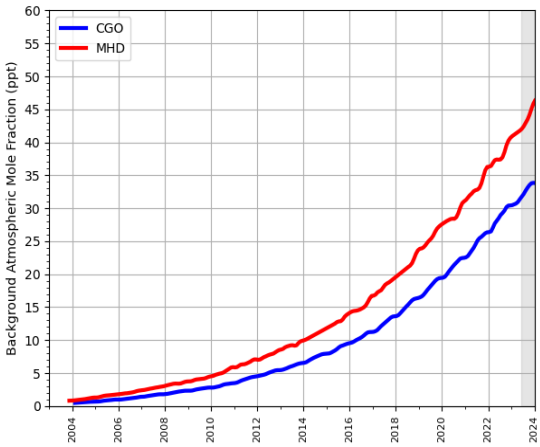

(d) HFC-32

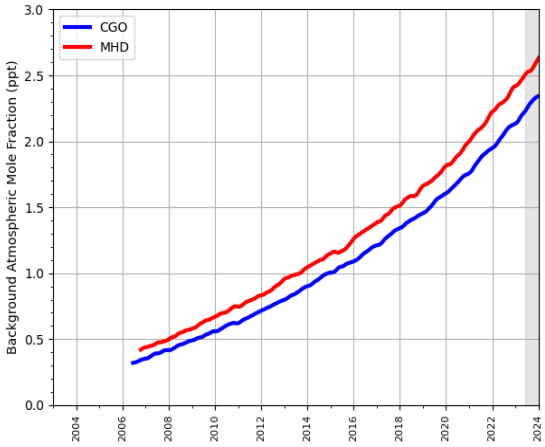

(e) HFC-227ea

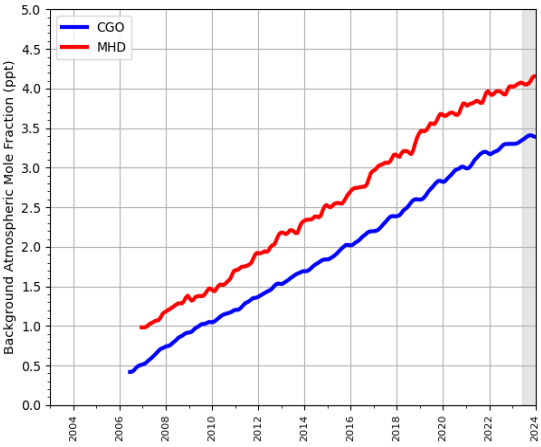

(f) HFC-245fa

Figure 2.3.2: Background Northern Hemisphere monthly concentrations of four HFCs estimated from MHD, Ireland observations are shown in red, and background Southern Hemisphere monthly concentrations from CGO, Tasmania are shown in blue. Grey shading represents provisional data.

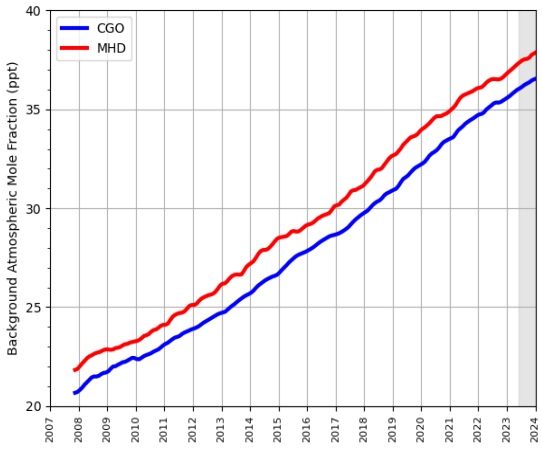

(a) HFC-23

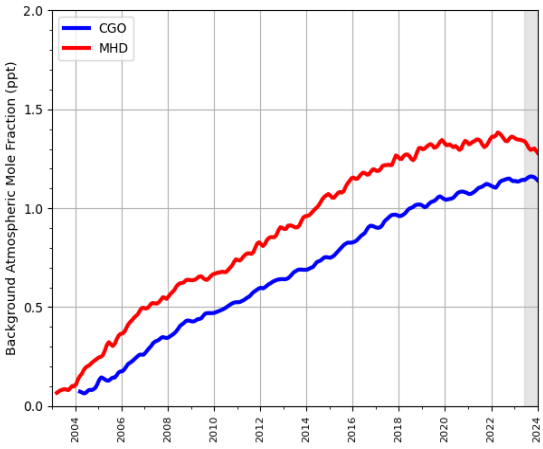

(b) HFC-365mfc

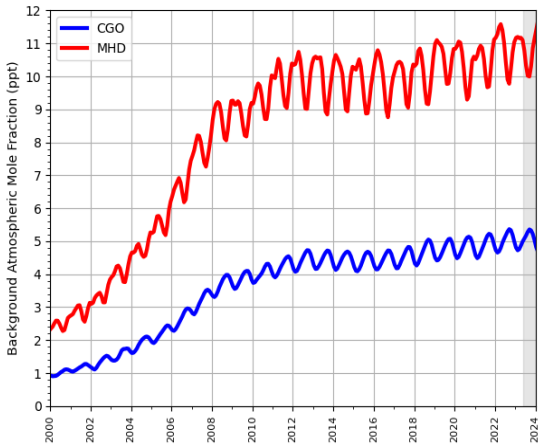

(c) HFC-152a

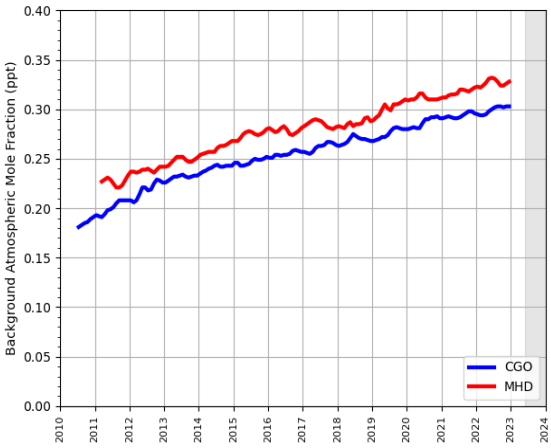

(d) HFC-43-10-mee

2.4 Perfluorocarbons (PFCs)

Figure 2.4.1: Background Northern Hemisphere monthly concentrations of four PFCs estimated from MHD, Ireland observations are shown in red, and background Southern Hemisphere monthly concentrations from CGO, Tasmania are shown in blue. Grey shading represents provisional data.

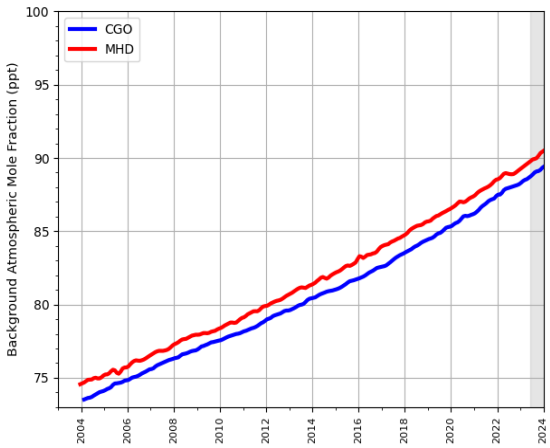

(a) PFC-14

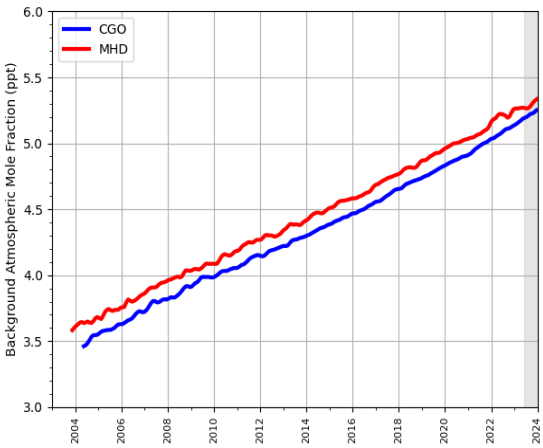

(b) PFC-116

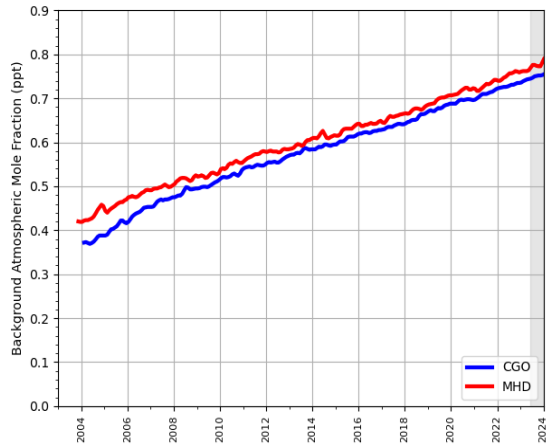

(c) PFC-218

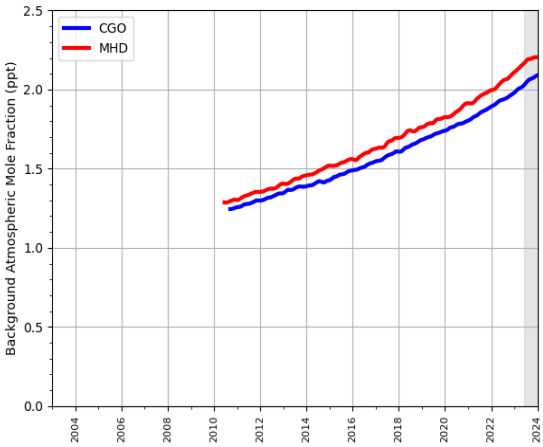

(d) PFC-318

3 Key findings

- General note: Currently, the presented inverse modelling estimates of Swiss emissions are limited by several factors. First, the applied transport model is not ideal for the complex topography of Switzerland and with an approximate horizontal resolution of 12 km much coarser than what is used in the national atmospheric support effort of the inventory reporting. Second, for a relatively small country like Switzerland, the applied inversion grids with a maximal horizontal resolution of about 25 km may cause mis-attribution of emissions from neighbouring countries. Third, important national observations (Beromünster tall tower) were not considered in this first round of PARIS inversions. Hence, observational constraint originates only from the Swiss site Jungfraujoch and from sites in neighbouring countries. The inclusion of Beromünster observations should reduce model uncertainty in future estimates. Due to these limitations results for CH_4 and N_2O are only presented for the period 2018-2023 when more observations in neighbouring countries became available.
- Methane (CH_4): Inverse results are in reasonable agreement with the inventory between 2018 and 2022 (Figure 4.0.2). Highest emissions are obtained along the Swiss Plateau, where agriculture is most intense (Figure 4.0.4). The inverse results indicate a pronounced seasonality in the methane emissions, related to agricultural emissions. The results show that these are maximum in winter (Figures 4.0.3 and 4.0.5). This is in contrast to previous studies and contradicts the expectation of little seasonal variability from the main emitting processes (enteric fermentation, manure management).
- Nitrous oxide (N_2O): Inverse results are significantly smaller, about half, than inventory estimates between 2018 and 2022 (Figure 5.0.2). As for CH_4, highest emissions are obtained along the Swiss Plateau. Contrary to expectations, high N_2O emissions are not limited to agricultural areas (Figure 5.0.4). Furthermore, large emissions in the Mulhouse area somewhat spread into the Basel region and may be mis-attributed. The inverse results indicate a weak seasonality in the nitrous oxide emissions with a maximum in autumn (Figures 5.0.3 and 5.0.5). This is in contrast to previous studies and contradicts the expectation of stronger emissions in spring/summer due to fertiliser application and enhance soil microbial activity.
- Hydrofluorocarbons (HFCs): From the current inverse modelling results, very little can be concluded about the Swiss HFC emissions. Both the coarse resolution of the transport model and the lack of observations in the Swiss atmospheric boundary layer make the inverse estimates very uncertain and hinder a direct comparison with the inventory.
- Perfluorocarbons (PFCs): From the current inverse modelling results very little can be concluded about the Swiss PFC emissions. Both the coarse resolution of the transport model and the lack of observations in the Swiss atmospheric boundary layer make the inverse estimates very uncertain and hinder a direct comparison with the inventory.
- Sulphur hexafluoride (SF_6): Similar to HFCs and PFCs, no conclusion can be drawn from the current uncertain inverse emission estimates of SF_6. In addition, large emissions in southwestern Germany will make it challenging to separate these from Swiss emissions.

Table 1: Emissions estimation for the main greenhouse gases of focus in $\mathrm{TgCO_2{-}eq \cdot yr^{-1}}$ according to the National Inventory Report (NIR) 2024 and the inversions done in the PARIS project. For the PARIS estimation, the mean of the 3 inversion models is displayed, along with a range of uncertainty estimated via the half distance between the maximum and minimum uncertainties of the different models.

		2018	2019	2020	2021	2022	2023
CH_4	NIR 2024	5.1	5.0	5.0	5.0	4.9	
	PARIS mean	4.1 ± 1.2	4.9 ± 1.2	4.8 ± 1.2	4.6 ± 1.2	5.1 ± 1.3	5.5 ± 1.7
N_2O	NIR 2024	3.1	3.1	3.0	2.9	2.5	
	PARIS mean	0.8 ± 0.5	1.4 ± 0.5	1.6 ± 0.5	1.4 ± 0.6	1.3 ± 0.5	1.1 ± 0.6
Total HFCs[(1)]	NIR 2024	1.4	1.4	1.3	1.3	1.3	
	PARIS mean	0.5 ± 0.2	0.5 ± 0.3	0.6 ± 0.3	0.5 ± 0.3	0.5 ± 0.3	0.3 ± 0.3
Total PFCs[(2)]	NIR 2024	0.02	0.02	0.02	0.01	0.01	
	PARIS mean	0.01 ± 0.02	0.02 ± 0.02	0.03 ± 0.03	0.03 ± 0.03	0.03 ± 0.04	0.02 ± 0.03
SF_6	NIR 2024	0.18	0.18	0.16	0.13	0.06	
	PARIS mean	0.04 ± 0.06	0.05 ± 0.07	0.08 ± 0.08	0.07 ± 0.07	0.06 ± 0.06	0.05 ± 0.07

(1) Sum of HFC emissions presented in Table 2, except HFC-4310mee.

(2) Sum of PFC emissions presented in Table 3.

4 Methane (CH_4)

Figure 4.0.1: Total source sensitivity of CH_4 observing sites as calculated by the NAME transport model for the year (left) 2018 and (right) 2023 and used in the inversions. Observing stations active in each year are marked with red dots. Areas with visible land surface represent regions for which emissions can be observed well from the network. Shaded or dark areas represent regions for which limited emission information can be obtained from the network.

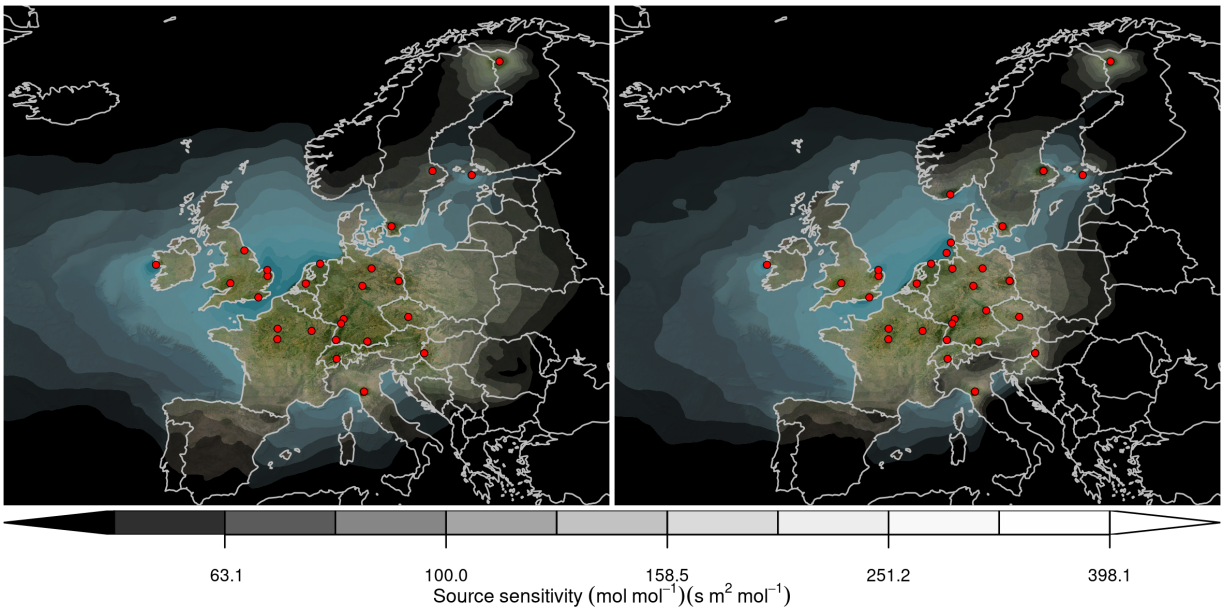

Figure 4.0.2: Verification of the Swiss emissions inventory estimates for CH_4 (zoom in to 2018-2023). Modelled annual emissions are given as the mean from all models (black line and grey shading) and the individual result from InTEM (blue line and shading). National inventory annual totals are given as grey bars.

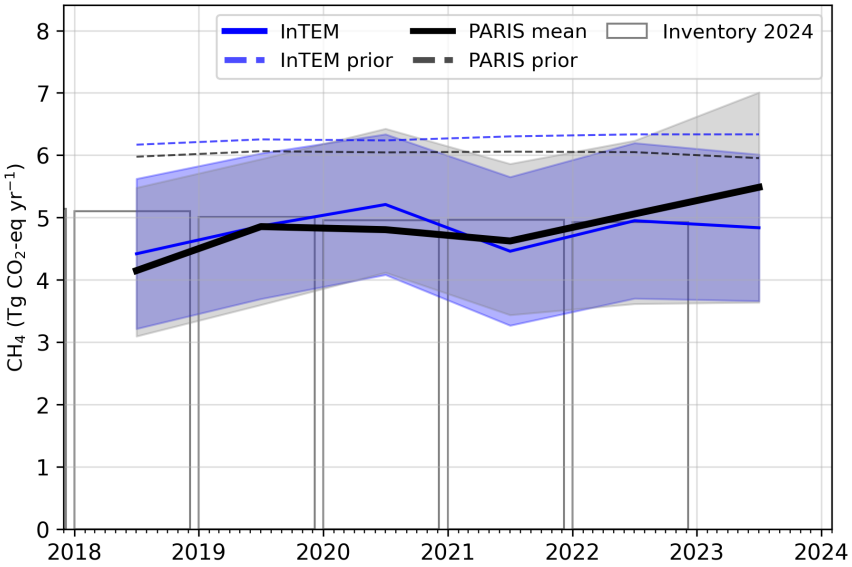

Figure 4.0.3: Verification of the Swiss emissions inventory estimates for CH_4 (zoom in to 2018-2023). Modelled monthly emissions are given as the mean from all models (black line and grey shading) and the individual result from InTEM (blue line and shading). National inventory annual totals are given as grey bars.

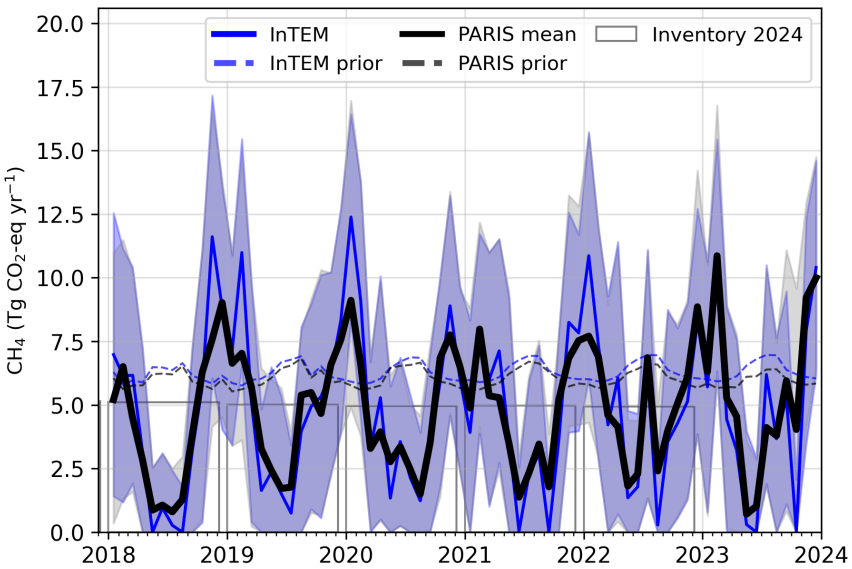

Figure 4.0.4: Spatial distribution of the Swiss average modelled emissions of CH_4 during the period of 2018-2023 (mean from all models). Observing stations are marked with red circles and highly-populated cities are marked with red triangles.

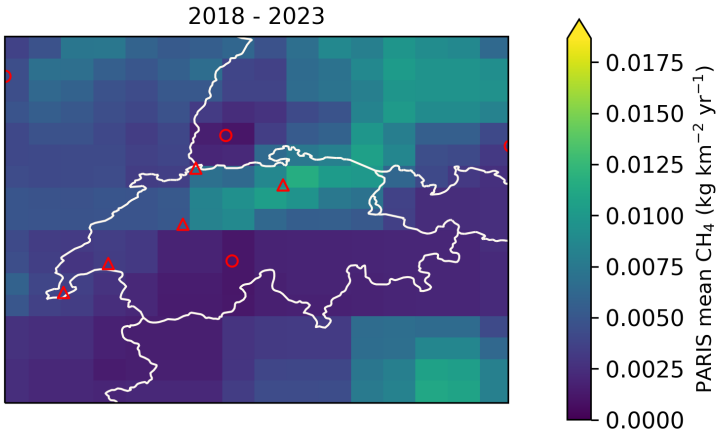

Figure 4.0.5: Spatial distribution of the seasonal deviation from the mean. The deviation is defined as the modelled Swiss seasonally averaged CH_4 emissions over 2018-2023 minus the average over the whole period. The mean across all models is shown. Observing stations are marked with red circles and highly-populated cities are marked with red triangles.

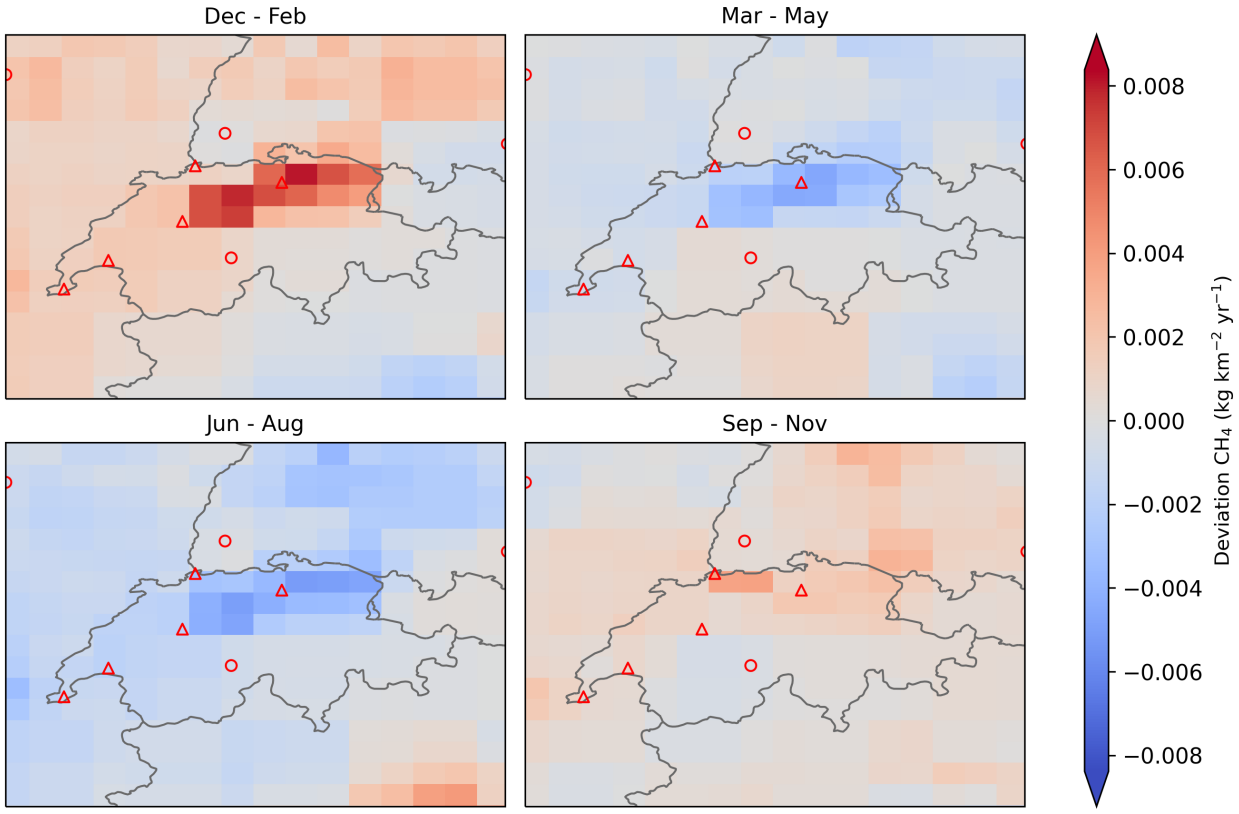

5 Nitrous Oxide (N_2O)

Figure 5.0.1: Total source sensitivity of N_2O observing sites as calculated by the NAME transport model for the year (left) 2018 and (right) 2023 and used in the inversions. Observing stations active in each year are marked with red dots. Areas with visible land surface represent regions for which emissions can be observed well from the network. Shaded or dark areas represent regions for which limited emission information can be obtained from the network.

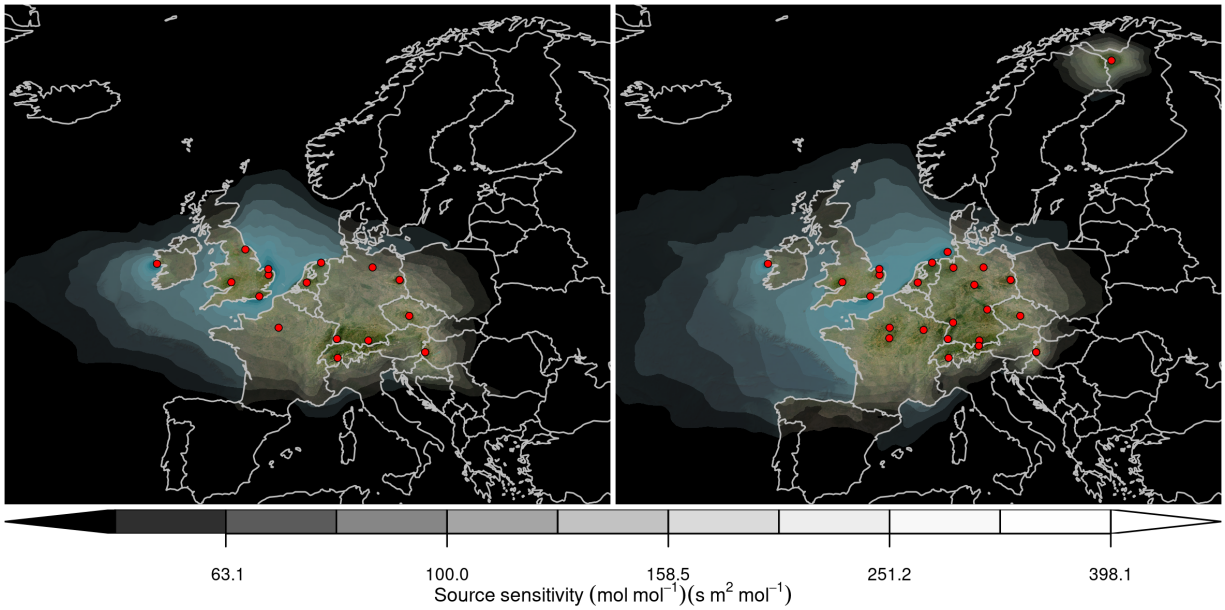

Figure 5.0.2: Verification of the Swiss emissions inventory estimates for N_2O (zoom in to 2018-2023). Modelled annual emissions are given as the mean from all models (black line and grey shading) and the individual result from InTEM (blue line and shading). National inventory annual totals are given as grey bars.

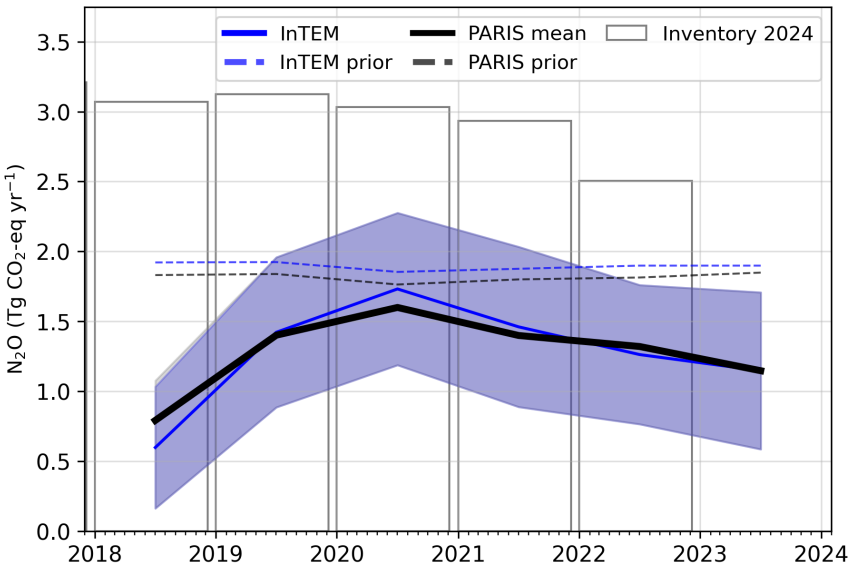

Figure 5.0.3: Verification of the Swiss emissions inventory estimates for N_2O (zoom in to 2018-2023). Modelled monthly emissions are given as the mean from all models (black line and grey shading) and the individual result from InTEM (blue line and shading). National inventory annual totals are given as grey bars.

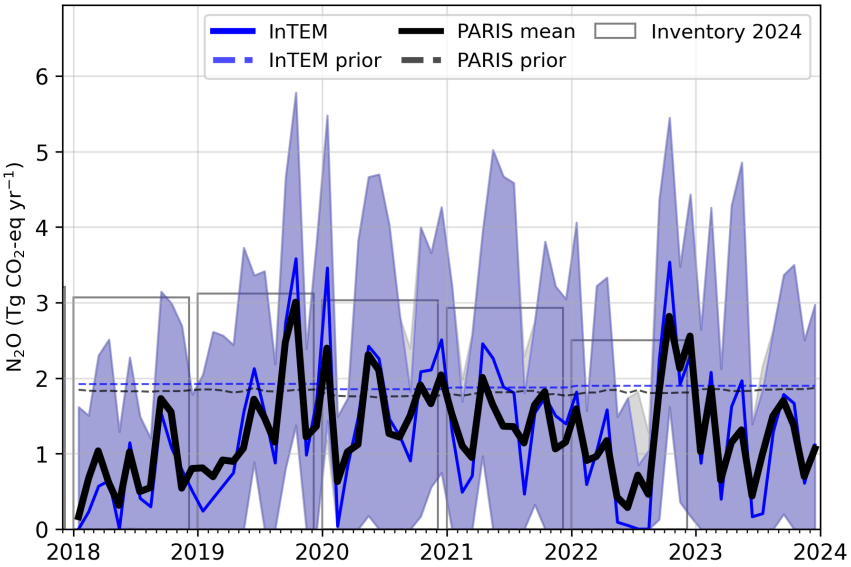

Figure 5.0.4: Spatial distribution of the Swiss average modelled emissions of N_2O during the period of 2018-2023 (mean from all models). Observing stations are marked with red circles and highly-populated cities are marked with red triangles.

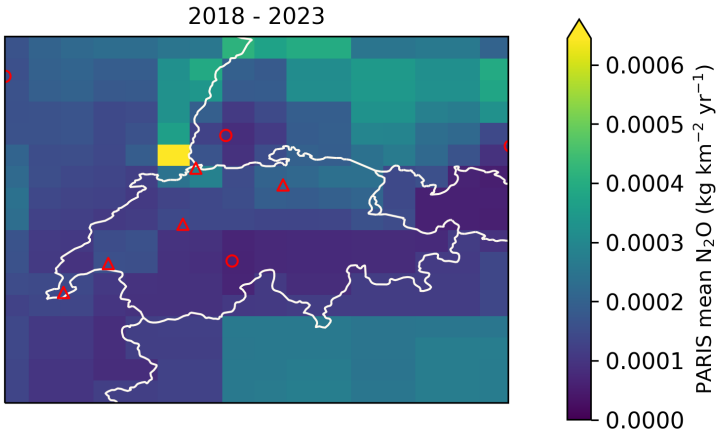

Figure 5.0.5: Spatial distribution of the seasonal deviation from the mean. The deviation is defined as the modelled Swiss seasonally averaged N_2O emissions over 2018-2023 minus the average over the whole period. The mean across all models is shown. Observing stations are marked with red circles and highly-populated cities are marked with red triangles.

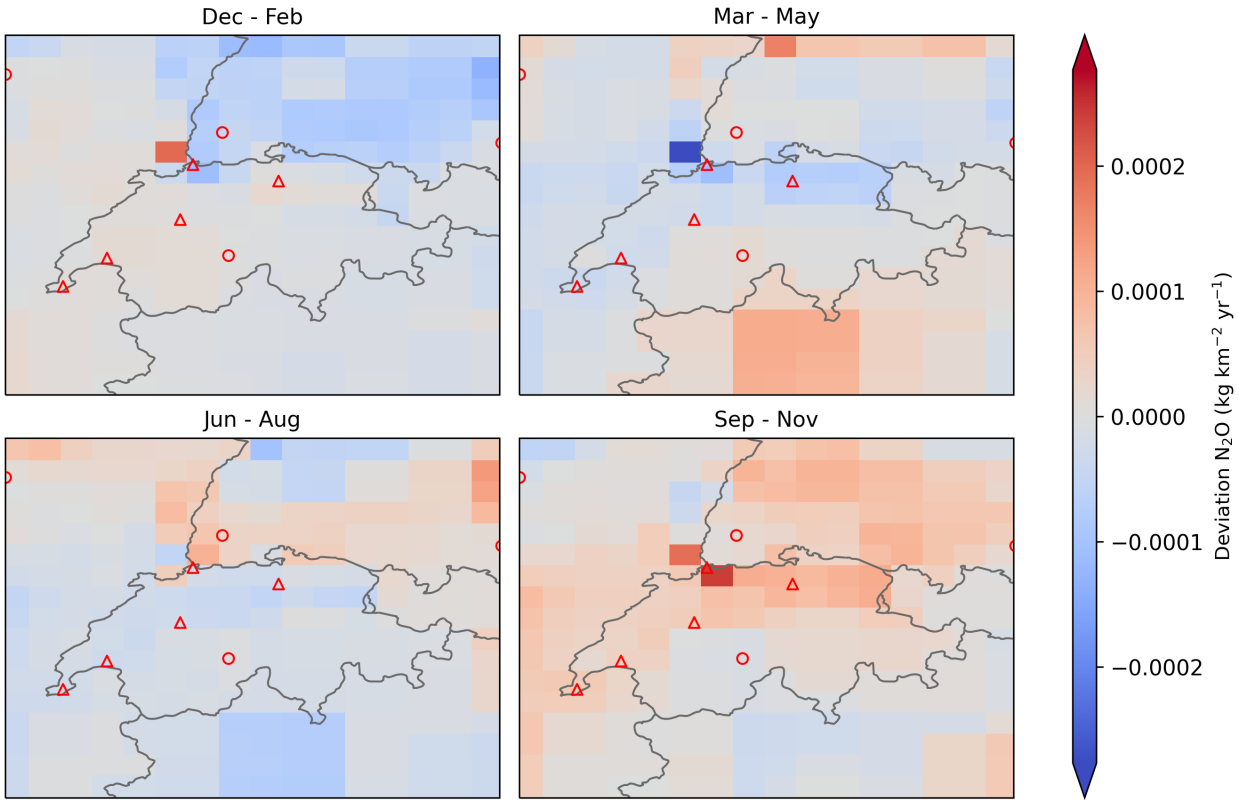

6 Hydrofluorocarbons (HFCs)

Figure 6.0.1: Total source sensitivity of HFCs/PFCs observing sites as calculated by the NAME transport model for the year (left) 2018 and (right) 2023 and used in the inversions. Observing stations active in each year are marked with red dots. Areas with visible land surface represent regions for which emissions can be observed well from the network. Shaded or dark areas represent regions for which limited emission information can be obtained from the network.

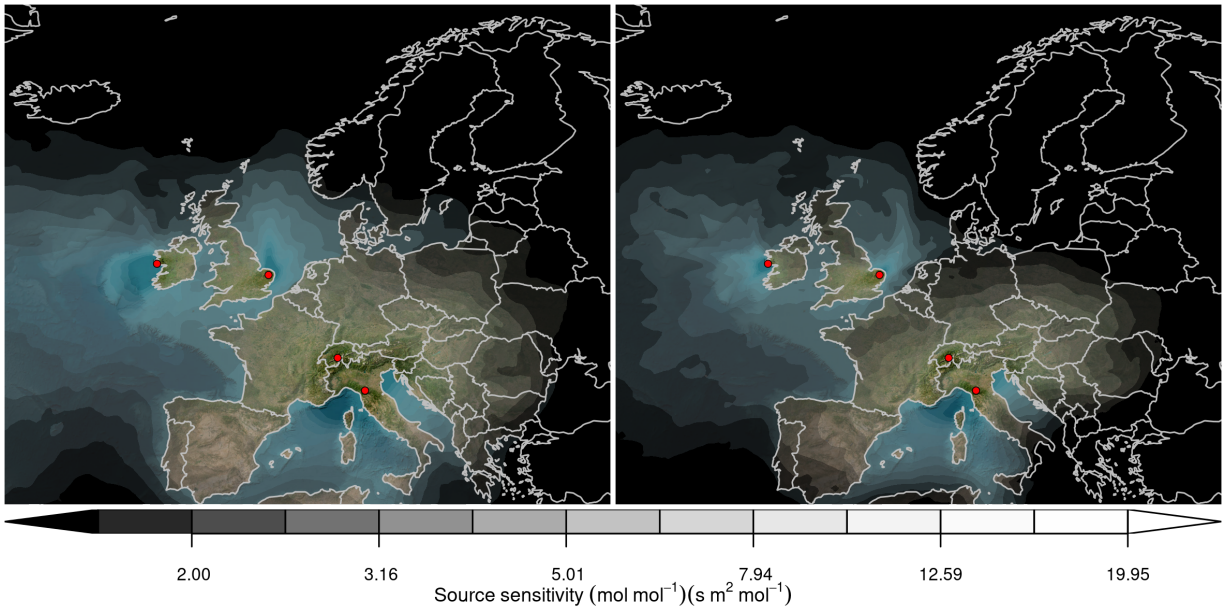

6.1 HFC-32

Figure 6.1.1: Verification of the Swiss emissions inventory estimates for HFC-32. Modelled annual emissions are given as the mean from all models (black line and grey shading) and the individual result from InTEM (blue line and shading). National inventory annual totals are given as grey bars.

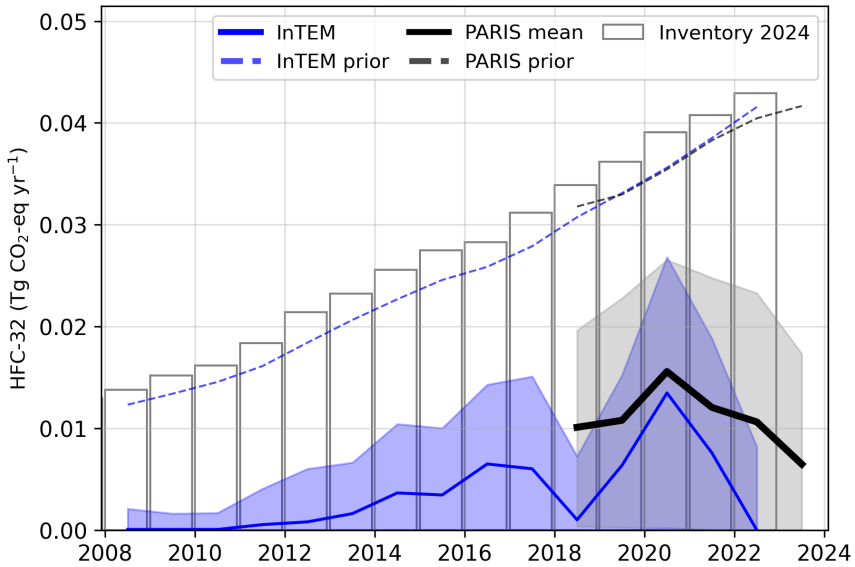

Figure 6.1.2: Spatial distribution of the Swiss average modelled emissions of HFC-32 during the period of 2018-2023 (mean from all models). Observing stations are marked with red circles and highly-populated cities are marked with red triangles.

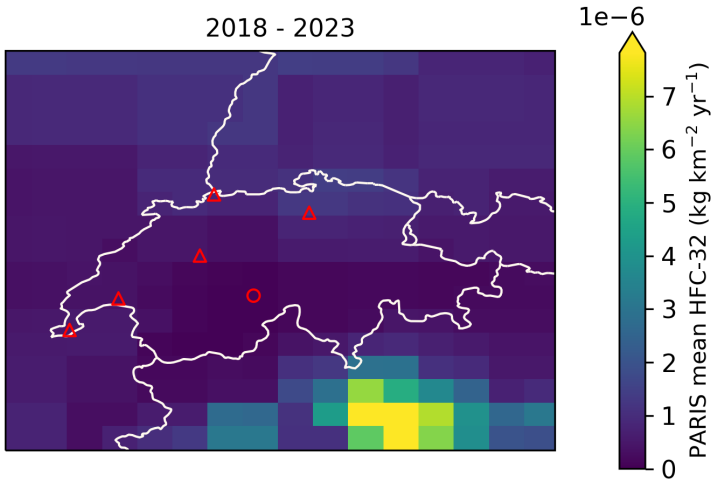

6.2 HFC-125

Figure 6.2.1: Verification of the Swiss emissions inventory estimates for HFC-125. Modelled annual emissions are given as the mean from all models (black line and grey shading) and the individual result from InTEM (blue line and shading). National inventory annual totals are given as grey bars.

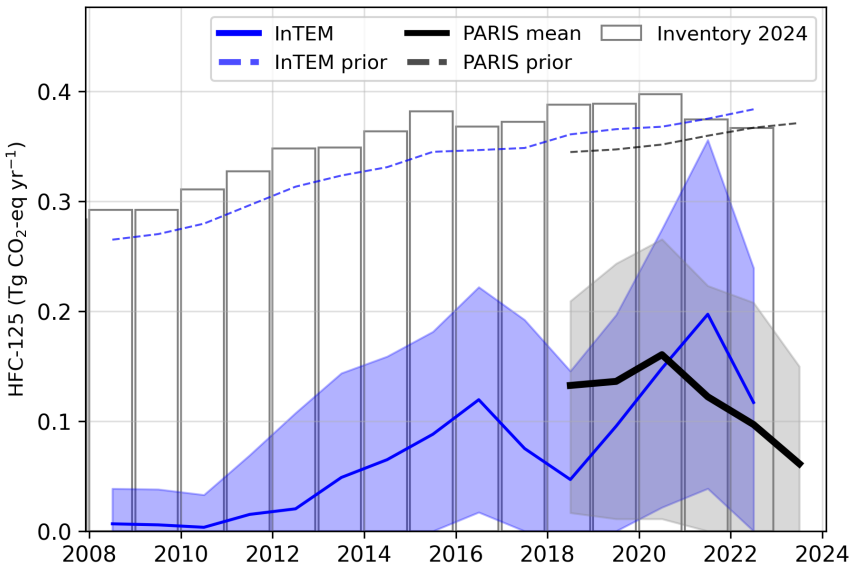

Figure 6.2.2: Spatial distribution of the Swiss average modelled emissions of HFC-125 during the period of 2018-2023 (mean from all models). Observing stations are marked with red circles and highly-populated cities are marked with red triangles.

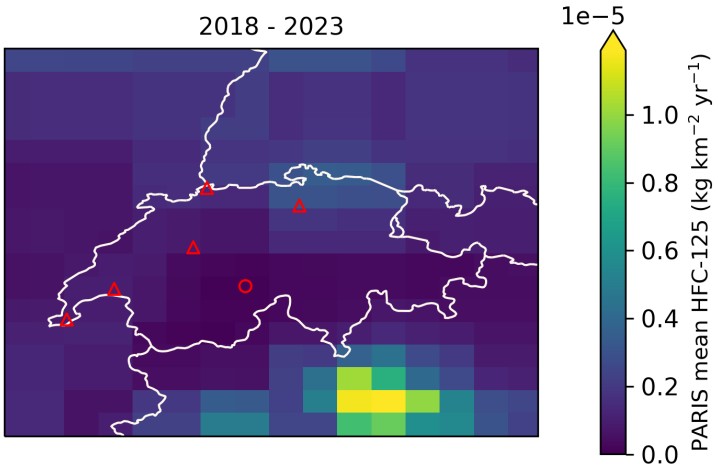

6.3 HFC-134a

Figure 6.3.1: Verification of the Swiss emissions inventory estimates for HFC-134a. Modelled annual emissions are given as the mean from all models (black line and grey shading) and the individual result from InTEM (blue line and shading). National inventory annual totals are given as grey bars.

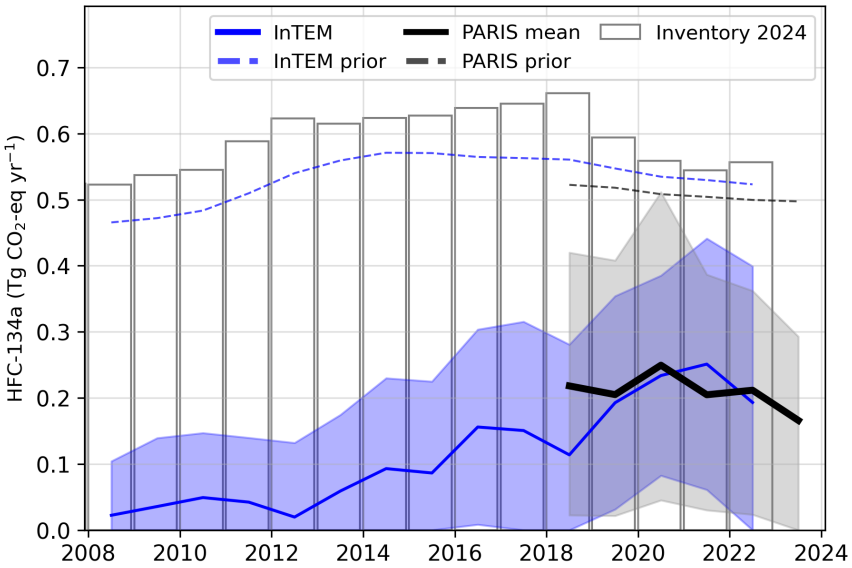

Figure 6.3.2: Spatial distribution of the Swiss average modelled emissions of HFC-134a during the period of 2018-2023 (mean from all models). Observing stations are marked with red circles and highly-populated cities are marked with red triangles.

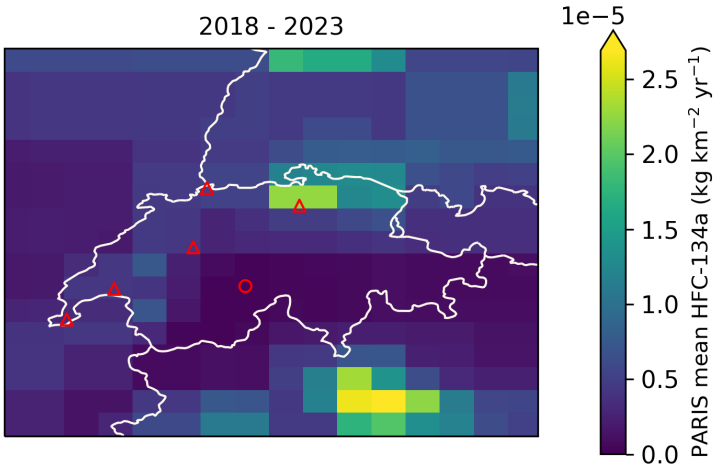

6.4 HFC-143a

Figure 6.4.1: Verification of the Swiss emissions inventory estimates for HFC-143a. Modelled annual emissions are given as the mean from all models (black line and grey shading) and the individual result from InTEM (blue line and shading). National inventory annual totals are given as grey bars.

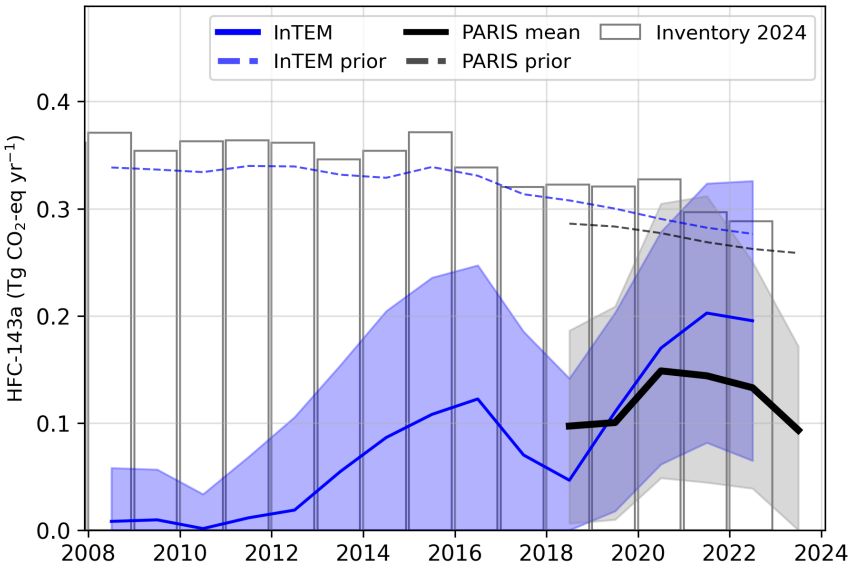

Figure 6.4.2: Spatial distribution of the Swiss average modelled emissions of HFC-143a during the period of 2018-2023 (mean from all models). Observing stations are marked with red circles and highly-populated cities are marked with red triangles.

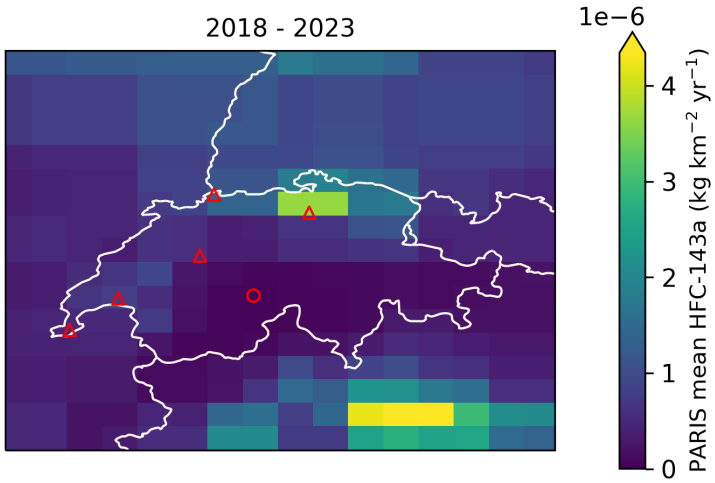

6.5 Total HFCs

Figure 6.5.1: Verification of the Swiss emissions inventory estimates for total HFCs. Modelled annual emissions are given as the mean from all models (black line and grey shading) and the individual result from InTEM (blue line and shading). National inventory annual totals are given as grey bars.

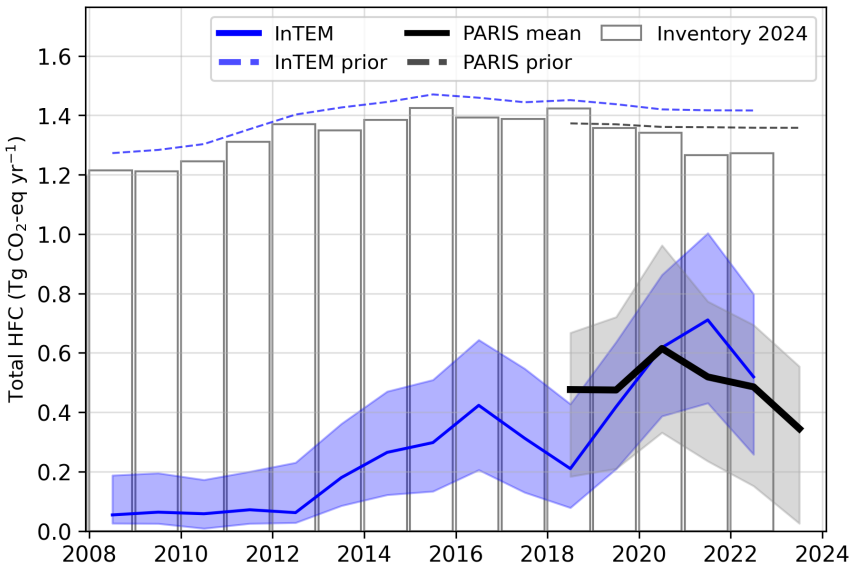

Table 2: Emissions estimation for HFCs in $\mathrm{TgCO_2{-}eq \cdot yr^{-1}}$ according to the National Inventory Report (NIR) 2024 and the inversions done in the PARIS project. For the PARIS estimation, the mean of the 3 inversion models is displayed, along with a range of uncertainty estimated via the half distance between the maximum and minimum uncertainties of the different models.

		2018	2019	2020	2021	2022	2023
HFC-23	NIR 2024	0.0072	0.0091	0.0119	0.0037	0.0040	
	PARIS mean	0.010 ± 0.024	0.014 ± 0.037	0.028 ± 0.074	0.027 ± 0.072	0.024 ± 0.059	0.013 ± 0.025
HFC-32	NIR 2024	0.0339	0.0362	0.0391	0.0408	0.0429	
	PARIS mean	0.01 ± 0.01	0.01 ± 0.01	0.02 ± 0.01	0.01 ± 0.01	0.01 ± 0.01	0.01 ± 0.01
HFC-125	NIR 2024	0.3876	0.3885	0.3971	0.3742	0.3664	
	PARIS mean	0.13 ± 0.10	0.14 ± 0.12	0.16 ± 0.13	0.12 ± 0.11	0.10 ± 0.10	0.06 ± 0.07
HFC-134a	NIR 2024	0.6607	0.5941	0.5589	0.5441	0.5569	
	PARIS mean	0.22 ± 0.20	0.21 ± 0.19	0.25 ± 0.23	0.20 ± 0.18	0.21 ± 0.17	0.17 ± 0.15
HFC-143a	NIR 2024	0.3227	0.3206	0.3273	0.2966	0.2881	
	PARIS mean	0.10 ± 0.09	0.10 ± 0.10	0.15 ± 0.13	0.14 ± 0.13	0.13 ± 0.11	0.09 ± 0.09
HFC-152a	NIR 2024	0.0001	0.0001	0.0000	0.0000	0.0000	
	PARIS mean	0.001 ± 0.002	0.001 ± 0.002	0.001 ± 0.003	0.001 ± 0.003	0.001 ± 0.002	0.000 ± 0.001
HFC-227ea	NIR 2024	0.0065	0.0043	0.0024	0.0025	0.0024	
	PARIS mean	0.004 ± 0.005	0.004 ± 0.004	0.004 ± 0.006	0.003 ± 0.004	0.004 ± 0.005	0.004 ± 0.005
HFC-245fa	NIR 2024	0.0002	0.0002	0.0002	0.0002	0.0002	
	PARIS mean	0.002 ± 0.002	0.001 ± 0.002	0.001 ± 0.002	0.001 ± 0.002	0.001 ± 0.002	0.000 ± 0.001
HFC-365mfc	NIR 2024	0.0038	0.0037	0.0036	0.0038	0.0109	
	PARIS mean	0.002 ± 0.002	0.002 ± 0.003	0.005 ± 0.007	0.005 ± 0.007	0.004 ± 0.006	0.001 ± 0.001
HFC-4310mee	NIR 2024	0.0007	0.0007	0.0002	0.0000	0.0000	
	PARIS mean	0.001 ± 0.002	0.001 ± 0.002	0.001 ± 0.002	0.001 ± 0.003	0.001 ± 0.003	[1]

[1] HFC-4310mee emissions were not estimated for 2023 due to lack of atmospheric observations.

7 Perfluorocarbons (PFCs)

7.1 PFC-14

Figure 7.1.1: Verification of the Swiss emissions inventory estimates for PFC-14. Modelled annual emissions are given as the mean from all models (black line and grey shading) and the individual result from InTEM (blue line and shading). National inventory annual totals are given as grey bars.

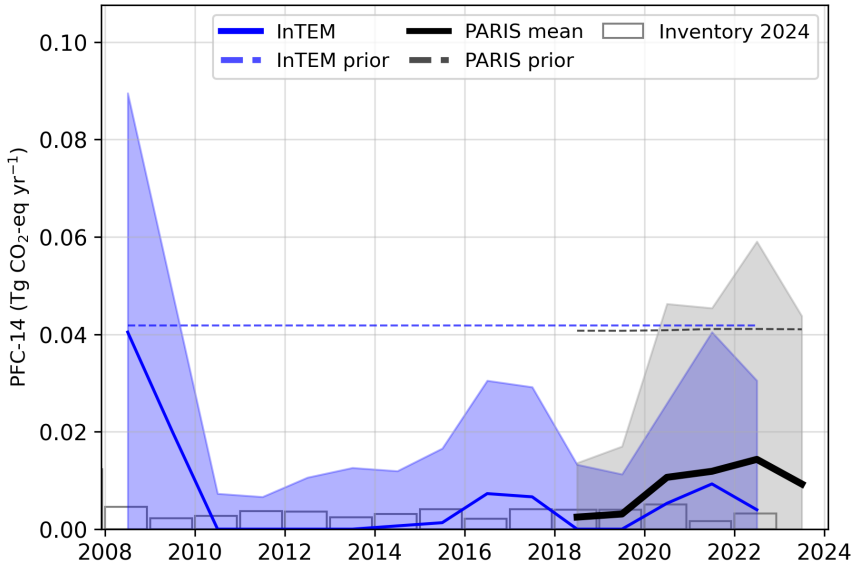

Figure 7.1.2: Spatial distribution of the Swiss average modelled emissions of PFC-14 during the period of 2018-2023 (mean from all models). Observing stations are marked with red circles and highly-populated cities are marked with red triangles.

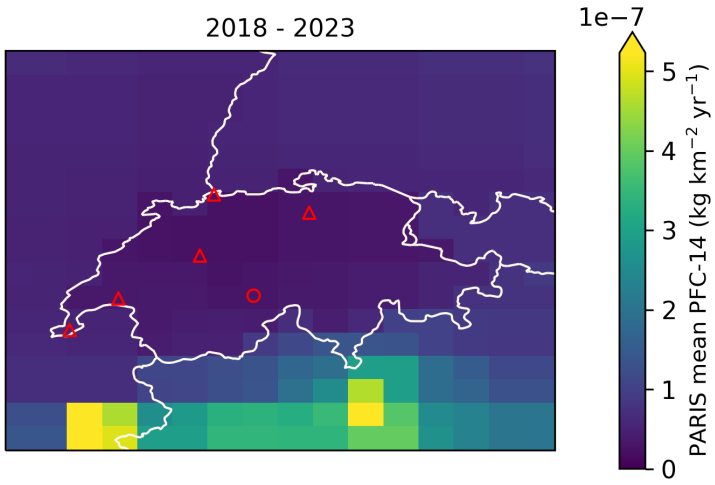

7.2 PFC-116

Figure 7.2.1: Verification of the Swiss emissions inventory estimates for PFC-116. Modelled annual emissions are given as the mean from all models (black line and grey shading) and the individual result from InTEM (blue line and shading). National inventory annual totals are given as grey bars.

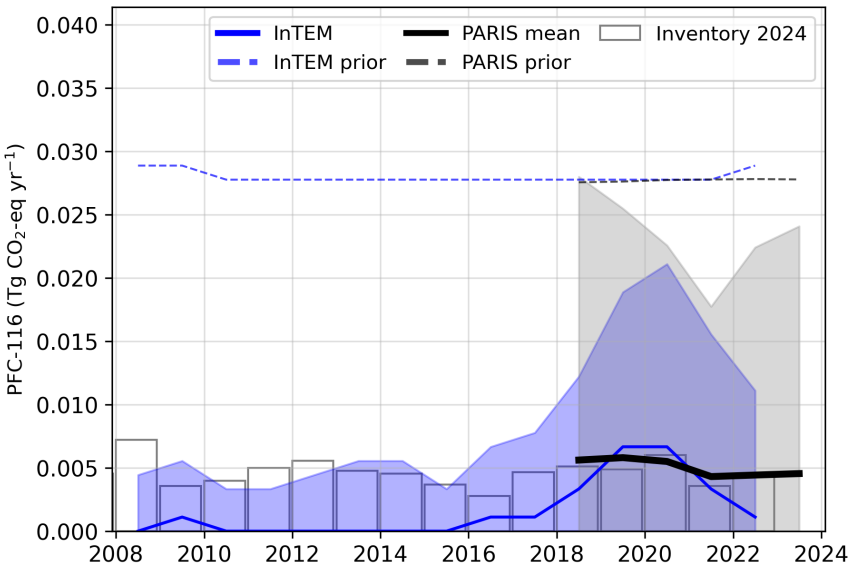

Figure 7.2.2: Spatial distribution of the Swiss average modelled emissions of PFC-116 during the period of 2018-2023 (mean from all models). Observing stations are marked with red circles and highly-populated cities are marked with red triangles.

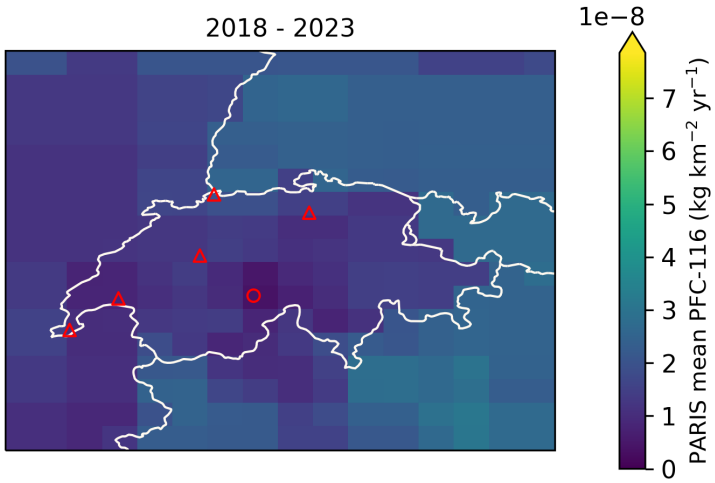

7.3 PFC-218

Figure 7.3.1: Verification of the Swiss emissions inventory estimates for PFC-218. Modelled annual emissions are given as the mean from all models (black line and grey shading) and the individual result from InTEM (blue line and shading). National inventory annual totals are given as grey bars.

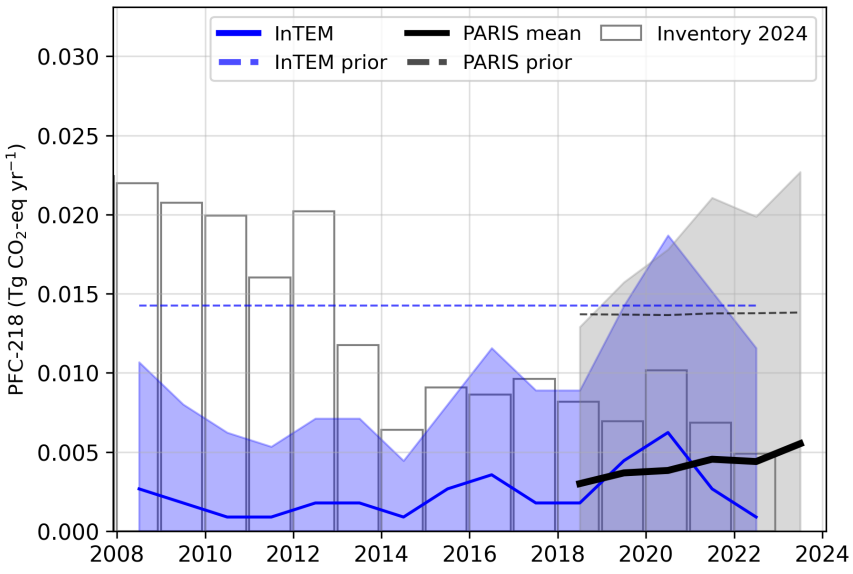

Figure 7.3.2: Spatial distribution of the Swiss average modelled emissions of PFC-218 during the period of 2018-2023 (mean from all models). Observing stations are marked with red circles and highly-populated cities are marked with red triangles.

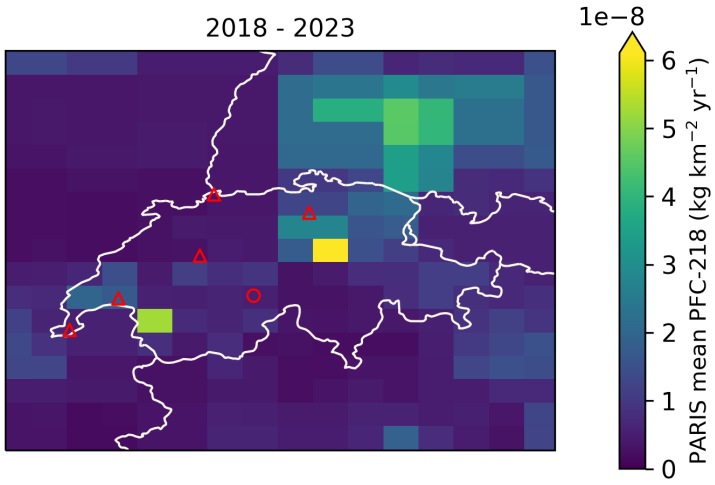

7.4 PFC-318

Figure 7.4.1: Verification of the Swiss emissions inventory estimates for PFC-318. Modelled annual emissions are given as the mean from all models (black line and grey shading) and the individual result from InTEM (blue line and shading). National inventory annual totals are given as grey bars.

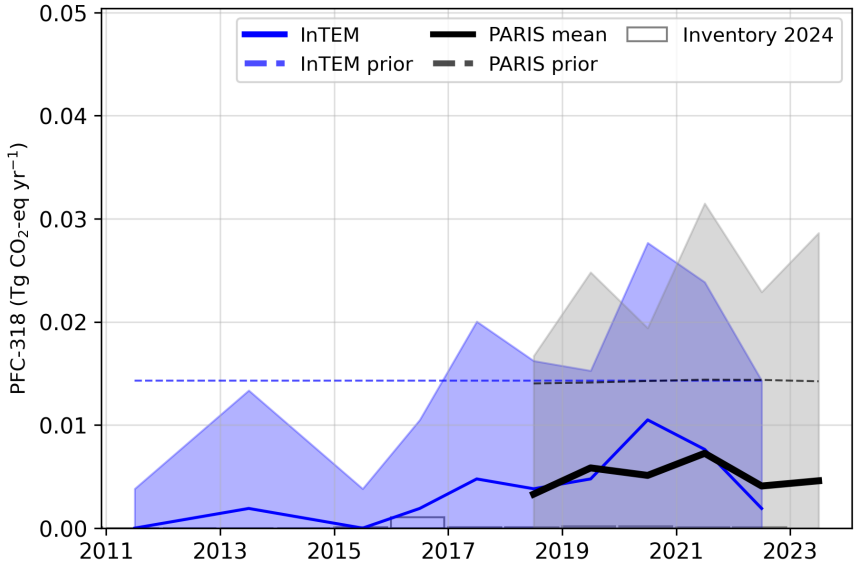

Figure 7.4.2: Spatial distribution of the Swiss average modelled emissions of PFC-318 during the period of 2018-2023 (mean from all models). Observing stations are marked with red circles and highly-populated cities are marked with red triangles.

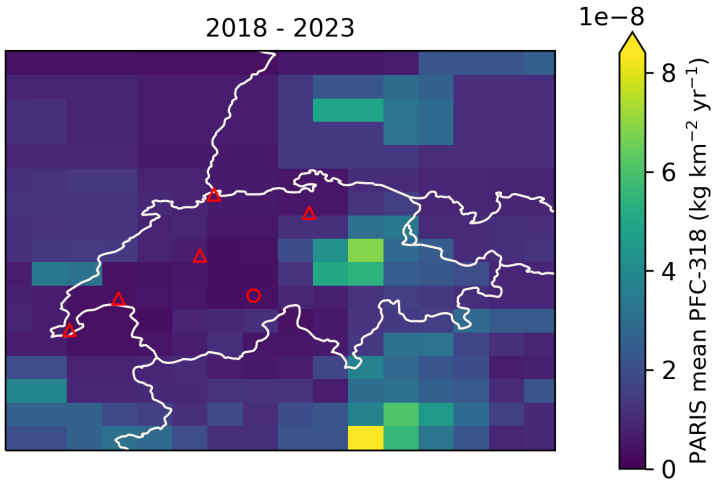

7.5 Total PFCs

Figure 7.5.1: Verification of the Swiss emissions inventory estimates for total PFCs. Modelled annual emissions are given as the mean from all models (black line and grey shading) and the individual result from InTEM (blue line and shading). National inventory annual totals are given as grey bars.

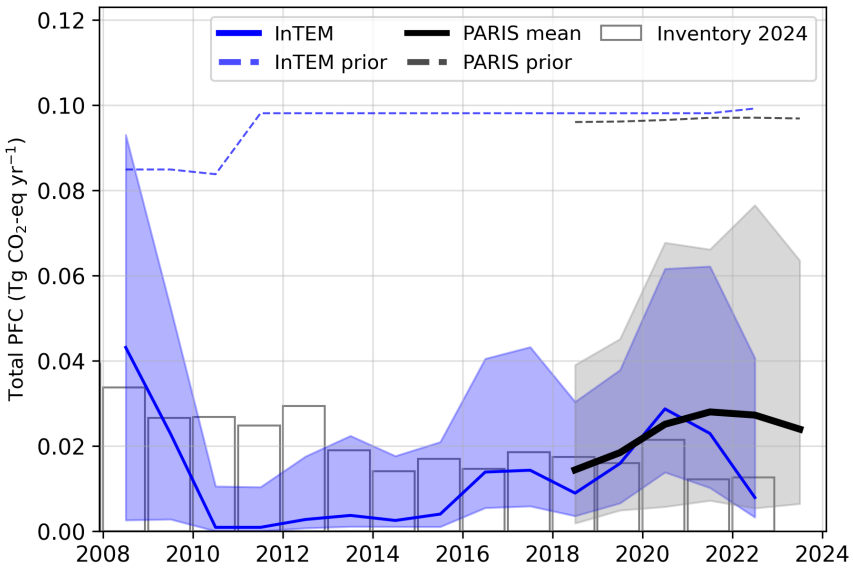

Table 3: Emissions estimation for PFCs in $\mathrm{TgCO_2{-}eq \cdot yr^{-1}}$ according to the National Inventory Report (NIR) 2024 and the inversions done in the PARIS project. For the PARIS estimation, the mean of the 3 inversion models is displayed, along with a range of uncertainty estimated via the half distance between the maximum and minimum uncertainties of the different models.

		2018	2019	2020	2021	2022	2023
PFC-14	NIR 2024	0.0040	0.0040	0.0051	0.0017	0.0032	
	PARIS mean	0.002 ± 0.007	0.003 ± 0.008	0.011 ± 0.023	0.012 ± 0.023	0.014 ± 0.030	0.009 ± 0.022
PFC-116	NIR 2024	0.0051	0.0049	0.0060	0.0036	0.0043	
	PARIS mean	0.006 ± 0.014	0.006 ± 0.013	0.006 ± 0.011	0.004 ± 0.009	0.004 ± 0.011	0.005 ± 0.012
PFC-218	NIR 2024	0.0082	0.0069	0.0101	0.0069	0.0049	
	PARIS mean	0.003 ± 0.006	0.004 ± 0.008	0.004 ± 0.009	0.005 ± 0.011	0.004 ± 0.010	0.006 ± 0.011
PFC-318	NIR 2024	0.0001	0.0002	0.0002	0.0001	0.0001	
	PARIS mean	0.003 ± 0.008	0.006 ± 0.012	0.005 ± 0.010	0.007 ± 0.016	0.004 ± 0.011	0.005 ± 0.014

8 Sulphur hexafluoride (SF_6)

Figure 8.0.1: Total source sensitivity of SF_6 observing sites as calculated by the NAME transport model for the year (left) 2018 and (right) 2023 and used in the inversions. Observing stations active in each year are marked with red dots. Areas with visible land surface represent regions for which emissions can be observed well from the network. Shaded or dark areas represent regions for which limited emission information can be obtained from the network.

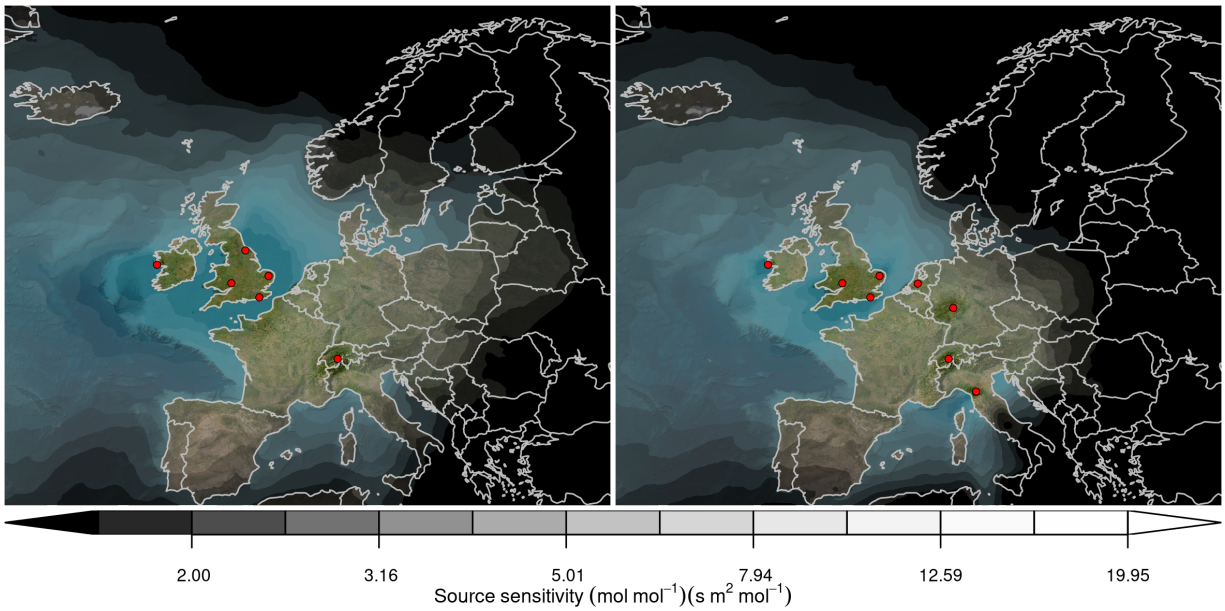

Figure 8.0.2: Verification of the Swiss emissions inventory estimates for SF_6. Modelled annual emissions are given as the mean from all models (black line and grey shading) and the individual result from InTEM (blue line and shading). National inventory annual totals are given as grey bars.

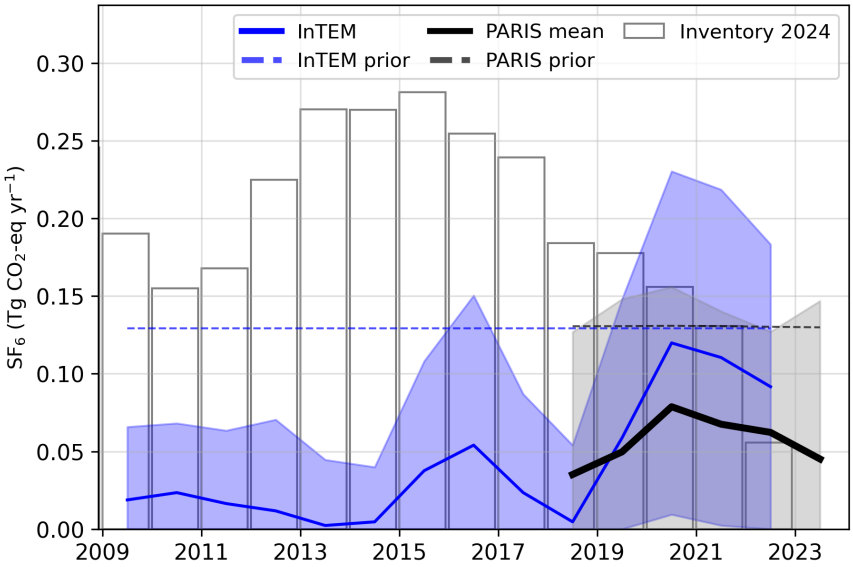

Figure 8.0.3: Spatial distribution of the Swiss average modelled emissions of SF_6 during the period of 2018-2023 (mean from all models). Observing stations are marked with red circles and highly-populated cities are marked with red triangles.

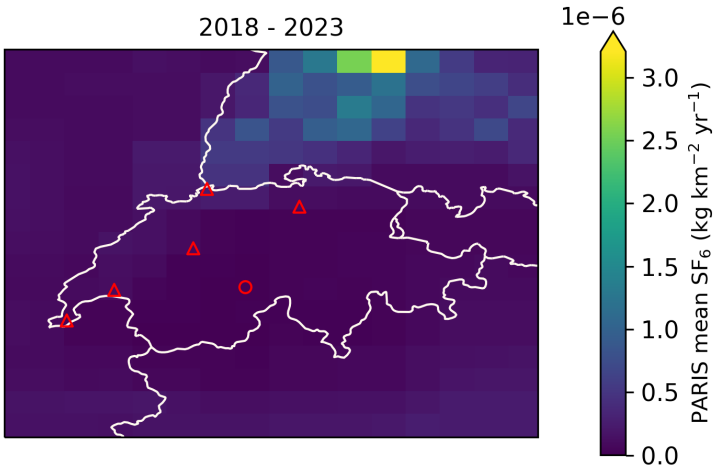

References

European Commission: Joint Research, Centre et al. (2023). *GHG emissions of all world countries – 2023*. Publications Office of the European Union. DOI: 10.2760/953322.

Ganesan, A. L. et al. (2014). "Characterization of uncertainties in atmospheric trace gas inversions using hierarchical Bayesian methods". In: *Atmospheric Chemistry and Physics* 14.8, pp. 3855–3864. DOI: 10.5194/acp-14-3855-2014. URL: http://www.atmos-chem-phys.net/14/3855/2014/http://www.atmos-chem-phys.net/14/3855/2014/acp-14-3855-2014.pdf.

Ganesan, A. L. et al. (2015). "Quantifying methane and nitrous oxide emissions from the UK and Ireland using a national-scale monitoring network". In: *Atmos. Chem. Phys.* 15.11, pp. 6393–6406. DOI: 10.5194/acp-15-6393-2015. URL: https://www.atmos-chem-phys.net/15/6393/2015/https://www.atmos-chem-phys.net/15/6393/2015/acp-15-6393-2015.pdf.

Henne, S. et al. (2016). "Validation of the Swiss methane emission inventory by atmospheric observations and inverse modelling". In: *Atmospheric Chemistry and Physics* 16.6, pp. 3683–3710. DOI: 10.5194/acp-16-3683-2016. URL: http://www.atmos-chem-phys.net/16/3683/2016/.

Jones, A.R. et al. (2007). "The U.K. Met Office's next-generation atmospheric dispersion model, NAME III, in Borrego C. and Norman A.-L. (Eds)". In: *Air Pollution Modeling and its Application XVII (Proceedings of the 27th NATO/CCMS International Technical Meeting on Air Pollution Modelling and its Application), Springer*, pp. 580–589.

Katharopoulos, I. et al. (2023). "Impact of transport model resolution and a priori assumptions on inverse modeling of Swiss F-gas emissions". In: *Atmos. Chem. Phys.* 23.22, pp. 14159–14186. DOI: 10.5194/acp-23-14159-2023. URL: https://acp.copernicus.org/articles/23/14159/2023/.

Manning, A. J. et al. (2021). "Evidence of a recent decline in UK emissions of hydrofluorocarbons determined by the InTEM inverse model and atmospheric measurements". In: *Atmospheric Chemistry and Physics* 21.16, pp. 12739–12755. DOI: 10.5194/acp-21-12739-2021. URL: https://acp.copernicus.org/articles/21/12739/2021/.

Rigby, M. et al. (2019). "Increase in CFC-11 emissions from eastern China based on atmospheric observations". In: *Nature* 569, pp. 546–550. DOI: 10.1038/s41586-019-1193-4. URL: https://doi.org/10.1038/s41586-019-1193-4.

Draft Inventory Annex
UK 2024

18th November, 2024

1 Introduction

In this document, global concentration trends and national emissions estimates derived from atmospheric observations ("inverse estimates") are presented for each reported gas. Comparing the emissions submitted in national inventories with those calculated using atmospheric observations allows for emissions to be assessed using two fundamentally different approaches. Substantial differences can highlight areas that could warrant further investigation.

Global concentration trends for each gas are first shown using annual average concentrations from Mace Head, Ireland (Northern Hemisphere) and Kennaook/Cape Grim, Tasmania, Australia (Southern Hemisphere). Data from these stations were selected to exclude regionally-polluted air masses and therefore represents northern and southern hemispheric concentration trends. Mace Head observations were supported by the National Aeronautics and Space Administration (NASA) and the UK Department of Energy, Security and Net Zero (DESNZ), and Kennaook/Cape Grim observations by NASA and the Australian Bureau of Meteorology.

Observations of European concentrations of greenhouse gases used to derive national inverse emission estimates were collected from many different networks and providers. Methane and nitrous oxide concentrations originated from the European ICOS (Integrated Carbon Observation System) network, the UK DECC (Deriving Emissions related to Climate Change) network and other national or individual initiatives. F-gas observations were made by affiliates of the AGAGE (Advanced Global Atmospheric Gases Experiment) network. Observations from from additional stations across Europe were supported by the Horizon-EU PARIS (Process Attribution of Regional Emissions) project. The observation stations used to derive emissions for each gas are shown in the corresponding sections of this document.

Inversion-based emissions estimates were derived using one atmospheric transport model but with multiple inverse models allowing a better quantification of the uncertainties associated with inverse modelling. The atmospheric transport model provides the link between surface fluxes and concentrations measured at the observing stations. Although the uncertainty associated with the atmospheric transport model is considered in the statistical inversion approach, it may be underestimated when only using a single transport model. The atmospheric transport model used is the Numerical Atmospheric dispersion Modelling Environment (NAME) (Jones et al., 2007), a backwards-running Lagrangian Particle Dispersion Model (LPDM) that simulates the recent transport of air to each observing station. The NAME model has been widely used in the estimation of greenhouse gases emissions (Ganesan et al., 2015; Rigby et al., 2019; Manning et al., 2021).

The three inverse methods used are InTEM (Inversion Technique for Emission Modelling, Manning et al., 2021), ELRIS (Empa Lagrangian Regional Inversion System, Henne et al., 2016; Katharopoulos et al., 2023), and RHIME (Regional Hierarchical Inverse Modelling Environment, Ganesan et al., 2014). All three inverse methods estimate emissions within Europe along with boundary conditions that account for the concentration of the air entering Europe. All three systems started from the same set of a priori emissions that were either derived from the global EDGAR emission inventory (version 8, European Commission: Joint Research et al., 2023) or a uniform land-based emission, depending on the gas. A natural emission component, from the WETCHARTS product, was included in the methane prior. The same observational dataset was used by each inverse model, but data selection (i.e., filtering datasets for specific conditions) and treatment of uncertainties were chosen separately and hence differ. The three methods also differ in their statistical approaches for estimating emissions.

Emission estimates are presented for the period 2008-2023. Emissions for the full 2008-2023 period were derived with the InTEM model only, while emissions from 2018-2023 are presented as a combined result using the three inverse models.

For the 2008-2023 InTEM results, a 2-year inversion resolution, incrementing annually, was used for all gases except CH_4nd N_2, where the resolution was monthly. For the recent 2018-2023 period, for all three models, the inversion resolution was one month for CH_4 and N_2O in order to capture the seasonality of the emissions, a one-year average over these results is also presented. For the fluorinated gases, a 1-year

inversion resolution was adopted, with a 3-year moving average applied to the results. The uncertainty shown is the minimum/maximum of the uncertainties from the three results.

2 Global Concentration Trends

2.1 Methane (CH_4)

Figure 2.1.1: Background Northern Hemisphere monthly concentrations of CH_4 estimated from MHD, Ireland observations are shown in red, and background Southern Hemisphere monthly concentrations from CGO, Tasmania are shown in blue. Grey shading represents provisional data.

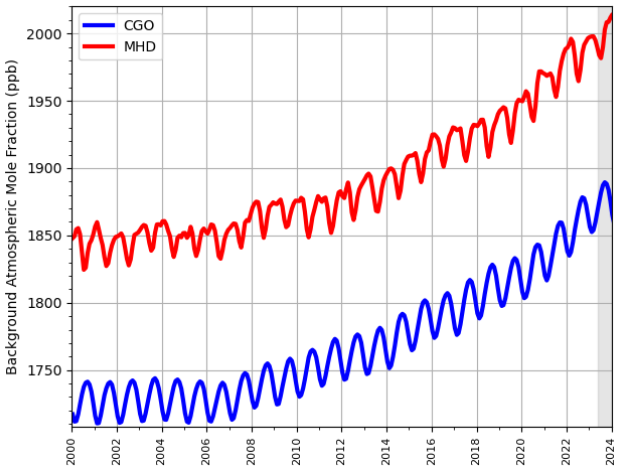

2.2 Nitrous Oxide (N_2O)

Figure 2.2.1: Background Northern Hemisphere monthly concentrations of N_2O estimated from MHD, Ireland observations are shown in red, and background Southern Hemisphere monthly concentrations from CGO, Tasmania are shown in blue. Grey shading represents provisional data.

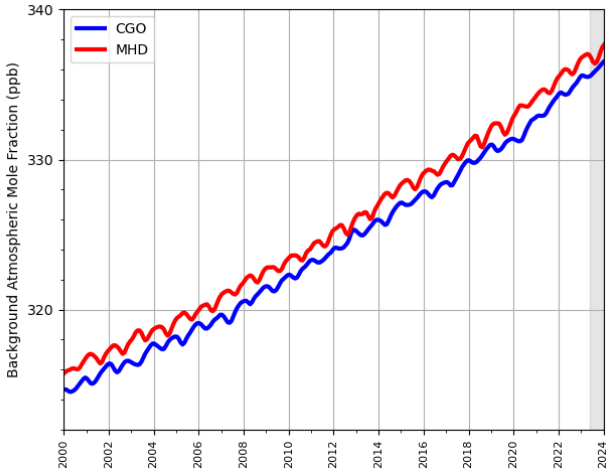

2.3 Hydrofluorocarbons (HFCs)

Figure 2.3.1: Background Northern Hemisphere monthly concentrations of six HFCs estimated from MHD, Ireland observations are shown in red, and background Southern Hemisphere monthly concentrations from CGO, Tasmania are shown in blue. Grey shading represents provisional data.

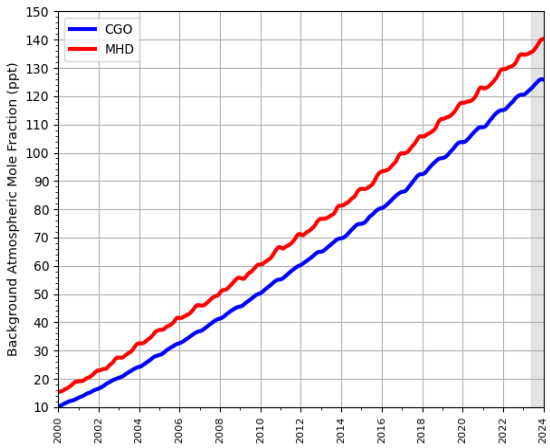

(a) HFC-134a

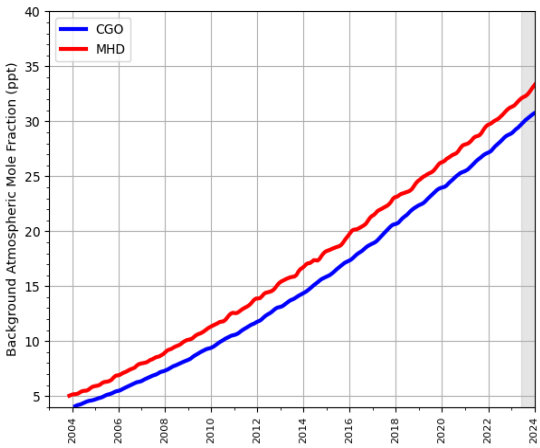

(b) HFC-143a

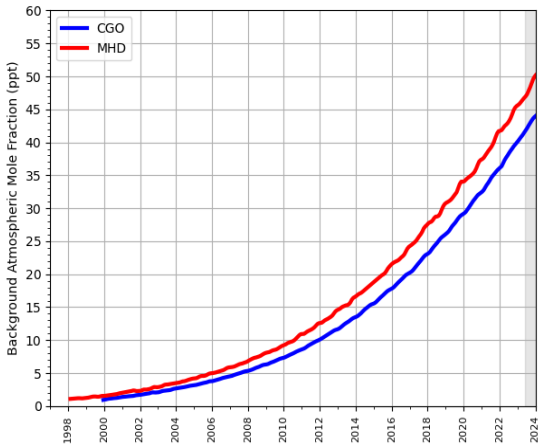

(c) HFC-125

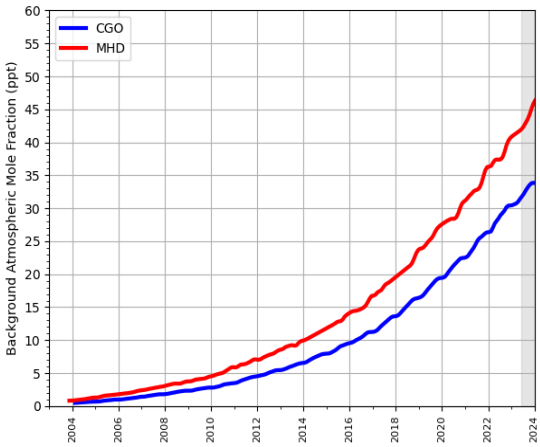

(d) HFC-32

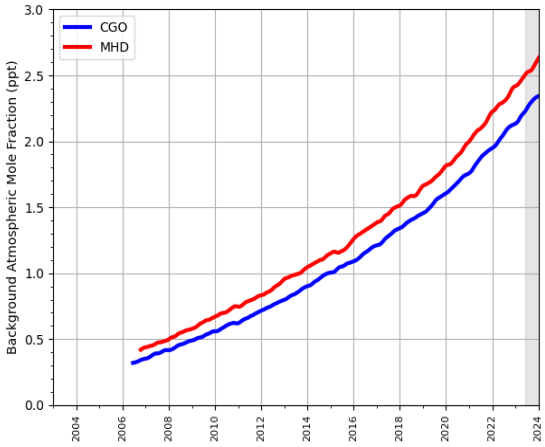

(e) HFC-227ea

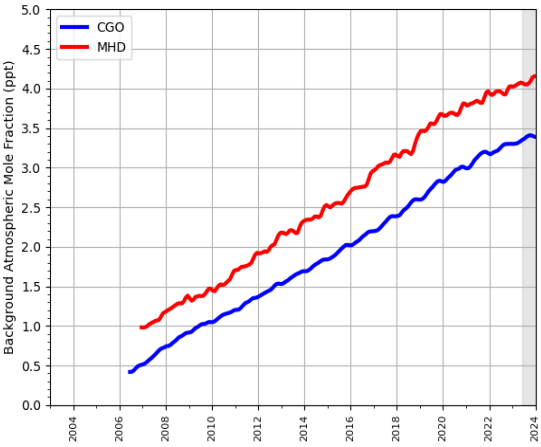

(f) HFC-245fa

Figure 2.3.2: Background Northern Hemisphere monthly concentrations of four HFCs estimated from MHD, Ireland observations are shown in red, and background Southern Hemisphere monthly concentrations from CGO, Tasmania are shown in blue. Grey shading represents provisional data.

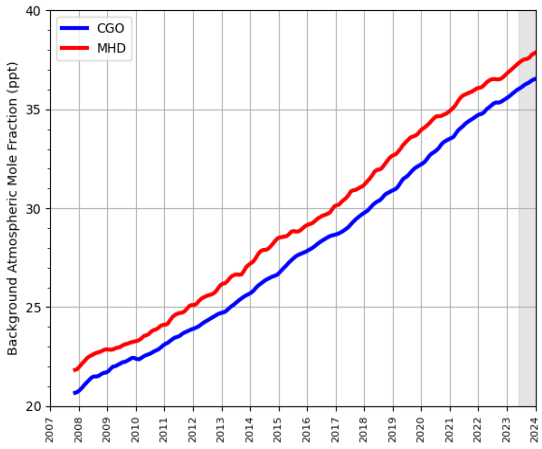

(a) HFC-23

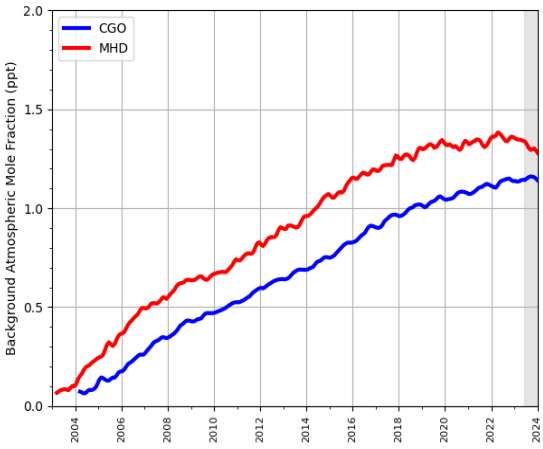

(b) HFC-365mfc

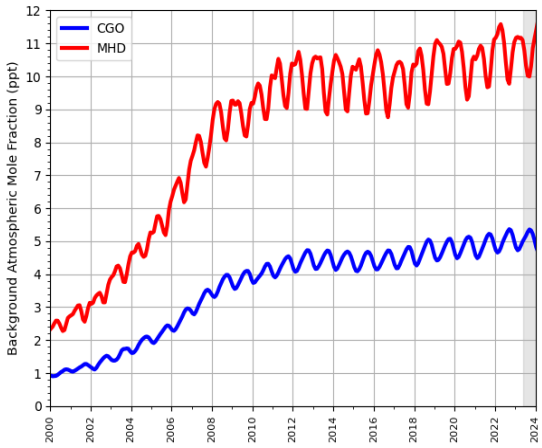

(c) HFC-152a

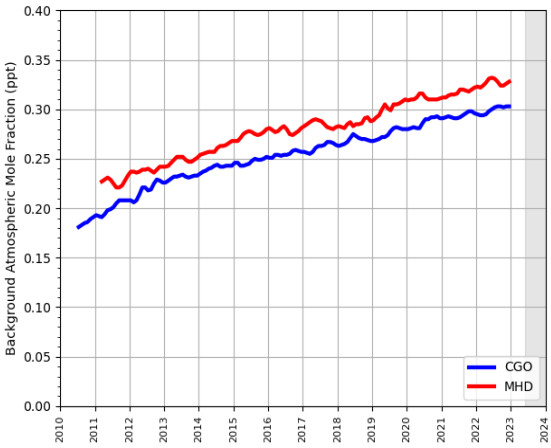

(d) HFC-43-10-mee

2.4 Perfluorocarbons (PFCs)

Figure 2.4.1: Background Northern Hemisphere monthly concentrations of four PFCs estimated from MHD, Ireland observations are shown in red, and background Southern Hemisphere monthly concentrations from CGO, Tasmania are shown in blue. Grey shading represents provisional data.

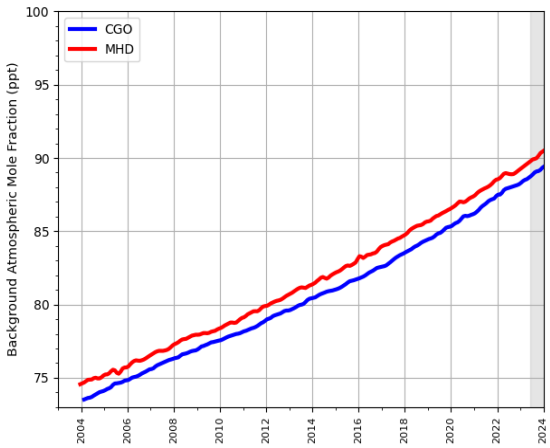

(a) PFC-14

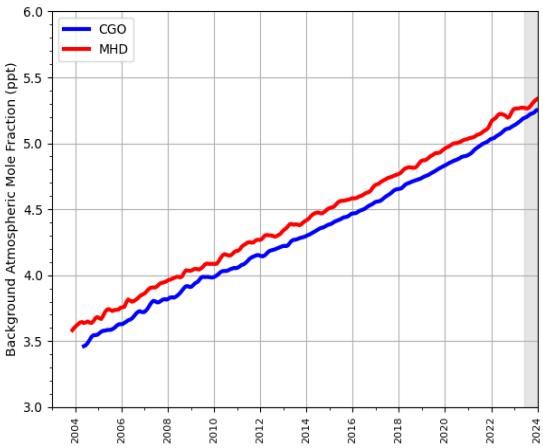

(b) PFC-116

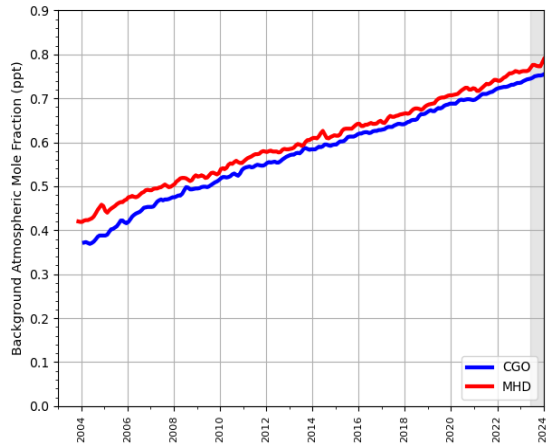

(c) PFC-218

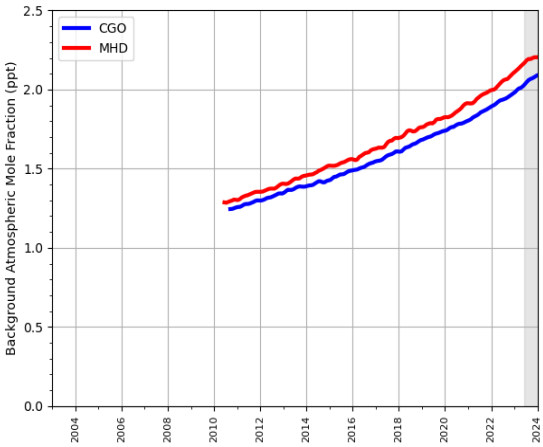

(d) PFC-318

3 Key findings

- Methane (CH_4): Inversion results are around 10-20% lower than the inventory estimates between 2017 and 2023. The inclusion of additional observational data from 2017 has had an impact on the UK estimates even though no additional observational data were added close to the UK. This impact requires further investigation. There does not appear to be a strong seasonal cycle in the emissions.
- Nitrous oxide (N_2O): Inversion results are around 20% higher than the inventory estimates. In all years the inverse models estimate a pronounced seasonal cycle in emissions with the maximum in late spring or early summer.
- Hydrofluorocarbons (HFCs): The emissions estimates from the inverse models generally agree, within the uncertainties, with those reported in the inventory.
- Perfluorocarbons (PFCs): The inverse results reveal some notable areas of emission, in NW and NE of England for PFC-14 and PFC-116 and in the NW of England for PFC-218. The inverse model estimates are higher than those reported in the inventory although the uncertainties are very high.
- Sulphur hexafluoride (SF_6): The trend and magnitude estimated by the inversions is consistent with that reported inventory 2018-2023. In earlier years, 2009-2017, the InTEM estimates are somewhat higher. The spatial distribution appears to be largely population-based.
- The observational coverage of the UK is generally very good. Scotland is the least well constrained area, especially for HFCs and PFCs.

Table 1: Emissions estimation for the main greenhouse gases of focus in $\mathrm{TgCO_2{-}eq \cdot yr^{-1}}$ according to the National Inventory Report (NIR) 2024 and the inversions done in the PARIS project. For the PARIS estimation, the mean of the 3 inversion models is displayed, along with a range of uncertainty estimated via the half distance between the maximum and minimum uncertainties of the different models.

		2018	2019	2020	2021	2022	2023
CH_4	NIR 2024	61	60	58	57	56	
	PARIS mean	49 ± 7	49 ± 6	44 ± 6	48 ± 5	46 ± 6	41 ± 6
N_2O	NIR 2024	20	20	19	19	18	
	PARIS mean	25 ± 2	23 ± 2	21 ± 2	23 ± 2	21 ± 2	21 ± 3
Total HFCs[(1)]	NIR 2024	9.7	9.0	8.2	7.6	7.1	
	PARIS mean	9.0 ± 0.8	8.3 ± 0.7	7.4 ± 0.7	7.2 ± 0.7	7.5 ± 0.7	7.3 ± 0.8
Total PFCs[(2)]	NIR 2024	0.1	0.2	0.2	0.2	0.1	
	PARIS mean	0.4 ± 0.2	0.4 ± 0.2	0.4 ± 0.2	0.4 ± 0.2	0.5 ± 0.3	0.6 ± 0.3
SF_6	NIR 2024	0.6	0.5	0.4	0.4	0.3	
	PARIS mean	0.6 ± 0.2	0.5 ± 0.2	0.5 ± 0.2	0.4 ± 0.2	0.4 ± 0.2	0.4 ± 0.2

(1) Sum of HFC emissions presented in Table 2, except HFC-4310mee.
(2) Sum of PFC emissions presented in Table 3.

4 Methane (CH_4)

Figure 4.0.1: Total source sensitivity of CH_4 observing sites as calculated by the NAME transport model for the year (left) 2018 and (right) 2023 and used in the inversions. Observing stations active in each year are marked with red dots. Areas with visible land surface represent regions for which emissions can be observed well from the network. Shaded or dark areas represent regions for which limited emission information can be obtained from the network.

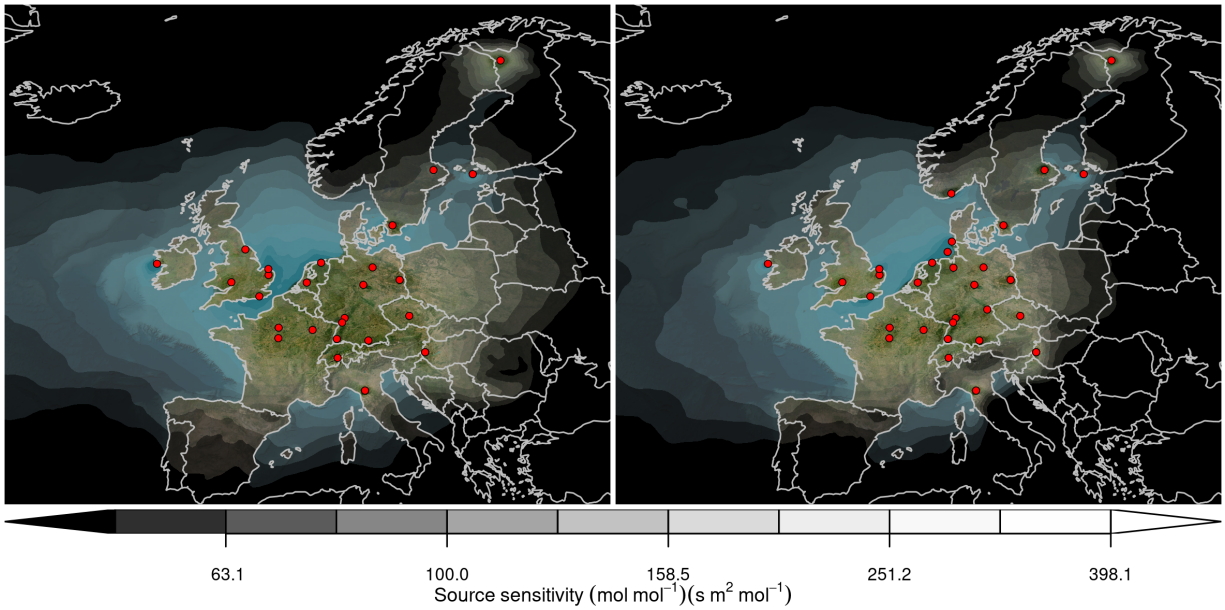

Figure 4.0.2: Verification of the UK emissions inventory estimates for CH_4. Modelled annual emissions are given as the mean from all models (black line and grey shading) and the individual result from InTEM (blue line and shading). National inventory annual totals are given as grey bars.

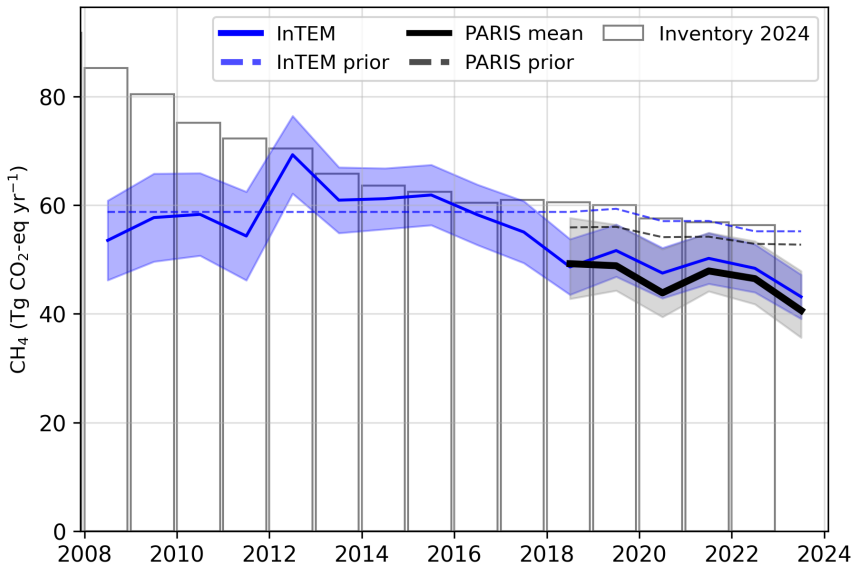

Figure 4.0.3: Verification of the UK emissions inventory estimates for CH_4 (zoom in to 2018-2023). Modelled annual emissions are given as the mean from all models (black line and grey shading) and the individual result from InTEM (blue line and shading). National inventory annual totals are given as grey bars.

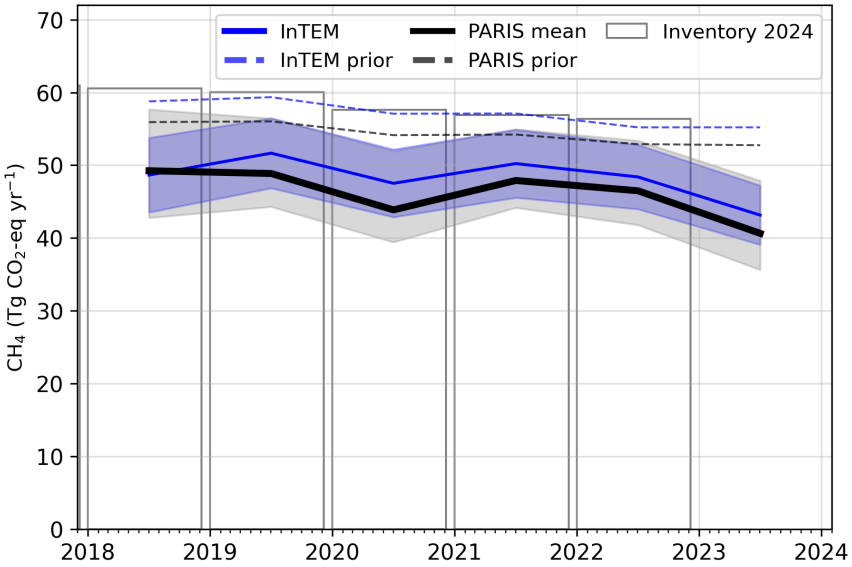

Figure 4.0.4: Verification of the UK emissions inventory estimates for CH_4 (zoom in to 2018-2023). Modelled monthly emissions are given as the mean from all models (black line and grey shading) and the individual result from InTEM (blue line and shading). National inventory annual totals are given as grey bars.

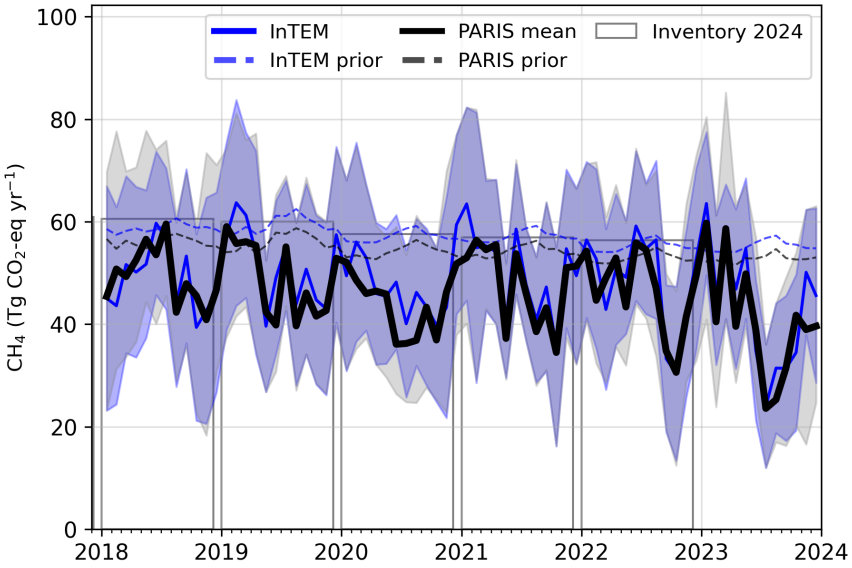

Figure 4.0.5: Spatial distribution of the UK average modelled emissions of CH_4 during the period of 2018-2023 (mean from all models). Observing stations are marked with red circles and highly-populated cities are marked with red triangles.

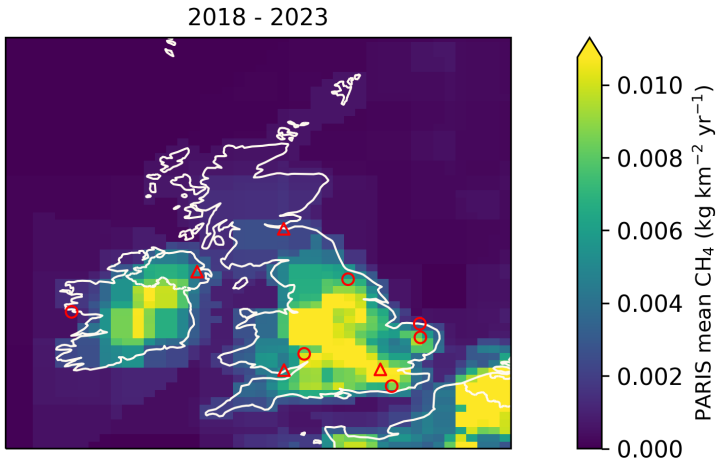

Figure 4.0.6: Spatial distribution of the seasonal deviation from the mean. The deviation is defined as the modelled UK seasonally averaged CH_4 emissions over 2018-2023 minus the average over the whole period. The mean across all models is shown. Observing stations are marked with red circles and highly-populated cities are marked with red triangles.

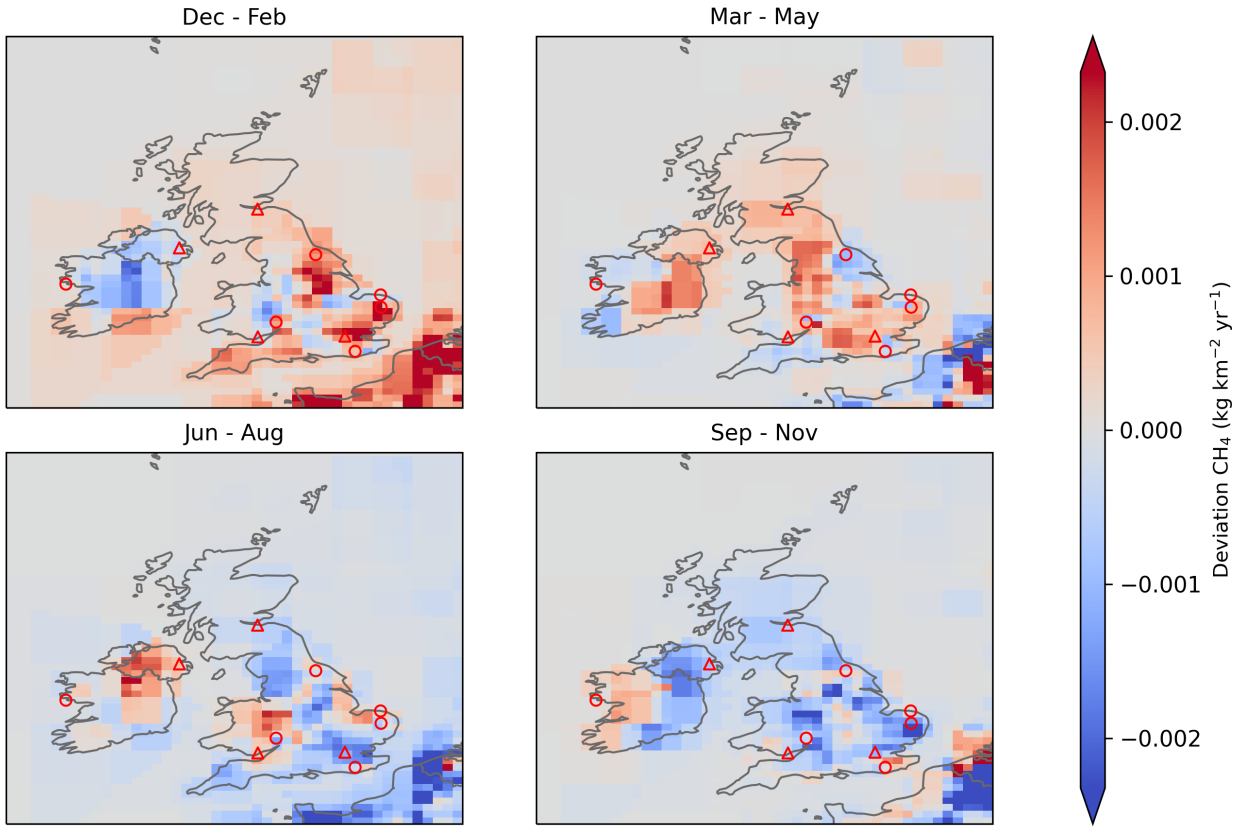

5 Nitrous Oxide (N_2O)

Figure 5.0.1: Total source sensitivity of N_2O observing sites as calculated by the NAME transport model for the year (left) 2018 and (right) 2023 and used in the inversions. Observing stations active in each year are marked with red dots. Areas with visible land surface represent regions for which emissions can be observed well from the network. Shaded or dark areas represent regions for which limited emission information can be obtained from the network.

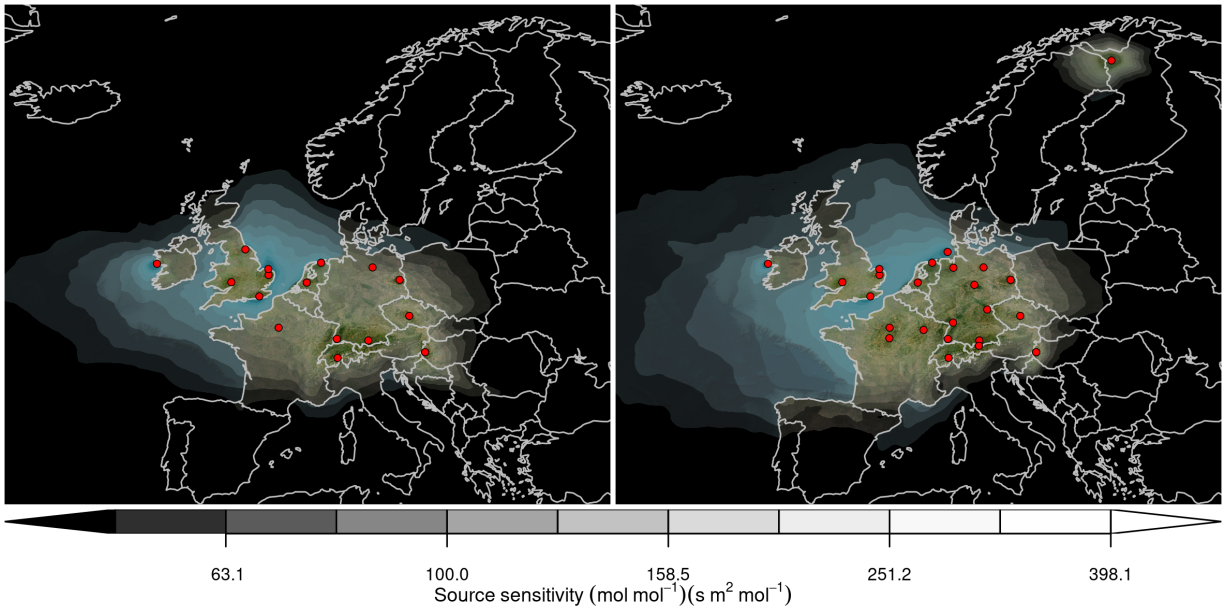

Figure 5.0.2: Verification of the UK emissions inventory estimates for N_2O. Modelled annual emissions are given as the mean from all models (black line and grey shading) and the individual result from InTEM (blue line and shading). National inventory annual totals are given as grey bars.

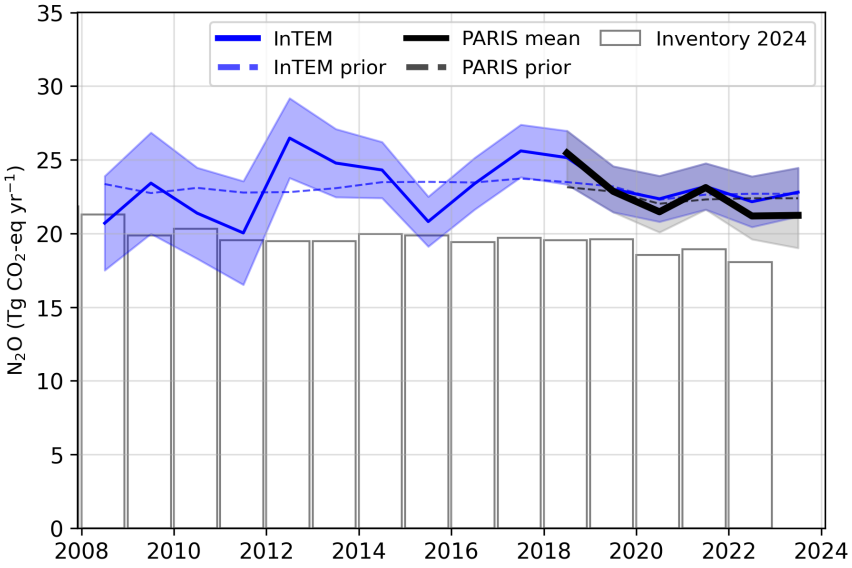

Figure 5.0.3: Verification of the UK emissions inventory estimates for N_2O (zoom in to 2018-2023). Modelled annual emissions are given as the mean from all models (black line and grey shading) and the individual result from InTEM (blue line and shading). National inventory annual totals are given as grey bars.

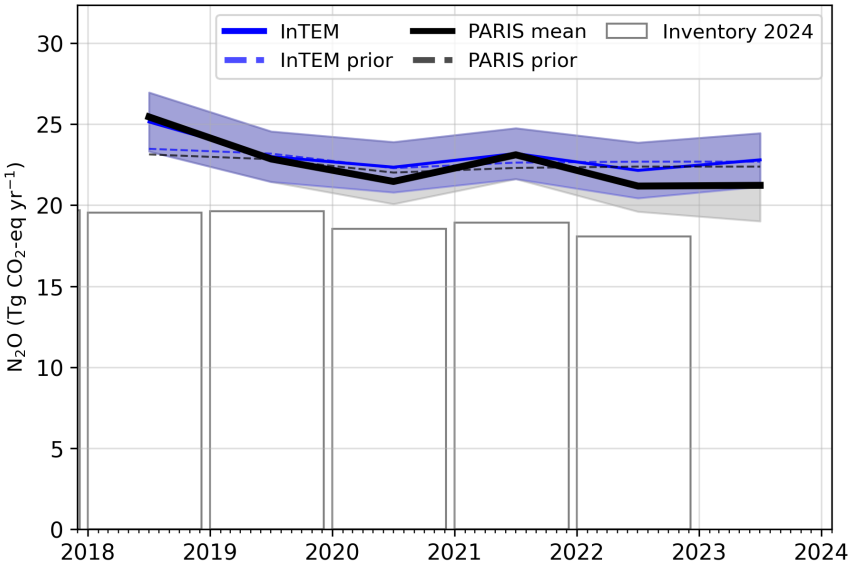

Figure 5.0.4: Verification of the UK emissions inventory estimates for N_2O (zoom in to 2018-2023). Modelled monthly emissions are given as the mean from all models (black line and grey shading) and the individual result from InTEM (blue line and shading). National inventory annual totals are given as grey bars.

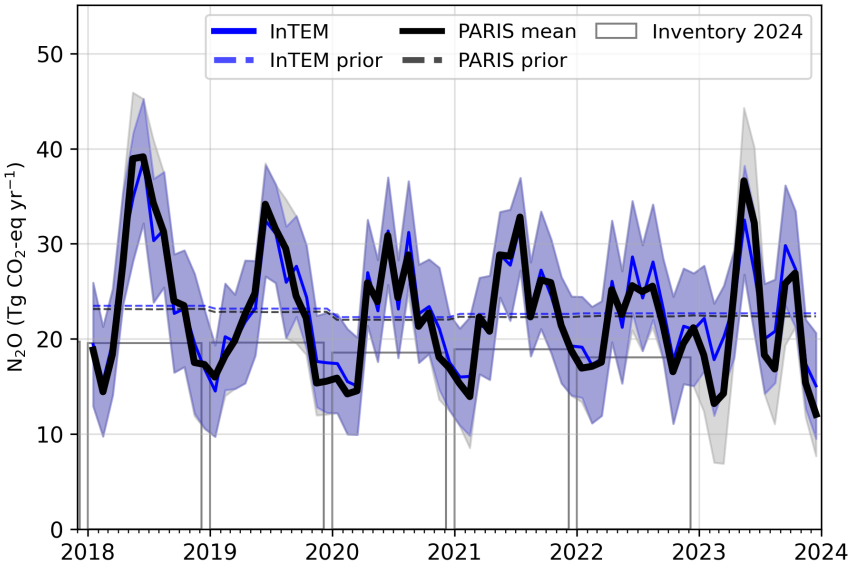

Figure 5.0.5: Spatial distribution of the UK average modelled emissions of N_2O during the period of 2018-2023 (mean from all models). Observing stations are marked with red circles and highly-populated cities are marked with red triangles.

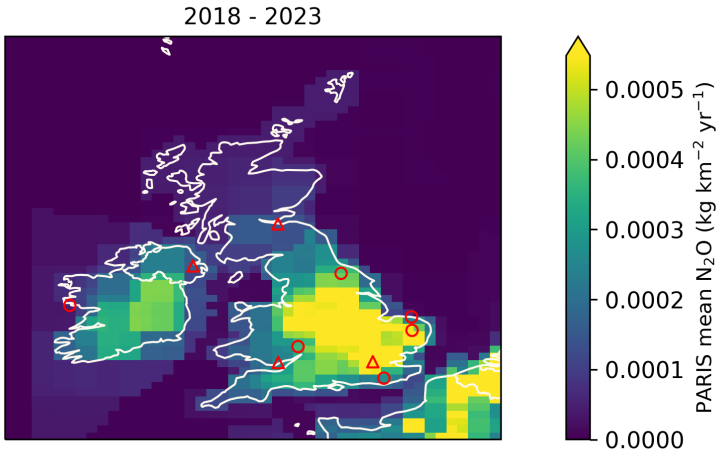

Figure 5.0.6: Spatial distribution of the seasonal deviation from the mean. The deviation is defined as the modelled UK seasonally averaged N_2O emissions over 2018-2023 minus the average over the whole period. The mean across all models is shown. Observing stations are marked with red circles and highly-populated cities are marked with red triangles.

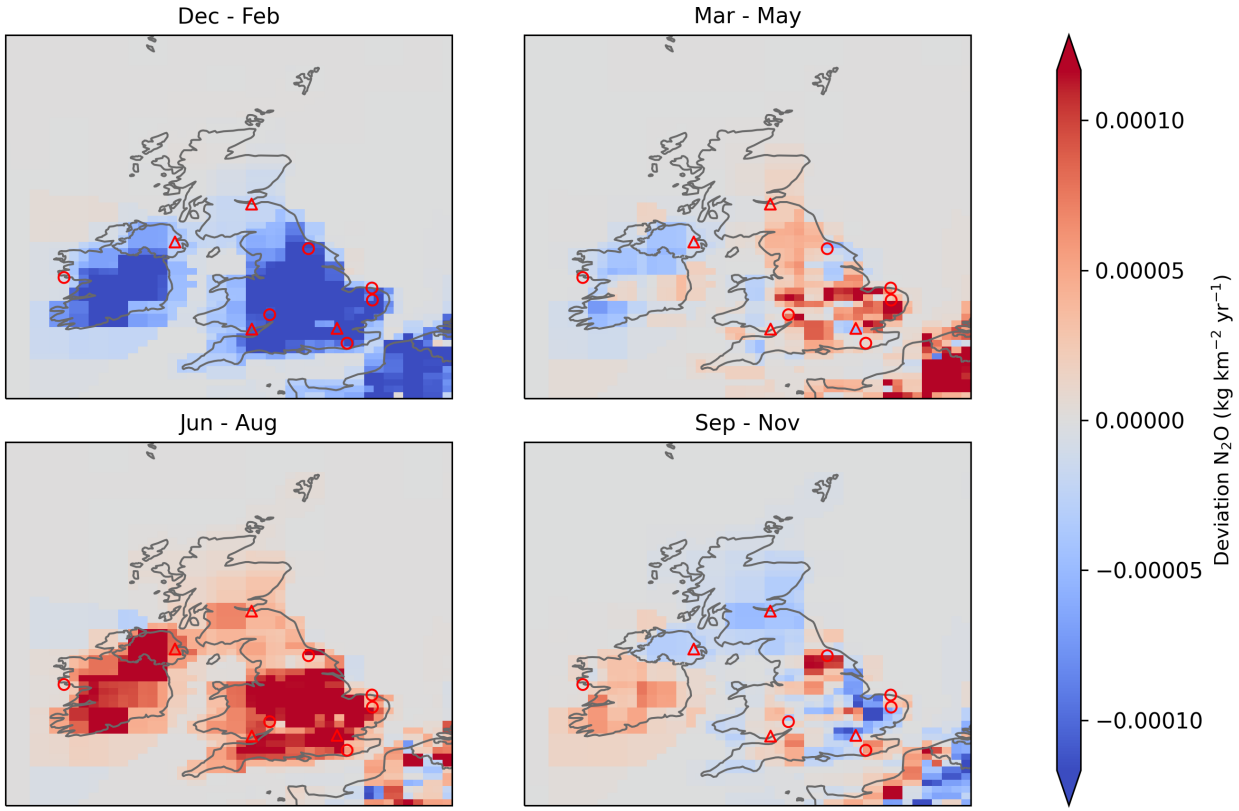

6 Hydrofluorocarbons (HFCs)

Figure 6.0.1: Total source sensitivity of HFCs/PFCs observing sites as calculated by the NAME transport model for the year (left) 2018 and (right) 2023 and used in the inversions. Observing stations active in each year are marked with red dots. Areas with visible land surface represent regions for which emissions can be observed well from the network. Shaded or dark areas represent regions for which limited emission information can be obtained from the network.

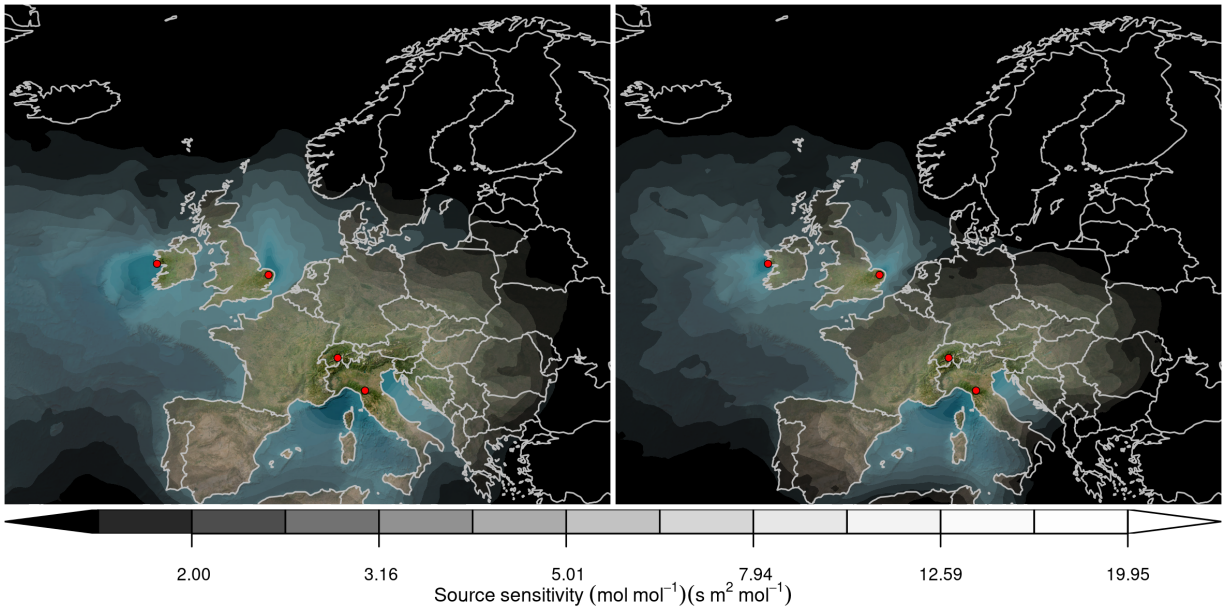

6.1 HFC-32

Figure 6.1.1: Verification of the UK emissions inventory estimates for HFC-32. Modelled annual emissions are given as the mean from all models (black line and grey shading) and the individual result from InTEM (blue line and shading). National inventory annual totals are given as grey bars.

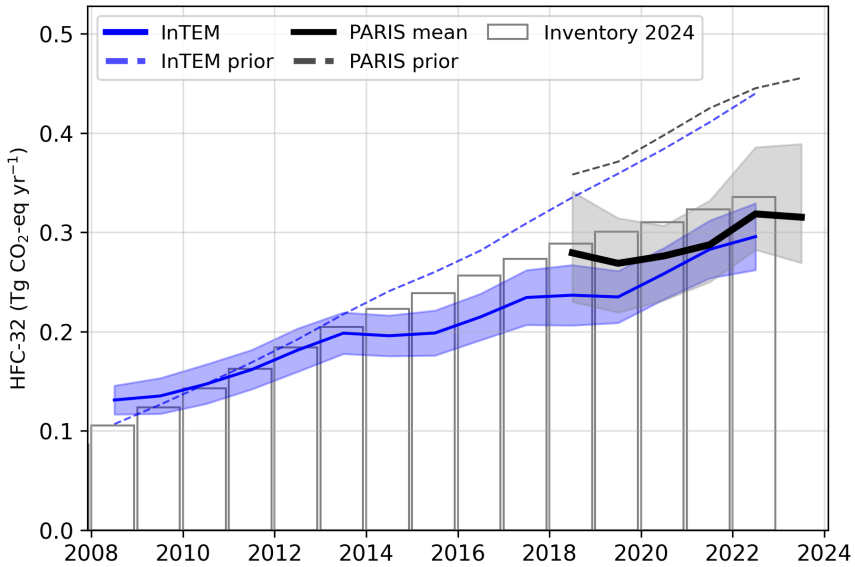

Figure 6.1.2: Spatial distribution of the UK average modelled emissions of HFC-32 during the period of 2018-2023 (mean from all models). Observing stations are marked with red circles and highly-populated cities are marked with red triangles.

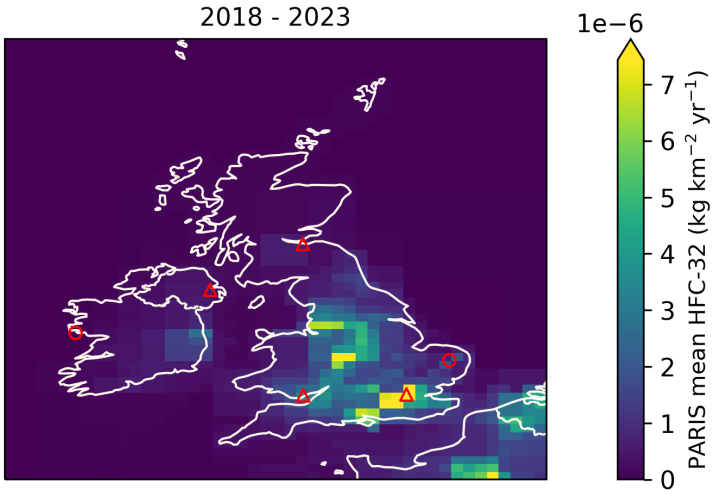

6.2 HFC-125

Figure 6.2.1: Verification of the UK emissions inventory estimates for HFC-125. Modelled annual emissions are given as the mean from all models (black line and grey shading) and the individual result from InTEM (blue line and shading). National inventory annual totals are given as grey bars.

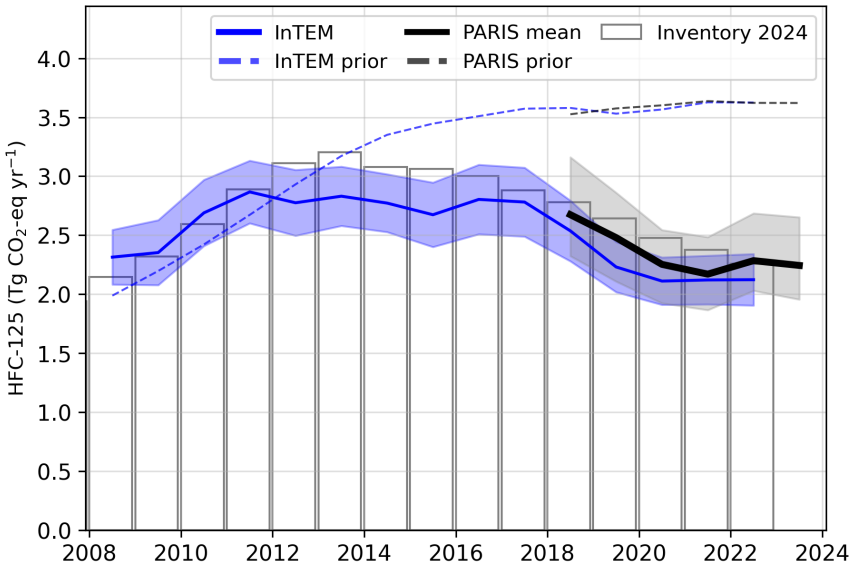

Figure 6.2.2: Spatial distribution of the UK average modelled emissions of HFC-125 during the period of 2018-2023 (mean from all models). Observing stations are marked with red circles and highly-populated cities are marked with red triangles.

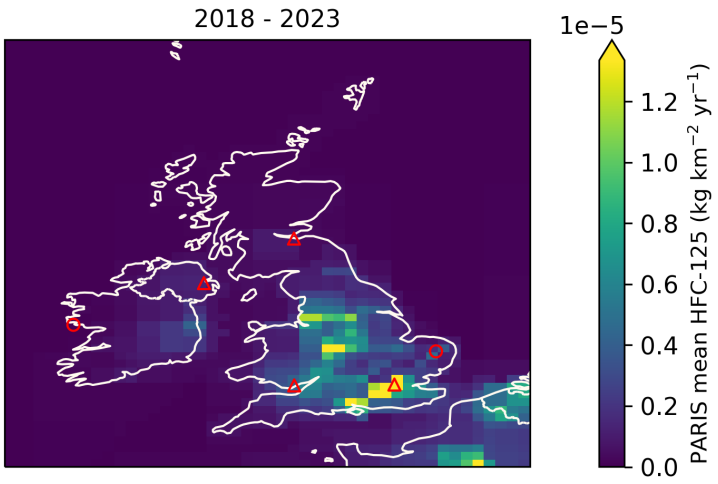

6.3 HFC-134a

Figure 6.3.1: Verification of the UK emissions inventory estimates for HFC-134a. Modelled annual emissions are given as the mean from all models (black line and grey shading) and the individual result from InTEM (blue line and shading). National inventory annual totals are given as grey bars.

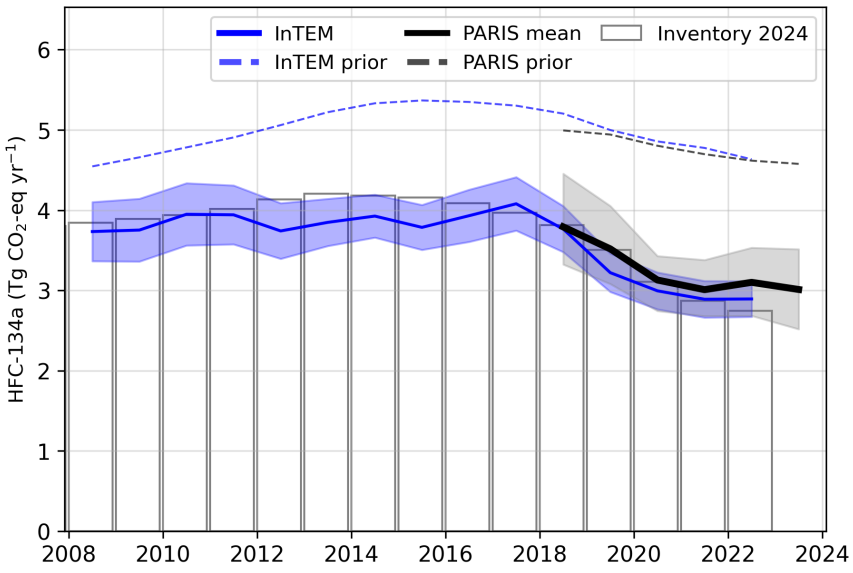

Figure 6.3.2: Spatial distribution of the UK average modelled emissions of HFC-134a during the period of 2018-2023 (mean from all models). Observing stations are marked with red circles and highly-populated cities are marked with red triangles.

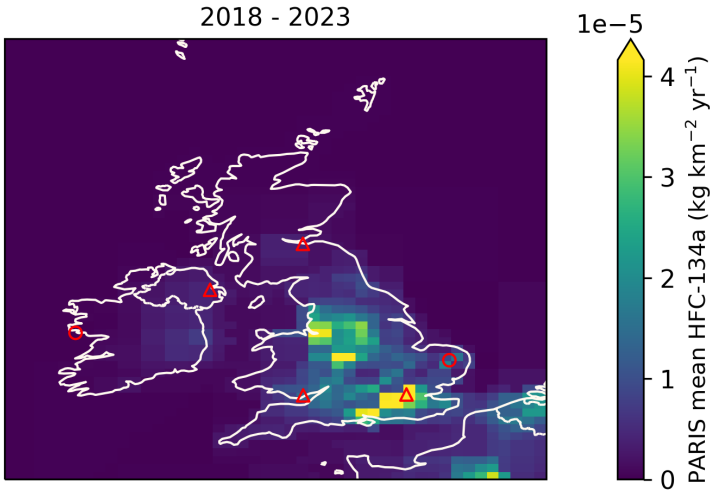

6.4 HFC-143a

Figure 6.4.1: Verification of the UK emissions inventory estimates for HFC-143a. Modelled annual emissions are given as the mean from all models (black line and grey shading) and the individual result from InTEM (blue line and shading). National inventory annual totals are given as grey bars.

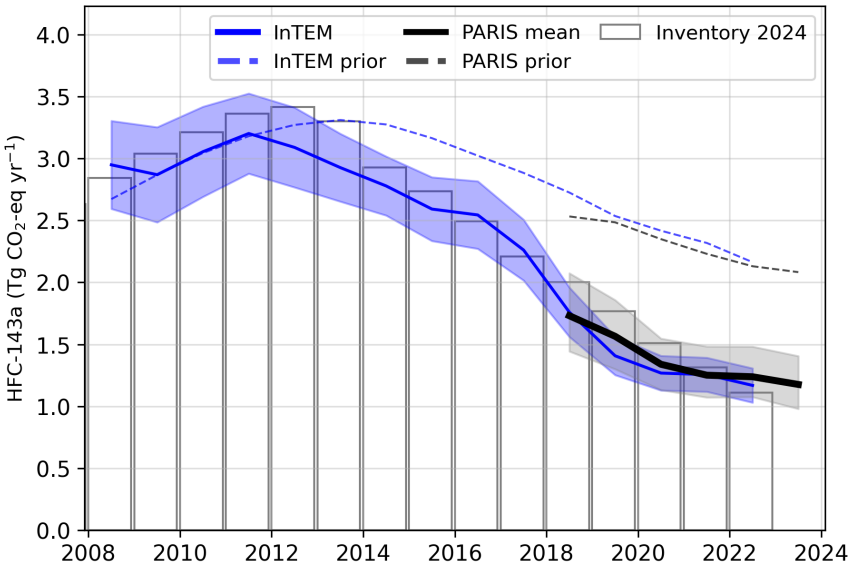

Figure 6.4.2: Spatial distribution of the UK average modelled emissions of HFC-143a during the period of 2018-2023 (mean from all models). Observing stations are marked with red circles and highly-populated cities are marked with red triangles.

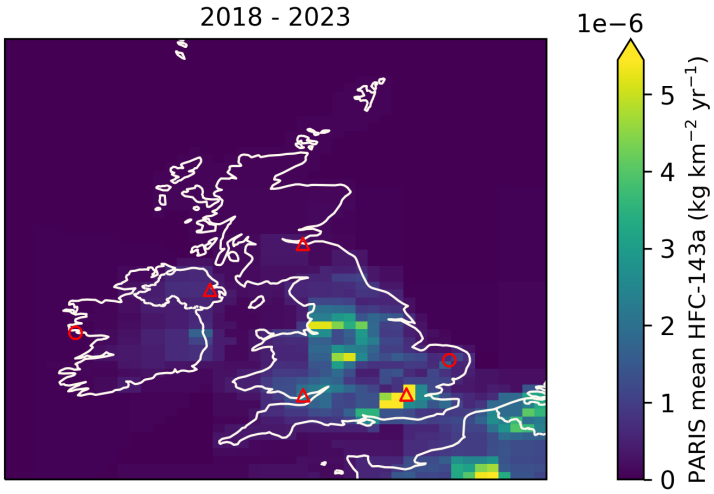

6.5 Total HFCs

Figure 6.5.1: Verification of the UK emissions inventory estimates for total HFCs. Modelled annual emissions are given as the mean from all models (black line and grey shading) and the individual result from InTEM (blue line and shading). National inventory annual totals are given as grey bars.

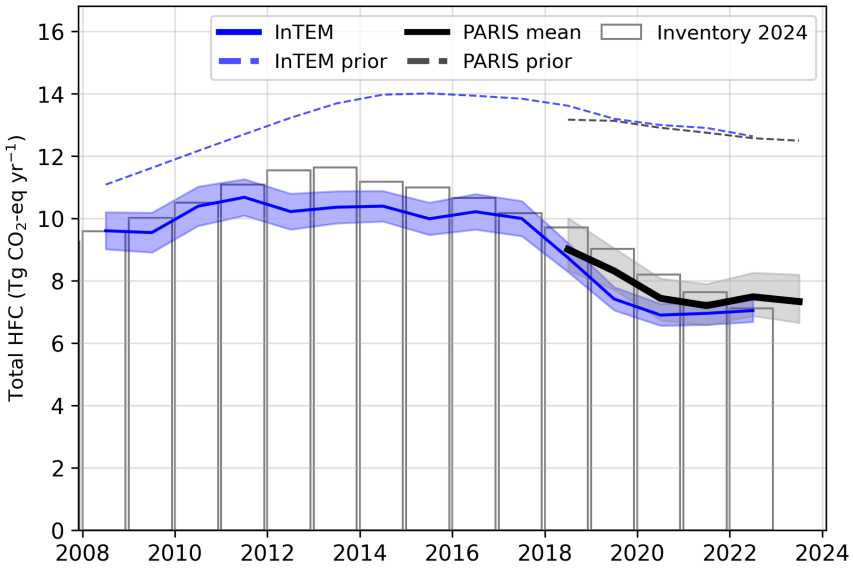

Table 2: Emissions estimation for HFCs in $\mathrm{TgCO_2{-}eq \cdot yr^{-1}}$ according to the National Inventory Report (NIR) 2024 and the inversions done in the PARIS project. For the PARIS estimation, the mean of the 3 inversion models is displayed, along with a range of uncertainty estimated via the half distance between the maximum and minimum uncertainties of the different models.

		2018	2019	2020	2021	2022	2023
HFC-23	NIR 2024	0.01	0.01	0.01	0.01	0.01	
	PARIS mean	0.16 ± 0.19	0.14 ± 0.20	0.14 ± 0.24	0.21 ± 0.31	0.27 ± 0.42	0.33 ± 0.50
HFC-32	NIR 2024	0.29	0.30	0.31	0.32	0.34	
	PARIS mean	0.28 ± 0.06	0.27 ± 0.05	0.28 ± 0.04	0.29 ± 0.04	0.32 ± 0.05	0.32 ± 0.06
HFC-125	NIR 2024	2.78	2.64	2.48	2.38	2.26	
	PARIS mean	2.67 ± 0.42	2.48 ± 0.38	2.25 ± 0.31	2.17 ± 0.31	2.28 ± 0.33	2.24 ± 0.35
HFC-134a	NIR 2024	3.81	3.50	3.11	2.87	2.75	
	PARIS mean	3.79 ± 0.57	3.52 ± 0.49	3.13 ± 0.34	3.01 ± 0.35	3.10 ± 0.42	3.01 ± 0.50
HFC-143a	NIR 2024	2.00	1.77	1.51	1.31	1.11	
	PARIS mean	1.73 ± 0.32	1.56 ± 0.28	1.34 ± 0.21	1.25 ± 0.21	1.24 ± 0.20	1.18 ± 0.21
HFC-152a	NIR 2024	0.04	0.04	0.03	0.03	0.03	
	PARIS mean	0.02 ± 0.01	0.02 ± 0.01	0.01 ± 0.01	0.01 ± 0.01	0.01 ± 0.01	0.01 ± 0.01
HFC-227ea	NIR 2024	0.57	0.57	0.56	0.52	0.46	
	PARIS mean	0.22 ± 0.06	0.21 ± 0.06	0.19 ± 0.05	0.18 ± 0.06	0.18 ± 0.07	0.18 ± 0.08
HFC-245fa	NIR 2024	0.08	0.08	0.08	0.08	0.06	
	PARIS mean	0.06 ± 0.02	0.05 ± 0.02	0.05 ± 0.02	0.05 ± 0.01	0.04 ± 0.01	0.03 ± 0.01
HFC-365mfc	NIR 2024	0.11	0.11	0.11	0.10	0.08	
	PARIS mean	0.07 ± 0.02	0.06 ± 0.02	0.05 ± 0.02	0.04 ± 0.02	0.04 ± 0.01	0.03 ± 0.01
HFC-4310mee	NIR 2024	0.02	0.02	0.02	0.02	0.02	
	PARIS mean	0.01 ± 0.01	0.01 ± 0.01	0.01 ± 0.01	0.01 ± 0.01	0.01 ± 0.01	[1]

[1] HFC-4310mee emissions were not estimated for 2023 due to lack of atmospheric observations.

7 Perfluorocarbons (PFCs)

7.1 PFC-14

Figure 7.1.1: Verification of the UK emissions inventory estimates for PFC-14. Modelled annual emissions are given as the mean from all models (black line and grey shading) and the individual result from InTEM (blue line and shading). National inventory annual totals are given as grey bars.

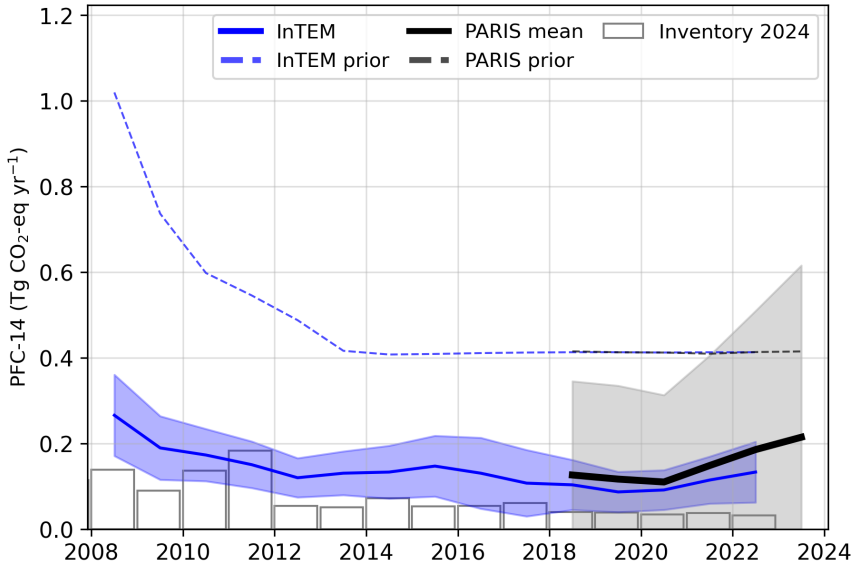

Figure 7.1.2: Spatial distribution of the UK average modelled emissions of PFC-14 during the period of 2018-2023 (mean from all models). Observing stations are marked with red circles and highly-populated cities are marked with red triangles.

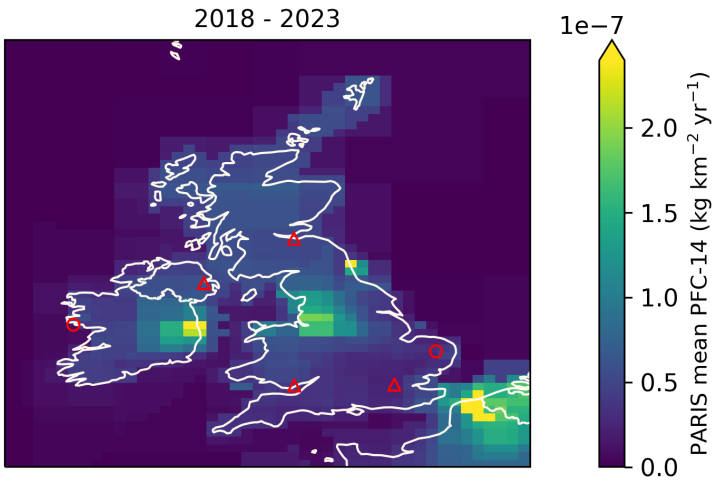

7.2 PFC-116

Figure 7.2.1: Verification of the UK emissions inventory estimates for PFC-116. Modelled annual emissions are given as the mean from all models (black line and grey shading) and the individual result from InTEM (blue line and shading). National inventory annual totals are given as grey bars.

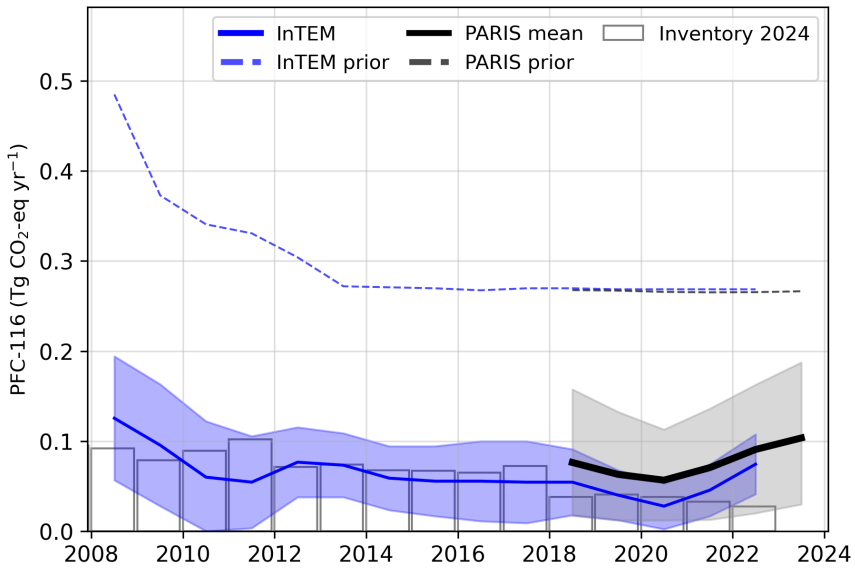

Figure 7.2.2: Spatial distribution of the UK average modelled emissions of PFC-116 during the period of 2018-2023 (mean from all models). Observing stations are marked with red circles and highly-populated cities are marked with red triangles.

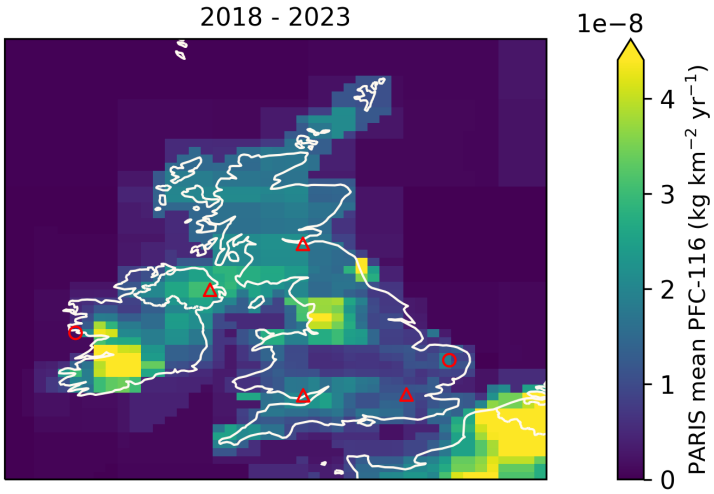

7.3 PFC-218

Figure 7.3.1: Verification of the UK emissions inventory estimates for PFC-218. Modelled annual emissions are given as the mean from all models (black line and grey shading) and the individual result from InTEM (blue line and shading). National inventory annual totals are given as grey bars.

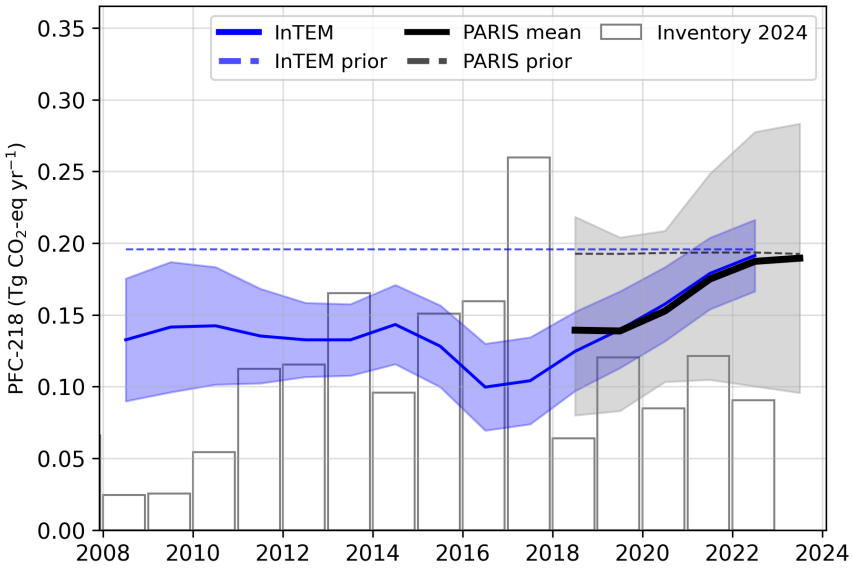

Figure 7.3.2: Spatial distribution of the UK average modelled emissions of PFC-218 during the period of 2018-2023 (mean from all models). Observing stations are marked with red circles and highly-populated cities are marked with red triangles.

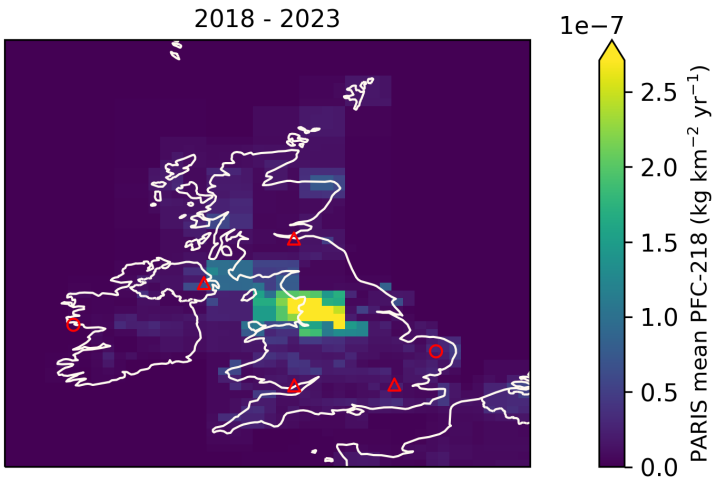

7.4 PFC-318

Figure 7.4.1: Verification of the UK emissions inventory estimates for PFC-318. Modelled annual emissions are given as the mean from all models (black line and grey shading) and the individual result from InTEM (blue line and shading). National inventory annual totals are given as grey bars.

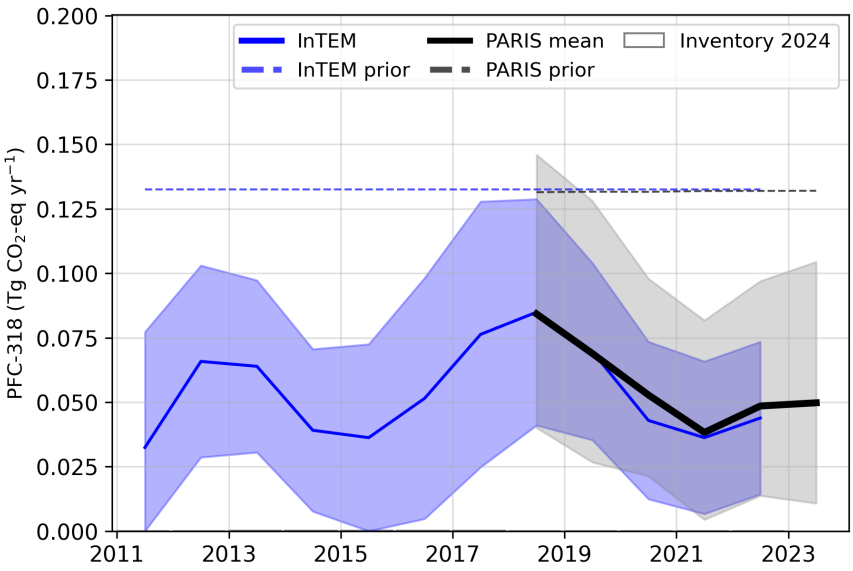

Figure 7.4.2: Spatial distribution of the UK average modelled emissions of PFC-318 during the period of 2018-2023 (mean from all models). Observing stations are marked with red circles and highly-populated cities are marked with red triangles.

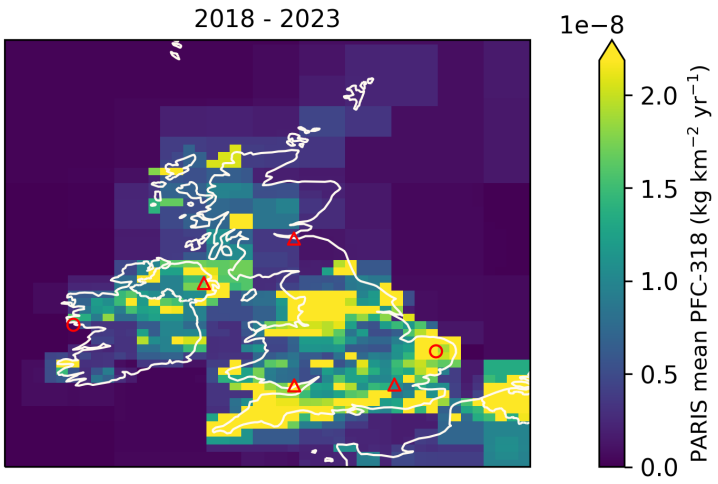

7.5 Total PFCs

Figure 7.5.1: Verification of the UK emissions inventory estimates for total PFCs. Modelled annual emissions are given as the mean from all models (black line and grey shading) and the individual result from InTEM (blue line and shading). National inventory annual totals are given as grey bars.

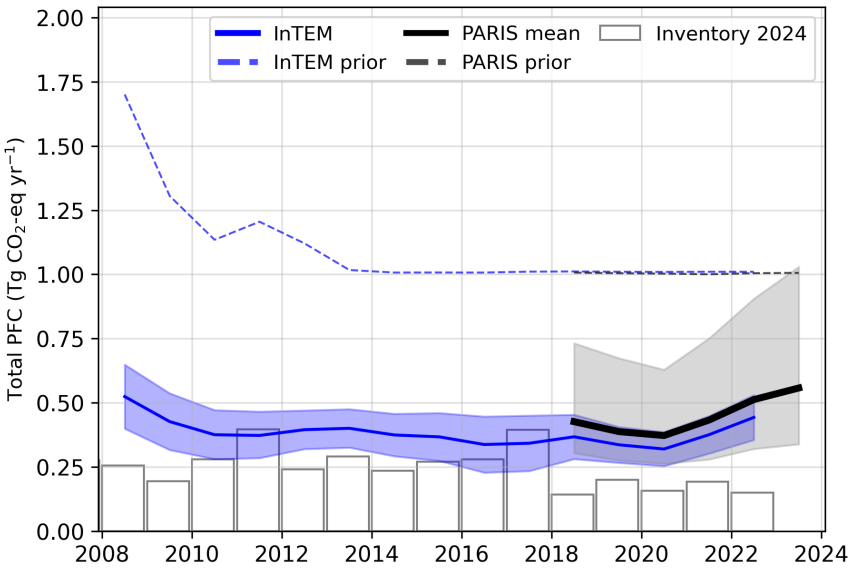

Table 3: Emissions estimation for PFCs in $\mathrm{TgCO_2{-}eq \cdot yr^{-1}}$ according to the National Inventory Report (NIR) 2024 and the inversions done in the PARIS project. For the PARIS estimation, the mean of the 3 inversion models is displayed, along with a range of uncertainty estimated via the half distance between the maximum and minimum uncertainties of the different models.

		2018	2019	2020	2021	2022	2023
PFC-14	NIR 2024	0.04	0.04	0.03	0.04	0.03	
	PARIS mean	0.13 ± 0.17	0.12 ± 0.17	0.11 ± 0.16	0.15 ± 0.20	0.19 ± 0.25	0.21 ± 0.31
PFC-116	NIR 2024	0.04	0.04	0.04	0.03	0.03	
	PARIS mean	0.08 ± 0.07	0.06 ± 0.06	0.06 ± 0.05	0.07 ± 0.06	0.09 ± 0.07	0.10 ± 0.08
PFC-218	NIR 2024	0.06	0.12	0.08	0.12	0.09	
	PARIS mean	0.14 ± 0.07	0.14 ± 0.06	0.15 ± 0.05	0.17 ± 0.07	0.19 ± 0.09	0.19 ± 0.09
PFC-318	NIR 2024	0.00	0.00	0.00	0.00	0.00	
	PARIS mean	0.08 ± 0.05	0.07 ± 0.05	0.05 ± 0.04	0.04 ± 0.04	0.05 ± 0.04	0.05 ± 0.05

8 Sulphur hexafluoride (SF_6)

Figure 8.0.1: Total source sensitivity of SF_6 observing sites as calculated by the NAME transport model for the year (left) 2018 and (right) 2023 and used in the inversions. Observing stations active in each year are marked with red dots. Areas with visible land surface represent regions for which emissions can be observed well from the network. Shaded or dark areas represent regions for which limited emission information can be obtained from the network.

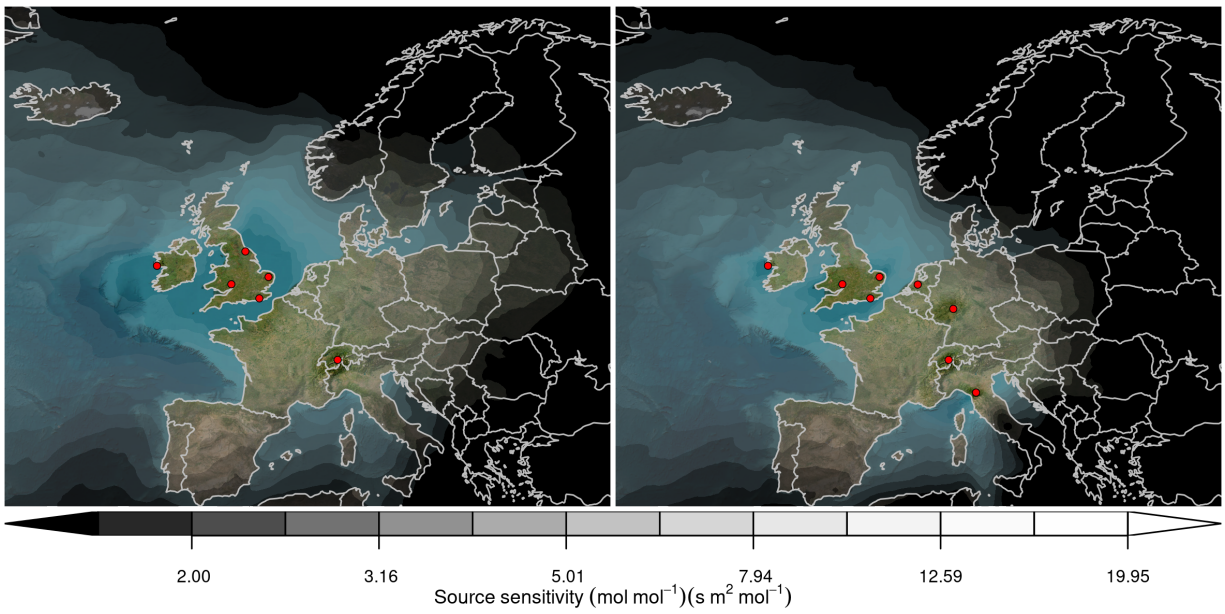

Figure 8.0.2: Verification of the UK emissions inventory estimates for SF_6. Modelled annual emissions are given as the mean from all models (black line and grey shading) and the individual result from InTEM (blue line and shading). National inventory annual totals are given as grey bars.

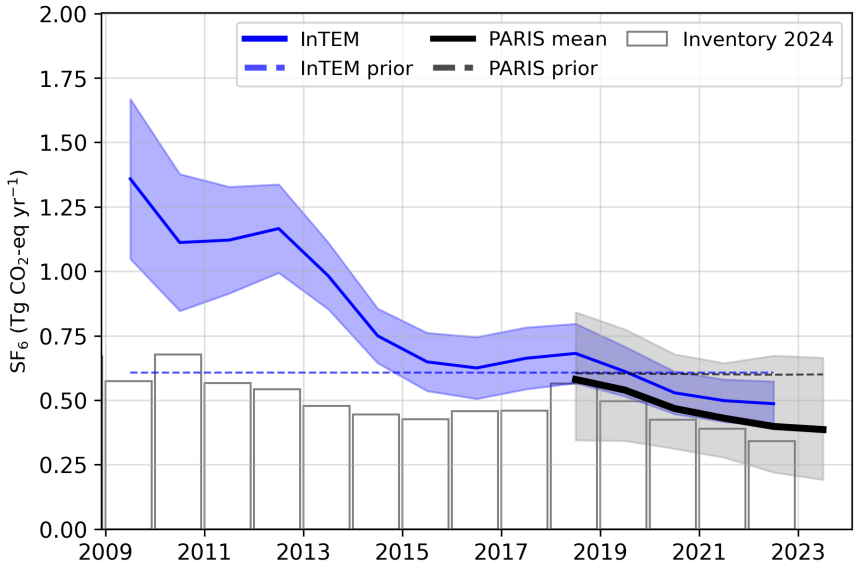

Figure 8.0.3: Spatial distribution of the UK average modelled emissions of SF_6 during the period of 2018-2023 (mean from all models). Observing stations are marked with red circles and highly-populated cities are marked with red triangles.

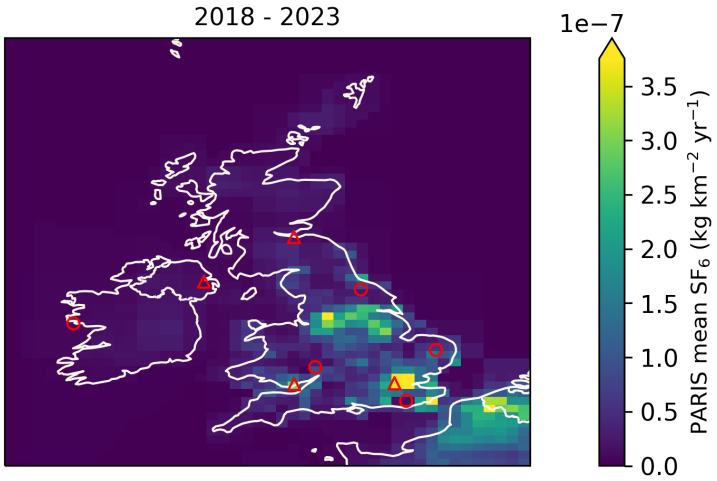

References

European Commission: Joint Research, Centre et al. (2023). *GHG emissions of all world countries – 2023*. Publications Office of the European Union. DOI: 10.2760/953322.

Ganesan, A. L. et al. (2014). "Characterization of uncertainties in atmospheric trace gas inversions using hierarchical Bayesian methods". In: *Atmospheric Chemistry and Physics* 14.8, pp. 3855–3864. DOI: 10.5194/acp-14-3855-2014. URL: http://www.atmos-chem-phys.net/14/3855/2014/http://www.atmos-chem-phys.net/14/3855/2014/acp-14-3855-2014.pdf.

Ganesan, A. L. et al. (2015). "Quantifying methane and nitrous oxide emissions from the UK and Ireland using a national-scale monitoring network". In: *Atmos. Chem. Phys.* 15.11, pp. 6393–6406. DOI: 10.5194/acp-15-6393-2015. URL: https://www.atmos-chem-phys.net/15/6393/2015/https://www.atmos-chem-phys.net/15/6393/2015/acp-15-6393-2015.pdf.

Henne, S. et al. (2016). "Validation of the Swiss methane emission inventory by atmospheric observations and inverse modelling". In: *Atmospheric Chemistry and Physics* 16.6, pp. 3683–3710. DOI: 10.5194/acp-16-3683-2016. URL: http://www.atmos-chem-phys.net/16/3683/2016/.

Jones, A.R. et al. (2007). "The U.K. Met Office's next-generation atmospheric dispersion model, NAME III, in Borrego C. and Norman A.-L. (Eds)". In: *Air Pollution Modeling and its Application XVII (Proceedings of the 27th NATO/CCMS International Technical Meeting on Air Pollution Modelling and its Application), Springer*, pp. 580–589.

Katharopoulos, I. et al. (2023). "Impact of transport model resolution and a priori assumptions on inverse modeling of Swiss F-gas emissions". In: *Atmos. Chem. Phys.* 23.22, pp. 14159–14186. DOI: 10.5194/acp-23-14159-2023. URL: https://acp.copernicus.org/articles/23/14159/2023/.

Manning, A. J. et al. (2021). "Evidence of a recent decline in UK emissions of hydrofluorocarbons determined by the InTEM inverse model and atmospheric measurements". In: *Atmospheric Chemistry and Physics* 21.16, pp. 12739–12755. DOI: 10.5194/acp-21-12739-2021. URL: https://acp.copernicus.org/articles/21/12739/2021/.

Rigby, M. et al. (2019). "Increase in CFC-11 emissions from eastern China based on atmospheric observations". In: *Nature* 569, pp. 546–550. DOI: 10.1038/s41586-019-1193-4. URL: https://doi.org/10.1038/s41586-019-1193-4.

Draft Inventory Annex
Ireland 2024

19th November, 2024

1 Introduction

In this document, global concentration trends and national emissions estimates derived from atmospheric observations ("inverse estimates") are presented for each reported gas. Comparing the emissions submitted in national inventories with those calculated using atmospheric observations allows for emissions to be assessed using two fundamentally different approaches. Substantial differences can highlight areas that could warrant further investigation.

Global concentration trends for each gas are first shown using annual average concentrations from Mace Head, Ireland (Northern Hemisphere) and Kennaook/Cape Grim, Tasmania, Australia (Southern Hemisphere). Data from these stations were selected to exclude regionally-polluted air masses and therefore represents northern and southern hemispheric concentration trends. Mace Head observations were supported by the National Aeronautics and Space Administration (NASA) and the UK Department of Energy, Security and Net Zero (DESNZ), and Kennaook/Cape Grim observations by NASA and the Australian Bureau of Meteorology.

Observations of European concentrations of greenhouse gases used to derive national inverse emission estimates were collected from many different networks and providers. Methane and nitrous oxide concentrations originated from the European ICOS (Integrated Carbon Observation System) network, the UK DECC (Deriving Emissions related to Climate Change) network and other national or individual initiatives. F-gas observations were made by affiliates of the AGAGE (Advanced Global Atmospheric Gases Experiment) network. Observations from from additional stations across Europe were supported by the Horizon-EU PARIS (Process Attribution of Regional Emissions) project. The observation stations used to derive emissions for each gas are shown in the corresponding sections of this document.

Inversion-based emissions estimates were derived using one atmospheric transport model but with multiple inverse models allowing a better quantification of the uncertainties associated with inverse modelling. The atmospheric transport model provides the link between surface fluxes and concentrations measured at the observing stations. Although the uncertainty associated with the atmospheric transport model is considered in the statistical inversion approach, it may be underestimated when only using a single transport model. The atmospheric transport model used is the Numerical Atmospheric dispersion Modelling Environment (NAME) (Jones et al., 2007), a backwards-running Lagrangian Particle Dispersion Model (LPDM) that simulates the recent transport of air to each observing station. The NAME model has been widely used in the estimation of greenhouse gases emissions (Ganesan et al., 2015; Rigby et al., 2019; Manning et al., 2021).

The three inverse methods used are InTEM (Inversion Technique for Emission Modelling, Manning et al., 2021), ELRIS (Empa Lagrangian Regional Inversion System, Henne et al., 2016; Katharopoulos et al., 2023), and RHIME (Regional Hierarchical Inverse Modelling Environment, Ganesan et al., 2014). All three inverse methods estimate emissions within Europe along with boundary conditions that account for the concentration of the air entering Europe. All three systems started from the same set of a priori emissions that were either derived from the global EDGAR emission inventory (version 8, European Commission: Joint Research et al., 2023) or a uniform land-based emission, depending on the gas. A natural emission component, from the WETCHARTS product, was included in the methane prior. The same observational dataset was used by each inverse model, but data selection (i.e., filtering datasets for specific conditions) and treatment of uncertainties were chosen separately and hence differ. The three methods also differ in their statistical approaches for estimating emissions.

Emission estimates are presented for the period 2008-2023. Emissions for the full 2008-2023 period were derived with the InTEM model only, while emissions from 2018-2023 are presented as a combined result using the three inverse models.

For the 2008-2023 InTEM results, a 2-year inversion resolution, incrementing annually, was used for all gases except CH_4nd N_2, where the resolution was monthly. For the recent 2018-2023 period, for all three models, the inversion resolution was one month for CH_4 and N_2O in order to capture the seasonality of the emissions, a one-year average over these results is also presented. For the fluorinated gases, a 1-year

inversion resolution was adopted, with a 3-year moving average applied to the results. The uncertainty shown is the minimum/maximum of the uncertainties from the three results.

2 Global Concentration Trends

2.1 Methane (CH_4)

Figure 2.1.1: Background Northern Hemisphere monthly concentrations of CH_4 estimated from MHD, Ireland observations are shown in red, and background Southern Hemisphere monthly concentrations from CGO, Tasmania are shown in blue. Grey shading represents provisional data.

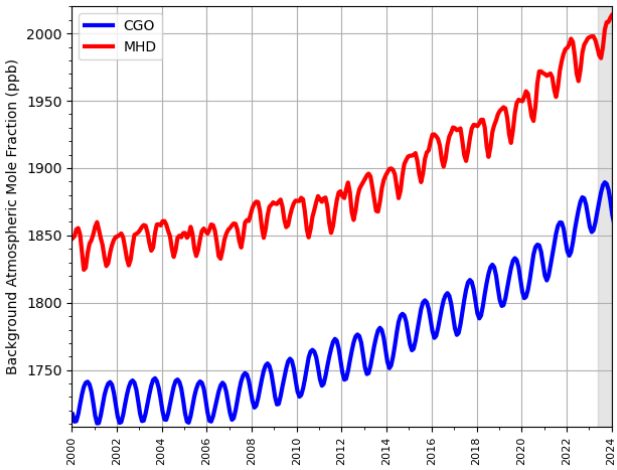

2.2 Nitrous Oxide (N_2O)

Figure 2.2.1: Background Northern Hemisphere monthly concentrations of N_2O estimated from MHD, Ireland observations are shown in red, and background Southern Hemisphere monthly concentrations from CGO, Tasmania are shown in blue. Grey shading represents provisional data.

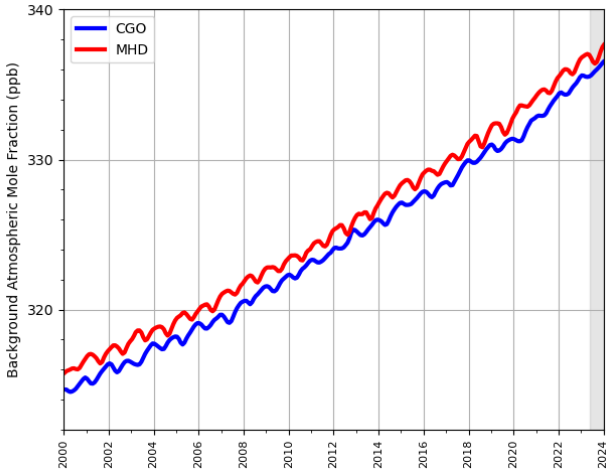

2.3 Hydrofluorocarbons (HFCs)

Figure 2.3.1: Background Northern Hemisphere monthly concentrations of six HFCs estimated from MHD, Ireland observations are shown in red, and background Southern Hemisphere monthly concentrations from CGO, Tasmania are shown in blue. Grey shading represents provisional data.

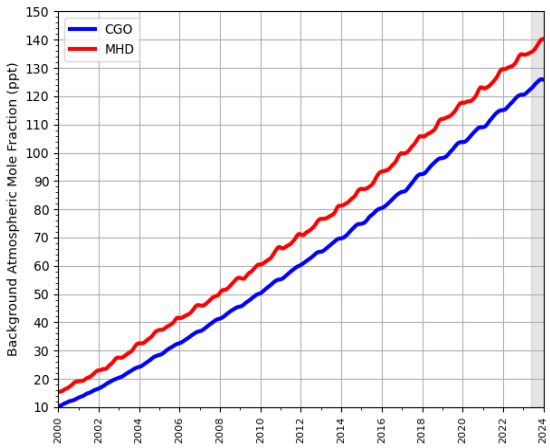

(a) HFC-134a

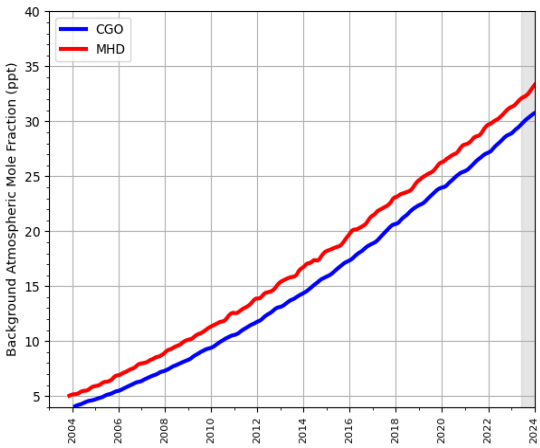

(b) HFC-143a

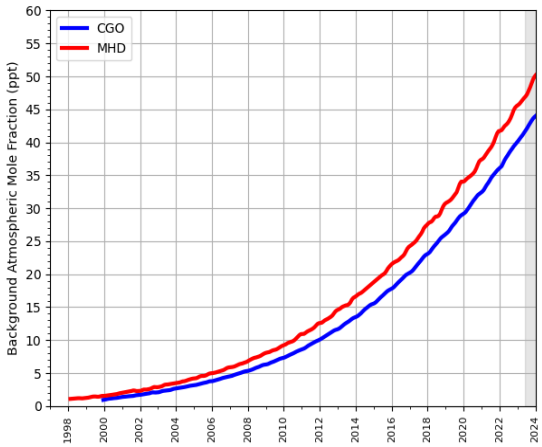

(c) HFC-125

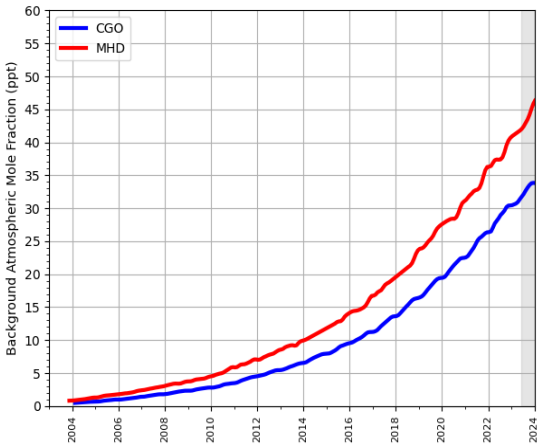

(d) HFC-32

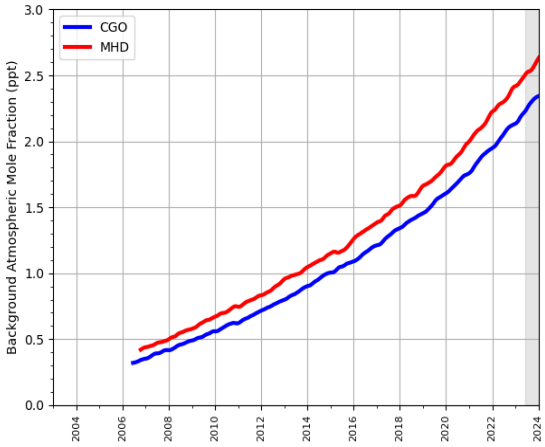

(e) HFC-227ea

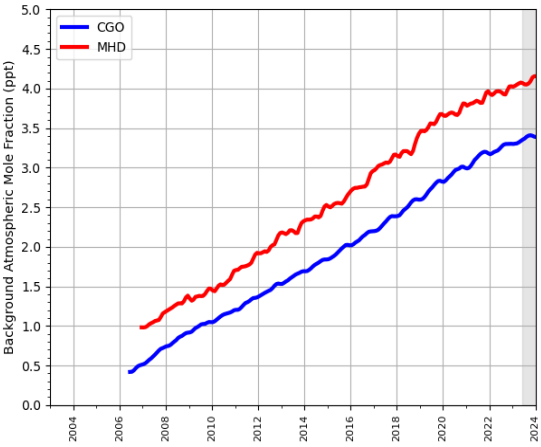

(f) HFC-245fa

Figure 2.3.2: Background Northern Hemisphere monthly concentrations of four HFCs estimated from MHD, Ireland observations are shown in red, and background Southern Hemisphere monthly concentrations from CGO, Tasmania are shown in blue. Grey shading represents provisional data.

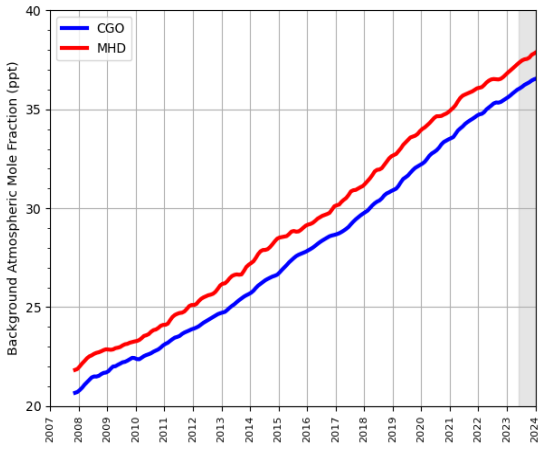

(a) HFC-23

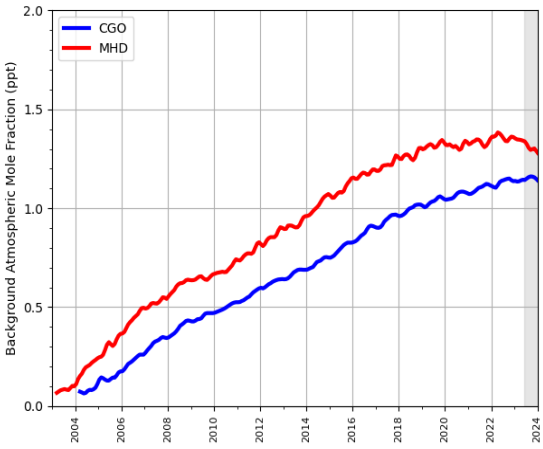

(b) HFC-365mfc

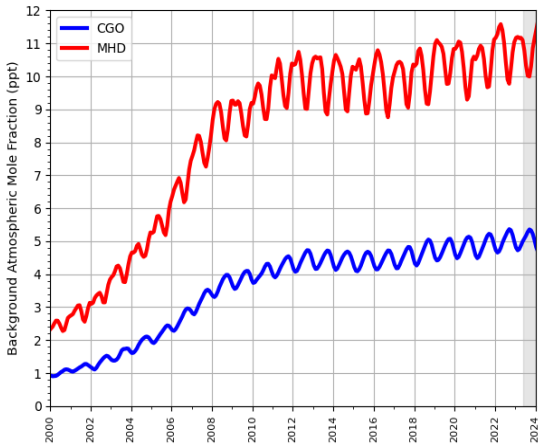

(c) HFC-152a

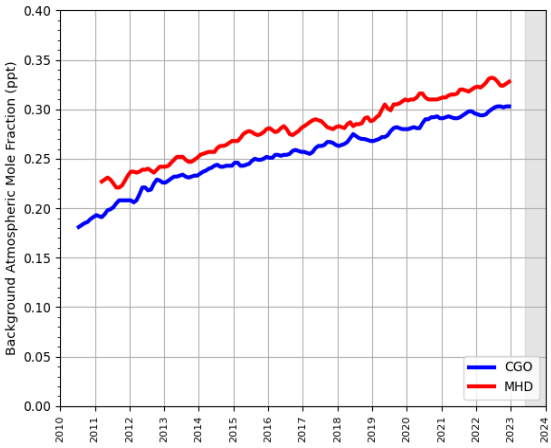

(d) HFC-43-10-mee

2.4 Perfluorocarbons (PFCs)

Figure 2.4.1: Background Northern Hemisphere monthly concentrations of four PFCs estimated from MHD, Ireland observations are shown in red, and background Southern Hemisphere monthly concentrations from CGO, Tasmania are shown in blue. Grey shading represents provisional data.

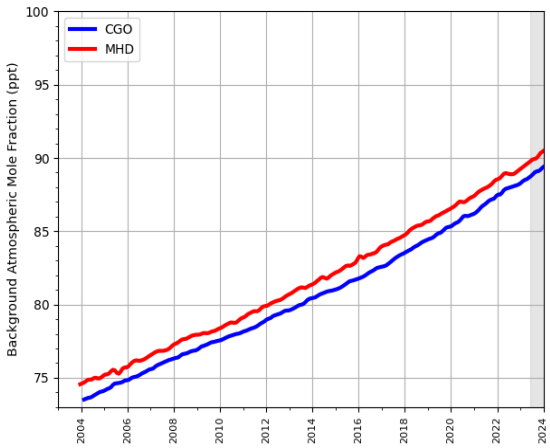

(a) PFC-14

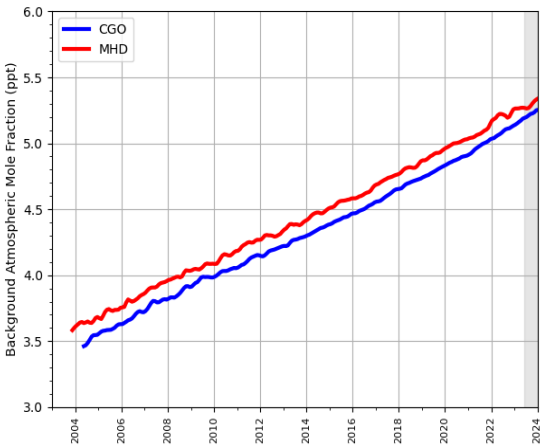

(b) PFC-116

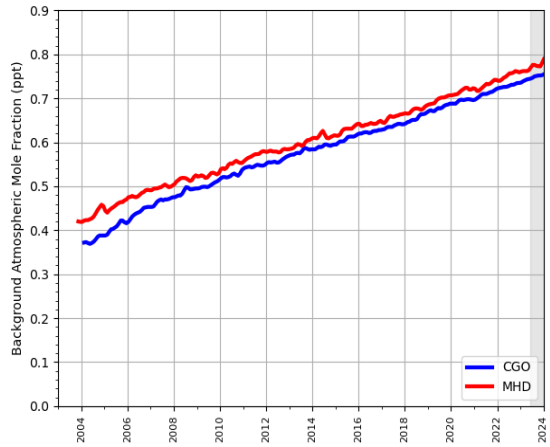

(c) PFC-218

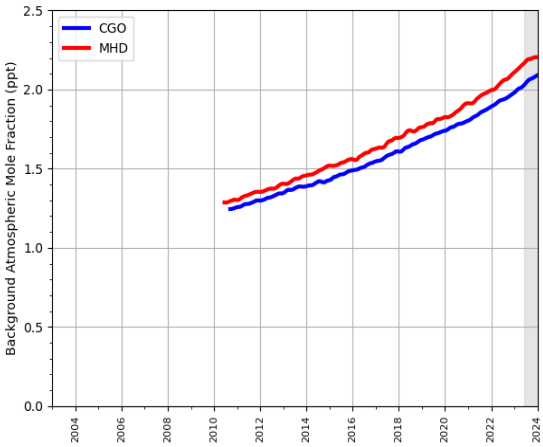

(d) PFC-318

3 Key findings

- Methane (CH_4): Inversion results are around 10-15% lower than the inventory estimates between 2017 and 2023. The inclusion of additional observational data from 2017 has had an impact on the inverse estimates even though no additional observational data were added close to Ireland. This impact requires further investigation. There does not appear to be a strong seasonal cycle in the emissions.
- Nitrous oxide (N_2O): Inversion results are around 20% higher than the inventory estimates. In all years the inverse models estimate a pronounced seasonal cycle in emissions with the maximum in late spring or early summer.
- Hydrofluorocarbons (HFCs): The emissions estimates from the inverse models generally agree, within the uncertainties, with those reported in the inventory. The very sharp drop in the inventory emissions in 2018 for HFC-143a is not seen in the inversions, they have a more steady decline.
- Perfluorocarbons (PFCs): The inverse results reveal some notable areas of emission, near Dublin for PFC-14 and near Cork for PFC-116. The inverse model estimates are very low and uncertain for PFC-218 and PFC-318. Overall the inverse estimates agree, within the uncertainties, with those reported.
- Sulphur hexafluoride (SF_6): The trend estimated by the inversions is consistent with that reported inventory 2018-2023, although the inverse results are higher, albeit with high uncertainty. In earlier years, 2009-2017, the InTEM estimates are somewhat higher.
- The observational coverage of Ireland is acceptable.

Table 1: Emissions estimation for the main greenhouse gases of focus in $\mathrm{TgCO_2{-}eq \cdot yr^{-1}}$ according to the National Inventory Report (NIR) 2024 and the inversions done in the PARIS project. For the PARIS estimation, the mean of the 3 inversion models is displayed, along with a range of uncertainty estimated via the half distance between the maximum and minimum uncertainties of the different models.

		2018	2019	2020	2021	2022	2023
CH_4	NIR 2024	21	21	21	21	22	
	PARIS mean	17 ± 5	16 ± 3	17 ± 3	16 ± 4	17 ± 3	16 ± 6
N_2O	NIR 2024	6	6	6	6	6	
	PARIS mean	8 ± 1	8 ± 1	8 ± 1	8 ± 1	7 ± 1	7 ± 1
Total HFCs[(1)]	NIR 2024	0.8	0.8	0.6	0.7	0.7	
	PARIS mean	1.0 ± 0.4	1.0 ± 0.4	0.9 ± 0.3	0.7 ± 0.3	0.6 ± 0.2	0.6 ± 0.3
Total PFCs[(2)]	NIR 2024	0.0	0.1	0.1	0.1	0.1	
	PARIS mean	0.1 ± 0.1	0.1 ± 0.1	0.1 ± 0.1	0.1 ± 0.1	0.1 ± 0.1	0.1 ± 0.1
SF_6	NIR 2024	0.0	0.0	0.0	0.0	0.0	
	PARIS mean	0.1 ± 0.0	0.1 ± 0.0	0.1 ± 0.0	0.0 ± 0.0	0.0 ± 0.0	0.0 ± 0.0

(1) Sum of HFC emissions presented in Table 2, except HFC-4310mee.

(2) Sum of PFC emissions presented in Table 3.

4 Methane (CH_4)

Figure 4.0.1: Total source sensitivity of CH_4 observing sites as calculated by the NAME transport model for the year (left) 2018 and (right) 2023 and used in the inversions. Observing stations active in each year are marked with red dots. Areas with visible land surface represent regions for which emissions can be observed well from the network. Shaded or dark areas represent regions for which limited emission information can be obtained from the network.

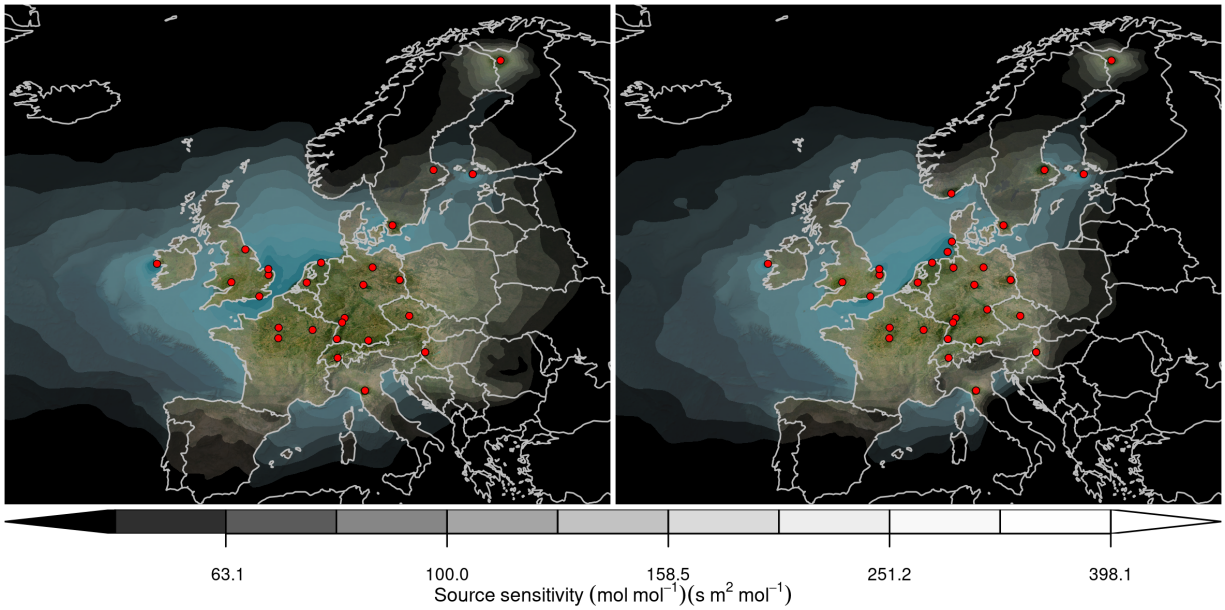

Figure 4.0.2: Verification of the Irish emissions inventory estimates for CH_4. Modelled annual emissions are given as the mean from all models (black line and grey shading) and the individual result from InTEM (blue line and shading). National inventory annual totals are given as grey bars.

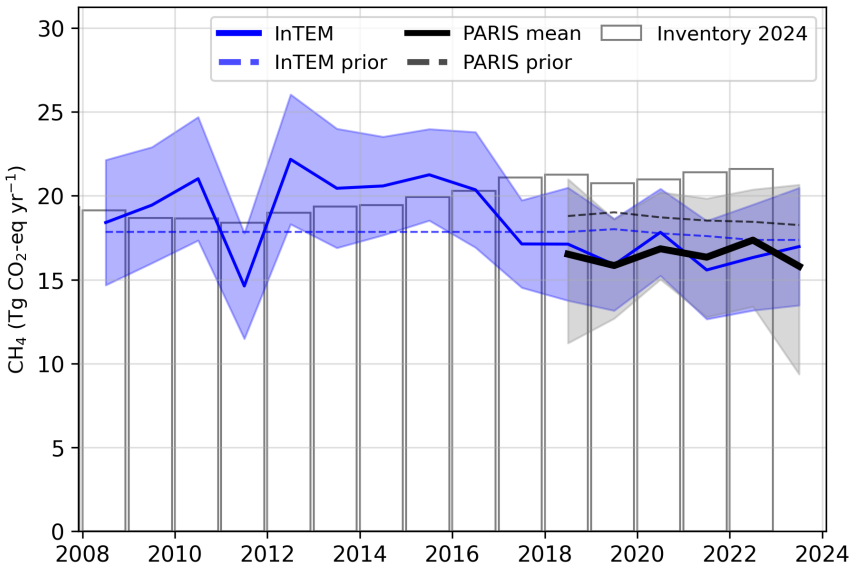

Figure 4.0.3: Verification of the Irish emissions inventory estimates for CH_4 (zoom in to 2018-2023). Modelled annual emissions are given as the mean from all models (black line and grey shading) and the individual result from InTEM (blue line and shading). National inventory annual totals are given as grey bars.

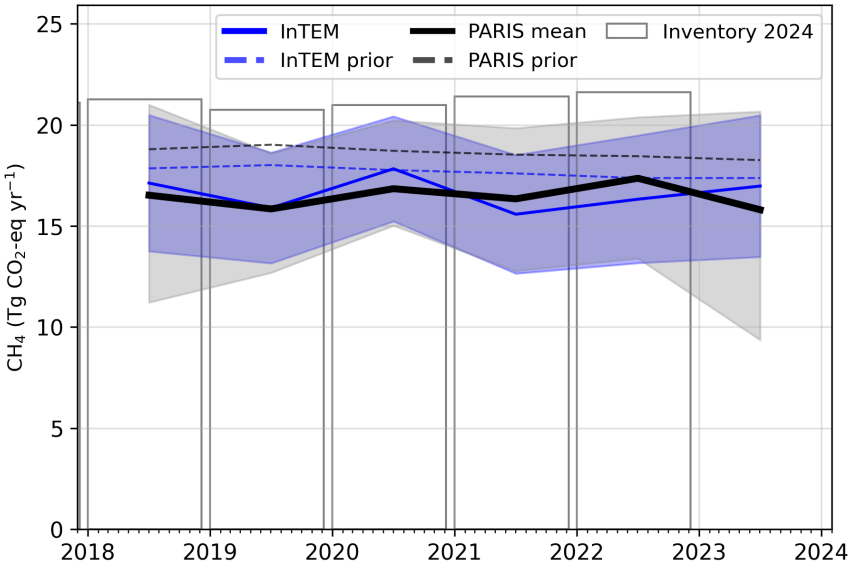

Figure 4.0.4: Verification of the Irish emissions inventory estimates for CH_4 (zoom in to 2018-2023). Modelled monthly emissions are given as the mean from all models (black line and grey shading) and the individual result from InTEM (blue line and shading). National inventory annual totals are given as grey bars.

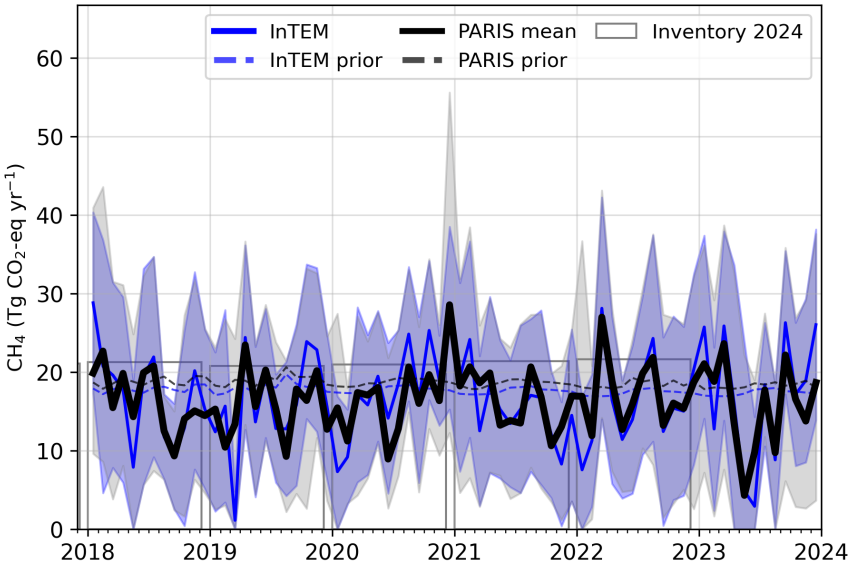

Figure 4.0.5: Spatial distribution of the Irish average modelled emissions of CH_4 during the period of 2018-2023 (mean from all models). Observing stations are marked with red circles and highly-populated cities are marked with red triangles.

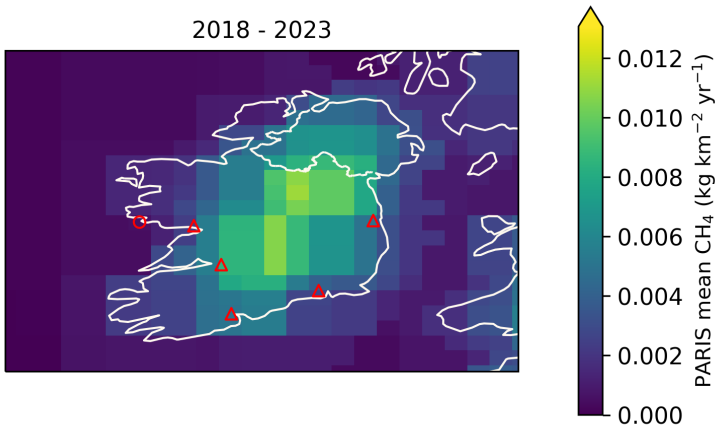

Figure 4.0.6: Spatial distribution of the seasonal deviation from the mean. The deviation is defined as the modelled Irish seasonally averaged CH_4 emissions over 2018-2023 minus the average over the whole period. The mean across all models is shown. Observing stations are marked with red circles and highly-populated cities are marked with red triangles.

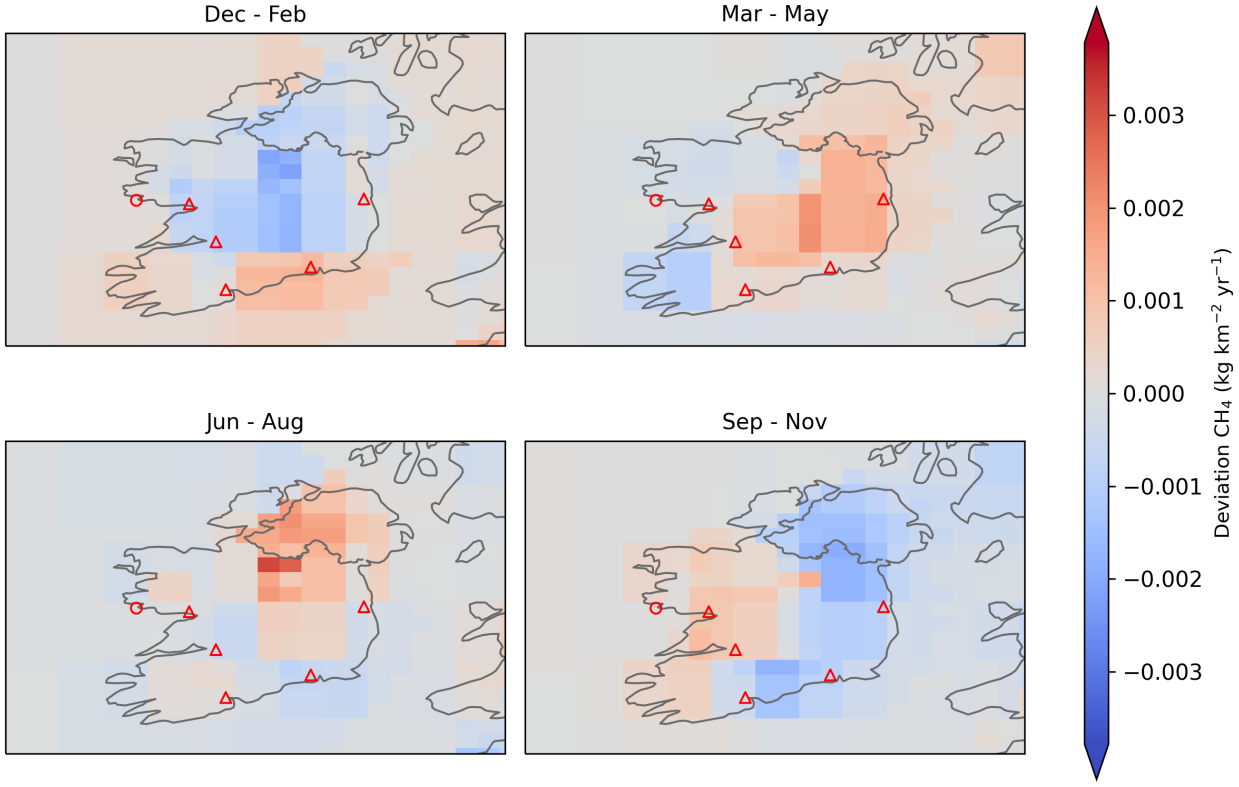

5 Nitrous Oxide (N_2O)

Figure 5.0.1: Total source sensitivity of N_2O observing sites as calculated by the NAME transport model for the year (left) 2018 and (right) 2023 and used in the inversions. Observing stations active in each year are marked with red dots. Areas with visible land surface represent regions for which emissions can be observed well from the network. Shaded or dark areas represent regions for which limited emission information can be obtained from the network.

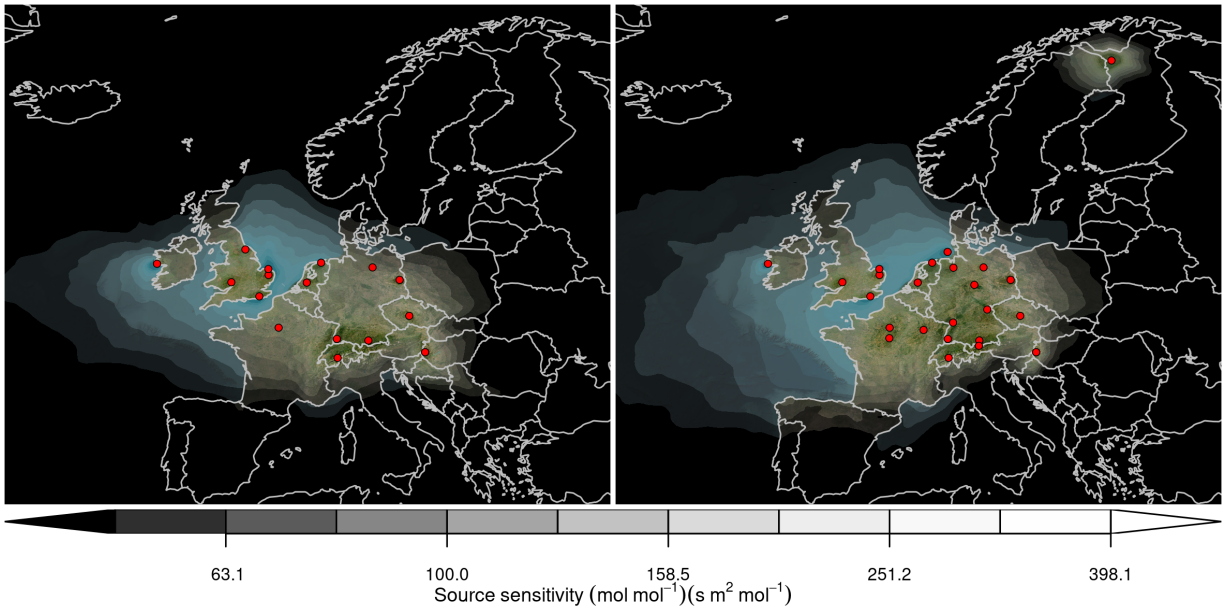

Figure 5.0.2: Verification of the Irish emissions inventory estimates for N_2O. Modelled annual emissions are given as the mean from all models (black line and grey shading) and the individual result from InTEM (blue line and shading). National inventory annual totals are given as grey bars.

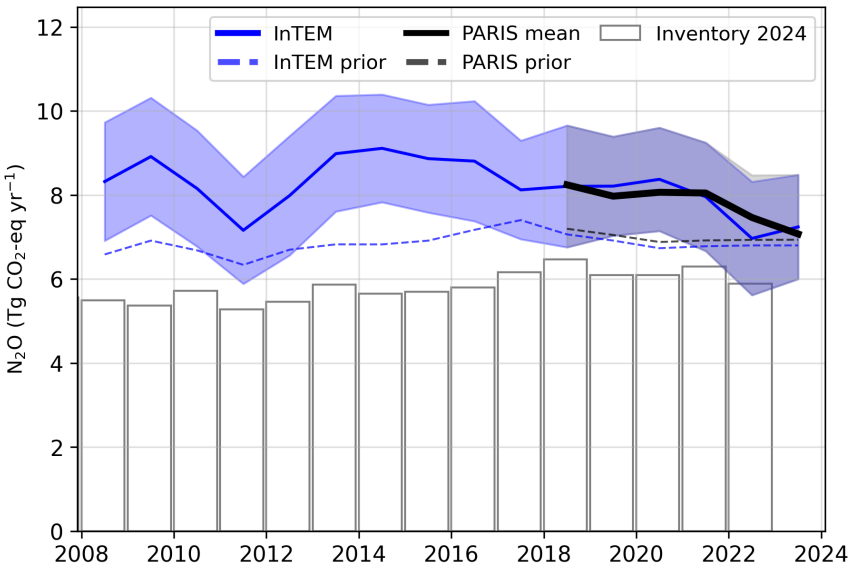

Figure 5.0.3: Verification of the Irish emissions inventory estimates for N_2O (zoom in to 2018-2023). Modelled annual emissions are given as the mean from all models (black line and grey shading) and the individual result from InTEM (blue line and shading). National inventory annual totals are given as grey bars.

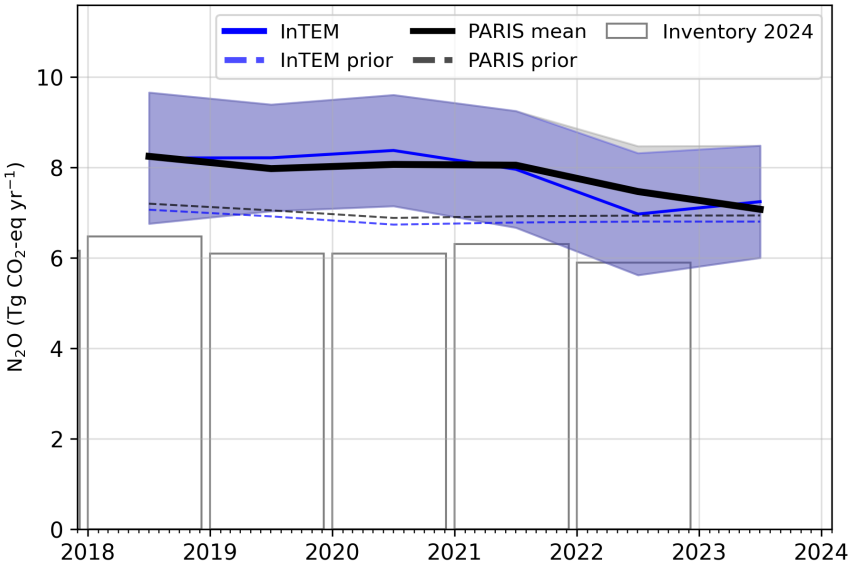

Figure 5.0.4: Verification of the Irish emissions inventory estimates for N_2O (zoom in to 2018-2023). Modelled monthly emissions are given as the mean from all models (black line and grey shading) and the individual result from InTEM (blue line and shading). National inventory annual totals are given as grey bars.

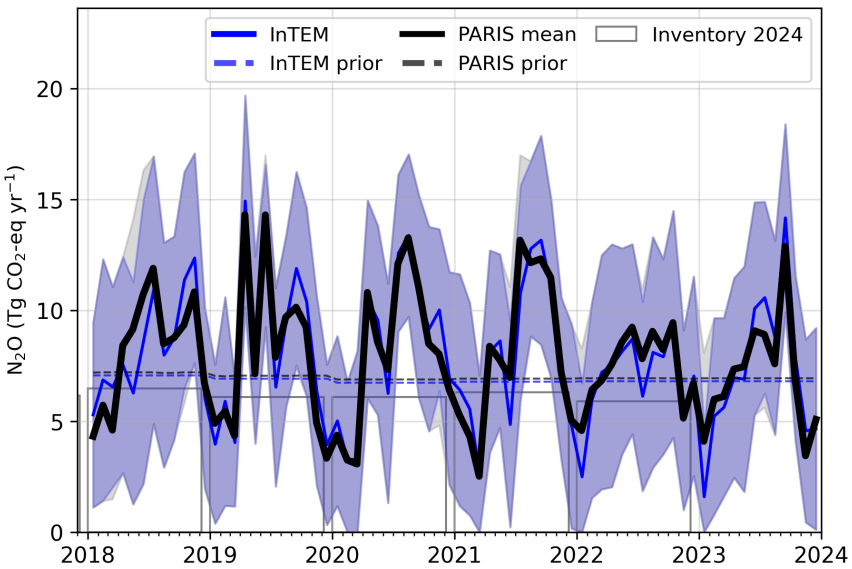

Figure 5.0.5: Spatial distribution of the Irish average modelled emissions of N_2O during the period of 2018-2023 (mean from all models). Observing stations are marked with red circles and highly-populated cities are marked with red triangles.

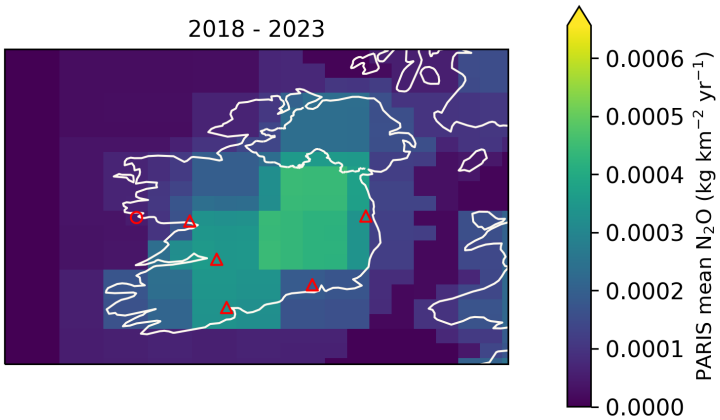

Figure 5.0.6: Spatial distribution of the seasonal deviation from the mean. The deviation is defined as the modelled Irish seasonally averaged N_2O emissions over 2018-2023 minus the average over the whole period. The mean across all models is shown. Observing stations are marked with red circles and highly-populated cities are marked with red triangles.

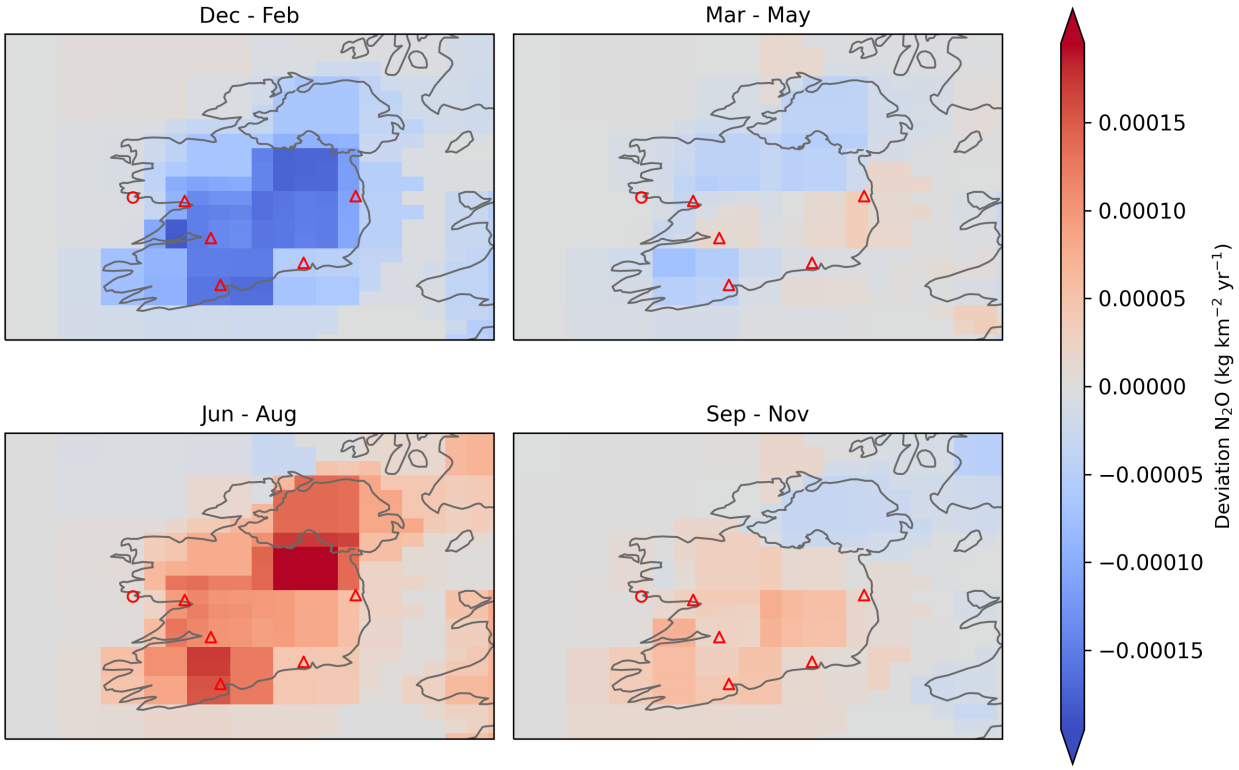

6 Hydrofluorocarbons (HFCs)

Figure 6.0.1: Total source sensitivity of HFCs/PFCs observing sites as calculated by the NAME transport model for the year (left) 2018 and (right) 2023 and used in the inversions. Observing stations active in each year are marked with red dots. Areas with visible land surface represent regions for which emissions can be observed well from the network. Shaded or dark areas represent regions for which limited emission information can be obtained from the network.

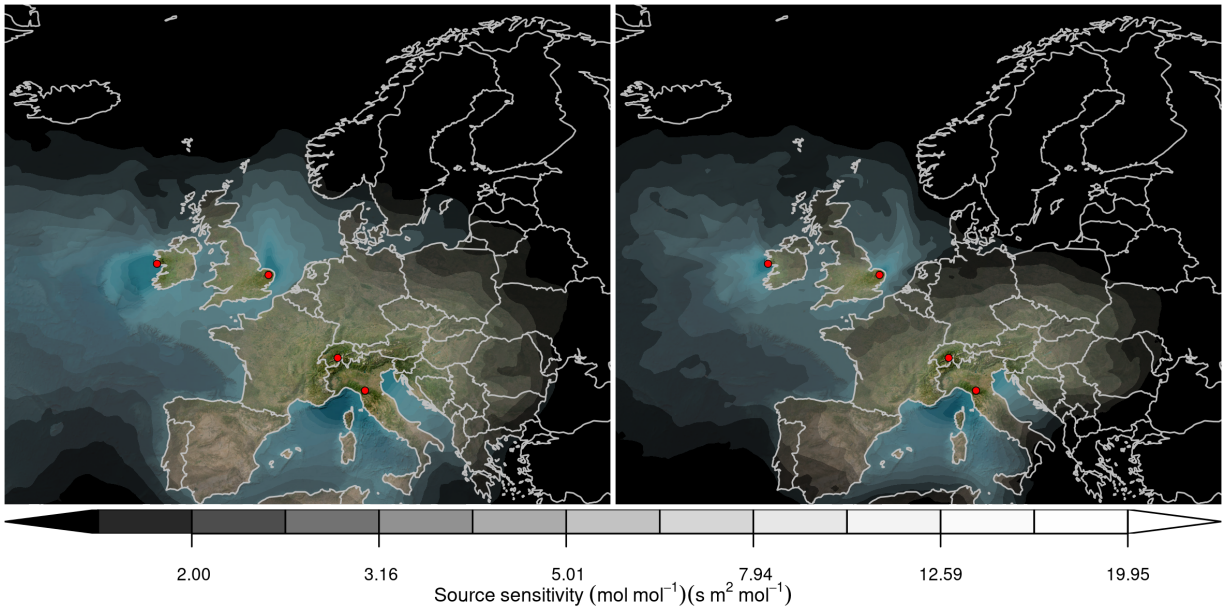

6.1 HFC-32

Figure 6.1.1: Verification of the Irish emissions inventory estimates for HFC-32. Modelled annual emissions are given as the mean from all models (black line and grey shading) and the individual result from InTEM (blue line and shading). National inventory annual totals are given as grey bars.

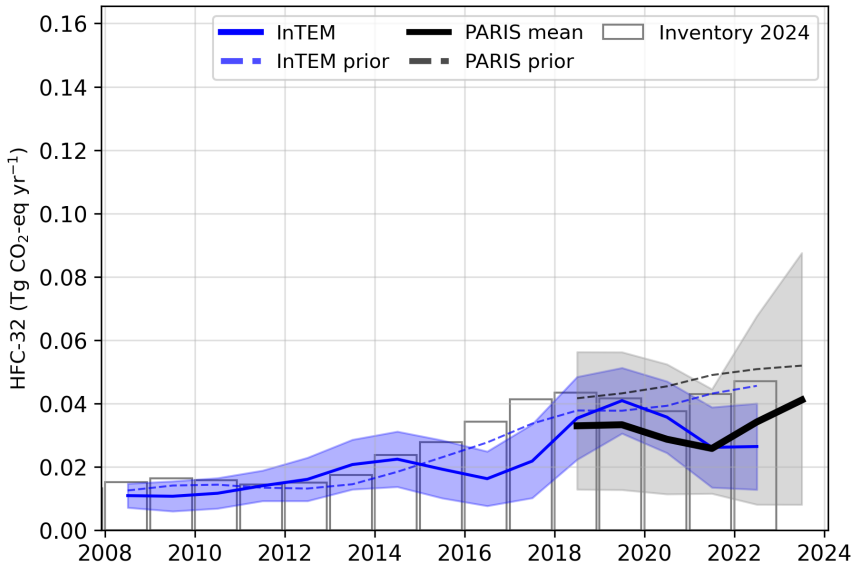

Figure 6.1.2: Spatial distribution of the Irish average modelled emissions of HFC-32 during the period of 2018-2023 (mean from all models). Observing stations are marked with red circles and highly-populated cities are marked with red triangles.

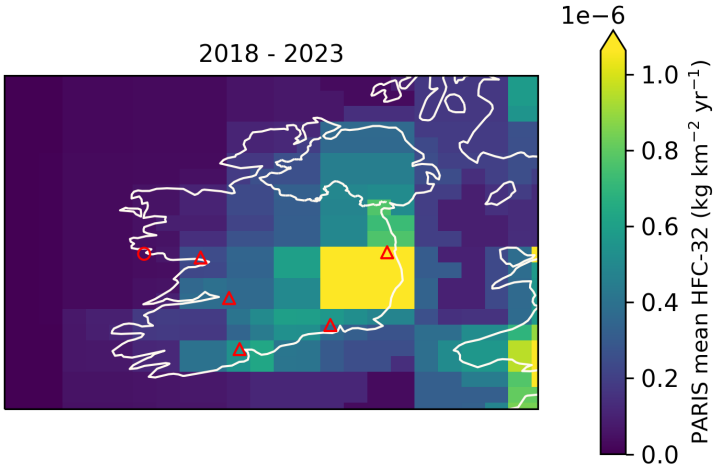

6.2 HFC-125

Figure 6.2.1: Verification of the Irish emissions inventory estimates for HFC-125. Modelled annual emissions are given as the mean from all models (black line and grey shading) and the individual result from InTEM (blue line and shading). National inventory annual totals are given as grey bars.

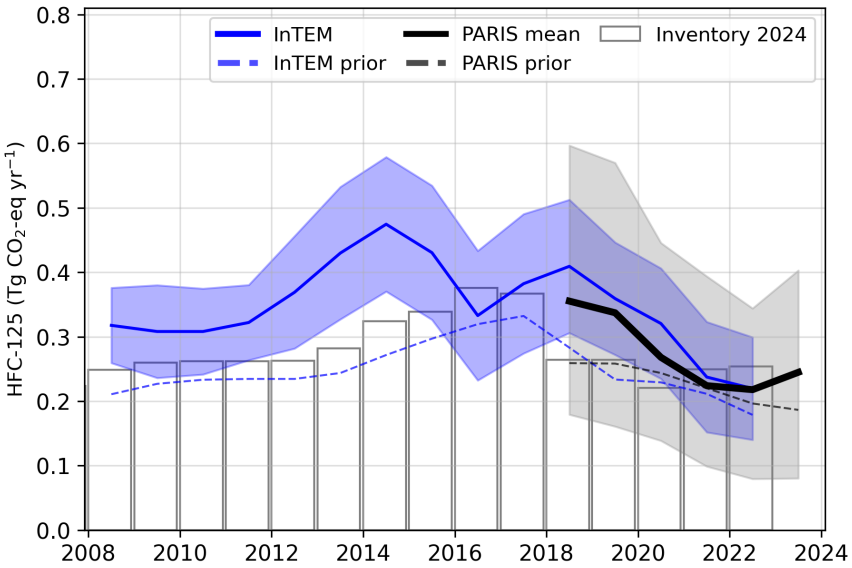

Figure 6.2.2: Spatial distribution of the Irish average modelled emissions of HFC-125 during the period of 2018-2023 (mean from all models). Observing stations are marked with red circles and highly-populated cities are marked with red triangles.

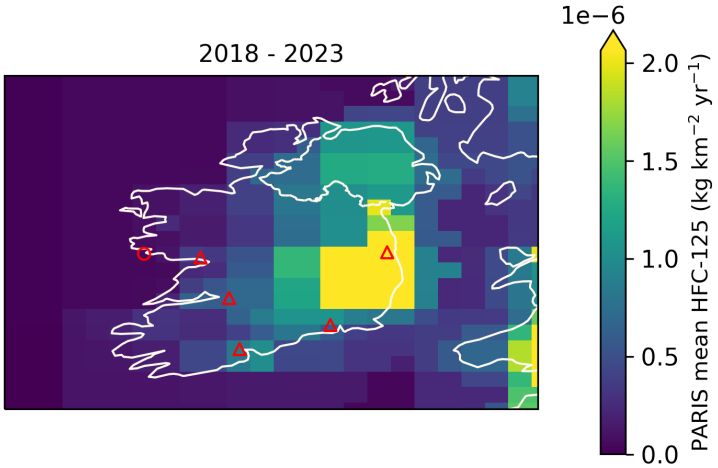

6.3 HFC-134a

Figure 6.3.1: Verification of the Irish emissions inventory estimates for HFC-134a. Modelled annual emissions are given as the mean from all models (black line and grey shading) and the individual result from InTEM (blue line and shading). National inventory annual totals are given as grey bars.

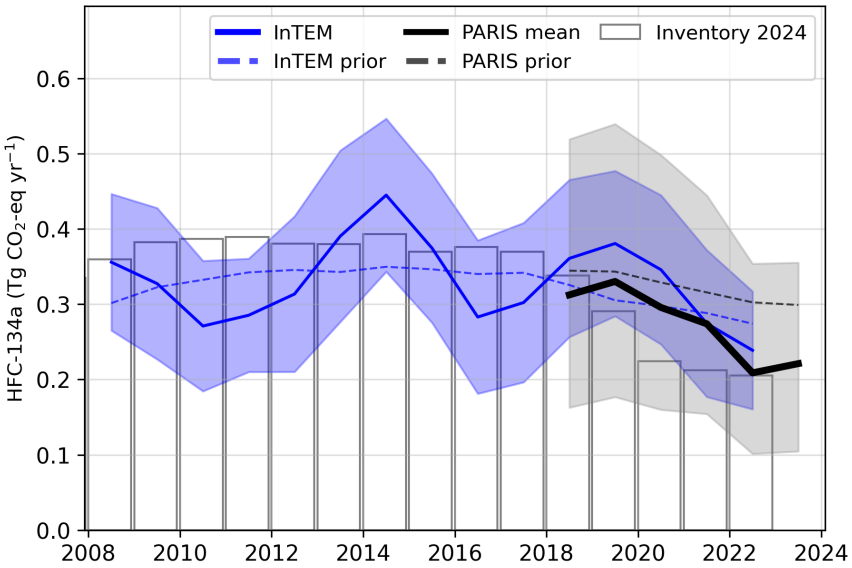

Figure 6.3.2: Spatial distribution of the Irish average modelled emissions of HFC-134a during the period of 2018-2023 (mean from all models). Observing stations are marked with red circles and highly-populated cities are marked with red triangles.

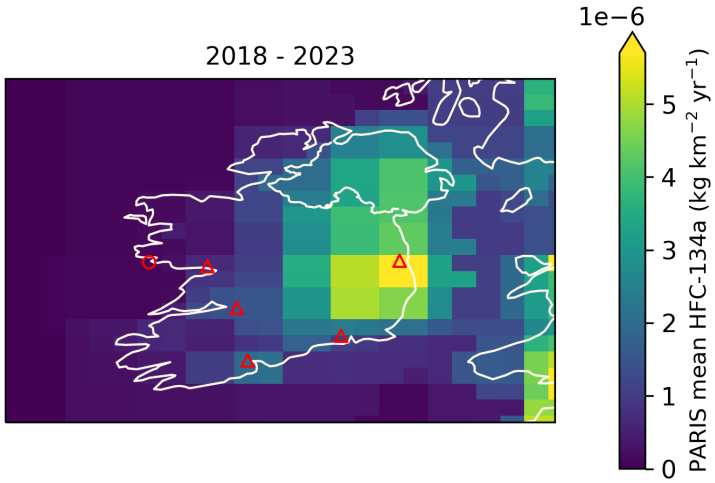

6.4 HFC-143a

Figure 6.4.1: Verification of the Irish emissions inventory estimates for HFC-143a. Modelled annual emissions are given as the mean from all models (black line and grey shading) and the individual result from InTEM (blue line and shading). National inventory annual totals are given as grey bars.

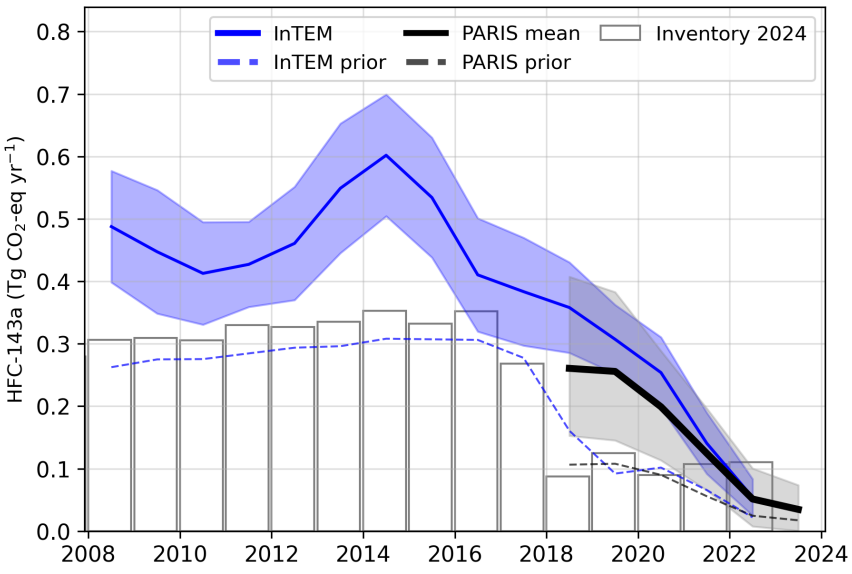

Figure 6.4.2: Spatial distribution of the Irish average modelled emissions of HFC-143a during the period of 2018-2023 (mean from all models). Observing stations are marked with red circles and highly-populated cities are marked with red triangles.

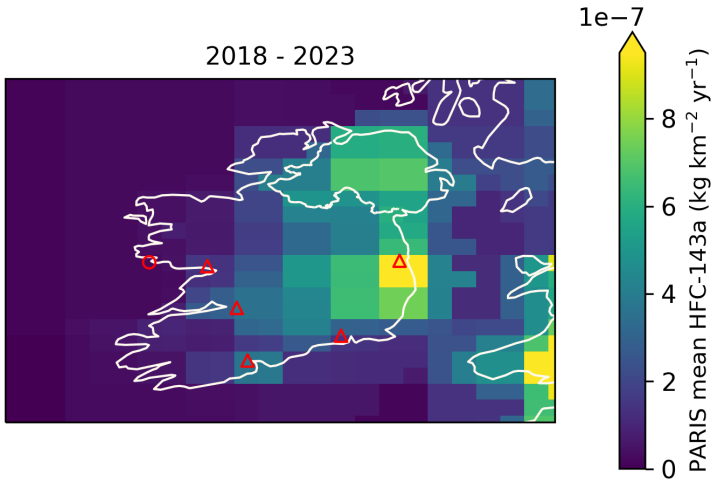

6.5 Total HFCs

Figure 6.5.1: Verification of the Irish emissions inventory estimates for total HFCs. Modelled annual emissions are given as the mean from all models (black line and grey shading) and the individual result from InTEM (blue line and shading). National inventory annual totals are given as grey bars.

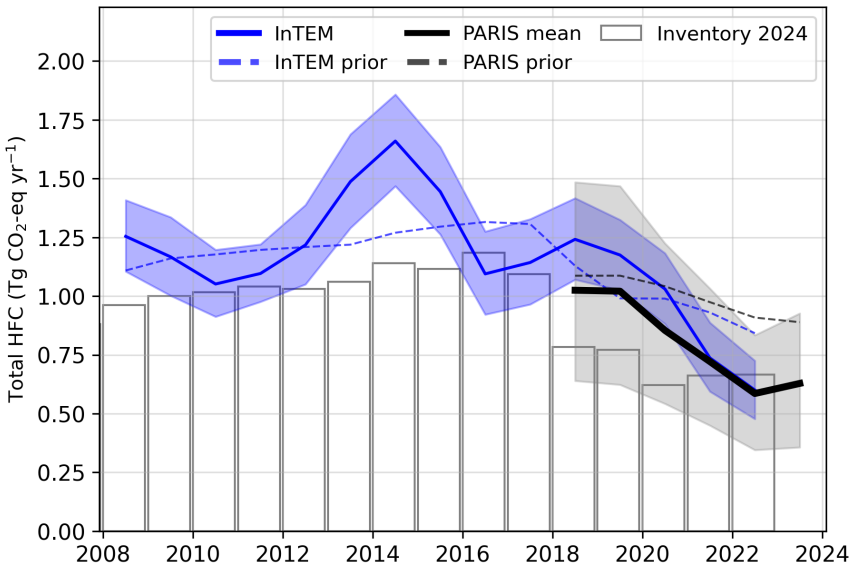

Table 2: Emissions estimation for HFCs in $\mathrm{TgCO_2{-}eq \cdot yr^{-1}}$ according to the National Inventory Report (NIR) 2024 and the inversions done in the PARIS project. For the PARIS estimation, the mean of the 3 inversion models is displayed, along with a range of uncertainty estimated via the half distance between the maximum and minimum uncertainties of the different models.

		2018	2019	2020	2021	2022	2023
HFC-23	NIR 2024	0.00	0.00	0.00	0.00	0.00	
	PARIS mean	0.03 ± 0.06	0.03 ± 0.05	0.03 ± 0.05	0.05 ± 0.07	0.05 ± 0.07	0.06 ± 0.08
HFC-32	NIR 2024	0.04	0.04	0.04	0.04	0.05	
	PARIS mean	0.03 ± 0.02	0.03 ± 0.02	0.03 ± 0.02	0.03 ± 0.02	0.03 ± 0.03	0.04 ± 0.04
HFC-125	NIR 2024	0.26	0.26	0.22	0.25	0.25	
	PARIS mean	0.36 ± 0.21	0.34 ± 0.20	0.27 ± 0.15	0.22 ± 0.15	0.22 ± 0.13	0.24 ± 0.16
HFC-134a	NIR 2024	0.34	0.29	0.22	0.21	0.21	
	PARIS mean	0.31 ± 0.18	0.33 ± 0.18	0.30 ± 0.17	0.27 ± 0.15	0.21 ± 0.13	0.22 ± 0.13
HFC-143a	NIR 2024	0.09	0.13	0.09	0.11	0.11	
	PARIS mean	0.26 ± 0.13	0.26 ± 0.12	0.20 ± 0.09	0.12 ± 0.07	0.05 ± 0.05	0.03 ± 0.04
HFC-152a	NIR 2024	0.00	0.00	0.00	0.00	0.00	
	PARIS mean	0.00 ± 0.00	0.00 ± 0.00	0.00 ± 0.00	0.00 ± 0.00	0.00 ± 0.00	0.00 ± 0.00
HFC-227ea	NIR 2024	0.04	0.04	0.04	0.04	0.04	
	PARIS mean	0.01 ± 0.01	0.01 ± 0.01	0.01 ± 0.01	0.01 ± 0.01	0.01 ± 0.01	0.01 ± 0.01
HFC-245fa	NIR 2024	0.00	0.00	0.00	0.00	0.00	
	PARIS mean	0.01 ± 0.01	0.01 ± 0.01	0.01 ± 0.01	0.00 ± 0.01	0.00 ± 0.00	0.00 ± 0.00
HFC-365mfc	NIR 2024	0.00	0.00	0.00	0.00	0.00	
	PARIS mean	0.01 ± 0.01	0.01 ± 0.01	0.01 ± 0.01	0.01 ± 0.01	0.01 ± 0.00	0.01 ± 0.00
HFC-4310mee	NIR 2024	0.00	0.00	0.00	0.00	0.00	
	PARIS mean	0.00 ± 0.00	0.00 ± 0.00	0.00 ± 0.00	0.00 ± 0.00	0.00 ± 0.00	[1]

[1] HFC-4310mee emissions were not estimated for 2023 due to lack of atmospheric observations.

7 Perfluorocarbons (PFCs)

7.1 PFC-14

Figure 7.1.1: Verification of the Irish emissions inventory estimates for PFC-14. Modelled annual emissions are given as the mean from all models (black line and grey shading) and the individual result from InTEM (blue line and shading). National inventory annual totals are given as grey bars.

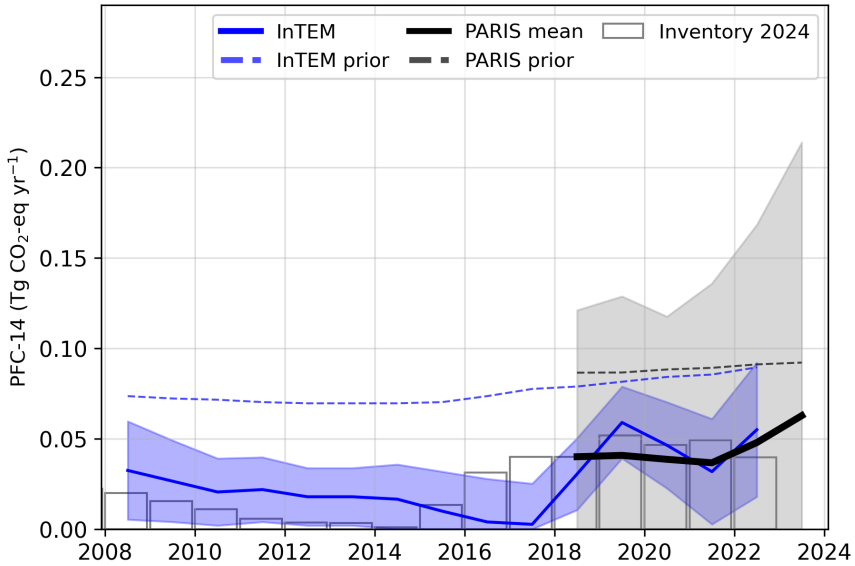

Figure 7.1.2: Spatial distribution of the Irish average modelled emissions of PFC-14 during the period of 2018-2023 (mean from all models). Observing stations are marked with red circles and highly-populated cities are marked with red triangles.

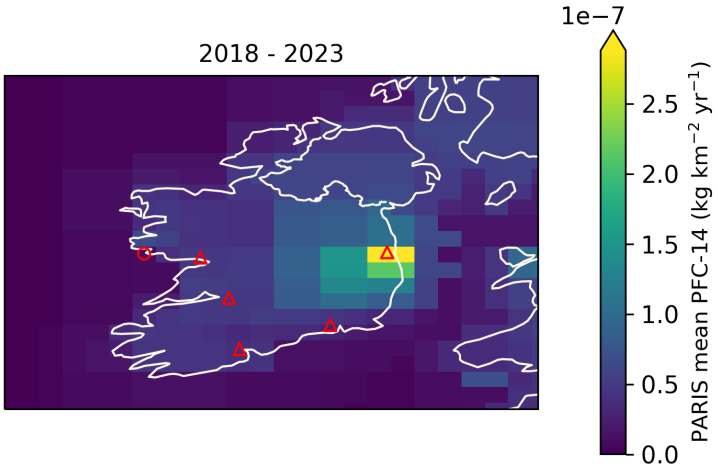

7.2 PFC-116

Figure 7.2.1: Verification of the Irish emissions inventory estimates for PFC-116. Modelled annual emissions are given as the mean from all models (black line and grey shading) and the individual result from InTEM (blue line and shading). National inventory annual totals are given as grey bars.

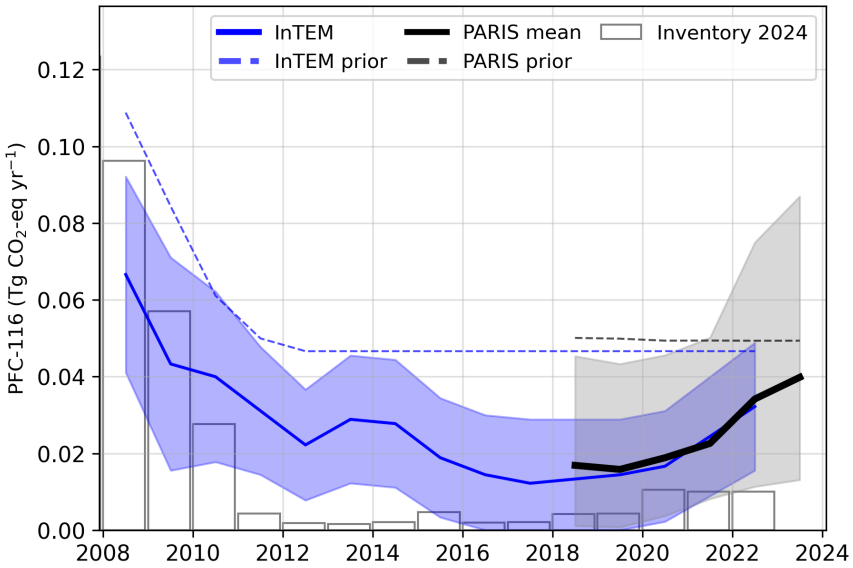

Figure 7.2.2: Spatial distribution of the Irish average modelled emissions of PFC-116 during the period of 2018-2023 (mean from all models). Observing stations are marked with red circles and highly-populated cities are marked with red triangles.

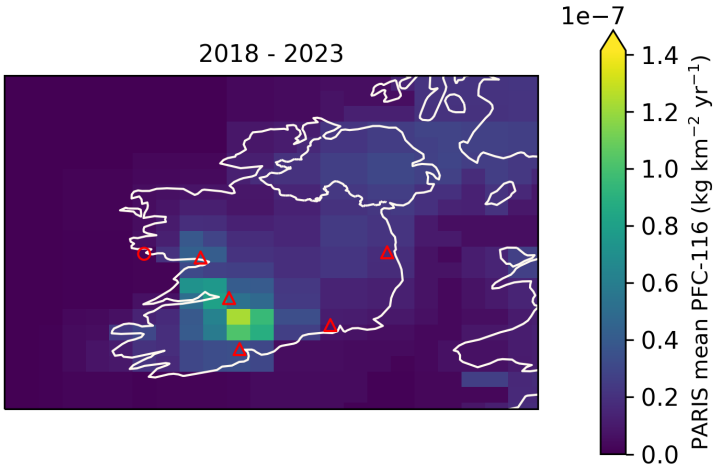

7.3 PFC-218

Figure 7.3.1: Verification of the Irish emissions inventory estimates for PFC-218. Modelled annual emissions are given as the mean from all models (black line and grey shading) and the individual result from InTEM (blue line and shading). National inventory annual totals are given as grey bars.

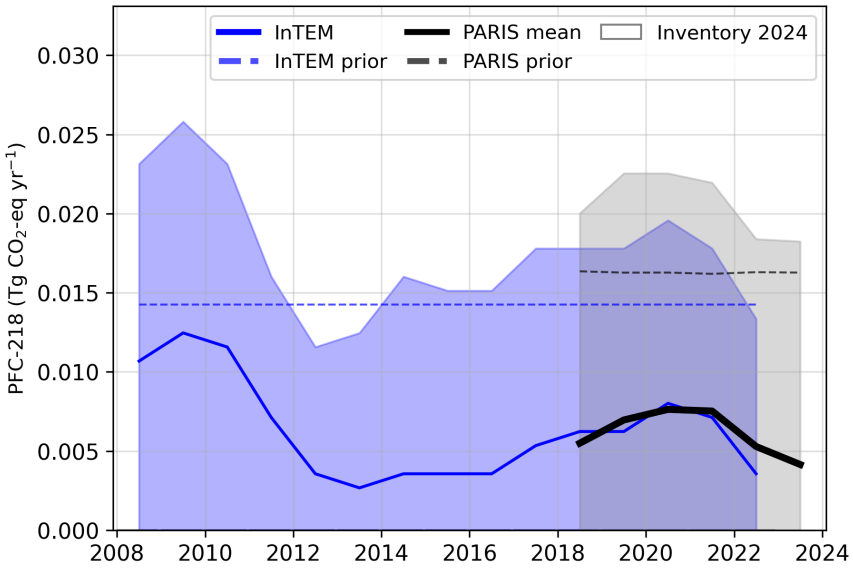

Figure 7.3.2: Spatial distribution of the Irish average modelled emissions of PFC-218 during the period of 2018-2023 (mean from all models). Observing stations are marked with red circles and highly-populated cities are marked with red triangles.

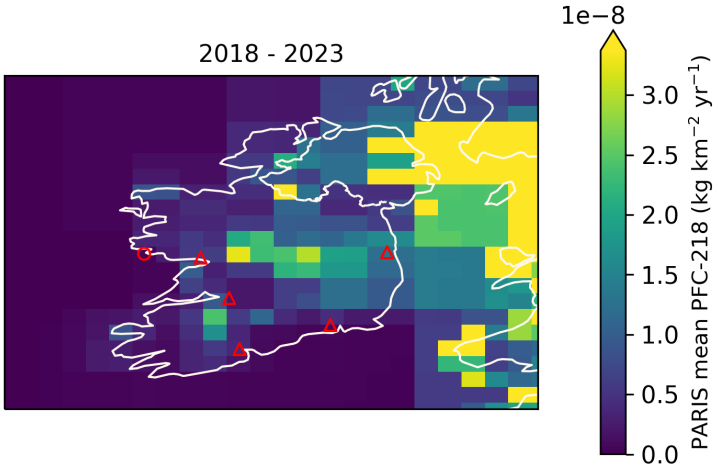

7.4 PFC-318

Figure 7.4.1: Verification of the Irish emissions inventory estimates for PFC-318. Modelled annual emissions are given as the mean from all models (black line and grey shading) and the individual result from InTEM (blue line and shading). National inventory annual totals are given as grey bars.

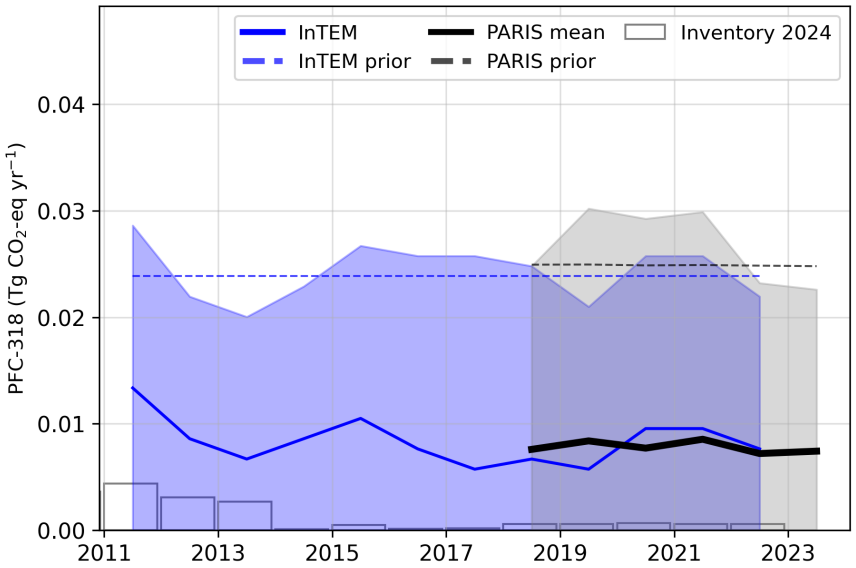

Figure 7.4.2: Spatial distribution of the Irish average modelled emissions of PFC-318 during the period of 2018-2023 (mean from all models). Observing stations are marked with red circles and highly-populated cities are marked with red triangles.

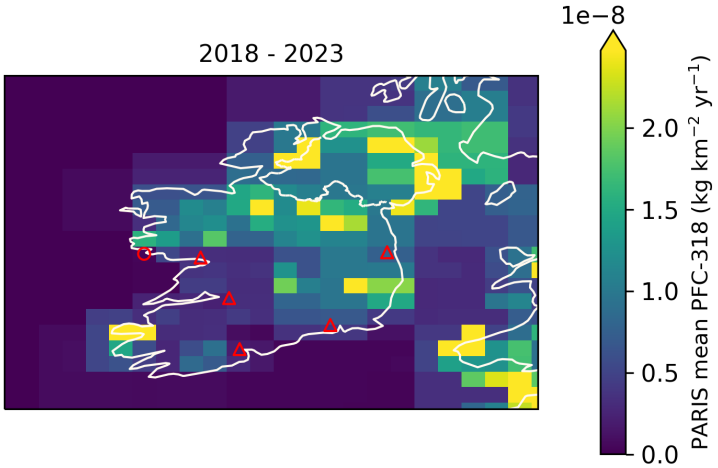

7.5 Total PFCs

Figure 7.5.1: Verification of the Irish emissions inventory estimates for total PFCs. Modelled annual emissions are given as the mean from all models (black line and grey shading) and the individual result from InTEM (blue line and shading). National inventory annual totals are given as grey bars.

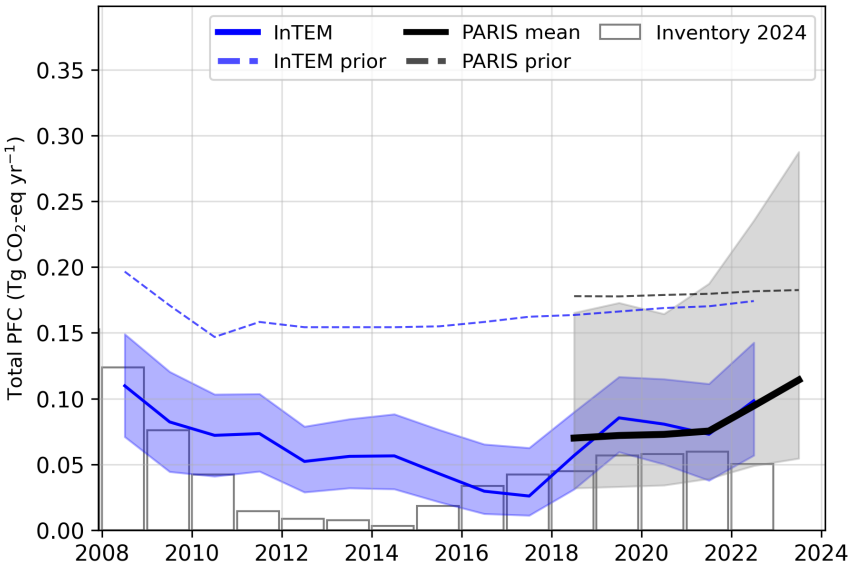

Table 3: Emissions estimation for PFCs in $\mathrm{TgCO_2{-}eq \cdot yr^{-1}}$ according to the National Inventory Report (NIR) 2024 and the inversions done in the PARIS project. For the PARIS estimation, the mean of the 3 inversion models is displayed, along with a range of uncertainty estimated via the half distance between the maximum and minimum uncertainties of the different models.

		2018	2019	2020	2021	2022	2023
PFC-14	NIR 2024	0.04	0.05	0.05	0.05	0.04	
	PARIS mean	0.04 ± 0.06	0.04 ± 0.06	0.04 ± 0.06	0.04 ± 0.07	0.05 ± 0.08	0.06 ± 0.11
PFC-116	NIR 2024	0.00	0.00	0.01	0.01	0.01	
	PARIS mean	0.02 ± 0.02	0.02 ± 0.02	0.02 ± 0.02	0.02 ± 0.02	0.03 ± 0.03	0.04 ± 0.04
PFC-218	NIR 2024	0.00	0.00	0.00	0.00	0.00	
	PARIS mean	0.01 ± 0.01	0.01 ± 0.01	0.01 ± 0.01	0.01 ± 0.01	0.01 ± 0.01	0.00 ± 0.01
PFC-318	NIR 2024	0.00	0.00	0.00	0.00	0.00	
	PARIS mean	0.01 ± 0.01	0.01 ± 0.02	0.01 ± 0.01	0.01 ± 0.01	0.01 ± 0.01	0.01 ± 0.01

8 Sulphur hexafluoride (SF_6)

Figure 8.0.1: Total source sensitivity of SF_6 observing sites as calculated by the NAME transport model for the year (left) 2018 and (right) 2023 and used in the inversions. Observing stations active in each year are marked with red dots. Areas with visible land surface represent regions for which emissions can be observed well from the network. Shaded or dark areas represent regions for which limited emission information can be obtained from the network.

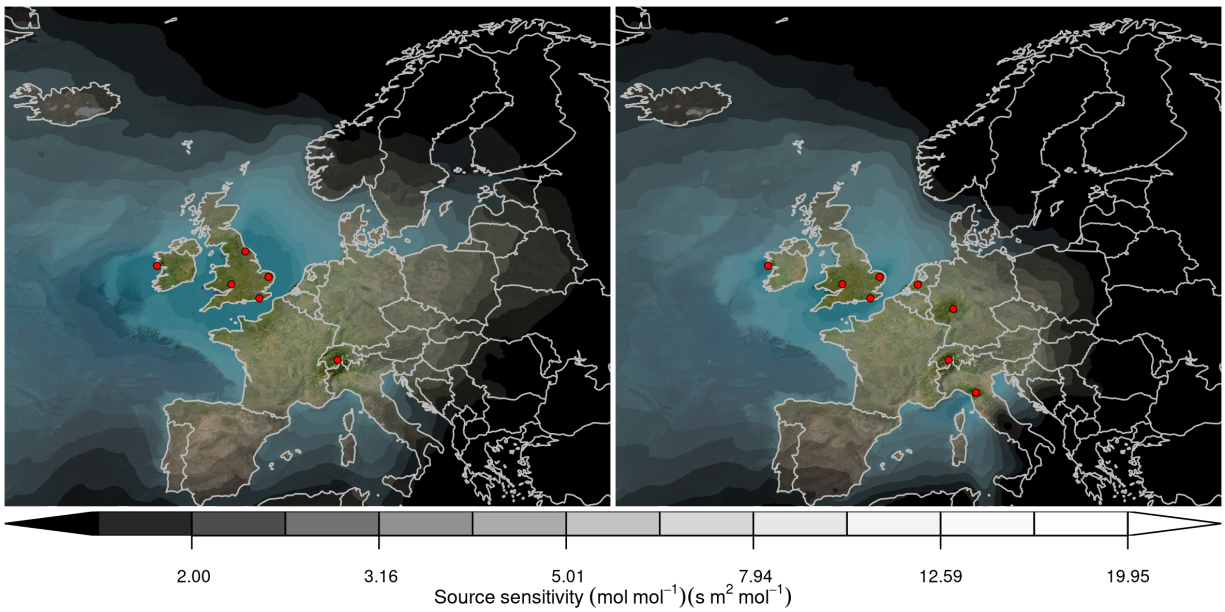

Figure 8.0.2: Verification of the Irish emissions inventory estimates for SF_6. Modelled annual emissions are given as the mean from all models (black line and grey shading) and the individual result from InTEM (blue line and shading). National inventory annual totals are given as grey bars.

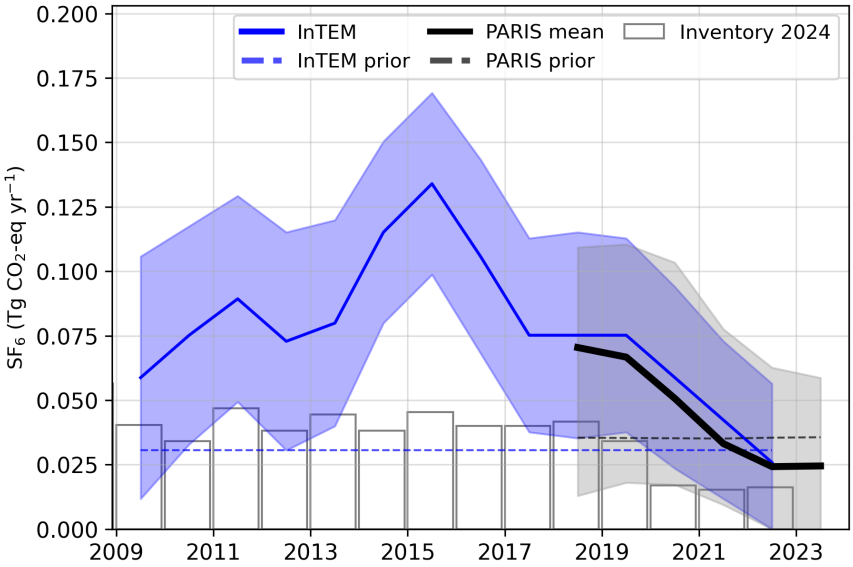

Figure 8.0.3: Spatial distribution of the Irish average modelled emissions of SF_6 during the period of 2018-2023 (mean from all models). Observing stations are marked with red circles and highly-populated cities are marked with red triangles.

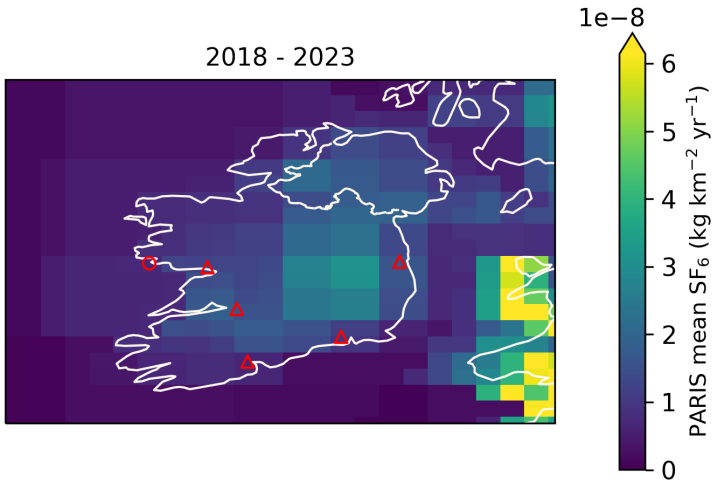

References

European Commission: Joint Research, Centre et al. (2023). *GHG emissions of all world countries – 2023*. Publications Office of the European Union. DOI: 10.2760/953322.

Ganesan, A. L. et al. (2014). "Characterization of uncertainties in atmospheric trace gas inversions using hierarchical Bayesian methods". In: *Atmospheric Chemistry and Physics* 14.8, pp. 3855–3864. DOI: 10.5194/acp-14-3855-2014. URL: http://www.atmos-chem-phys.net/14/3855/2014/http://www.atmos-chem-phys.net/14/3855/2014/acp-14-3855-2014.pdf.

Ganesan, A. L. et al. (2015). "Quantifying methane and nitrous oxide emissions from the UK and Ireland using a national-scale monitoring network". In: *Atmos. Chem. Phys.* 15.11, pp. 6393–6406. DOI: 10.5194/acp-15-6393-2015. URL: https://www.atmos-chem-phys.net/15/6393/2015/https://www.atmos-chem-phys.net/15/6393/2015/acp-15-6393-2015.pdf.

Henne, S. et al. (2016). "Validation of the Swiss methane emission inventory by atmospheric observations and inverse modelling". In: *Atmospheric Chemistry and Physics* 16.6, pp. 3683–3710. DOI: 10.5194/acp-16-3683-2016. URL: http://www.atmos-chem-phys.net/16/3683/2016/.

Jones, A.R. et al. (2007). "The U.K. Met Office's next-generation atmospheric dispersion model, NAME III, in Borrego C. and Norman A.-L. (Eds)". In: *Air Pollution Modeling and its Application XVII (Proceedings of the 27th NATO/CCMS International Technical Meeting on Air Pollution Modelling and its Application), Springer*, pp. 580–589.

Katharopoulos, I. et al. (2023). "Impact of transport model resolution and a priori assumptions on inverse modeling of Swiss F-gas emissions". In: *Atmos. Chem. Phys.* 23.22, pp. 14159–14186. DOI: 10.5194/acp-23-14159-2023. URL: https://acp.copernicus.org/articles/23/14159/2023/.

Manning, A. J. et al. (2021). "Evidence of a recent decline in UK emissions of hydrofluorocarbons determined by the InTEM inverse model and atmospheric measurements". In: *Atmospheric Chemistry and Physics* 21.16, pp. 12739–12755. DOI: 10.5194/acp-21-12739-2021. URL: https://acp.copernicus.org/articles/21/12739/2021/.

Rigby, M. et al. (2019). "Increase in CFC-11 emissions from eastern China based on atmospheric observations". In: *Nature* 569, pp. 546–550. DOI: 10.1038/s41586-019-1193-4. URL: https://doi.org/10.1038/s41586-019-1193-4.